

UNIVERSITY OF BIRMINGHAM

A NANOTOXICOLOGY INVESTIGATION: EXPLORING THE IMPACTS OF SILVER AND GOLD NANOPARTICLES SIZE ON CELL SIGNALLING PATHWAYS IN LUNG CELL LINES

by

HANOUF BAFHAID

A thesis submitted to the University of Birmingham for the degree of

DOCTOR OF PHILOSOPHY

School of Pharmacy

The Institute of Clinical Sciences

College of Medical and Dental Sciences

University of Birmingham

October 2020

Abstract

Metal-containing nanoparticles (NPs), including silver nanoparticles (AgNPs) and gold nanoparticles (AuNPs) have shown great promise in several biomedical applications. It is of importance to predict their potential adverse effects upon their cellular exposure. In this study, we hypothesise that cellular exposure to different NPs chemical compositions (AgNPs and AuNPs) with various NPs sizes (10, 40 and 80 nm) can mediate distinct biological responses in 2D and 3D cell culture models of human lung cells. The overarching aims of this study were to assess the toxicity of AgNPs and AuNPs of different sizes in normal human lung fibroblast cells (MRC-5) and human lung adenocarcinoma epithelial cells (A549) and investigate the influence of both NPs on the PI3K/AKT and Wnt/β-catenin signalling pathways. Cell viability data demonstrated the high biocompatibility of AuNPs compared to AgNPs on both cell lines. In addition, AgNPs elicited size-, concentration- and time-dependent toxicity in both lung cells. Similar responses were observed in A549 exposed to AuNPs but not MRC-5 treated with AuNPs, which illustrates high sensitivity to large sized AuNPs (80 nm). AgNPs, compared to AuNPs, induced significant oxidative stress via the overproduction of reactive oxygen species and depletion of intracellular glutathione levels. Both AgNPs and AuNPs provoked G2/M phase cell cycle arrest and mitochondrial-dysfunction mediated apoptosis in both cell lines. The A549 3D spheroidal model demonstrated lower sensitivity upon exposure to both types of NPs compared to the 2D monolayer model, but presented size-dependent toxicity when exposed to AgNPs. It was revealed that both AgNPs and AuNPs may trigger apoptosis via attenuation of the PI3K/AKT pathway activity and suppression of cell proliferation and cell cycle progression via dysregulation of Wnt/β-catenin signalling activity. Overall, this work shows the

influential effects of NPs composition and size on cellular toxicity and could propose a potential use of AgNPs and AuNPs as therapeutic targets in the PI3K/AKT and Wnt/β-catenin cell signalling pathways.

Acknowledgment

I would like to express my heartfelt gratitude to my supervisor Dr Hanene Ali-Boucetta for her time, guidance and support throughout this project. Also, I would like to extend my thanks to Dr Zubair Ahmed and Dr Youcef Mehellou for their help and contributions in this work.

I gratefully acknowledge the Saudi ministry of higher education for funding this project.

Special thanks to my parents and all my family for their endless support and constant encouragement during very difficult times.

Finally, I would like to thanks all my lab colleagues and friends for their assistance and motivation throughout my PhD journey.

Table of Contents

1. Chapter 1. Introduction 1

1.1 Background 2

1.2 Silver and gold nanoparticles 3

1.2.1 Synthesis of AgNPs and AuNPs 4

1.2.2 Biomedical applications of AgNPs and AuNPs 5

1.3 The importance of Nanotoxicology 7

1.4 Toxicity of AgNPs and AuNPs 8

1.4.1 Postulated mechanisms underlying AgNPs and AuNPs toxicity 8

1.4.2 *In vitro* nanotoxicity assessments of AgNPs and AuNPs 12

1.4.3 Impact of physicochemical properties of AgNPs and AuNPs on toxicity 15

1.4.3.1 Effect of particle size 16

1.4.3.2 Effect of particle morphology 22

1.4.3.3 Effect of particle surface charge and surface modification 25

1.4.3.4 Effect of particle chemical composition 30

1.5 AgNPs and AuNPs mediate oxidative stress by modulating cell signalling pathways……32

1.5.1 Impact of physicochemical properties of AgNPs and AuNPs on modulation of oxidative stress mediated cell signalling pathways 36

1.5.2 Effect of AgNPs and AuNPs on other cell signalling pathways 42

1.6 Research aims and objectives 46

2. Chapter 2. Materials and methods 48

2.1 Materials 49

2.1.1 Nanoparticles 49

2.1.2 Cell lines and cell culture reagents 49

2.1.3 Chemicals 50
2.1.4 Assay Kits 51
2.2 Methods 52
2.2.1 Characterisations of AgNPs and AuNPs of different sizes 52
2.2.1.1 Transmission electron microscopy (TEM) 52
2.2.1.2 Dynamic light scattering (DLS)/ Zetasizer 52
2.2.1.3 Ultraviolet-Visible (UV-Vis) spectroscopy 52
2.2.2 Toxicological assessment of AgNPs and AuNPs of different sizes in 2D *in vitro* cell culture model 53
2.2.2.1 Cell culture 53
2.2.2.2 LIVE/DEAD™ fixable far-red dead cell stain assay: cell viability assessment of sodium citrate stabiliser 53
2.2.2.3 Modified lactate dehydrogenase (mLDH) assay: cell viability assessment ... 54
2.2.2.4 Thiazolyl blue tetrazolium bromide (MTT) assay: cell metabolic activity measurement 56
2.2.2.5 Cellular uptake of AgNPs and AuNPs 57
2.2.2.5.1 Side-scattered light intensity analysis by flow cytometry: cell granularity assessment 57
2.2.2.5.2 Quantifications of intracellular NPs by inductively coupled plasma mass spectrometry (ICP-MS): silver and gold ions measurement 58
2.2.2.6 Mechanisms of AgNPs and AuNPs toxicity 60
2.2.2.6.1 CellROX™ deep red reagent for oxidative stress detection: ROS measurement 60
2.2.2.6.2 GSH/GSSG-Glo™ assay: glutathione measurement 61
2.2.2.6.3 Alexa Fluor® 488 Annexin V/Dead Cell Apoptosis assay: apoptosis cell death detection 62

2.2.2.6.4 MitoProbe™ TMRM assay by Flow Cytometry: mitochondrial membrane potential health assessment 63

2.2.2.6.5 FxCycle™ PI/RNase Staining Solution assay: cell cycle progression analysis……64

2.2.2.6.6 mLDH assay: Cell recovery post AgNPs and AuNPs treatment 65

2.2.3 Toxicological assessment of AgNPs and AuNPs of different sizes in 3D *in vitro* cell culture model 65

2.2.3.1 Spheroids preparation 65

2.2.3.2 Spheroids morphology and size changes 66

2.2.3.3 LIVE/DEAD™ cell imaging assay: spheroids cytotoxicity assessment 66

2.2.4 Impacts of AgNPs and AuNPs of different sizes on cell signalling pathways... 67

2.2.4.1 Western blot technique: protein detection 67

2.2.4.2 Bradford assay: protein concentration measurement prior to western blotting……70

2.2.4.3 Cytoplasmic/nuclear localisation of β-catenin..... 70

2.2.4.4 Immunohistochemistry analysis (IHC) of β-catenin expression..... 73

2.2.4.5 Wnt/β-catenin pathway activation by Lithium Chloride (LiCl) 73

2.2.4.6 Wnt/β-catenin pathway activation by Wnt agonist I 75

2.2.5 Statistical data analysis..... 77

3. Chapter 3. Toxicological assessment of AgNPs of different sizes 78

3.1 Introduction..... 79

3.2 Characterisations of AgNPs of different sizes..... 79

3.2.1 Results and discussion..... 80

3.2.1.1 Size measurement 80

3.2.1.2 Surface charge analysis..... 82

3.2.1.3 AgNPs stability in cell culture media 83

3.3 Toxicological assessment of AgNPs of different sizes in a 2D *in vitro* cell culture model……85

3.3.1 Results and discussion 85

3.3.1.1 Cell viability assessment of sodium citrate stabiliser 85

3.3.1.2 Cell viability assessment of AgNPs of different sizes 88

3.3.1.3 Changes in cell morphology post AgNPs treatment 95

3.3.1.4 Cellular uptake of AgNPs 98

3.3.1.4.1 Cell granularity assessment by flow cytometry 98

3.3.1.4.2 Intracellular Ag ions quantification by ICP-MS 102

3.3.1.5 The mechanisms of AgNPs toxicity assessment..... 105

3.3.1.5.1 Oxidative stress detection..... 105

3.3.1.5.2 Glutathione measurement..... 110

3.3.1.5.3 Apoptosis detection 112

3.3.1.5.4 Mitochondrial membrane potential health assessment..... 119

3.3.1.5.5 Cell cycle progression analysis 122

3.3.1.5.6 Cells recovery post AgNPs treatment 126

3.3.1.5.7 NPs- assay interference 129

3.4 Toxicological assessment of AgNPs of different sizes in a 3D *in vitro* cell culture model……...130

3.4.1 Results and discussion 130

3.4.1.1 Spheroids preparation 130

3.4.1.2 Spheroids morphology and size changes 133

3.4.1.3 Spheroids cytotoxicity assessment..... 136

4. Chapter 4. Toxicological assessment of AuNPs of different sizes 139

4.1 Introduction..... 140

4.2 Characterisations of AuNPs of different sizes 140

4.2.1 Results and discussion 141
4.2.1.1 Size measurement 141
4.2.1.2 Surface charge analysis 143
4.2.1.3 AuNPs stability in cell culture media 143
4.3 Toxicological assessment of AuNPs of different sizes in a 2D *in vitro* cell culture model……...145
4.3.1 Results and discussion 145
4.3.1.1 Cell viability assessment of sodium citrate stabiliser 145
4.3.1.2 Cell viability assessment of AuNPs of different sizes 146
4.3.1.3 Changes in cell morphology post AuNPs treatment 153
4.3.1.4 Cellular uptake of AuNPs 156
4.3.1.4.1 Cell granularity assessment by flow cytometry 156
4.3.1.5 The mechanisms of AuNPs toxicity assessment 160
4.3.1.5.1 Oxidative stress detection 160
4.3.1.5.2 Glutathione measurement 162
4.3.1.5.3 Apoptosis detection 164
4.3.1.5.4 Mitochondrial membrane potential health assessment 168
4.3.1.5.5 Cell cycle progression analysis 171
4.3.1.5.6 Cells recovery post AuNPs treatment 174
4.3.1.5.7 NPs- assay interference 177
4.4 Toxicological assessment of AuNPs of different sizes in a 3D *in vitro* cell culture model……...177
4.4.1 Results and discussion 178
4.4.1.1 Spheroids morphology and size changes 178
4.4.1.2 Spheroids cytotoxicity assessment 181

5. Chapter 5. Impacts of AuNPs and AgNPs on PI3K/AKT and Wnt/β-catenin cell signalling pathways 183

5.1 Introduction 184

5.2 The influences of AuNPs and AgNPs of different sizes on the PI3K/AKT cell signalling pathway 185

5.2.1 Results and discussion 188

5.2.1.1 The impacts of AuNPs on the PI3K/AKT cell signalling pathway 188

5.2.1.2 The impacts of AgNPs on the PI3K/AKT cell signalling pathway 201

5.3 The influences of AuNPs and AgNPs of different sizes on the Wnt/β-catenin cell signalling pathway 215

5.3.1 Results and discussion 218

5.3.1.1 The impacts of AuNPs on the Wnt/β-catenin cell signalling pathway 218

5.3.1.2 The impacts of AgNPs on the Wnt/β-catenin cell signalling pathway 226

5.3.1.2.1 The effects of AgNPs on β-catenin and GSK-3β proteins phosphorylation…. 231

5.3.1.2.2 The effects of AgNPs on the membrane proteins expression of Wnt/β-catenin signalling pathway 236

5.3.1.2.3 Cytoplasmic/nuclear localisation of β-catenin 243

5.3.1.2.4 Wnt/β-catenin signalling pathway activation by Wnt activators 246

6. Chapter 6. General discussion and future work 255

6.1 General discussion 256

6.2 Future directions 265

6.3 Conclusion 267

7. Chapter 7. References 269

8. Chapter 8. Appendix 298

List of Figures

Figure 1.1. Postulated toxicity mechanisms of AgNPs and AuNPs 9

Figure 1.2. Synopsis of *in vitro* nanotoxicity assessments 14

Figure 1.3. Schematic representation of AgNPs and AuNPs impact on MAPK, AKT and p53 cell signalling pathways 33

Figure 2.1. Schematic flow chart of cytoplasmic and nuclear fractions sample preparation 72

Figure 2.2. Schematic flow chart of cells treated with LiCl and Ag10 74

Figure 2.3. Schematic flow chart of cells treated with Wnt agonist I and Ag10 76

Figure 3.1. TEM micrographs and the size distributions of AgNPs of different sizes 81

Figure 3.2. Cell viability assessment of MRC-5 and A549 cells treated with sodium citrate. 87

Figure 3.3. Cytotoxicity assessment of MRC-5 and A549 cells following exposure to AgNPs of different sizes using mLDH assay 89

Figure 3.4. Cytotoxicity assessment of MRC-5 and A549 cells following the exposure to AgNPs of different sizes using MTT assay 92

Figure 3.5. Cell morphological changes of MRC-5 cells treated with AgNPs of different sizes 96

Figure 3.6. Cell morphological changes of A549 cells treated with AgNPs of different sizes 97

Figure 3.7. SSC light intensity analysis of cellular uptake of AgNPs in MRC-5 cells by flow cytometry 100

Figure 3.8. SSC light intensity analysis of cellular uptake of AgNPs in A549 cells by flow cytometry 101

Figure 3.9. Cellular uptake of AgNPs in MRC-5 and A549 cells analysed by ICP-MS 103

Figure 3.10. Oxidative stress detection in MRC-5 and A549 cells following the exposure to AgNPs of different sizes using CellRox deep red reagent 107

Figure 3.11. GSH/GSSG ratio quantification of MRC-5 and A549 cells following the exposure to AgNPs of different sizes using GSH/GSSG-Glo™ Assay 111

Figure 3.12. Apoptosis cell death analysis of MRC-5 cells following the exposure to AgNPs of different sizes using Annexin V and PI by flow cytometry. 115

Figure 3.13. Apoptosis cell death analysis in A549 cells following the exposure to AgNPs of different sizes using Annexin V and PI by flow cytometry 116

Figure 3.14. Detection of mitochondrial membrane potential state in MRC-5 and A549 cells following the exposure to AgNPs of different sizes using MitoProbe, TMRM assay by flow cytometry 120

Figure 3.15. Cell Cycle progression analysis in MRC-5 and A549 cells following the exposure to AgNPs of different sizes using FxCycle™ PI/RNase Staining by flow cytometry 124

Figure 3.16. Recovery of MRC-5 and A549 cells following the exposure to AgNPs of different sizes 127

Figure 3.17. Growth curve of A549 spheroids 132

Figure 3.18. A549 spheroids morphological changes following the exposure to Ag10 134

Figure 3.19. A549 spheroids morphological changes following the exposure to Ag80 135

Figure 3.20. Cytotoxicity assessment of A549 spheroids following the exposure to Ag10 and Ag80. 137

Figure 4.1. TEM micrographs and the size distributions of AuNPs of different sizes 142

Figure 4.2. Cytotoxicity assessment of MRC-5 and A549 cells following the exposure to AuNPs of different sizes using mLDH assay 147

Figure 4.3. Cytotoxicity assessment of MRC-5 and A549 cells following the exposure to AuNPs of different sizes using MTT assay 149

Figure 4.4. Cell morphological changes of MRC-5 cells treated with AuNPs of different sizes 154

Figure 4.5. Cell morphological changes of A549 cells treated with AuNPs of different sizes 155

Figure 4.6. SSC light intensity analysis of cellular uptake of AuNPs in MRC-5 cells by flow cytometry 158

Figure 4.7. SSC light intensity analysis of cellular uptake of AuNPs in A549 cells by flow cytometry 159

Figure 4.8. Oxidative stress detection of MRC-5 and A549 cells following the exposure to AuNPs of different sizes using CellRox deep red reagent 161

Figure 4.9. GSH/GSSG ratio quantification of MRC-5 and A549 cells following the exposure to AuNPs of different sizes using GSH/GSSG-Glo Assay. 163

Figure 4.10. Apoptosis cell death analysis of MRC-5 cells following the exposure to AuNPs of different sizes using Annexin V and PI by flow cytometry 165

Figure 4.11. Apoptosis cell death analysis of A549 cells following the exposure to AuNPs of different sizes using Annexin V and PI by flow cytometry. 166

Figure 4.12. Detection of mitochondrial membrane potential state of MRC-5 and A549 cells following the exposure to AuNPs of different sizes using MitoProbe, TMRM assay by flow cytometry 170

Figure 4.13. Cell Cycle progression analysis of MRC-5 and A549 cells following the exposure to AuNPs of different sizes using FxCycle™ PI/RNase Staining by flow cytometry. 172

Figure 4.14. Recovery of MRC-5 and A549 cells following the exposure to AuNPs of different sizes 175

Figure 4.15. A549 spheroids morphological changes following the exposure to Au10..... 179

Figure 4.16. A549 spheroids morphological changes following the exposure to Au80..... 180

Figure 4.17. Cytotoxicity assessment of A549 spheroids following exposure to Au10 and Au80. 181

Figure 5.1. Schematic representation of PI3K/AKT pathway..... 187

Figure 5.2. The protein expression analysis of PDK1 following MRC-5 cells exposure to Au10 and Au80 of different concentrations for 24 hours. 189

Figure 5.3. The protein expression analysis of PDK1 following A549 cells exposure to Au10 and Au80 of different concentrations for 24 hours. 190

Figure 5.4. The protein expression analysis of mTOR following MRC-5 cells exposure to Au10 and Au80 of different concentrations for 24 hours 191

Figure 5.5. The protein expression analysis of mTOR following A549 cells exposure to Au10 and Au80 of different concentrations for 24 hours. 192

Figure 5.6. The protein expression analysis of PTEN following MRC-5 cells exposure to Au10 and Au80 of different concentrations for 24 hours. 193

Figure 5.7. The protein expression analysis of PTEN following A549 cells exposure to Au10 and Au80 of different concentrations for 24 hours 194

Figure 5.8. The protein expression analysis of AKT following MRC-5 cells exposure to Au10 and Au80 of different concentrations for 24 hours. 195

Figure 5.9. The protein expression analysis of AKT following A549 cells exposure to Au10 and Au80 of different concentrations for 24 hours 196

Figure 5.10. The protein expression analysis of phospho-c-Raf (Ser259) following MRC-5 cells exposure to Au10 and Au80 of different concentrations for 24 hours 198

Figure 5.11. The protein expression analysis of phospho-c-Raf (Ser259) following A549 cells exposure to Au10 and Au80 of different concentrations for 24 hours 199

Figure 5.12. The protein expression analysis of PDK1 following MRC-5 cells exposure to Ag10 and Ag80 of different concentrations for 24 hours 202

Figure 5.13. The protein expression analysis of PDK1 following A549 cells exposure to Ag10 and Ag80 of different concentrations for 24 hours 203

Figure 5.14. The protein expression analysis of phospho-PDK1 (Ser241) following MRC-5 cells exposure to Ag10 and Ag80 of different concentrations for 24 hours 204

Figure 5.15. The protein expression analysis of phospho-PDK1 (Ser241) following A549 cells exposure to Ag10 and Ag80 of different concentrations for 24 hours 205

Figure 5.16. The protein expression analysis of mTOR following MRC-5 cells exposure to Ag10 and Ag80 of different concentrations for 24 hours 206

Figure 5.17. The protein expression analysis of mTOR following A549 cells exposure to Ag10 and Ag80 of different concentrations for 24 hours 207

Figure 5.18. The protein expression analysis of PTEN following MRC-5 cells exposure to Ag10 and Ag80 of different concentrations for 24 hours 208

Figure 5.19. The protein expression analysis of PTEN following A549 cells exposure to Ag10 and Ag80 of different concentrations for 24 hours 209

Figure 5.20. The protein expression analysis of AKT following MRC-5 cells exposure to Ag10 and Ag80 of different concentrations for 24 hours. 210

Figure 5.21. The protein expression analysis of AKT following A549 cells exposure to Ag10 and Ag80 of different concentrations for 24 hours 211

Figure 5.22. The protein expression analysis of phospho-c-Raf (Ser259) following MRC-5 cells exposure to Ag10 and Ag80 of different concentrations for 24 hours 212

Figure 5.23. The protein expression analysis of phospho-c-Raf (Ser259) following A549 cells exposure to Ag10 and Ag80 of different concentrations for 24 hours 213

Figure 5.24. Schematic representation of Wnt/ β-catenin signalling pathway 217

Figure 5.25. The protein expression analysis of β-catenin following MRC-5 cells exposure to Au10 and Au80 of different concentrations for 24 hours 219

Figure 5.26. The protein expression analysis of β-catenin following A549 cells exposure to Au10 and Au80 of different concentrations for 24 hours 220

Figure 5.27. The protein expression analysis of GSK-3β following MRC-5 cells exposure to Au10 and Au80 of different concentrations for 24 hours 221

Figure 5.28. The protein expression analysis of GSK-3β following A549 cells exposure to Au10 and Au80 of different concentrations for 24 hours. 222

Figure 5.29. The protein expression analysis of phospho-GSK-3β (Ser9) following MRC-5 cells exposure to Au10 and Au80 of different concentrations for 24 hours. 223

Figure 5.30. The protein expression analysis of phospho-GSK-3β (Ser9) following A549 cells exposure to Au10 and Au80 of different concentrations for 24 hours. 224

Figure 5.31. The protein expression analysis of β-catenin following MRC-5 cells exposure to Ag10 and Ag80 of different concentrations for 24 hours 227

Figure 5.32. The protein expression analysis of β-catenin following A549 cells exposure to Ag10 and Ag80 of different concentrations for 24 hours 228

Figure 5.33. The protein expression analysis of GSK-3β following MRC-5 cells exposure to Ag10 and Ag80 of different concentrations for 24 hours 229

Figure 5.34. The protein expression analysis of GSK-3β following A549 cells exposure to Ag10 and Ag80 of different concentrations for 24 hours. 230

Figure 5.35. The protein expression analysis of phospho-β-catenin (Thr41/Ser45) and non-phospho-(Active) β-catenin (Ser33/37/Thr41) following MRC-5 cells exposure to Ag10 of different concentrations for 24 hours 232

Figure 5.36. The protein expression analysis of phospho-β-catenin (Ser675) and phospho-β-catenin (Ser552) following MRC-5 cells exposure to Ag10 of different concentrations for 24 hours..... 233

Figure 5.37. The protein expression analysis of phospho-GSK-3β (Ser9) following MRC-5 cells exposure to Ag10 and Ag80 of different concentrations for 24 hours 234

Figure 5.38. The protein expression analysis of phospho-GSK-3β (Ser9) following A549 cells exposure to Ag10 and Ag80 of different concentrations for 24 hours. 235

Figure 5.39. The protein expression analysis of LRP6 following MRC-5 cells exposure to Ag10 and Ag80 of different concentrations for 24 hours 237

Figure 5.40. The protein expression analysis of LRP6 following A549 cells exposure to Ag10 and Ag80 of different concentrations for 24 hours 238

Figure 5.41. The protein expression analysis of Dvl2 following MRC-5 cells exposure to Ag10 and Ag80 of different concentrations for 24 hours 239

Figure 5.42. The protein expression analysis of Dvl2 following A549 cells exposure to Ag10 and Ag80 of different concentrations for 24 hours 240

Figure 5.43. The protein expression analysis of N-Cadherin following MRC-5 cells exposure to Ag10 and Ag80 of different concentrations for 24 hours 241

Figure 5.44. The protein expression analysis of N-Cadherin following A549 cells exposure to Ag10 and Ag80 of different concentrations for 24 hours 242

Figure 5.45. The protein expression analysis of β-catenin localisation in the cytoplasm and nucleus following MRC-5 cells exposure to Ag10 of different concentrations for 24 hours..... 244

Figure 5.46. Microscopic images of β-catenin localisation following MRC-5 cells exposure to Ag10 of different concentrations for 24 hours 245

Figure 5.47. The protein expression analysis of β-catenin and GSK-3β following MRC-5 cells exposure to LiCl and Ag10..... 247

Figure 5.48. The protein expression analysis of β-catenin and GSK-3β following MRC-5 cells exposure to Ag10 and Wnt agonist I 249

Figure 6.1. Schematic illustration summarised the current study findings of AgNPs and AuNP mechanisms of toxicity and their impacts on cell signalling pathways..... 260

Figure A1. Standard curves of Ag10 and Ag80 in water using ICP MS……..……...…300

Figure A2. Analysis of AgNPs and AuNPs interference with CellRox™ deep red assay…..…..……..301

Figure A3. Analysis of AgNPs and AuNPs interference with Alexa Fluor® 488 Annexin V/Dead cell apoptosis assay……..……301

Figure A4. Analysis of AgNPs and AuNPs interference with MitoProbe™,TMRM assay...…...…….302

Figure A5. Analysis of AgNPs and AuNPs interference with FxCycle™ PI/RNase Staining…...……302

List of Tables

Table 1.1. *In vitro* studies of the size impacts on AuNPs and AgNPs toxicity. 19

Table 1.2. *In vitro* studies of the morphology impacts on AuNPs and AgNPs toxicity 24

Table 1.3. *In vitro* studies of the surface charge/modification impacts on AuNPs and AgNPs toxicity 28

Table 1.4. *In vitro* studies of the NPs composition impacts on toxicity 31

Table 1.5. *In vitro* studies on the impact of AgNPs and AuNPs on cell signalling pathways 38

Table 2.1. Chemicals 50

Table 2.2. Assay kits 51

Table 2.3. Modification steps performed during the sample digestions for ICP-MS 59

Table 2.4. Western blot buffers 69

Table 2.5. Resolving gel preparation (15 ml) 70

Table 2.6. Stacking gel preparation (5 ml) 70

Table 3.1. Summary the characterisations of AgNPs 82

Table 3.2. The stability of AgNPs in EMEM with or without (10%) FBS by measuring the size using DLS 84

Table 3.3. The CC50 values of MRC-5 and A549 cells treated with AgNPs of different sizes 90

Table 4.1. Summary of the characterisations of AuNPs 143

Table 4.2. The stability of AuNPs in EMEM with or without (10%) FBS by measuring the size using DLS 144

Table 4.3. The CC50 values of MRC-5 and A549 cells treated with AuNPs of different sizes 150

Table 5.1. Summary of AuNPs impacts on the protein expressions involved in PI3K/AKT and Wnt/β-catenin signalling pathways in lung cell lines 252

Table 5.2. Summary of AgNPs impacts on the protein expressions involved in PI3K/AKT and Wnt/β-catenin signalling pathways in lung cell lines 253

Table A1. Stability measurement of AgNPs in Ham's F-12 Nutrient Mixture……..…..……..299

Table A2. Stability measurement of AuNPs in Ham's F-12 Nutrient Mixture……..……299

List of Abbreviations

λ max	Maximum absorption wavelength
2D	Two-dimensional
3D	Three-dimensional
A549	Human lung epithelial carcinoma cell
Ag	Silver
Ag10	Silver nanoparticles 10 nm
Ag40	Silver nanoparticles 40 nm
Ag80	Silver nanoparticles 80 nm
AgNPs	Silver nanoparticles
AKT	Protein kinase B
AMPK	5' adenosine monophosphate-activated protein kinase
APC	Adenomatous polyposis Coli
APS	Ammonium persulfate
ARPE-19	Retinal pigment epithelial cell
ATM	Ataxia-telangiectasia mutated
Au	Gold
Au10	Gold nanoparticles 10 nm
Au40	Gold nanoparticles 40 nm
Au80	Gold nanoparticles 80 nm
AuNPs	Gold nanoparticles
BEAS-2B	Normal human bronchial epithelial cell
BSA	Bovine serum albumin
Caco-2	Human colorectal adenocarcinoma cell
CC50	50% cytotoxic concentration
CCCP	Carbonyl cyanide 3-chlorophenylhydrazone
CK1	Casein kinase 1
CTAB	Cetyl trimethyl ammonium bromide
CuO	Copper oxide
DLS	Dynamic light scattering
DMSO	Dimethyl sulfoxide
DNA-PKcs	DNA-dependent protein kinase
DPBS	Dulbecco’s phosphate-buffered saline
DSBs	Double strand breaks
DTT	1,4-dithiothreitol
DU145	Human prostate cancer cell
Dvl	Dishevelled
EDTA	Ethylenediaminetetraacetic acid
EGTA	Ethylene glycol tetra acetic acid
EMEM	Eagle minimum essential medium
ERK	Extracellular signal-regulated kinases
EUE	Human epithelial embryonic cell
FBS	Foetal bovine serum
GAPDH	Glyceraldehyde 3-phosphate dehydrogenase
GS	Reduced glutathione

GSK-3β	Glycogen synthase kinase-3 β
GSSG	Oxidized glutathione
HBEC3-kt	Normal human bronchial epithelial cell
HCl	Hydrochloric acid
HCT116	Human colon cancer cell
HDF	Human dermal fibroblast cell
HepG2	Human hepatoblastoma cell
HNO_3	Nitric acid
HO-1	Heme oxygenase-1
HRP	Horseradish Peroxidase
hrs	Hours
HT29	Human colorectal adenocarcinoma cell
IL	Interleukin
ICP-MS	Inductively coupled plasma mass spectrometry
IMR-90	Normal human fibroblast cell
JAK	Janus kinase
JNK	c-Jun N-terminal kinase
Jukart	Human T lymphocyte cell
KCl	Potassium chloride
L132	Human lung epithelial cell
LC3	Light chain 3
LiCl	Lithium chloride
LRP5/6	Low-density lipoprotein receptor related protein 5/6
M059K	Human glioblastoma cell
MAPK	Mitogen-activated protein kinases
MCF-7	Human breast cancer cell
MDA-MB-231	Human breast cancer cell
MDA-MB-468	Human breast cancer cell
MDR	Multiple drug resistance
MFI	Median fluorescence intensity
mins	Minutes
mLDH	Modified lactate dehydrogenase
MMP	Mitochondrial membrane potential
MRC-5	Human foetal lung fibroblast cell
mTOR	Mammalian target of rapamycin
mTORC1	Mammalian target of rapamycin complex 1
mTORC2	Mammalian target of rapamycin complex 2
MTT	Thiazolyl blue tetrazolium bromide
NaCl	Sodium chloride
NF-kB	Nuclear factor kappa-light-chain-enhancer of activated B cells
nm	Nanometre
NPs	Nanoparticles
NQO1	NADPH quinone oxidoreductase 1
PAA	Polyacrylic acid
PARP	Poly (ADP-ribose) polymerase
PAH	Polyelectrolyte poly(allylamine) hydrochloride

PC-3	Human prostate cancer cell
PDI	Polydispersity index
PDK1	Phosphoinositide dependent kinase 1
PEG	Polyethylene glycol
phospho-β-catenin	Phosphorylated β-catenin
phospho-c-Raf	Phosphorylated c-Raf
phospho-GSK-3β	Phosphorylated GSK-3β
phospho-PDK1	Phosphorylated PDK1
PI	Propidium iodide
PI3K	Phosphoinositide-3-kinase
PIP3	Phosphatidylinositol trisphosphates
PKA	Protein Kinase A
PMSF	Phenylmethylsulphonyl fluoride
PS	Phosphatidylserine
Pt	Platinum
PTEN	Phosphatase and tensin homolog
PVP	Polyvinylpyrrolidone
RAW 264.7	Macrophage cell
RIPA	Radioimmunoprecipitation assay
ROS	Reactive oxygen species
RTK	Receptor tyrosine kinase
SD	Standard deviation
SDS	Sodium dodecyl sulfate
Ser	Serine
SGC-7901	Human stomach cancer cells
SH-SY5Y	Human neuroblastoma cell
SILAC	Stable isotope labeling by amino acids in cell culture
SPR	Surface plasmon resonance
SSC	Side scattered
STAT	Signal transducer and activator of transcription
TBST	Tris-buffered saline and Tween 20
TCF/Lef	T-cell factor/ Lymphocyte enhancer binding factor
TEM	Transmission electron microscopy
TEMED	Tetramethyl-ethylene-diamine
Thr	Threonine
TiO_2	Titanium dioxide
TMRM	Tetramethyl rhodamine methyl
TNFα	Tumour necrosis factor alpha
Tyr	Tyrosine
U937	Human myeloid leukaemia cell
UV-Vis	Ultraviolet-visible
VEGFA	Vascular Endothelial Growth Factor A
Wnt	Wingless-related integration site
ZnO	Zinc oxide

Chapter 1

Introduction

1.1 Background

The nanotechnology field has developed rapidly and it has been widely incorporated in many areas, including food, cosmetic, textile, agricultural and biomedical industries (Singh et al., 2013, Gupta and Xie, 2018). Nanotechnology refers to manipulation of the molecular-scale materials into the nano-scale range mainly between 1 to 100 nanometre (nm) (Jeevanandam et al., 2018). Based on the material used, nanomaterials can be classified into different classes. For example carbon-based nanomaterials such as carbon nanotubes which made from graphene sheets and are suitable for biosensing applications due to their powerful electrocatalytic properties (Lin et al., 2004). Organic-based nanomaterials such as liposomes which composed of phospholipid bilayers and considered as efficient tools for drug delivery system (Green and Rose, 2006). Inorganic-based nanomaterials such as silver, zinc and iron oxide nanoparticles exhibit advanced optical characteristics. Superparamagnetic iron oxide nanoparticles (SPION) have effectively applied as magnetic resonance contrast agent (Bulte and Kraitchman, 2004).

Nanomaterials exhibit unique intrinsic mechanical, electrical, optical and thermal properties (Kahru and Ivask, 2013, Khan et al., 2019); thus, allowing the integration of nanomaterials into different disciplines. The prevalence of commercial products that contained nanomaterials were around 1814 products as listed in consumer products inventory (Vance et al., 2015). Moreover, metal and metal oxide nanoparticles (NPs) are the most commonly nanomaterials involved in consumer products with 42%. Metal NPs such as silver and gold NPs (AgNPs and AuNPs, respectively) and metal oxide NPs including zinc oxide, iron oxide and titanium dioxide NPs are most commonly used in industries and nanomedicine filed (Vance et al., 2015, Rastogi et al., 2017). Several biomedical applications have been reported for metal NPs, including their use as delivery vectors for proteins, genes, small molecules and monoclonal antibodies

(Klębowski et al., 2018, Zamora-Justo et al., 2019). Moreover, these NPs are widely used in sunscreens and chemical sensing because of their photocatalytic activities (Smijs and Pavel, 2011, Napi et al., 2019, Lu et al., 2015). Among all the metal-based NPs, AgNPs and AuNPs showed a particular interest as promising nanomaterials for biomedical applications, because AuNPs exhibit powerful chemical stability against physiological oxidation and AgNPs demonstrate strong antibacterial property (Arvizo et al., 2010, Prabhu and Poulose, 2012). However, the wide uses of AgNPs and AuNPs in medical field reveal the importance of investigating their safety profile and the potential risks among their exposure to human. Both AgNPs and AuNPs will be the focus of this research.

1.2 Silver and gold nanoparticles

AgNPs and AuNPs have unique advantages due to their high stability, high functional flexibility, large-scale production, large loading capacity and ease of size and shape optimisation (Katas et al., 2018). Both AgNPs and AuNPs show ability to scatter and absorb light by manipulating their surface plasmon resonance (SPR) (Katas et al., 2018, Arvizo et al., 2010). Moreover, AgNPs are considered the most prominent type of metal NPs that used commercially because of their antimicrobial properties. Around 24% of these products were composed of AgNPs (Vance et al., 2015). AgNPs are incorporated in huge industrial productions including: toothpastes, soaps, paints, textile, plastics and food packaging (Fabrega et al., 2011). AuNPs have been attracted a great attention for biomedical applications and greatly explored as nanocarrier for drug delivery and photothermal therapy, due to their extraordinary optical properties (Verma et al., 2008, Iodice et al., 2016). AuNPs are demonstrated as an inert metal with good biocompatibility. However, it was suggested that the small size of AuNPs can be significantly toxic (Bahadar et al., 2016). Though there are several studies that presumed that

AgNPs and AuNPs can induce detrimental effects in the human as well as the environment (Kakakhel et al., 2021, Teles et al., 2019, Kim et al., 2011, Vales et al., 2020).

1.2.1 Synthesis of AgNPs and AuNPs

Both AgNPs and AuNPs can be synthesised using different approaches, including green, physical and chemical methods (Haider and Kang, 2015). The green method is considered the most environmentally friendly and non-toxic method in which the AgNPs and AuNP can be synthesised through the utilisation of biological sources such as plant extracts, bacteria and fungi (Katas et al., 2018). This method depends on the use of natural source reducing and stabilising agent to reduce the metal salts to form the metal particles. The plant extract contains several components such as flavonoids and polysaccharides also, the bacteria and fungi contain enzymes and proteins which can act as a reducing agent (Ahmed et al., 2016). The physical method can be performed by laser ablation approach which produces uncontaminated NPs in the absence of using chemical reagents (Iravani et al., 2014). The process of metal particles formation by a laser beam that targets a metal plate immersed in organic solvent leading to form photo-ions then nucleation and growth of particles (Xu et al., 2020b). The type of solvent, the pulse duration and the laser wavelength are factors that can control the properties of AgNPs and AuNPs.

The most commonly used chemical approach is the Turkevich method through the reaction of metal salts with reducing agents (Chugh et al., 2018). Chloroauric acid and silver nitrate are used as the main source of gold and silver atoms, respectively (Katas et al., 2018). Sodium citrate is an example of a reducing and stabilising agent which associated with the surface of the particles and is crucial in metal particles synthesis to produce spherical, monodispersed AgNPs and AuNPs suspended in an aqueous solution. The concentration of reducing agent,

temperature and pH are factors that can impact the size and dispersity of the AgNPs and AuNPs in the dispersion (Quintero-Quiroz et al., 2019). Several stabilisers can be used such as polyvinylpyrrolidone, polyvinyl alcohol and polyethylene glycol to improve the AgNPs and AuNPs stability and avoid their aggregation (Zhao et al., 2013, Zhang and Zhang, 2014, Tam et al., 2013). The AgNPs and AuNPs will be used in this study were produced via the chemical method.

1.2.2 Biomedical applications of AgNPs and AuNPs

AgNPs exhibit a powerful antibacterial property and are therefore used in several pharmaceutical products, including wound dressings and implant coatings (Hameed et al., 2014, Wang et al., 2016). AgNPs-coated catheters showed high efficiency in sustained-release bactericidal effect against the development of infection as a complication of long-term catheter use (Wu et al., 2015). Due to their excellent antibacterial effects, AgNPs can destroy a wide range of gram-positive and gram-negative bacteria (Shao et al., 2018). Moreover, AgNPs exhibit high antifungal and antiviral activities (Monteiro et al., 2013, Elechiguerra et al., 2005). They can exhibit antimicrobial activities by damaging the microbial membrane via physical adherence to the cell wall of the microorganism, thereby compromising the membrane integrity and resulting in leakage of the cytoplasmic content (Durán et al., 2016). Another potential mechanism of AgNPs is their dissolution into silver ions; this results in the induction of reactive oxygen species (ROS) generation, which subsequently deactivate proteins and nucleotides of the microorganism (Durán et al., 2016). AgNPs thus have high potency against many drug-resistant microbial strains (Yuan et al., 2017). The killing of microorganisms or the suppression of their growth is suggested to be dependent on the physicochemical properties of AgNPs, such as their surface charge and size (Koduru et al., 2018).

AgNPs demonstrated as potential candidate for drug delivery systems for different therapeutic agents, such as anticancer and anti-inflammatory drugs (Muhammad et al., 2016, Karthik et al., 2018). Moreover, AgNPs have been shown to exhibit potent anticancer effects (Gomathi et al., 2020). The doxorubicin conjugated to chitosan-coated AgNPs was found to induce cell death of breast (*in vitro*) and subcutaneous (*in vivo*) tumours and enhance the sustained release of doxorubicin than doxorubicin alone (Mohamed, 2020).

Amongst all other metal NPs, AuNPs exhibit powerful optical characteristics and offer promising imaging tools for cancer therapy and diagnosis (Qian et al., 2008, Huo et al., 2012). AuNPs display powerful plasmonic property of localised SPR, which is involved in oscillation of electrons at the metal NPs surface when excited by light. Moreover, the shape and size of AuNPs are correlated with their optical properties of SPR (Bai et al., 2020). AuNPs have been utilised in photodynamic therapy for treating cancer or infectious diseases due to their high SPR absorption efficiency (García Calavia et al., 2018). Most of the conventional photosensitiser drugs are hydrophobic and need a delivery system in photodynamic therapy. A combination of photosensitisers and AuNPs demonstrated an ideal approach to tackle the challenges of photosensitiser drugs (Yao et al., 2016). Surface functionalisation of AuNPs with biological ligands can enhance the delivery of drug to a specific target. Moreover, AuNPs can absorb light and convert it to heating energy via the SPR phenomenon and promote singlet oxygen formation leading to extensive cell damage (Kim and Lee, 2018).

In addition, AuNPs are used in thermal ablation for treating cancer. Auroloase® is polyethylene glycol (PEG) coated silica-gold nanoshells for thermal ablation therapy. When light stimulation at near infra-red light is applied, gold nanoparticles absorb the light causing an increase in the temperature in the tumour area leading to solid tumour destruction (Schwartz et al., 2011, Stern

et al., 2016). This intravenous nanoparticle therapy is currently undergoing clinical trials. A biosensor is a device used to detect biological components, such as proteins, nucleotides and enzymes. AuNPs are being used within biosensors due to their ease of modification and biocompatibility (Peng and Miller, 2011).

1.3 The importance of Nanotoxicology

AgNPs and AuNPs have been intensively used in several areas, however, there is a lack information about the safety and the potential risk associated with the direct or indirect exposure of living organisms to those NPs. Therefore, it is important to study the nanotoxicity to determine the potential adverse effects of AgNPs and AuNPs and to investigate the biological process may perturb by cells exposure to these NPs (Fadeel, 2019). The size of AgNPs and AuNPs is anticipated to be the main factor influencing the behaviour of nano-scale particles, having greater impacts on living organisms than micro-scale particles belonging to the same materials (Yaqoob et al., 2020). The reduced size of AgNPs and AuNPs translates into a large surface area to volume ratio, which could induce particles reactivity and a complex interaction with physiological and biological systems. Other factors including surface charge morphology, chemical composition, surface functionalisation, solubility, hydrophobicity and aggregation of AgNPs and AuNPs can influence their interaction with biological systems (Adewale et al., 2019, Riaz Ahmed et al., 2017). Therefore, elucidating the safety profile of AgNPs and AuNPs is essential to protect human health and the environmental systems and enable the industry and regulatory agencies to maximise the applications of nanomaterials. Although intensive studies have focused on nanotoxicity and understanding the mechanisms underlying AgNPs and AuNPs toxicity, the outcomes can be contradictory due to the inadequate characterisation of these NPs (Krug, 2014).

1.4 Toxicity of AgNPs and AuNPs

1.4.1 Postulated mechanisms underlying AgNPs and AuNPs toxicity

Understanding the mechanisms underlying the toxicity of AgNPs and AuNPs are one of the essential aspects of nanotoxicological studies. AgNPs and AuNPs may directly interact with subcellular compartments, resulting in the disruption of normal biological functions (Khan, 2020). The large surface area of the AgNPs and AuNPs is the key factor influencing their interaction with cellular components, thereby contributing to toxicity (Khan, 2020).

The cellular exposure to AgNP and AuNPs can lead to an increase in the production of ROS, such as hydroxyl radical, superoxide and singlet oxygen, this is most likely to be the focal mechanism correlated to AgNPs and AuNPs toxicity (Foldbjerg et al., 2011, Li et al., 2010). The suggested mechanisms underlying AgNPs and AuNPs toxicity are illustrated in (**Figure 1.1**). The interaction of AgNPs and AuNPs with cells triggers a pro-oxidant effect by induction of ROS formation which mediate mitochondrial depolarisation, intracellular calcium influx and inflammatory response, (**Figure 1.1**) (Xue et al., 2016, Asharani et al., 2009a, Bin-Jumah et al., 2020, Schaeublin et al., 2011). The accumulation of a high level of ROS results in oxidative stress which is the imbalance of cellular redox haemostasis, thus lead to the oxidation of protein, DNA and lipid causing subsequent cell damage and, eventually, cell death (Khanna et al., 2015). AgNPs and AuNPs can also trigger oxidative stress by dysregulation of oxidative stress associated cell signalling pathways (Rinna et al., 2014, Falagan-Lotsch et al., 2016). Oxidative stress induced by AgNPs and AuNPs can lead to the suppression of the defence system and antioxidant activity, (**Figure 1.1**) (Avalos et al., 2014, Mateo et al., 2014). Cells exhibit a defence response to counteract the overproduction of free radicals by producing antioxidants, such as glutathione (GSH), vitamin E and vitamin C, or antioxidant enzymes, such as

superoxide dismutase, GSH peroxidase and catalase (Dasgupta et al., 2018, Manke et al., 2013, Ávalos et al., 2015). However, the process of ROS detoxification can lead to cell death (Piao et al., 2011, Martínez-Torres et al., 2018).

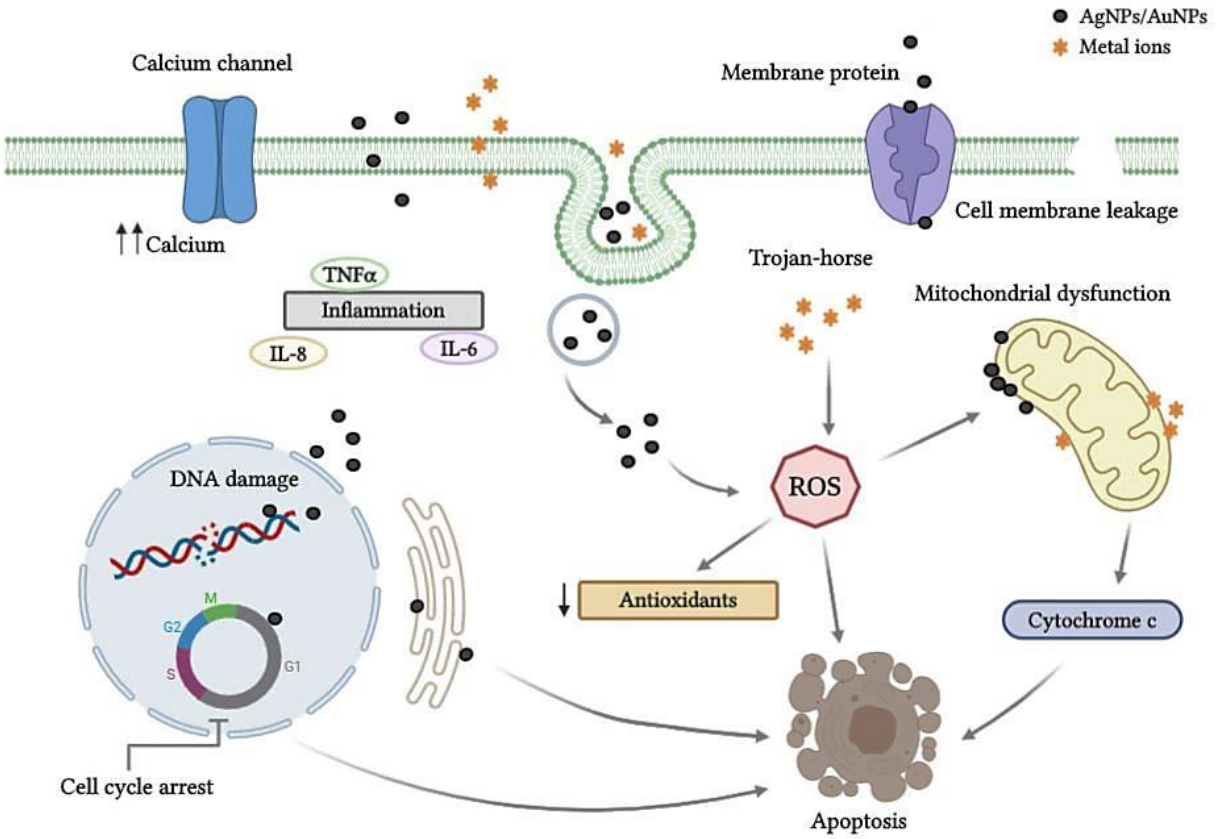


Figure 1.1. Postulated toxicity mechanisms of AgNPs and AuNPs. Scheme generated with BioRender.com.

In addition, AgNPs and AuNPs can induce DNA damage and chromosomal aberrations as a result of oxidative stress (Asharani et al., 2009a, Vales et al., 2020). AgNPs and AuNPs can induce endoplasmic reticulum stress which occurs in response to ROS formation and cellular stress. Sustained endoplasmic reticulum stress can ultimately trigger the apoptotic cascade, (**Figure 1.1**) (Simard et al., 2016, Noël et al., 2016). ROS-independent toxicity has also been suggested to be a mechanism that can be triggered by the accumulation of AgNPs on the plasma membrane surface, dissolution of AgNPs or direct binding of AgNPs to the death receptor (Greulich et al., 2012).

Another postulated mechanism underlying the toxicity of AgNPs involves the disruption of cell function via released silver ions, which penetrate the plasma membrane and contribute to the overall observed toxicity (Kittler et al., 2010). It was previously indicated that the toxicity of metal NPs is closely correlated with the release of chemical constituents, i.e. the dissolution of metal NPs (Smith et al., 2018, De Matteis et al., 2015). However, controversial debate exists regarding whether the AgNPs potential toxicity is induced by the influence of AgNPs themselves or both AgNPs and released metal ions. One group indicated that the toxicity of AgNPs is mainly associated with the effect of AgNPs themselves and not related to their dissolution (Kim et al., 2009, Sambale et al., 2015). For example, a study reported the CC50 value of AgNPs with 10 ppm which was drastically lower than the CC50 of silver nitrate which was used as a direct source of silver ions with 72 ppm in human lung epithelial cancer cell line (Sambale et al., 2015). Also, AgNPs showed to trigger apoptosis to a higher extent than silver nitrate. However, another group suggested that the AgNPs toxicity is mediated by silver ion release (Kittler et al., 2010, Beer et al., 2012). AgNPs found to induce cell death in the human lung epithelial cancer cell line via oxidative stress which was enhanced by the presence of silver

ions (Beer et al., 2012). Vrček et al. (2016) illustrated that the cellular membrane damage and cytotoxicity were significantly triggered by the exposure of silver nitrate to human hepatoblastoma cells (HepG2) compared to AgNPs indicating the role of released silver ion in promoting AgNPs toxicity.

Moreover, AgNPs may undergo dissolution due to the electrochemical potential of the biological medium which increases the potential interaction of released metal ions with the cells resulted in cell damage (Slavin et al., 2017). Additionally, it was presumed that AgNPs toxicity can occur due to the intracellular release of silver (Ag) ions by the Trojan horse-type mechanism, (**Figure 1.1**) (Hsiao et al., 2015). The trojan horse-type mechanism, wherein AgNPs penetrating the cell membrane can highly dissociate to form metal ions inside the cells by the acidic lysosome environment (Chernousova and Epple, 2013). Furthermore, it is evident that the size of AgNPs can significantly affect the rate of metal ions release, their cellular internalisation and subsequent adverse effects in cells (Wang et al., 2015).

In case of AuNPs, the reported toxicity of AuNPs was due to the effect of AuNPs themselves but not the gold ions (Barbasz and Oćwieja, 2016). The latter author reported no changes in cell viability in human promyelocytic leukaemia cells (HL-60) exposed to gold ions, whereas AuNPs showed significant cytotoxicity. However, the dissolution tendency of metal NPs is thought to be dependent on their chemical composition (Slavin et al., 2017). AuNPs can not easily oxidise and release gold ions because gold considers as least reactive metal (Balfourier et al., 2020).

As illustrated in **Figure 1.1**, the negative effects of AgNPs and AuNPs can be mediated by different mechanisms, thus, stressing on the importance of nanotoxicology assessments to understand the behaviour of these NPs toward their cellular exposure. Two key parameters are

essential in the nanotoxicity assessments which are: metal NPs characterisation and type of model system is used for toxicity investigation (Armstead and Li, 2016). The metal NPs characterisations include determination of their size, morphology, surface charge, stability and aggregation potential in biological fluids (Armstead and Li, 2016). The typical metal NPs model systems for nanotoxicity assessments are either *in vitro* cell culture model or *in vivo* model usually animals (Kumar et al., 2017b). The advantages of the *in vitro* model systems include lower cost and reduce the animal use for ethical aspects (Armstead and Li, 2016). Moreover, *in vitro* model systems allow to examine the metal NPs biocompatibility following exposure to several types of cells to determine the potential target of metal NPs to specific cell types or tissues and to identify the appropriate concentrations that can be used for the *in vivo* testing (Armstead and Li, 2016). However, it is still difficult to test the consequence of long term exposures and the complex interaction between different types of cells and thus considered as major drawbacks of *in vitro* study (Tellez-Gabriel et al., 2018).

1.4.2 *In vitro* nanotoxicity assessments of AgNPs and AuNPs

The assessment of the metal NPs potential adverse effects is necessary to determine the risk associated with their medical use (Kumar et al., 2017a). The *in vitro* methods which widely used for nanotoxicity assessment are summarised in **Figure 1.2**. The exposure to either AgNPs or AuNPs may cause structural and/or functional changes in cells, which may eventually result in cell death. Cell health can be evaluated by assessing cell proliferation or cytotoxicity, e.g. by measuring the metabolic activity of viable cells or by quantifying the amount of lactate dehydrogenase (LDH) released from a compromised membrane of dead cells (Hillegass et al., 2010). To gain further understanding about the mechanism underlying the toxicity of AgNPs and AuNPs, oxidative stress, which is thought to be the major toxicity mechanism, can be

measured directly by quantifying the existing intracellular ROS levels or indirectly by evaluating antioxidants levels, such as GSH and superoxide dismutase (Roesslein et al., 2013).

Moreover, AgNPs and AuNPs can disrupt mitochondrial activity, which can be assessed by analysing the mitochondrial membrane potential and caspase activity. AgNPs and AuNPs can also mediate several immunological responses, which can be assessed by measuring the levels of inflammatory biomarkers, including interleukin-8 (IL-8), IL-6 and tumour necrosis factor-alpha (TNFα) (Elsabahy and Wooley, 2013). Genotoxicity can be triggered by AgNPs and AuNPs, which can be assessed by evaluating the DNA damage such as single-strand breaks or double-strand breaks (DSBs) and by assessing the cell cycle progression checkpoints (Savage et al., 2019).

Finally, the mechanism of cell death as a result of AgNPs and AuNPs exposure can be assessed. The release of apoptotic markers, such as caspase-3 and caspase-9, can be quantified. Moreover, membrane alteration can be tested using Annexin V probe, which binds to the translocated phosphatidylserine to the outer layer of the cell membrane in cells undergoing apoptosis (Vanden Berghe et al., 2013). Cells undergoing apoptosis may have subsequent DNA fragmentation, which can be also measured (Kumar and Dhawan, 2013). Necrotic cell death can be detected by plasma membrane damage and the loss of cytoplasmic integrity (Cummings and Schnellmann, 2004). Apoptotic cells may eventually undergo secondary necrosis following prolonged incubation, which halts their metabolic activity and compromises the cell membrane. Therefore, careful consideration of the exposure time and investigation of multiple markers can help understand toxicity mechanisms (Terry L. Riss and Moravec, 2004). AgNP and AuNPs can triggered autophagy which can be detected by quantifying autophagosome formation by measuring the light chain 3 (LC3-II) and p62 biomarker levels (Zhang et al., 2016).

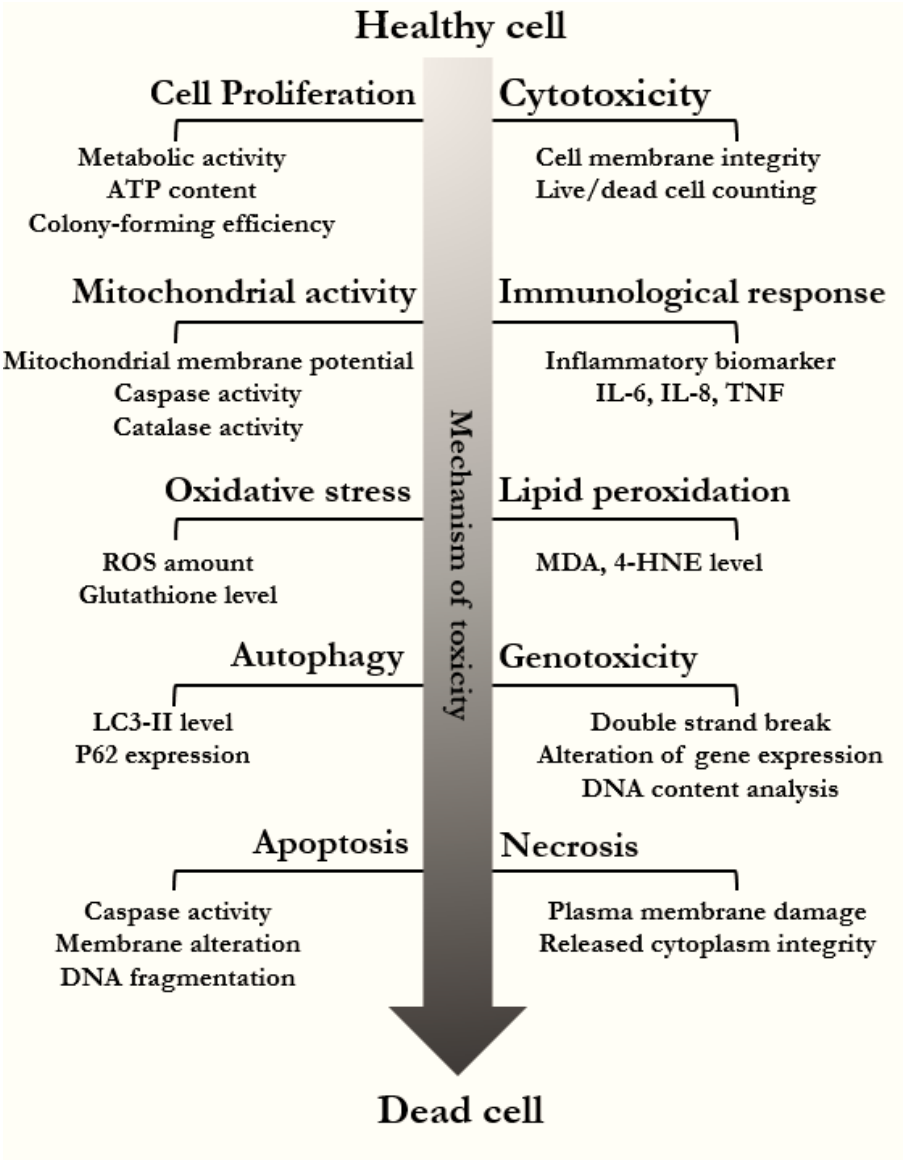


Figure 1.2. Synopsis of *in vitro* nanotoxicity assessments.

As demonstrated in the literature, several investigations can be performed to test the mechanism of AgNPs and AuNPs toxicity. Nevertheless, the assessment of the ROS generation is considered as most prominent examination for the metal NPs as they tend to induce oxidative stress (Fu et al., 2014). It is noteworthy that AgNPs and AuNPs may interfere with some *in vitro* endpoints as they exhibit optical properties. Therefore, it was suggested to validate the toxicity outcomes using two or more independent methods to avoid any misleading results (Dusinska et al., 2017).

1.4.3 Impact of physicochemical properties of AgNPs and AuNPs on toxicity

Several studies were conducted to test the effect of AgNPs and AuNPs in different types of cancer cell lines. Some of these studies were focused on the assessment of AgNPs and AuNPs as safe candidates for drug delivery system to enhance the efficiency of the cancer therapy (Kumar et al., 2017a, Liu et al., 2010). However, other studies were intended to investigate the potentially detrimental effect of AgNPs and AuNPs on cancer cells as a promising approach for cancer treatment (Rajeshkumar, 2016, Lin et al., 2014). This revealed that the ongoing research is devoted to utilise the unique properties of AgNPs and AuNPs and understand their nanotoxicity which can result in safe design nanomaterials-based delivery system as a positive indication of these NPs or to use their anticancer activity to destroy cancer cells. AgNPs and AuNPs physicochemical properties can significantly control their cellular behaviour. Moreover, cell type, duration of exposure and concentration are other factors that can also influence the AgNPs and AuNPs toxicity (Adewale et al., 2019, Riaz Ahmed et al., 2017). The toxicity studies presented inconsistent findings as matter of varying of AgNPs and AuNPs preparation methods, physicochemical properties and *in vitro* toxicity tested methods used (Fratoddi et al., 2015a,

Johnston et al., 2010). Therefore, building systematic nanotoxicology framework is necessary to validate the current literature and to develop AgNPs and AuNPs for medical applications.

1.4.3.1 Effect of particle size

A decrease in the diameter of NPs leads to an increase in their surface area and particle surface energy. Therefore, different sizes of NPs having the same composition may have different toxicity levels (Shin et al., 2015). In addition, the plasma membrane acts as a barrier; hence, the size of NPs can control their cellular uptake, cellular localisation and subsequent adverse events in cells (Gustafson et al., 2015). As shown in **Table 1.1**, the *in vitro* studies indicated the role of AuNPs and AgNPs size in determining their cellular response. Several studies revealed that the small size of AgNPs and AuNPs are more toxic than large ones (Mateo et al., 2014, Xia et al., 2017b, Perde-Schrepler et al., 2019, Miethling-Graff et al., 2014).

However, different hypotheses were generated regarding the impact of size on AgNPs and AuNPs. It was reported that the size of AgNPs play a major role in toxicity regardless of the surface coatings (Gliga et al., 2014). Gliga et al. (2014) demonstrated that the cytotoxicity and DNA damage potential of smaller PVP- and citrate-coated AgNPs sized 10 nm compared with that of larger ones (40, 50 and 75 nm) in a normal human bronchial epithelial cell line, BEAS-2B. The toxicity was amplified by the large surface area of small NPs, resulting in a high release rate of Ag ions by the Trojan horse-type mechanism. This finding was in agreement with that of Wang et al. (2014) in BEAS-2B cells treated with citrate- or PVP-coated AgNPs sized 20 and 110 nm. Another proposed meahcnaism on the impact of size on toxicity is that AgNPs sized less than 20 nm can easily transport into cells and result in the release of a high amount of Ag ions by the acidic environment of the lysosome, thereby inducing cytotoxicity and cell

damage (Riaz Ahmed et al., 2017). Similarly, Liu et al. (2010) postulated that small PVP-coated AgNPs can easily transport through the plasma membrane and dissociate to release Ag ions.

In addition, it was suggested that the size-dependent toxicity of AgNPs can be correlated to their aggregation potential. It was reported that the smaller size AgNPs (10 nm) tend to form large aggregate which are more toxic than larger AgNPs (20 nm) (Rosário et al., 2016). The study claimed that AgNPs (10 nm) formed large aggregates in cell culture medium which hinder their cellular uptake, however, these aggregates directly interact with cell membrane causing damage and induced necrosis. In contrary, AgNPs (20 nm) found to form smaller aggregates in cell culture medium compared to 10 nm size resulted in easier cellular internalisation and triggered apoptosis.

Another hypothesis claimed that AgNPs and AuNPs sizes ranging from 40 to 50 nm are the optimal size for high cellular internalisation, thereof trigger toxicity (Arvizo et al., 2012). It speculated that AuNPs sized around 50 nm can rapidly internalise into cells to a higher extent than AuNPs of larger size by a process is known as wrapping effect and is assumed to be greatly influenced by the AuNPs size (Chithrani and Chan, 2007). It is presumed that the wrapping of AuNPs sized 50 nm is fast which can generate high levels of free energy by ligand–receptor interaction, resulting in the intracellular accumulation of AuNPs. However, it is suggested that smaller AuNPs sized less than 50 nm need to be clustered together to produce sufficient free energy for complete wrapping on the membrane surface. For AuNPs size larger than 50 nm, the wrapping process is slow due to longer time is needed for the receptor diffusion kinetic resulted in lower AuNPs uptake, thereof induce less toxicity (Chithrani and Chan, 2007).

Contradictory studies postulated that AgNPs and AuNPs trigger cytotoxicity regardless of their size. No size-dependent reduction in the cell viability and oxidative stress induction of human

colorectal adenocarcinoma cells (Caco-2) and human breast cancer cells (MCF-7) was noted following incubation with AgNPs sized 20, 30, 60 and 110 nm (Van Der Zande et al., 2016). Lebedová et al. (2018) observed DNA damage following normal human bronchial epithelial cells (HBEC3-kt) incubation with AgNPs irrespective of their size (5 and 50 nm). Another study claimed that no detrimental effect in the cellular functions can be induced in human leukaemia exposed to AuNPs of different sizes (4, 12 and 18 nm) using several surface modification agents, including citrate, cetyltrimethylammonium bromide (CTAB), biotin and glucose (Connor et al., 2005).

The available information showed different suggestions about the AgNPs and AuNPs size impact on their cellular uptake as well as toxicity. The lack of consistency was found in these studies in terms of the manufacturer, concentration and the experimental conditions of AgNPs and AuNPs turn it difficult to build a critical correlation about their size impact on toxicity.

Table 1.1. *In vitro* studies of the size impacts on AuNPs and AgNPs toxicity.

Type of NPs	Size (nm)	Cell line	Concentration	Major findings	Reference
AuNPs	5, 10, 20, 40	Human lung epithelial carcinoma cells (A549 and 95D)	25 µg/ml	Smaller size AgNPs (5 nm) induced apoptosis and G0/G1 phase cell cycle arrest followed by AgNPs sized 10 nm No significant effect with AuNPs sized 20 and 40 nm	(Liu et al., 2014)
AuNPs	10, 30, 60	Human colorectal adenocarcinoma cells (HT-29) and human hepatoblastoma (HepG2) cells	10 ppb - 10 ppm	Size-, concentration- and time- dependent toxicity and DNA damage No significant effect with AuNPs sized (60 nm)	(Lopez-Chaves et al., 2018)
AuNPs	5, 10, 20, 30, 50, 100	Retinal pigment epithelial cells (ARPE-19) and human embryonic kidney cells (HEK293)	0.01 to 5 µg/ml	Reduction in cell viability was in order of 5>10>20>30 No significant toxic response with AuNPs sized 50 and 100 nm	(Karakoçak et al., 2016)
AuNPs	5, 20, 50	Human hepatoblastoma cells (HepG2)	1.67- 12.5 µg/ml	Size-dependent toxicity Smaller sized AuNPs (5 nm) induced cell cycle arrest in G1 phase, DNA damage and ROS generation	(Xia et al., 2017b)
AuNPs	30, 50, 90	Human leukaemia cells (HL-60) and human hepatoblastoma cells (HepG2)	1 -25 µg/ml	Size-dependent cytotoxicity effect, GSH depletion and ROS generation	(Mateo et al., 2014)
AuNPs	6.2, 24.3, 42.5, 61.2	Human hepatoblastoma cells (HepG2) and human cervical cancer cells (HeLa)	0.25- 1 mM	Size-dependent oxidative stress and cell damage	(Li et al., 2018)
AuNPs	3, 10, 25, 50	Human laryngeal carcinoma cells (HEp-2)	0.5- 50 µg/ml	Smaller sized AuNPs (3 nm) were more toxic compared with other sizes Other sizes induced similar cytotoxic responses	(Boyoglu et al., 2013)
AuNPs	18, 40, 60, 80	Human ovarian cancer cells (OVCAR5, OVCAR8, and SKOV3)	6.4 - 38.6 µg/ml	AuNPs sized (18 and 80 nm) showed higher cellular uptake and reduction in cell viability Larger AuNPs size (80 nm) triggered ROS generation	(Kumar et al., 2017a)
AuNPs	3, 5, 6, 8, 10, 17, 30, 45	Human prostate cancer cells (PC-3) and human breast cancer cells (MCF-7)	10- 130 µg/ml	AuNPs sized (3, 8, and 30 nm) were the most cytotoxic The other sizes of AuNPs were nontoxic	(Kumar and Ganesan, 2013)
AgNPs	10, 20	Human osteosarcoma cells (MG-63)	1 -100 µg/ml	AgNPs sized 10 nm were more toxic and triggered necrosis AgNPs sized 20 nm induced G0/G1 cell cycle arrest and cell undergo apoptosis	(Rosário et al., 2016)

Table 1.1. *In vitro* studies of the size impacts on AuNPs and AgNPs toxicity (continued).

Type of NPs	Size (nm)	Cell line	Concentration	Major findings	Reference
AgNPs	10, 20, 40, 60, 100	Human colon carcinoma cells (LoVo)	1 -10 µg/ml	Size-dependent ROS generation , trigger inflammatory response, mitochondrial dysfunction and apoptosis	(Miethling-Graff et al., 2014)
AgNPs	4.7, 42	Human leukaemia cells (HL-60) and human hepatoblastoma cells (HepG2)	0.84–500 µg/ml	Size-dependent cytotoxicity, ROS generation and GSH depletion HepG2 cells were more vulnerable to the AgNPs than HL-60	(Avalos et al., 2014)
AgNPs	4.7, 42	Normal human dermal fibroblasts	0·84–2000 µg/ml	Smaller sized AgNPs (4.7 nm) were more toxic, inducted ROS generation and GSH depletion	(Avalos et al., 2016)
AgNPs	20, 40	Human colon adenocarcinoma cells (Caco-2)	4- 100 µg/ml	Smaller sized AgNPs (20 nm) showed higher cytotoxicity and mediated necrosis cell death	(Böhmert et al., 2012)
AgNPs	10, 40, 75	Normal bronchial epithelial cells (BEAS-2B)	5-50 µg/ml	Size-dependent cytotoxicity and DNA damage Smaller AgNPs sized (10 nm) released high amount of silver ions compared with other AgNPs sizes	(Gliga et al., 2014)
AgNPs	5, 25, 50, 110	Cochlear cells (HEI-OC1) and human keratinocytes cells (HaCaT)	1.1-100 µg/ml	Size- and concentration-dependent reduction in cell viability and induction of ROS level	(Perde-Schrepler et al., 2019)
AgNPs	10, 20, 75, 110	Human colonic epithelial cells (T84)	20- 100 µg/ml	Size-dependent toxicity Smaller AgNPs sizes mediated modification in cell permeability and gene expression	(Williams et al., 2016)
AgNPs	2.6, 18	Human pancreas ductal adenocarcinoma cells (PANC-1) and human pancreas duct epithelial cells (hTERT-HPNE)	0.5- 50 µg/ml	Size- and concentration-dependent reduction in cell viability and induce cell death	(Zielinska et al., 2017)
AgNPs	5, 20, 50	Human lung epithelial carcinoma cells (A549), human stomach cancer cells (SGC-7901), human hepatoblastoma cells (HepG2) and human breast cancer cells (MCF-7)	0.01-100 µg/ml	Smaller AgNPs sized (5nm) were more toxic, induced ROS generation, cell cycle arrest at S phase and triggered apoptosis	(Liu et al., 2010)

Table 1.1. ***In vitro*** **studies of the size impacts on AuNPs and AgNPs toxicity (continued).**

Type of NPs	Size (nm)	Cell line	Concentration	Major findings	Reference
AgNPs	20, 110	Human bronchial epithelial cells (BEAS-2B)	6- 50 µg/ml	Size-dependent toxicity and induction of oxidative stress	(Wang et al., 2014)
AgNPs	4, 20, 70	Human monocytic cells (U937)	1.56- 50 µg/ml	Smaller AgNPs sized (4 nm) showed the highest cytotoxicity, induced ROS generation and increased in IL-8 release	(Park et al., 2011)
AgNPs	15, 30, 55	Alveolar macrophages	5-75 µg/ml	Size-dependent cytotoxicity, induction of oxidative stress and inflammatory response	(Carlson et al., 2008)
AgNPs	20, 40, 60, 80 (uncoated) 10, 50, 75 (coated)	Human colon cancer cells (HT29)	12.5 -50 µg/ml	Size-dependent cytotoxicity in both coated and uncoated AgNPs	(Nguyen et al., 2013)
AgNPs	20, 30, 60, 110	Human colorectal adenocarcinoma cells (Caco-2), and human breast cancer cells (MCF-7)	5- 25 µg/ml	AgNPs triggered oxidative stress and reduced cell viability Caco-2 cells showed a higher sensitivity to AgNPs than MCF-7 cells No size-dependent toxicity response	(Van Der Zande et al., 2016)

1.4.3.2 Effect of particle morphology

AgNPs and AuNPs can be manufactured with different shapes, including spheres, rods, cubes, prisms, stars and wires (Sukhanova et al., 2018, Lee and Jun, 2019). The morphology of AgNPs and AuNPs is thought to influence the biological response of the cells, as demonstrated in **Table 1.2**. It was assumed that the toxicity of AuNPs of different shapes is dependent on their cellular uptake which is greatly influenced by the AuNPs shapes and the high surface area available to contact with cell membrane (Li et al., 2012). Karakoçak et al. (2016) reported that rod-shaped AuNPs showed greater toxicity compared to spherical-shaped AuNPs (sized 5-30 nm), whereas low cellular internalisation and toxicity response were observed in cubic-shaped and spherical shapes of larger size (50-100 nm). It was presumed that spherical-shaped AuNPs require low amount of energy for cell membrane to bent which facilitate their internalisation compared to the cubic-shaped AuNPs (Karakoçak et al., 2016). Rod-shaped AuNPs showed toxicity due to the high surface curvature at the edge of rod-shaped which cause deformation in the cell membrane and resulted in cell damage. In contrast, a study by Falagan-Lotsch et al. (2016) demonstrated that high uptake efficiency of rod-shaped AuNPs compared to spherical-shaped counterpart, however both shaped AuNPs induced the gene expressions associated to oxidative stress to similar extent.

Contradictory observation was reported that the slow cellular uptake and low toxicity of rod-shaped AuNPs compared to spherical-shaped counterpart (Li et al., 2015). Rod-shaped AuNPs exhibit high aspect ratio and require strong membrane energy bending to maximise the contact area between AuNPs and cell membrane hence, a longer wrapping time is needed for their internalisation compared to spherical-shaped AuNPs (Malugin and Ghandehari, 2010).

In another study, the toxicity of spherical- and wire-shaped AgNPs in human lung cancer cell lines was compared. The results showed that the wire-shaped AgNPs were toxic, whereas the spherical AgNPs had better biocompatibility. The author suggested that wire-shaped AgNPs directly interact with the plasma membrane, causing a small puncture on the cell membrane and thereby damaging the cells. Contrarily, the spherical-shaped AgNPs internalised via endocytosis. The author also indicated that the observed toxicity was correlated with the actual AgNPs and not with Ag ions release (Stoehr et al., 2011).

As can be seen from **Table 1.2**, conflicting outcomes were reported regarding the influence of AgNPs and AuNPs shape on their cellular internalisation and toxicity. Unfortunately, the variability in the concentration and size used in several studies make a clear determination of the AgNPs and AuNPs shape effect difficult to conclude.

Table 1.2. *In vitro* studies of the morphology impacts on AuNPs and AgNPs toxicity.

Type of NPs	Morphology	Size (nm)	Cell line	Concentration	Major findings	Reference
AuNPs	Spherical cubic rod	5, 10, 20, 30, 50, 100 50 10 x 90	Retinal pigment epithelial cells (ARPE-19) and human embryonic kidney cells (HEK293)	0.01- 5 µg/ml	Rod-shaped AuNPs showed more toxicity than spherical-shaped AuNPs sized (10 nm) No cellular uptake and toxicity effect were reported with AuNPs cubic- and spherical-shaped of large size (> 50 nm)	(Karakoçak et al., 2016)
AuNPs	Spherical rod	14, 50, 75 14 x 50 7 x 42	Human cervical cancer cell (HeLa) and human glioblastoma cell (SNB19)	0.02 nM	Spherical-shaped AuNPs showed a higher uptake than rod-shaped ones	(Chithrani and Chan, 2007)
AuNPs	Spherical rod	30, 50, 90 10 x 35 10 x 45	Human prostate cancer cell (PC-3)	1.5-34 nM	Rod-shaped AuNPs were more internalised than spherical-shaped ones No toxicity observed with both shaped of AuNPs	(Malugin and Ghandehari, 2010)
AuNPs	Spherical star	61.46 33.69	Human skin fibroblasts	1.2- 400 µg/ml	Spherical-shaped AuNPs were more toxic than star- shaped ones	(Favi et al., 2015)
AuNPs	Spherical rod	18 16 x 84	Human dermal fibroblasts (HDF)	0.1 nM	Rod-shaped AuNPs were toxic and mediated oxidative stress No toxicity was observed with spherical-shaped AuNPs	(Falagan-Lotsch et al., 2016)
AgNPs	Spherical wire	30 25 x 100	Human lung epithelial carcinoma cells (A549)	2.25×10^{9} - 2.3×10^{10} particles/ml	Wires-shaped AgNPs were more cytotoxic No toxicity response was observed with the spherical-shaped AgNPs	(Stoehr et al., 2011)

1.4.3.3 Effect of particle surface charge and surface modification

The AgNPs and AuNPs surface charge, and surface modification can influence their response and behaviour in biological systems. As shown in **Table 1.3**, surface modifications and the net surface charge of AgNPs and AuNPs have been investigated in several studies. Metal-based NPs can be designed with a specific surface coating or functionalisation with different ligands in order to enhance targeting, specificity and stability to avoid their aggregation via electrostatic repulsion (El Badawy et al., 2010). However, surface modifications and the net surface charge of AgNPs and AuNPs can play a role in toxicity (Adewale et al., 2019). Therefore, it is important to assess the biocompatibility of the ligand and coating agents involved in AgNPs and AuNPs synthesis. Examples of common coating agents used for metal-based NPs include citrate, polymer and carbohydrate (Akter et al., 2018).

Controversial outcomes regarding the influence of surface charge in relation to metal NPs toxicity. Positively-charge AgNPs and AuNPs surface were assumed to induce more toxicity than negatively-charged ones (Surapaneni et al., 2018, Boyles et al., 2015, Marassi et al., 2018) or neutral surface AgNPs and AuNPs (Schaeublin et al., 2011, Marassi et al., 2018). It is presumed that a positive surface charge can significantly influence the toxicity of AgNPs and AuNPs as it facilitates their transportation into the negatively-charged phospholipid bilayer of the cell membrane by endocytosis due to electrostatic interaction (Marassi et al., 2018, Surapaneni et al., 2018). Thus, in contrast to negatively-charged surface, positively-charged metal-based NPs may result in the disruption of the plasma membrane by increasing the membrane permeability (Sukhanova et al., 2018). It has been reported that negatively and neutrally-charged AuNPs and AgNPs can hardly attach to and pass through the negatively-charged cell membrane surface (Cho et al., 2009, Marassi et al., 2018).

Other group elucidated the negatively-charged surface of AgNPs and AuNPs can promote the cellular adverse response than positively-charged ones (Barbasz et al., 2017, Sur et al., 2010). It was previously evident that citrate-coated AgNPs (negatively-charged) can trigger AgNPs toxicity in which carbohydrate-coated AgNPs were found to be more biocompatible with the human lung adenocarcinoma epithelial cells (A549) than citrate-coated AgNPs (Sur et al., 2010). Another study detected that high concentrations of citrate-coated AuNPs were found to be more toxic in human prostate cancer cells (PC-3) and MCF-7 cells than other negatively-charged coated AuNPs (starch- and Arabic gum-coated). The acidic nature of sodium citrate is thought to induce AuNPs toxicity (Vijayakumar and Ganesan, 2012). Another suggestion reported about citrate-coated AgNPs to induce toxicity due to the weak bond of citrate, which can easily be displaced with the biological medium, thereby increasing the ionic strength of the biological medium, disrupting AgNPs stability and subsequently promoting Ag ion release (Gliga et al., 2014).

In contrast, other studies have reported no impact of surface coating on AgNPs and AuNPs toxicity. Citrate- or PEG-coated AgNPs of a similar size (30 nm) showed similar biocompatibility when incubated with HepG2 cells (Bastos et al., 2017). The author revealed that the type of AgNPs coating did not play a role in triggering toxicity. The same author also proved that the apoptosis and cell cycle arrest at S and G2 phases mediated by both types of AgNPs was correlated to the effect of both AgNPs and their dissolved Ag ions. In another study, CTAB-coated (positively-charged) AuNPs showed more toxicity than polyacrylic acid (PAA)-coated (negatively-charged) and polyelectrolyte poly(allylamine) hydrochloride (PAH)-coated (positively-charged) AuNPs; the cytotoxicity of AuNPs was not correlated with their surface

charge but was correlated with the free CTAB in the solution; therefore, CTAB overcoating can promote NPs toxicity (Alkilany et al., 2009).

Another opinion indicated that the aggregation of both citrate- and PVP-coated AgNPs of the same size in the presence of serum proteins induced a similar toxicity profile in BEAS-2B cells, independent of AgNPs coating (Manson et al., 2011). Regardless of AgNPs and AuNPs properties, it was suggested that the aggregation of AgNPs and AuNPs may significantly impact their underlying toxicity, as the exposure to a high level of metal-based NPs can result in severe toxic effects (Bantz et al., 2014). Therefore, the aggregation can impede the original properties of metal NPs (Rose et al., 2012).

The collected data in **Table 1.3** presented conflicting conclusions due to the variations in the other properties of AgNPs and AuNPs which lead to ambiguity of whether the detected effects were due to the surface coating alone.

Table 1.3. *In vitro* studies of the surface charge/modification impacts on AuNPs and AgNPs toxicity.

Type of NPs	Surface charge/ modification	Cell line	Concentration	Major findings	Reference
AuNPs	Cetyl trimethyl ammonium bromide (CTAB), poly(diallyldimethyl ammonium chloride) (PDDAC) (positive) Polystyrene sulfonate (PSS), thiol functionalised carboxy poly (ethylene glycol) (HS-PEG-COOH) (negative)	Human lung epithelial carcinoma cells (A549)	50 100 µM	CTAB modified AuNPs (positively charged) showed the highest reduction in cell viability compared to other modified AuNPs	(Wang et al., 2013)
AuNPs	Citrate (negative) Cysteamine (positive)	Human breast cancer cells (MDA-MB-231 and MDA-MB-468)	25 µg/mL -1 mg/m	Cystamine AuNPs (Positively charged) showed more oxidative stress compared to citrate-coated AuNPs (negatively charged)	(Surapaneni et al., 2018)
AuNPs	Trimethyl ammonium-thanethiol (TMAT) (positive) Mercapto- ethanesulfonate (MES) (negative) Mercapto- ethoxy ethoxy ethanol (MEEE) (neutral)	Human keratinocyte cells (HaCaT)	5- 100 µg/ml	Positively and negatively charged AuNPs induced mitochondrial dysfunction and reduction in intracellular calcium No toxic effect with neutral AuNPs.	(Schaeublin et al., 2011)
AuNPs	Citrate (negative) Starch (negative) Arabic gum (negative)	Human prostate cancer cells (PC-3) and human breast cancer cells (MCF-7)	20- 140 µg/ml	Citrate-coated AuNPs mediated significant reduction in cell viability than starch- and gum Arabic-coated AuNPs	(Vijayakumar and Ganesan, 2012)
AuNPs	Citrate (negative) Cinnamic acid (negative)	Human breast cancer cells (MCF-7)	50- 250 µg/ml	Cinnamic acid-coated AuNPs were more cytotoxic and induce apoptosis in concentration- dependent manner compared to citrate-coated AuNPs	(Subramanian and Ponnuchamy, 2018)
AuNPs	Citrate (negative) 11-mercaptoundecanoic acid (negative)	Human hepatoblastoma cells (HepG2)	1 -200 µM	No cytotoxicity was observed with both types of AuNPs Slight induce of DNA damage was reported only with citrate-coated AuNPs	(Fraga et al., 2013)
AgNPs	Citrate (negative), Polyethylene glycol (PEG) (neutral), Bovine serum albumin (BSA) (negative)	Human skin keratinocyte cells (HaCaT)	10 -40 µg/ml	BSA-coated AgNPs were more toxic than citrate- and PEG-coated AgNPs	(Carrola et al., 2016)

Table 1.3. *In vitro* studies of the surface charge/modification impacts on AuNPs and AgNPs toxicity (continued).

Type of NPs	Surface coating/ modification	Cell line	Concentration	Major findings	Reference
AuNPs	Citrate (negative) Chitosan (positive)	THP-1-derived human macrophages	0.6- 3.2 µg/ml	Chitosan AuNPs (positively charged) showed more cytotoxicity and inflammatory response	(Boyles et al., 2015)
AgNPs	Bovine serum albumin (BSA) (negative) Chitosan (positive) Polyvinylpyrrolidone (PVP) (neutral)	Macrophage cells (RAW 264.7)	1.1-1000 µg/ml	All types of AgNPs reduced cell viability BSA-coated AgNPs were more toxic and induced inflammatory response	(Makama et al., 2018)
AgNPs	Citrate (negative), Glucose-, lactose-, oligonucleotide-modified AgNPs (positive)	Human lung epithelial carcinoma cells (A549)	7.5- 30 µg/ml	AgNPs surface modification with positively charged moiety improve biocompatibility	(Sur et al., 2010)
AgNPs	Citrate (negative) PEG (neutral)	Human keratinocyte cells (HaCaT)	20 -100 µg/ml	Both types AgNPs reduced cells viability and induced ROS generation Citrate-coated AgNPs were more toxic and induced cell cycle arrest at G2 phase	(Bastos et al., 2016)
AgNPs	Citrate (negative), PEG (neutral)	Human hepatoblastoma cells (HepG2)	1 -50 µg/ml	Citrate- and PEG-coated AgNPs triggered apoptosis and cell cycle arrest	(Bastos et al., 2017)
AgNPs	Unmodified (negative) Citrate (negative) Cysteamine hydrochloride (positive)	Histiocytic lymphoma (U-937) and human promyelocytic cells (HL-60)	5- 20 µg/ml	Citrate-coated AgNPs showed more toxicity Cysteamine-coated AgNPs showed lowest toxicity	(Barbasz et al., 2017)
AgNPs	Citrate (negative), Lactose (negative), 2-base long oligonucleotide (negative)	Primary human dermal fibroblast cells (HDF) and human lung epithelial carcinoma cells (A549)	12.5- 100 µg/ml	Citrate-coated AgNPs showed more cytotoxicity, induced DNA damage and apoptosis compared to other types of AgNPs	(Suresh et al., 2012)
AgNPs	Pristine (weakly negative), PVP (neutral), Citrate (negative), Hydroxyethyl cellulose-coated (HEC) (positive)	Human epidermoid carcinoma cells (A431) and human keratinocyte cells (HaCaT)	0.5- 2.5 µg/ml	PVP-coated AgNPs induced toxicity No toxicity was observed with pristine and citrate-coated AgNPs HEC-coated AgNPs showed a mild toxicity	(Marassi et al., 2018)
AgNPs	Uncoated (weakly negative), PVP (neutral), Citrate (negative)	Human colon cancer cells (HT29)	12.5 -50 µg/ml	Uncoated AgNPs showed highest toxicity and triggered oxidative stress PVP-coated AgNPs induced greater toxicity compared to citrate-coated AgNPs	(Nguyen et al., 2013)

1.4.3.4 Effect of particle chemical composition

The composition of metal NPs either AgNPs or AuNPs can behave differently and induce distinct biological responses. As illustrated in **Table 1.4**, several studies indicated the substantial toxicity of AgNPs compared to the low toxicity potential of AuNPs using the same size, surface coating and concentration. Metal ions can exert toxic effects causing cellular damage and it was suggested the potential toxic effect of AgNPs due to their dissolution. AgNPs are highly prone to oxidise and therefore release Ag ions which assumed to be the cause of toxicity (Soenen et al., 2015, Parnsamut and Brimson, 2015). On contrary, AuNPs exhibit low reactivity thereof display low toxicity. However, the safety profile of AuNPs remains debatable as several investigators have demonstrated the detrimental effect of the cellular exposure to AuNPs (Connor et al., 2005, Kumar et al., 2017a).

Table 1.4. *In vitro* studies of the NPs composition impacts on toxicity.

Type of NPs	Size (nm)	Coating	Cell line	Concentration	Major findings	Reference
AgNPs, AuNPs,	7, 31 32	Not reported	Human colorectal adenocarcinoma cells (HT29)	2- 10 µg/ml	AgNPs showed highest cytotoxicity AuNPs showed lowest toxic response	(Schneider et al., 2017)
AgNPs AuNPs	20, 40 20, 40	Peptide-coated	THP-1-derived human macrophages	10 -50 µg/ml	AuNPs were non toxic AgNPs showed toxicity and triggered oxidative stress	(Haase et al., 2011)
AgNPs AuNPs	5, 50 5, 50	Citrate	Normal human bronchial epithelial cells (HBEC3-kt)	0.5- 50 µg/ml	AgNPs showed highest toxicity with induction of DNA strand breaks AuNPs showed lowest toxicity Slight induce in DNA damage with smaller sized (5 nm) AuNPs	(Lebedová et al., 2018)
AgNPs AuNPs	10-50 10-50	Citrate	Human leukemic T cells (Jurkat) and human monocytic cells (U937)	2.5-50 ppm	AgNPs were more toxic than AuNPs AgNPs can easily oxidised than AuNPs AgNPs induced oxidative stress	(Parnsamut and Brimson, 2015)

1.5 AgNPs and AuNPs mediate oxidative stress by modulating cell signalling pathways

Nano-scale particles can behave differently than bulk-sized particles of the same material in a biological system (Rauch et al., 2013). Because of their small size, AgNPs and AuNPs can interact with different types of biological molecules, such as DNA, proteins and lipids. This interaction may lead to sustained modification and interruption of the normal biological processes and functions (Sengul and Asmatulu, 2020).

The role of AgNPs and AuNPs in modulating various cell signalling pathways remains unclear and the link between NPs and toxicity at the proteomic and transcriptomic levels is not well investigated (Marano et al., 2011). Understanding the mechanism underlying the effect of AgNPs and AuNPs in the cell signalling machinery may help develop a novel nanosystem for targeting or treating several diseases, including cancer (Basu et al., 2009). AuNPs and AgNPs can interact and interfere with different signalling transduction pathways, leading to different biological responses (Schaeublin et al., 2011, Parnsamut and Brimson, 2015). It was demonstrated that the activity of serine/ threonine kinases such as mitogen-activated protein kinase (MAPK) and phosphoinositide-3-kinase/protein kinase B (PI3K/AKT) can be modulated by both AuNPs and AgNPs. These pathways play roles in the regulation of redox haemostasis signalling cascades and found to be dysregulated when oxidative stress is induced by AuNPs and AgNPs (Rinna et al., 2014, Comfort et al., 2011).

MAPK pathways regulate crucial cellular biological processes including differentiation, apoptosis, proliferation, metabolism and cytokine production (Kyriakis and Avruch, 2001). The MAPK family consists of several subgroups, namely extracellular signal-regulated kinase (ERK), p38 and c-Jun N-terminal kinase (JNk) pathways. MAPK pathways are commonly

activated under the influence of cellular stress, including oxidative stress stimuli, and have been demonstrated to be involved in AgNPs- and AuNPs-mediated apoptosis (Zhu et al., 2016, Yi et al., 2010). Rinna et al. (2014) revealed that AgNPs exposure resulted in oxidative stress, which was mediated by the activation of the ERK pathway, in human epithelial embryonic cells (EUE). The activation of MAPK lead to increase the activity of ERK protein which consequently stimulate several transcription factors that regulate cells cycle progression and cell survival processes (**Figure 1.3**) (Roberts and Der, 2007).

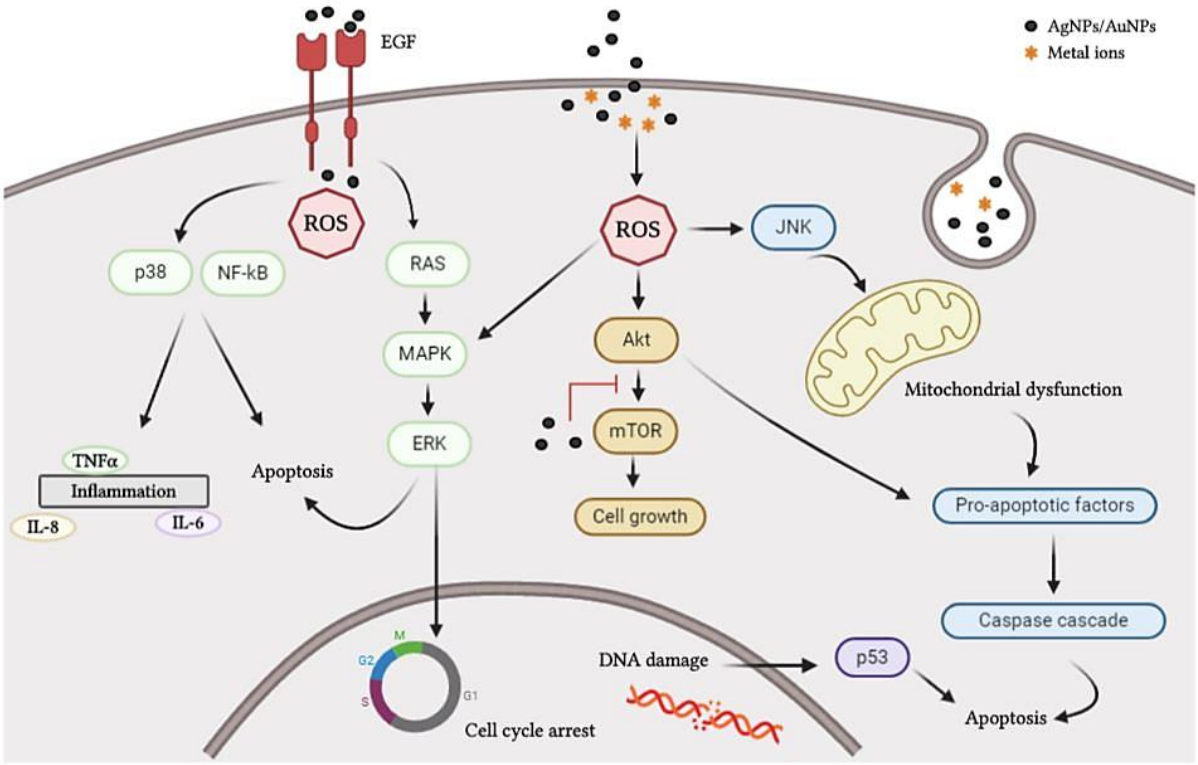


Figure 1.3. Schematic representation of AgNPs and AuNPs impact on MAPK, AKT and p53 cell signalling pathways. Scheme generated with BioRender.com.

The AKT signalling pathway regulates many cellular functions, such as cell proliferation and cell survival (Hemmings and Restuccia, 2012). Previous studies have proved that AgNPs and AuNPs can induce toxicity by modulating the activity of the AKT pathway (Zhu et al., 2016, Pan et al., 2014). The inhibition of AKT lead to deactivation of mammalian target of rapamycin (mTOR) and subsequent suppression of cell growth (**Figure 1.3**) (Xu et al., 2020a). Zhu et al. (2016) found that AgNPs induced apoptosis mediated by dysregulation of AKT, MAPK and p53 signalling cascades in human hepatocellular carcinoma cells (HepG2).

AgNPs and AuNPs potentiate toxicity by different mechanisms; oxidative stress triggered by the generation of ROS is one of the most postulated mechanism (Foldbjerg et al., 2009, Li et al., 2010). This process can be regulated by several pathways, including PI3K/AKT, MAPK and p53 signalling cascades, which eventually induce apoptosis and inhibition of cell proliferation (Manke et al., 2013). An increase in the accumulation of ROS level leads to the suppression of AKT activity and stimulates proapoptotic regulators, such as p38 (Wada and Penninger, 2004). Consequently, caspase-3 is activated, resulting in the cleavage of poly (ADP-ribose) polymerase (PARP), which mediates apoptosis (**Figure 1.3**).

Mitochondrial dysfunction is another mechanism underlying the toxicity of AgNPs and AuNPs (Bin-Jumah et al., 2020, Xue et al., 2016). Impaired cellular metabolic activity and mitochondrial membrane depolarisation can cause mitochondrial collapse. Both AgNPs and AuNPs may induce apoptosis via the JNK pathway, which induces cell death by mitochondria-mediated apoptosis in response to oxidative stress (Piao et al., 2011, Zhu et al., 2016, Jawaid et al., 2020). JNK induces the activation of proapoptotic proteins by the phosphorylation of Bcl-2. Therefore, proapoptotic proteins, including Bax, Bad and Bid, are induced and cytochrome c

is released into the cytoplasm, consequently activating caspase-3 and caspase-9 (**Figure 1.3**) (Aoki et al., 2002).

Nrf2 is a redox-sensitive transcription factors that regulates the activation of antioxidant enzymes in cells as a defence system in response to oxidative stress (Anedda et al., 2013). Nrf2 activity can be induced by AgNPs and AuNPs lead to Keap-1 oxidation, which triggers the translocation of Nrf2 into the nucleus and thereby stimulates antioxidants, such as haem oxygenase-1 (HO-1) and NADPH quinone oxidoreductase 1 (NQO1) (Lim et al., 2012a, Lai et al., 2015). Under the conditions of high oxidative stress, ROS stimulate MAPKs by activating the growth receptor, inhibiting MAPK phosphatases (MKPs) and simulating redox-sensitive kinases to induce proinflammatory cytokines, such as IL-8, IL-2, IL-6 and TNF-α (Thannickal and Fanburg, 2000).

p38 protein is activated by the presence of ROS, which lead to stimulation of inflammatory response through induction of the TNF-α cascade (**Figure 1.3**). Therefore, subsequent disruption of the cell membrane and apoptosis are induced (Fehaid and Taniguchi, 2018). The release of Ag ions via the Trojan horse-type mechanism is presumed to be the key factor associated with the activation of this pathway (Park et al., 2010).

Imbalance in redox haemostasis as a result of the overproduction of ROS induced by AgNPs and AuNPs may cause DNA damage, which is accompanied by the activation of p53 and leads to apoptosis (**Figure 1.3**) (P. J et al., 2016, Schaeublin et al., 2011). p53 is a tumour suppressor gene and it is activated by its phosphorylation at serine 15 which induced the apoptotic machinery, thereby activating proapoptotic proteins (Bax) and downregulating antiapoptotic proteins (Bcl-2 and Bcl-xl) (Aubrey et al., 2018). p53-mediated apoptosis has been reported in the colon cancer cells (HCT116) after treatment with starch-coated AgNPs (Satapathy et al.,

2013). A similar finding has been reported in in the lung epithelial carcinoma cells (A549) exposed to AgNPs (P. J et al., 2016). As previously demonstrated the AgNPs and AuNPs physiochemical properties are associated with their toxicity response, thus can also provoke distinct cell signalling responses upon cellular exposure to different AgNPs AuNPs physicochemical properties.

1.5.1 Impact of physicochemical properties of AgNPs and AuNPs on modulation of oxidative stress mediated cell signalling pathways

Few studies have reported that different AgNPs and AuNPs physicochemical properties can trigger different signalling events. As shown in **Table 1.5**, the AgNPs and AuNPs morphology, size, surface modification as well as cell type can mediate and target different cell signalling pathways at both transcriptional and translational levels. The composition of NPs may result in distinct alterations in signalling cascades. Both AgNPs and AuNPs were found to inhibit cell proliferation at different levels in human T-lymphocyte cells (Jurkat cells) and human myeloid leukaemia cells (U937). It was reported that AgNPs mediated the inactivation of ERK pathway resulted in suppression of cell proliferation, whereas AuNPs inhibited cell proliferation via dysregulation of JNK pathway without influencing ERK pathway (Parnsamut and Brimson, 2015).

The cell type-dependent alteration of proapoptotic proteins by AuNPs in human prostate cancer cells (DU145), breast cancer cells (MDA-MB-231) and lung epithelial cells (L132) was assessed in a previous study (Coulter et al., 2012). Significant upregulation of cleaved caspase-9 and PARP expression was observed in DU145 and MDA-MB-231 cells, while no changes were observed in L132 cells. Another study demonstrated cell-type specific response via upregulation of protein related to DNA damage (Lim et al., 2012b). AgNPs were found to

induce the phosphorylation of the histone H2AX at serine 139, one of the key markers for DNA DSB (Lim et al., 2012b), in normal human fibroblasts (IMR-90) and human glioblastoma cells (M059K). However, only M059K cells exposed to AgNPs showed upregulated expression of the ataxia-telangiectasia mutated (ATM) protein, a major transducer activated in response to DNA DSB.

AgNPs and AuNPs of different coating may trigger distinct level of cell signalling pathway modulation. In a previous study, both citrate- and PEG-coated AgNPs were shown to arrest the cells at G2 phase by reduction in the gene expression of cyclin B1 (*CCNB1*) and cyclin E1 (*CCNE1*) in HepG2 cells (Bastos et al., 2017). In the same study, no sign of apoptosis was noticed as downregulation of apoptotic genes, including *Bcl-3* and *Bax*, was reported in both coated AgNPs. However, PEG-coated AgNPs showed significant alteration on the proteins expression compared to the other AgNPs coating even at low concentration of AgNPs (5 µg/ml). On other hand, another study revealed that apoptotic cell death induced in MCF-7 cells via the upregulation of caspase-6, caspase-9, PARP, Bax and Bcl-2 expression on exposure to AgNPs and AuNPs (Jeyaraj et al., 2015).

The size of AgNPs and AuNPs may influence the extent of the signalling outcome. AgNPs sized 18 nm were found to increase the expression of the proapoptotic protein Bax more significantly than AgNPs sized 2.6 nm (Zielinska et al., 2017). However, compared to larger AgNPs, smaller AgNPs caused a significant elevation in LC3-II and p53 levels (Zielinska et al., 2017). On the other hand, Van Der Zande et al. (2016) revealed that the exposure to different AgNPs sizes (20, 30, 60, 110 nm) triggered the same effect regardless of the AgNPs sizes in Caco-2 and MCF-7 cells. AgNPs of different sizes showed an induction in oxidative stress by upregulating the expression of genes responsible for oxidative stress including *Hsps* and *HMOX1* genes.

Table 1.5. *In vitro* studies on the impact of AgNPs and AuNPs on cell signalling pathways.

Type of NPs	NPs characteristics			Cell signalling assessment					Reference
	Size (nm)	Surface coating/ modification	Shape	Cell line	Concentration	Exposure time	Major findings	Activity	
AgNPs	20, 30, 60, 110	Citrate (negative)	Spherical	Human colorectal adenocarcinoma cells (Caco-2), and human breast cancer cells (MCF-7)	5- 25 µg/ml	6- 24 hrs	AgNPs of all sizes upregulated genes responsible for oxidative stress	↑ Hsps ↑ HMOX1 ↑ SRXN1 ↑ OKL38	(Van Der Zande et al., 2016)
AgNPs	5, 35	Citrate (negative)	Spherical	Osteosarcoma cells (U2Os), (Saos-2)	10- 100 µM	24- 48 hrs	Both sizes of AgNPs activated p53 and caspase-3 lead to mitochondrial dysfunction and apoptosis	↑ p53 ↑ caspase 3	(Kovács et al., 2016)
AgNPs	2.6, 18	Not reported	Spherical	Human pancreas ductal adenocarcinoma cells (PANC-1) and human pancreas duct epithelial cells (hTERT-HPNE)	0.5- 50 µg/ml	24 hrs	Both sizes of AgNPs activated pro-apoptotic protein (Bax) and it was more significant with sized 18 nm AgNPs Both AgNPs elevated LC3-II and p53 levels and it was significant with smaller size (2.6 nm)	↑Bax ↑P53 ↑LC3-II	(Zielinska et al., 2017)
AgNPs	5, 100	PVP (weakly negative)	Spherical	Human macrophage cells (U937)	0.39- 25 µg/ml	24 hrs	Smaller sized AgNPs significantly induced gene expressions related to oxidative stress and inflammation	↑ HO-1 ↑ Hsp70 ↑ IL-8	(Lim et al., 2012a)
AuNPs	10, 70	Neutral	Not reported	Human neutrophil	1 -100 µg/ml	24 hrs	Both sizes AuNPs mediated apoptosis caspase-dependent pathway by upregulating caspases-3,-7 and -9	↑ caspase-3,7,9	(Noël et al., 2016)
AgNPs	30	Citrate (negative), Poly(ethylene glycol) (PEG) (neutral)	Spherical	Human hepatoblastoma cells (HepG2)	1-50 µg/ml	24- 48 hrs	PEG-coated AgNPs induced the cell cycle gene expression related to S and G2 phases activity PEG-coated reduced gene expression related to apoptotic cascade	↓ BCL2 ↓ Bax ↓ CCNB1 ↓ CCNE1	(Bastos et al., 2017)

Table 1.5. *In vitro* studies on the impact of AgNPs and AuNPs on cell signalling pathways (continued).

Type of NPs	NPs characteristics			Cell signalling assessment					Reference
	Size (nm)	Surface coating/ modification	Shape	Cell line	Concentration	Exposure time	Major findings	Activity	
AgNPs	30- 50	Sodium borohydride (negative), Tannic acid (negative)	Not reported	Human epithelium carcinoma cells (A431) and human lung epitehlial carcinoma (A549)	25- 75 µg/ml	24 hrs	Tannic acid -coated AgNPs induced protein expressions related to oxidative stress in a concentration-dependent manner No changes were observed with sodium borohydride-AgNPs	↑pp38 ↑TNF-a ↑Hsp70	(Kaur and Tikoo, 2013)
AuNPs	18 16 × 48	Citrate (negative) Polyacrylic acid (PAA) (positive) PAA (positive) Poly(ethylene glycol) (PEG) (neutral)	Spherical Rod	Human dermal fibroblast cells (HDF)	0.1 nM	24 hrs	PEG-coated rods-shaped AuNPs induced drastic modifications to gene expression responsible for antioxidant, inflammation and oxidative stress Others AuNPs mediated similar responses but to less extent	↑VEGFA ↑CCL2 ↑PRDX1 ↑NQO1 ↑EDN1 ↑HspA5	(Falagan-Lotsch et al., 2016)
AuNPs	1.5	Trimethyl ammonium-thanethiol (TMAT) (positive) Mercapto-ethanesulfonate (MES) (negative), Mercapto- ethoxy ethoxy ethanol (MEEE) (neutral)	Spherical	Human keratinocyte cells (HaCaT)	5- 100 µg/ml	24 hrs	Charged AuNPs and more significantly negatively charged AuNPs triggered apoptosis by activation of p53 and caspase-3 genes Neutral AuNPs reduced the gene expression of apoptosis related gene p53 and caspase-3 and mediated necrosis	↑/↓ p53 ↑/↓ Caspase-3	(Schaeublin et al., 2011)

Table 1.5. *In vitro* studies on the impact of AgNPs and AuNPs on cell signalling pathways (continued).

Type of NPs	NPs characteristics			Cell signalling assessment					Reference
	Size (nm)	Surface coating/ modification	Shape	Cell line	Concentration	Exposure time	Major findings	Activity	
AgNPs	30	Citrate (negative), Poly(ethylene glycol) (PEG) (neutral)	Spherical	Human keratinocytes cells (HaCaT)	10- 40 µg/ml	24- 48 hrs	PEG-coated AgNPs mediated intrinsic apoptosis by activation of BCL-2, BAX and caspase-3 Citrate-coated AgNPs triggered cell cycle arrest at G2 phase by significant reduction of gene expression related to cyclin B1 activity	↑ BCL-2 ↑ Bax ↑ Caspase-3 ↓CCNB1	(Bastos et al., 2016)
AgNPs	20	PVP (weakly negative)	Spherical	Normal human fibroblasts (IMR-90) and human glioblastoma cells (M059K)	20- 100 µg/ml	48 hrs	AgNPs influenced the gene expression involved in genotoxicity and it was more significant in MO59K cells compared to normal human cells	↑γ-H2AX ↑DNA-PKcs ↑ATM	(Lim et al., 2012b)
AuNPs	1.9	Not reported	Spherical	Human prostate cancer cell (DU145), breast cancer cells (MDA-MB-231) and lung epithelial cells (L132)	12 µM	24 hrs	AuNPs triggered apoptosis by increases of cleaved caspase-9 and cleaved PARP which were drastic in MDA-MB-231 cells followed by DU145 cells No response was observed in L132 cells	↑cleaved caspase-9 ↑PARP	(Coulter et al., 2012)
AgNPs, AuNPs	10	Citrate (negative)	Spherical	Human epithelial cells (A-431)	5- 25 µg/ml	24 hrs	Both AgNPs and AuNPs suppressed epidermal growth factor (EGF) signal and inhibited AKT and Erk phosphorylation Only AuNPs inhibited AKT activity by deactivation of IkB kinase (IKK) signalling	↓ EGF ↓ pAKT ↓pErk ↓ p-IKK	(Comfort et al., 2011)
AgNPs, AuNPs	10-50	Citrate (negative)	Spherical	Human T lymphocyte cells (Jurkat) and human monocytic cells (U937)	7.5-25 ppm	5 min – 24 hrs	AgNPs inhibited ERK protein expression whereas AuNPs upregulated ERK expression AgNPs repressed TNF-α production AuNPs downregulated IL-2 expression	↑/↓ ERK ↓TNF-α ↓IL-2	(Parnsamut and Brimson, 2015)

The release of metal ions may induce distinct cell signalling transduction pathways. Eom and Choi (2010) exposed human Jurkat cells to AgNPs and Ag ions and found that AgNPs induced apoptosis and DNA damage by the activation of p38, MAPK pathways and upregulation of p-H2AX, a DNA damage marker. However, significant induction was not noted in Jurkat cells treated with Ag ions, indicating that the pivotal toxicity is correlated with AgNPs rather than Ag ions.

The surface charge of AgNPs and AuNPs can elicit different responses. Negatively charged (Mercapto- ethanesulfonate) and positively charged (Trimethyl ammonium-thanethiol) AuNPs were found to stimulate apoptotic cell death via the upregulation of caspase-3 and p53 levels; however, no significant modification in the levels of apoptotic markers was noted on treatment with neutrally charged AuNPs (Mercapto- ethoxy ethoxy ethanol) (Schaeublin et al., 2011).

The impact of the shape of AgNPs and AuNPs on cell signalling events was investigated in a previous study. Human dermal fibroblast (HDF) cells were incubated with AuNPs using two different shapes and surface coatings: citrate- and PAA-coated spherical-shaped AuNPs and PAA- and PEG-coated rod-shaped AuNPs (Falagan-Lotsch et al., 2016). No effect of shape was observed on the oxidative stress gene expression levels following 24 hours of treatment, but surface coating had an effect on the gene expression levels. The expression of genes responsible for oxidative stress, apoptosis and antioxidant activities were greatly altered by PEG-coated rods in HDF cells (Falagan-Lotsch et al., 2016).

The composition of NPs (AgNPs or AuNPs) was displayed to induce different cell signalling pathway effects. Both Jukart and U937 were exposed to citrate-coated AgNPs and AuNPs and resulted in reduction of cell proliferation via influencing distinct cell signalling pathways.

AgNPs showed to suppressed the protein activity of ERK pathway and TNF-α production. For cells exposed to AuNPs illustrated the opposite effect in which ERK and TNF-α expression were upregulated but AuNPs reported to inhibit cell proliferation by attenuation of JNK pathway (Parnsamut and Brimson, 2015).

1.5.2 Effect of AgNPs and AuNPs on other cell signalling pathways

AgNPs and AuNPs can affect the activity of other cell signalling pathways such as Wingless-related integration site (Wnt)/β-catenin signalling pathway which regulates cell proliferation, communication and adhesion (Macdonald et al., 2009). The disruption of this pathway may contribute to several human diseases, such as cancer and osteoporosis (Macdonald et al., 2009). Few evidence was found in the literature investigated the potential effect of AuNPs or AgNPs on this pathway. One study exposed the human breast cancer cells (MDA-MB-231 and MDA-MB-468) to citrate-coated AuNPs (negatively charged) and cysteamine-coated AuNPs (positively charged). Both AuNPs significantly inhibited cell proliferation by interrupting the Wnt/β-catenin pathway via β-catenin destabilisation and subsequently suppressing the level of cyclin D1, which is required for cell cycle progression. The pathway modification was significantly greater with cysteamine-coated AuNPs (Surapaneni et al., 2018).

The AMP-activated protein kinase (AMPK) is another signalling pathway which plays key roles in controlling cellular energy and growth (Mihaylova and Shaw, 2011). The AMPK pathway acts as a metabolic sensor that is activated upon the reduction of intracellular ATP production (Mihaylova and Shaw, 2011). Another function of this pathway is the regulation of the mammalian target of rapamycin complex 1 (mTORC1) pathway, which triggers the autophagy process. AgNPs have been found to induce the autophagy process in a human

neuroblastoma cell line (SH-SY5Y) by increasing the intracellular calcium level, which induces endoplasmic reticulum stress and activates the MAPK pathway, resulting in the downregulation of mTOR levels (Li et al., 2019).

In summary, the existing *in vitro* studies evident the toxicity of AgNPs and AuNPs which emphasises the significance of careful consideration of the risk–benefit ratio when using these NPs for different purposes. A comprehensive understanding of the impact of physicochemical properties of AgNPs and AuNPs on their underlying toxicity remains challenging as the major obstacles were the variation on the their synthesis methods, concentration, physiochemical properties and the experimental conditions.

The composition of metal-based NPs can play critical role in determining their detrimental effect. Metal-based NPs mainly AgNPs and AuNPs were extensively explored because of their promising properties for biomedical applications. The toxicity of AuNPs is still under debate and the conclusions from the existing literature remain contradictory (Fratoddi et al., 2015b). The toxicity of AgNPs is suggested to occur by their dissolution into Ag ions in the extracellular or intracellular matrix (Kittler et al., 2010, Hsiao et al., 2015). Therefore, the present research will focus on AgNPs and AuNPs to investigate the impact of two different metal-based NPs composition in relation to toxicity.

AgNPs and AuNPs size play an important role in controlling their toxicity. Size-dependent toxicity was observed in most studies (**Table 1.1**). However, some investigators have suggested that AgNPs and AuNPs with the size of 50 nm is the optimal size that leads to an increase in the NPs internalisation, thereof induce toxicity. However, it is thought that the size of AgNPs and AuNPs is not the primary factor determining their associated toxicity. Rather, the total number of AgNPs and AuNPs present in a specific volume plays a critical role in

determining the behaviours of these NPs in a biological system (Oberdörster et al., 2005). Therefore, the present research will focus on studying the impact of different sizes of AgNPs and AuNPs on toxicity.

The effect of physicochemical properties of AgNPs and AuNPs on modulating cell signalling pathways can be correlated with NPs-induced toxicity (**Table 1.5**). AgNPs and AuNPs can trigger oxidative stress mediated by alteration in cell signalling pathways. However, AgNPs and AuNPs can interfere with several other transduction pathways that have not yet been investigated. Both AgNPs and AuNPs can alter various cell signalling pathways, which opens a new avenue for their application as potential therapeutics for treating diseases. The present research will study the AgNPs and AuNPs modulation effects on PI3K/AKT and Wnt/β-catenin pathways as both pathways have not well been investigated yet.

All of the reviewed *in vitro* nanotoxicology studies in this chapter were performed in two dimensional (2D) monolayer cell culture as one of the most well-known preclinical *in vitro* methods for biological compound testing prior to *in vivo* studies. The advantages of using the 2D monolayer method includes the low cost as well as the ease of cell maintenance and growth. However, there are some limitations of this method, mainly the lack of complexity in mimicking original tissue (Breslin and O'driscoll, 2013). Several methods have been developed and gained prominence for creating more accurate and representative models of *in vivo* tissue, which helps minimise or replace the use of animal models. The three dimensional (3D) culture model is one useful method for biological compound screening, novel mechanism detection, and biomarker identification (Breslin and O'driscoll, 2013). 3D culture model demonstrated better representation of *in vivo* condition. The present study will investigate the AgNPs and AuNPs toxicity mainly focused on a 2D culture model and also will assess both NPs toxicity on a 3D multicellular tumour spheroids model to compare the AgNPs and AuNPs

influence in two different cell culture models. It was observed from the literature the potential risk of lung toxicity however, there is a lack in the consistency of the toxicity evaluation corresponding to AgNPs and AuNPs properties (Hadrup et al., 2020, Adewale et al., 2019). Two immortalised lung cell lines were selected for 2D and 3D cell culture models in this study to assess the toxicity of AgNPs and AuNPs of different sizes which are human Caucasian lung carcinoma epithelial (A549) and human foetal lung fibroblast (MRC-5) cell lines. A549 cell line is a type of epithelial lung cancer cell in the proximal alveolar space which is the initial place to come into contact with nanomaterials in the epithelium of the respiratory tract system (Yurdasiper et al., 2018). As A549 cells represent a direct and sensitive region for nanomaterials deposition, this cell line is one of the most commonly lung cancer cell model used in the *in vitro* studies to investigate the lung toxicity of the nanomaterials via environmental exposure (Theodorou et al., 2014). Moreover, A549 cell model is used for developing a drug to treat lung cancer (Brown et al., 2010, Foldbjerg et al., 2011). Fibroblast cells consider as ideal representative cells privilege to their existence in all organs. MRC-5 cell line in lung regulates the extracellular matrix thereof this cell type is widely used as an *in vitro* model for toxicity testing (Riaz Ahmed et al., 2017). MRC-5 cell lines will be involved in this work as a healthy cells model to assess how the normal cells would behave upon AgNPs and AuNPs exposure for their safety concerns. Therefore, it was of interest to compare the toxicity profile of AgNPs and AuNPs of different sizes in the non-cancerous (MRC-5) and cancerous (A549) lung cells in this project.

1.6 Research aims and objectives

The safety profile of AgNPs and AuNPs can limit their medical application and hinder their clinical usability. The *in vitro* studies revealed a significant relationship between the physicochemical properties of AgNPs and AuNPs and the observed toxicity. In the present research, we hypothesised that the exposure of cells to different metal NPs chemical compositions (AgNPs and AuNPs) and using different AgNPs and AuNPs sizes can induce distinct toxicological responses. The primary aim of this study was to create a systematic toxicological investigation in order to study the potential toxicity of AgNPs and AuNPs of the same sizes (10, 40 and 80 nm) in healthy and cancerous lung cell lines in an *in vitro* model. This study was also interested to compare the AgNPs and AuNPs cytotoxicity in the 2D monolayer and 3D multicellular spheroids models. Moreover, it was hypothesised that AgNPs and AuNPs can mediate toxicity by modulating PI3K/AKT and Wnt/β-catenin signalling pathways, which regulate cell proliferation, oxidative stress, cell cycle progression and apoptosis.

The specific objectives were as follows:

- AgNPs and AuNPs were characterised to determine their physicochemical properties including size, morphology, surface charge and their stability in the cell culture medium.
- The cytotoxicity profile of both AgNPs and AuNPs of different sizes was assessed to identify the effect of the concentration, size, composition and exposure time on their toxicity in a 2D cell culture model of the human lung cell lines.
- The cellular uptake of AgNPs and AuNPs was investigated in a 2D cell culture model of the human lung cell lines to compare the influence of both AgNPs and AuNPs on their cellular internalisation.

- The molecular mechanisms underlying the toxicity of AgNPs and AuNPs of different sizes, including oxidative stress and cell death mechanisms, were assessed in a 2D cell culture model of the human lung cell lines.

- The toxicity of AgNPs and AuNPs of different sizes was examined in a 3D multicellular spheroid cell culture model of the cancerous lung cell line.

- The impact of AgNPs and AuNPs of different sizes on PI3K/AKT and Wnt/β-catenin signalling pathways in a 2D cell culture model of the human lung cell lines were studied by investigating the protein expression level that related to these pathways.

Chapter 2

Materials and methods

2.1 Materials

2.1.1 Nanoparticles

Three sizes of AgNPs and AuNPs were investigated in this study (10, 40, and 80 nm). Ag10 (10 nm) and Ag40 (40 nm) were obtained from Sigma-Aldrich (Dorset, UK). Ag80 (80 nm) were purchased from NanoComposix (San Diego, CA, USA). The three AgNPs sizes (10, 40 and 80 nm) were provided at a concentration of 0.02 mg/ml in an aqueous buffer containing sodium citrate as a stabiliser. The particle concentrations of Ag10, Ag40, and Ag80 were $3.6x10^{12}$, $5.7x10^{10}$ and $7.6x10^{9}$ particles/ml, respectively.

Au10 (10 nm), Au40 (40 nm), and Au80 (80 nm) were obtained from BBI Solutions (Cardiff, UK). The AuNPs were provided at concentrations of 57.6, 58.2 and 56.9 µg/ml for Au10, Au40 and Au80, respectively. The three AuNPs sizes were stabilised in sodium citrate. The concentrations in particles/ml for Au10, Au40 and Au80 were 5.70×10^{12}, 9.00×10^{10} and 1.10×10^{10} particles/ml, respectively.

2.1.2 Cell lines and cell culture reagents

Human foetal lung fibroblast (MRC-5) and human Caucasian lung carcinoma epithelial (A549) cell lines were purchased from Public Health England (Salisbury, UK). Ham's F-12 Nutrient Mix medium, Dulbecco's phosphate-buffered saline (DPBS), heat-inactivated foetal bovine serum (FBS), L-glutamine (200 mM), Trypsin 0.25%- EDTA (1X) and Penicillin-streptomycin (5,000 U/ml) were purchased from Gibco (Paisley, UK). Eagle's minimum essential medium (EMEM) and MEM non-essential amino acid solution (100X) were from Sigma-Aldrich (Dorset, UK).

2.1.3 Chemicals

Table 2.1. Chemicals.

Chemical	Supplier
1,4-dithiothreitol (DTT) 2-mercaptoethanol Agar Ammonium persulfate (APS) Benzamidine Bovine serum albumin (BSA) Bradford reagent Bromophenol blue Dimethy sulfoxide (DMSO) Ethylenediaminetetraacetic acid (EDTA) Ethylene glycol tetra acetic acid (EGTA) Tetramethyl-ethylen-diamine (TEMED) Etoposide Glycerol HEPES Lithium chloride (LiCl) Menadione Potassium chloride (KCl) Radioimmunoprecipitation assay (RIPA) buffer Skim milk powder Sodium Chloride (NaCl) Sodium Dodecyl Sulfate (SDS) Sodium Fluoride Sodium Orthovanadate Sodium Pyrophosphate Sucrose Thiazolyl Blue Tetrazolium Bromide (MTT) Tris-HCl Triton X-100 Topotecan Hydrochloride Hydrate	Sigma-Aldrich (Dorset, UK)
Wnt agonist I	Cayman Chemical Company (Cambridge, UK)

Table 2.1. Chemicals (continued).

Chemicals	Supplier
Tween 20 Phenylmethylsulfonyl fluoride (PMSF)	PanReac AppliChem ITW reagents (Barcelona, Spain)
Hydrochloric acid 37% in water RPMI 1640 Medium, no phenol red Pierce™ Bovine Serum Albumin Standard Ampules, 2 mg/ml Vectashield Hardset Antifade Mounting Medium with DAPI	Thermo Scientific (Paisley, UK)
Acrylamide/Bisacrylamide 37.5:1, 30% soln. Paraformaldehyde, 16% w/v aq. soln. Methanol free Ponceau stain, 0.2% v/v in 5% acetic acid Staurosporin	Alfa Aesar (Lancashire, UK)
Tris base	Roche (Welwyn Garden City, UK)
Glycine Nitric acid 67-69%	VWR International (Bristol, UK)
Amersham ECL western blotting detection reagents	GE Healthcare Life Sciences (Buckinghamshire, UK)
DC Protein assay	Bio-Rad (Watford, UK)
10% NP-40, Detergent, 10% solution in water	Abcam (Cambridge, UK)

2.1.4 Assay Kits

Table 2.2. Assay kits.

Assay kit	Supplier
Alexa Fluor® 488 Annexin V/Dead Cell Apoptosis Kit CellROX™ deep red reagent Kit LIVE/DEAD™ cell imaging Kit LIVE/DEAD™ fixable far red dead cell stain Kit MitoProbe™ TMRM assay Kit for flow cytometry FxCycle™ PI/RNase Staining Solution	Invitrogen by Thermo Fisher Scientific (Paisley, UK)
CytoTox 96® Non-Radioactive Cytotoxicity Assay GSH/GSSG-Glo™ Assay	Promega (Southampton, UK)

2.2 Methods

2.2.1 Characterisations of AgNPs and AuNPs of different sizes

2.2.1.1 Transmission electron microscopy (TEM)

The different sizes of AgNPs and AuNPs were imaged using TEM Jeol-2100, operating at a voltage of 80 keV. A drop of NPs sample was air dried on a formvar carbon film on a copper grid (EM Resolutions Ltd, Sheffield, UK). The particle diameter distribution in nm for each size of AgNPs and AuNPs was measured for 200 particles using ImageJ software (version 2.0.0).

2.2.1.2 Dynamic light scattering (DLS)/ Zetasizer

The z-average size of both AgNPs and AuNPs of different sizes was measured using Malvern Zetasizer (Malvern Instruments Ltd, Worcestershire, UK) at 25°C. The size and surface charge of AgNPs and AuNPs were measured at (10 µg/ml) and (26 µg/ml), respectively in ultrapure water. The z-average size of the particles was determined by the changes in the intensity of scattered light that crossed the particles. The technique is based on Brownian motion of spherical NPs in the sample over time. The zeta potential of NPs was used to measure the NPs surface charge based on the electrophoretic mobility. At least three different NPs batches from the supplier were measured.

2.2.1.3 Ultraviolet-Visible (UV-Vis) spectroscopy

The surface plasmon resonance of the NPs displays optical properties. The UV-Vis spectra of AgNPs (10 µg/ml) and AuNPs (26 µg/ml) in ultrapure water were determined using UV-Vis spectrophotometer-2600 (Shimadzu Corporation, Kyoto, Japan). The instrument was set to scan the wavelengths from 200 to 700 nm with spectral bandwidth of 1 nm.

2.2.2 Toxicological assessment of AgNPs and AuNPs of different sizes in 2D *in vitro* cell culture model

2.2.2.1 Cell culture

A549 cells were maintained in Ham's F-12 Nutrient Mix medium. The medium was supplemented with (10%) FBS and (1%) penicillin-streptomycin. MRC-5 cells were maintained in EMEM and supplemented with (10%) FBS, (1%) penicillin-streptomycin, (1%) L-glutamine, and (1%) MEM non-essential amino acid. The cells were incubated in 5% CO_2 at 37°C. Both cells were passaged using trypsin 0.25% -EDTA (1X). Cells were split at 75%–85% of cell confluence and seeded in an appropriate cell culture well-plate for the desired experiments. The passage numbers of both cell lines were considered throughout the experiments in which the cells were maintained at passage number between 5 to 15.

2.2.2.2 LIVE/DEAD™ fixable far-red dead cell stain assay: cell viability assessment of sodium citrate stabiliser

Assay principle: Cell viability was measured by flow cytometry using a LIVE/DEAD™ fixable far-red dead cell stain kit. The assay is based on a fluorescent dye reaction with free amines inside cells and on the cell surface. The fluorescent reactive dye binds to amines on the cell surface of intact live cells, resulting in a weak fluorescent signal. However, in dead cells the fluorescent reactive dye interacts with both amines on the cell surface and intracellular amines and generates a strong fluorescent signal. This assay was used to investigate the potential toxicity of sodium citrate stabiliser alone as both AgNPs and AuNPs were stabilised in sodium citrate.

Experimental protocol: MRC-5 cells were seeded in 12-well plate at a density of 1×10^5 cells/well in 1.5 ml of cell culture medium and allowed to adhere overnight in 5% CO_2 at

37°C. A stock solution of sodium citrate (2 mM) was prepared in ultrapure water and then used to prepare different concentrations of sodium citrate in cell culture medium. Cells were exposed for 24 hours to sodium citrate at concentrations of (1.25, 1.5, and 1.7 mM) which were equivalent to the concentrations used in AgNPs and AuNPs treatment. 20% dimethyl sulfoxide (DMSO) was used as a positive control incubated with cells for 24 hours. Cells were trypsinised and centrifuged at 1,500 rpm for 10 minutes at 4°C (VWR International Centrifuge, Darmstadt, Germany). As manufacturer instructed, cells were re-suspended in 1 ml of DPBS, and 1 µl of fluorescent reactive dye reconstituted in DMSO was added to each sample. The cell suspension was mixed well and incubated for 30 minutes at room temperature, protected from light. Around 10,000 events were measured on a BD LSRFortessa X20 cell analyser (BD Biosciences, Franklin Lakes, NJ, USA) at an excitation and emission maxima of 650/665 nm. Two separate experiments were carried-out, and data were analysed using FlowJo software (v10.6.1) (FlowJo LLC, Ashland, OR, USA).

2.2.2.3 Modified lactate dehydrogenase (mLDH) assay: cell viability assessment

Assay principle: The modified LDH assay was carried out using the CytoTox 96® Non-Radioactive Cytotoxicity Assay (Ali-Boucetta et al., 2011). The mLDH is a colorimetric assay that quantifies the amount of LDH released from the intact cells following the addition of lysing solution. The released LDH leads to iodonitro-tetrazolium violet (INT) conversion into a red formazan. The colour intensity generated is proportional to the amount of LDH released from the live cells that survived after exposure to the NPs. This assay was used as indirect way to measure the cell survival post incubation with NPs.

Experimental protocol: MRC-5 and A549 cells were seeded in 96-well plate at a density of 9×10^3 and 7×10^3, respectively in 0.1 ml of cell culture medium and allowed to adhere

overnight in 5% CO_2 at 37°C. Higher cell density was used while seeding MRC-5 cell line in 96 well-plate to reach cell confluency between 75%–85%. Both cells were treated with AgNPs of different sizes at a concentration range of 0.625–15 µg/ml, AuNPs of different sizes at a concentration range of 19–55 µg/ml, and sodium citrate at concentration of 1 mM for 3, 24, and 48 hours. 20% DMSO was used as a positive control. At each exposure time, the media was discarded from each well and cells were lysed by adding 9% Triton X-100 dissolved in ultrapure water (10 µl) and RPMI 1640 phenol-free medium (100 µl). Cells were left to lyse for 1 hour at 37°C and then the lysates collected and transferred into a fresh microcentrifuge tube. Cell lysates were centrifuged at 13,000 rpm for 5 minutes, and the supernatant of cell lysates (50 µl) was transferred into a fresh 96-well cell culture plate. As the manufacturer instructed, substrate mix (50 µl) was added to each well and incubated for 15 minutes at room temperature protected from light. Stop solution (50 µl) was then added to each well, and the absorbance was measured at 490 nm using a multi-mode microplate reader (BMG Labtech GmbH, Ortenberg, Germany). The data represented at least three independent experiments using different NPs batches from the supplier. The obtained absorbances were used to calculate the percentage of cell viability compared to the naive (untreated group) using the following equation:

$$\text{Cell viability (\%)} = \left(\frac{\text{Absorbance of the sample}}{\text{Mean absorbance of the naive}}\right) \text{X } 100$$

After 24 hours exposure, changes in cell morphology were investigated by imaging the cells using an optical microscope (Primovert, Carl Zeiss AG, Suzhou, China). The cytotoxic concentration of NPs that cause 50% reduction in cell viability is known as CC50. The CC50

values of cells treated with a range of concentration of AgNPs and AuNPs were estimated from a dose-response inhibition curve fitted to normalise the response based on the control group using a nonlinear regression model to produce a curve between 100% to 0% with hill slope of 0.1 in GraphPad Prism software version 8.1.2 (San Diego, CA, USA).

2.2.2.4 Thiazolyl blue tetrazolium bromide (MTT) assay: cell metabolic activity measurement

Assay principle: A colorimetric assay measures the metabolic activity of viable cells. A reduction of yellow MTT salt to purple formazan crystals occurs by mitochondrial reductase in the metabolic active cells. The colour intensity of purple formazan produced is proportional to the number of metabolically active cells that survived after exposure to the NPs.

Experimental protocol: MRC-5 and A549 cells were seeded in 96-well plate at a density of 9×10^3 and 7×10^3, respectively in 0.1 ml of cell culture medium and allowed to adhere overnight in 5% CO_2 at 37°C. Both cells were then treated with AgNPs of different sizes at a concentration range of 1.25–15 µg/ml and AuNPs of different sizes at a concentration range of 19–55 µg/ml for 24 and 48 hours. At each exposure time, the media was aspirated and cells were washed with DPBS to remove any excess NPs. Fresh media containing MTT were added at a final concentration of 0.5 mg/ml to each well and incubated for 4 hours at 37°C. The media was carefully aspirated to avoid disruption of purple formazan crystals of viable cells. DMSO (100 µl) was added to each well to solubilise the formed crystal and incubated for 15 minutes at 37°C. The absorbance was measured at 570 nm on a multi-mode microplate reader. The experiment was performed at least three times. The percentage of cell survival was calculated from the obtained absorbance based on the following equation:

$$\text{Cell survival (\%)} = \left(\frac{\text{Absorbance of the sample}}{\text{Mean absorbance of the naive}}\right) \text{X } 100$$

The CC50 values of AgNPs and AuNPs of different sizes were also estimated from the MTT data. The CC50 values were obtained from a dose-response inhibition curve fitted to normalise the response based on the control group using a nonlinear regression model to produce a curve between 100% to 0% with hill slop of 0.1 in GraphPad Prism software version 8.1.2 (San Diego, CA, USA).

2.2.2.5 Cellular uptake of AgNPs and AuNPs

2.2.2.5.1 Side-scattered light intensity analysis by flow cytometry: cell granularity assessment

Assay principle: NPs cellular internalisation was measured by the changes in the cellular granularity of cells treated with NPs compared to cells free of NPs (Jochums et al., 2017). The NPs attached to the cell membrane as well as intracellular NPs cause increases in cell granularity, which is detected by measuring side-scattered (SSC) light intensity by flow cytometry.

Experimental protocol: MRC-5 and A549 cells were seeded in 24-well plate at a density of 5×10^4 cells/well in 0.5 ml of cell culture medium and allowed to adhere overnight in 5% CO_2 at 37°C. Both cells were then treated with several concentrations of AgNPs of different sizes (7.5, 10, and 12.5 µg/ml) and AuNPs of different sizes (26, 36, and 41 µg/ml) for 24 and 48 hours. At each exposure time, the medium was discarded, and the cells were washed with DPBS to remove excess NPs. The cells were detached by trypsinisation and centrifuged at 1,500 rpm for 10 minutes at 4°C. Cells were then re-suspended in DPBS (0.5 ml) and analysed

immediately by measuring 10,000 events using the BD LSRFortessa X20 cell analyser. The generated data were interpreted using FlowJo software (v10.6.1).

2.2.2.5.2 Quantifications of intracellular NPs by inductively coupled plasma mass spectrometry (ICP-MS): silver and gold ions measurement

Assay principle: The mass concentration of silver (Ag) and gold (Au) ions internalised in the cells following exposure to AgNPs or AuNPs were quantified using ICP-MS technique. Cells treated with NPs required digestion in acidic mixture before analysis. In the ICP, the sample is evaporated by argon gas at high temperature converted NPs into ions. The amount of metal ions is determined by the detector in MS as a mass/charge ratio. This method provides the total amount of the metal ions regardless the original state of the NPs presented in the sample as NPs or metal ions (Ortenzio et al., 2019).

Experimental protocol

A. Standard curve: Several concentrations of Ag10 and Ag80 were prepared in ultrapure water ranges from 0 to 15 µg/ml at a final volume of 1 ml. Each sample was performed in four replicates. Samples were incubated for 24 hours at 37°C and acid mixture (1 ml) was added using aqua regia which consists of hydrochloric acid (HCl) and nitric acid (HNO_3) in a ratio of 3:1. The digestion process was conducted in closed glass vials at 80°C using an oven for 20 hours. Samples were diluted to 2% HNO_3 in ultrapure water. Samples were then filtered using a 0.2 µm cellulose nitrate syringe filter and analysed on ICP-MS (NexION 300X, Perkin Elmer, Waltham, MA, USA) to quantify the Ag amount. Rhodium (Rh 103) was used as an internal standard for Ag (Ag 107). The equation of the standard curve for Ag10 in water was $Y= 1.0614X - 0.4492$ ($R^2= 0.9903$) and for Ag80 in water was $Y= 0.8618X + 0.008$ ($R^2= 1$) (**Figure A1**).

For Au10 and Au80, the similar protocol as above was performed. A range of concentration from 0 to 46 µg/ml were prepared in ultrapure water, in four replicates. Platinum (Pt 195) was used as an internal standard for Au (Au 197). The amounts of Au detected for the standard curve were very low compared to the starting concentrations even after performing several modifications in the sample digestion (**Table 2.3)**. The protocol optimisation of this experiment could not be completed because of the time constraint of the project.

Table 2.3. Modification steps performed during the sample digestions for ICP-MS.

	Modification steps performed during the sample digestions	**Amount of Au (µg/ml)**
1	Samples digested with (70%) HNO_3 for 2 hours with periodic ultrasonic bath sonication then aqua regia was added and samples incubated for overnight at 80°C.	1.41
2	Samples digested with aqua regia for 48 hours at 80°C with periodic ultrasonic bath sonication.	0.38
3	Samples digested with aqua regia for 4 hours at 80°C with periodic ultrasonic bath sonication.	0.32
4	Samples digested with aqua regia for 2 hours in ultrasonic bath sonication then (70%) HNO_3 was added and samples incubated overnight at 80°C.	0.32
5	Samples digested with aqua regia for 2 hours with periodic probe sonication then (70%) HNO_3 was added and samples incubated overnight at 80°C.	0.21
6	Samples digested with aqua regia for 2 hours with periodic ultrasonic bath sonication then samples incubated overnight at 80°C.	1.38

B. Quantifying intracellular Ag amount: MRC-5 and A549 cells were seeded in 6-well plate at a density of 5×10^5 cells/well in 3 ml of cell culture medium and allowed to adhere overnight in 5% CO_2 at 37°C. Cells were then treated with Ag10 and Ag80 at concentration of 2.5, 5, and 10 µg/ml for 24 hours; each sample was performed in triplicate. After 24 hours of exposure, the media containing unbound NPs were transferred into a fresh tube. Then, the cells were washed gently with DPBS (0.5 ml) and the washing solution residue was added to the same tube of the media containing unbound NPs. Cells were then trypsnised (0.3 ml) and centrifuged at 13,000 rpm for 5 minutes at 4°C. Cell pellets were acid digested with (1 ml)

aqua regia, HCl: HNO_3 (3:1). Media containing unbound NPs (1 ml) were also acid digested by adding aqua regia (1 ml). The same steps were followed as described in the standard curve sample preparation.

2.2.2.6 Mechanisms of AgNPs and AuNPs toxicity

2.2.2.6.1 CellROX™ deep red reagent for oxidative stress detection: ROS measurement

Assay principle: The level of ROS in live cells was measured using CellROX™ deep red reagent. The CellRox reagent is a cell-permeable, non-fluorescent dye that generates a robust fluorescent signal upon its oxidation in the presence of ROS.

Experimental protocol: MRC-5 and A549 cells were seeded in 12-well plate at a density of 1×10^5 cells/well in 1.5 ml of cell culture medium and allowed to adhere overnight in 5% CO_2 at 37°C. The cells were then treated with several concentrations of AgNPs of different sizes (7.5, 10, and 12.5 µg/ml) and AuNPs of different sizes (26, 36, and 41 µg/ml) for 24 hours. Menadione was incubated with the cells for 1 hour at a final concentration of 50 µM as a positive control. Following 24 hours incubation, cells were collected by cell trypsinisation and centrifuged at 1,500 rpm for 10 minutes at 4°C. As manufacturer instructed, cells were stained with CellRox deep red reagent (1 ml) at a final concentration of 5 µM in RPMI 1640 medium (phenol-free) for 1 hour at 37°C, protected from light. Cells were then centrifuged at 1,500 rpm for 10 minutes at 4°C, and re-suspended in RPMI 1640 medium (1 ml) for analysis. Around 10,000 events were measured on the BD LSRFortessa X20 cell analyser. The maximum excitation and emission spectra for CellRox deep red reagent were 640/665 nm. Three separate experiments were carried-out. The elicited data were analysed on FlowJo software (v10.6.1).

2.2.2.6.2 GSH/GSSG-Glo™ assay: glutathione measurement

Assay principle: GSH/GSSG-Glo™ Assay is a luminescence-based assay that measures the amount of reduced and oxidised glutathione (GSH and GSSG, respectively) in live cells. The assay is performed based on two reactions. The first reaction quantifies the total glutathione (GSH + GSSG) by adding a reducing agent to convert the whole cellular glutathione into the reduced form. The second reaction measures the GSSG alone by adding a blocking reagent (N-Ethylmaleimide) that reacts with GSH forming a non-luminescent product. The final step is to calculate the GSH/GSSG ratio based on the luminescence signal obtained from both reactions.

Experimental protocol: MRC-5 and A549 cells were seeded in a white 96-well plate at a density of 9×10^3 and 7×10^3, respectively in 0.1 ml of cell culture medium and allowed to attach overnight in 5% CO_2 at 37°C. Both cells were then treated with several concentrations of AgNPs of different sizes (7.5, 10, and 12.5 µg/ml) and AuNPs of different sizes (26, 36, and 41 µg/ml) for 24 hours. Menadione (50 µM) used as a positive control which was incubated with the cells for 1 hour. After 24 hours incubation, the media containing NPs were removed, and the cells were washed with DPBS to remove any left absorbed NPs. As manufacturer instructed, cells were divided into two groups based on the reaction. A total glutathione lysis reagent (50 µl/well) was added to the first group and oxidised glutathione lysis reagent (50 µl/well) was added to the second group. The plate was placed on a shaker for 5 minutes at room temperature. Luciferin generation reagent (50 µl/well) was added to both groups with gentle shaking and incubated for 30 minutes at room temperature. The final step was adding luciferin detection reagent (100 µl/well) to both groups with gentle shaking and incubating for 15 minutes at room temperature. Luminescence light was measured on the multi-mode

microplate reader. The experiment was repeated twice, and the GSH/GSSG ratio was calculated from the generated luminescent signal light (RLU) using the following equation:

$$\text{GSH/GSSG ratio} = \frac{\text{(Net RLU of treated total glutathione – Net RLU of treated GSSG)}}{\text{(Netl RLU of treated GSSG /2)}}$$

2.2.2.6.3 Alexa Fluor® 488 Annexin V/Dead Cell Apoptosis assay: apoptosis cell death detection

Assay principle: The mode of cell death was investigated using an Alexa Fluor® 488 Annexin V/Dead Cell Apoptosis kit. Two stains were used to distinguish between apoptotic and necrotic cell populations. Alexa Fluor® 488 annexin V dye expresses high binding affinity to the outer layer phosphatidyl serine (PS), indicating cell apoptosis. Propidium iodide (PI) is a cell-impermeable dye for intact cells but PI stain intercalates DNA of compromised cell membrane indicating cell necrosis.

Experimental protocol: MRC-5 and A549 cells were seeded in 12-well plate at a density of 1×10^5 cells/well in 1.5 ml of cell culture medium and allowed to adhere overnight in 5% CO_2 at 37°C. The cells were then treated with several concentrations of AgNPs of different sizes (7.5, 10, and 12.5 µg/ml) and AuNPs of different sizes (26, 36, and 41 µg/ml) for 24 and 48 hours. Cells were incubated with (10%) DMSO for 24 hours and Staurosporine (1µM) for 6 hours as the positive necrotic and apoptotic controls, respectively. Cells were detached and centrifuged at 1,500 rpm for 10 minutes at 4°C. As manufacturer instructed, cells were re-suspended in Annexin binding buffer (1X-100 µl). PI (1 µl) and Alexa Fluor® 488 Annexin V (5 µl) dyes were both added to the cell suspension and incubated for 15 minutes at room temperature, protected from light. Prior to analysis, the samples were diluted by adding the Annexin binding buffer (1X-400 µl). The samples were assessed on the BD LSRFortessa X20

cell analyser by measuring 10,000 cells. To avoid signal overlap between the emission spectra of the two stains, electronic compensation was performed. The maximum excitation and emission spectra of Alexa Fluor® 488 Annexin V stain were 488/499 nm, and for the PI stain were 535/617 nm. Three separate experiments were carried-out. The elicited data were analysed on FlowJo software (v10.6.1).

2.2.2.6.4 MitoProbe™ TMRM assay by Flow Cytometry: mitochondrial membrane potential health assessment

Assay principle: The cellular mitochondrial membrane potential health was measured using a MitoProbe™ TMRM Kit for Flow Cytometry. Tetramethylrhodamine, methyl ester (TMRM), is a fluorescent cationic lipid soluble dye that accumulates in hyperpolarised mitochondria in healthy cells expressed by a bright signal. Disruption in the mitochondrial membrane potential of damaged cells exhibits a decrease in the TMRM signal.

Experimental protocol: MRC-5 and A549 cells were seeded in 12-well plate at a density of 1×10^5 cells/well in 1.5 ml of cell culture medium and allowed to adhere overnight in 5% CO_2 at 37°C. The cells were then treated with several concentrations of AgNPs of different sizes (7.5, 10, and 12.5 µg/ml) and AuNPs of different sizes (26, 36, and 41 µg/ml) for 24 hours. Carbonyl cyanide 3-chlorophenylhydrazone (CCCP) is a potent mitochondrial membrane depolarisation inducer and was used in this experiment as a positive control. CCCP was added to cell-free of NPs at a final concentration of 50 µM for 5 minutes in 5% CO_2 at 37°C. After exposure, the cells were detached and centrifugated at 1,500 rpm for 10 minutes at 4°C. As manufacturer instructed, cells were re-suspended in cell culture medium (1 ml) and TMRM reagent solution was added on each sample at a final concentration of 20 nM for 30 minutes in 5% CO_2 at 37°C. The cells were centrifuged at 1,500 rpm for 5 minutes at 4°C, and re-suspended in DPBS (0.5 ml) for analysis. The samples were analysed by the BD LSRFortessa

X20 cell analyser, counting 10,000 events per sample. The TMRM reagent was excited at 561 nm with an approximate maximum emission wavelength of 585 nm. Three separate experiments were carried-out. The elicited data were analysed on FlowJo software (v10.6.1).

2.2.2.6.5 FxCycle™ PI/RNase Staining Solution assay: cell cycle progression analysis

Assay principle: The cellular DNA content was quantified using FxCycle™ PI/RNase Staining Solution. The PI reagent emits fluorescence through binding to DNA. A histogram was elicited by flow cytometry based on PI dye intensity quantification. The cell distribution was demonstrated in three cell cycle phases (G1, S, and G2). Cells in the S phase express a brighter signal than in the G1 phase. Cells in the G2 phase, the period following the DNA synthesis show twice the intensity of cells in the G1 phase. PI dye may also bind to RNA; therefore, the staining solution contains RNase to degrade RNA.

Experimental protocol: MRC-5 and A549 cells were seeded in 12-well plate at a density of 1×10^5 cells/well in 1.5 ml of cell culture medium and allowed to adhere overnight in 5% CO_2 at 37°C. The cells were then treated with several concentrations of AgNPs of different sizes (7.5, 10, and 12.5 µg/ml) and AuNPs of different sizes (26, 36, and 41 µg/ml) for 24 and 48 hours. Topotecan (1 µM) and Etoposide (10 µM) which arrested the cell cycle at G1/S and G2/M phases , respectively, were used as positive controls in this experiment following 24 hours incubation with cells. At each exposure time, the cells were detached using trypsin and collected in a fresh tube. The samples were spun at 1,500 rpm for 10 minutes at 4°C. Cell pellets were re-suspended in ultrapure water (0.25 ml). To fix the cells, cold 70% ethanol (2 ml) was added dropwise to each sample with gentle vortexing of the cells. Following that, the samples were stored at 4°C until the time of samples analysis. The cells were then harvested and washed once with DPBS. As manufacturer instructed, the cell pellet was stained by adding

FxCycle™ PI/RNase staining solution and incubated for 30 minutes at room temperature, protected from light. Around 10,000 events of each sample were counted using the BD LSRFortessa X20 cell analyser. The approximate maximum excitation and emission fluorescence wavelengths of the staining solution (PI) were 535/617 nm. Three separate experiments were carried-out. The elicited data were analysed on FlowJo software (v10.6.1).

2.2.2.6.6 mLDH assay: Cell recovery post AgNPs and AuNPs treatment

Assay principle: The cells ability to survive and resume normal proliferation following exposure to toxic concentrations of NPs for 1 day was examined by investigating the percentage of cell viability of treated cells compared to the untreated group.

Experimental protocol: MRC-5 and A549 cells were seeded in 96-well plate at a density of 9×10^3 and 7×10^3 cells/well, respectively in 0.1 ml of cell culture medium and allowed to adhere overnight in 5% CO_2 at 37°C. Both cells were then treated with AgNPs of different sizes at a concentration range of 5–12.5 µg/ml and AuNPs of different sizes at a concentration range of 26–41 µg/ml for 1 day. After 1 day, the medium was discarded, and the cells were gently washed with DPBS to remove unbound AgNPs and AuNPs. Fresh medium was added to the cells and incubated for 1, 2, and 3 days. The medium was changed again after 1.5 day. At each time point of cells recovery, the cell viability was measured using mLDH assay following the same protocol described in section 2.2.2.3.

2.2.3 Toxicological assessment of AgNPs and AuNPs of different sizes in 3D *in vitro* cell culture model

2.2.3.1 Spheroids preparation

3D lung multicellular tumour spheroids were prepared using the liquid overlay method (Metzger et al., 2011). The 96-well plate was pre-coated with sterile 1% agar dissolved in

water (50 µl/well). A549 cells were then seeded in 96-well plate at a density of 8×10^3 cells/well in 0.1 ml of cell culture medium and incubated for 7 days in 5% CO_2 at 37°C. A549 spheroids were imaged every day for 7 days using an optical microscope. The growth curve of spheroids was calculated by measuring spheroid circumference sizes using ImageJ software (version 2.0.0).

2.2.3.2 Spheroids morphology and size changes

A549 spheroids were prepared as previously describe in section 2.2.3.1. At day 4, the spheroids were treated with Ag10 and Ag80 (5 and 12.5 µg/ml), and Au10 and Au80 (26 and 41 µg/ml) for 24 and 48 hours. (20%) DMSO was used as a positive control. At each exposure time, the changes in spheroid integrity were imaged using optical microscopy. The circumference size of at least 20 spheroids was calculated before and after exposure to AgNPs and AuNPs by ImageJ software (version 2.0.0).

2.2.3.3 LIVE/DEAD™ cell imaging assay: spheroids cytotoxicity assessment

Assay principle: The cytotoxicity of NPs on spheroids was measured using LIVE/DEAD™ cell imaging assay. A green fluorescent cell-permeable dye emits fluorescence upon dye conversion by intracellular esterase. A bright green fluorescent signal indicates live cells. In contrast, a red fluorescent cell-impermeable dye emits fluorescence once the dye binds to DNA. A strong red fluorescent signal indicates membrane-compromised dead cells.

Experimental protocol: A549 spheroids were treated on day 4 with Ag10, Ag80 at concentrations of 5 and 12.5 µg/ml, and Au10, Au80 at concentrations of 26 and 41 µg/ml for 48 hours. At least 16 spheroids per treatment were centrifuged at 1,000 rpm for 2 minutes at 4°C. The media was then carefully discarded to avoid disruption of spheroids. Spheroids were then re-suspended in DPBS (100 µl) and gently transferred to 8-chamber culture slides (Falcon

Fisher Scientific, Loughborough, UK). As manufacturer instructed, the spheroids were stained with a staining mixture and incubated for 15 minutes at 20°C, protected from light. Stained spheroids were immediately imaged using a confocal laser microscope Zeiss LSM 780 (Carl Zeiss Microscopy, Jena, Germany). The excitation and emission maxima of the green fluorescent dye were 488/515 nm and for the red fluorescent dye were 570/602 nm.

2.2.4 Impacts of AgNPs and AuNPs of different sizes on cell signalling pathways

2.2.4.1 Western blot technique: protein detection

Assay principle: Western blot is a semi-quantitative technique used to investigate specific proteins from a complex mixture of cell lysate. Proteins are separated based on their molecular weight by SDS-polyacrylamide gel electrophoresis (SDS-PAGE). The separated proteins are then transferred into a nitrocellulose membrane, which was detected by a specific primary antibody to the target protein. Then secondary antibody binds to the primary antibody, which conjugated with Horseradish Peroxidase (HRP) enzyme that generates luminescence upon adding enhanced chemiluminescence to the membrane.

Experimental protocol: MRC-5 and A549 cells were seeded in 6-well plate at a density of 5×10^5 cells/well in 3 ml of cell culture medium and allowed to adhere overnight in 5% CO_2 at 37°C. Both cells were then treated with AgNPs of different sizes at a concentration range of 1.25–10 µg/ml and AuNPs of different sizes at a concentration range of 16–41 µg/ml. After 24 hours incubation, the media was discarded and the cells were lysed on an ice plate using cold NP40 lysis buffer (100 µl) containing a protease inhibitor mixture (**Table 2.4**). Radioimmunoprecipitation assay (RIPA) lysis buffer (100 µl) was used to lyse cells of membrane proteins. Cell lysates centrifuged at 10,000 rpm for 10 minutes at 4°C. Supernatants were collected, and the total protein concentrations were measured using the Bradford assay

as described in section 2.2.4.2. Resolving (**Table 2.5**) and stacking (**Table 2.6**) gels were prepared to load the protein samples. The percentage of resolving gel was prepared according to the molecular weight of the protein of interest. Cell lysate samples were loaded (20 µg/20 µl) on SDS-polyacrylamide gel to separate the proteins by electrophoresis and run the gel at 180 V for 1 hour in running buffer (**Table 2.4**). The protein ladder (5 µl) was loaded as a marker of molecular weight size. Then the proteins were transferred from the gel to nitrocellulose membrane (Amersham Pharmacia Biotech K.K., UK) at 85 V for 1.5 hour in transfer buffer (**Table 2.4**). Nitrocellulose membranes were stained with Ponceau stain and washed with ultrapure water. Membrane blocking was performed as the following step for 1 hour using blocking buffer (**Table 2.4**), and then washed with Tris-buffered saline and Tween 20 (TBST) buffer (**Table 2.4**). Membranes were incubated with a primary antibody of the protein of interest at certain dilutions, according to the supplier instructions, and incubated overnight at 4°C with gentle shaking. To remove nonspecific binding of the antibody, the membranes were washed with TBST buffer and then incubated for 1 hour with Antirabbit-IgG, HRP-linked secondary antibody at 25°C with gentle agitation. Membranes were washed again with TBST buffer, and then enhanced chemiluminescence (ECL) was added on the membrane to develop signals that visualised and imaged on G: Box Chemi XRQ (Syngene, Cambridge, UK). The intensity of developed bands in different lanes was quantified using the ImageJ software (version 2.0.0). Glyceraldehyde 3-phosphate dehydrogenase (GAPDH) was used as a loading in all experiments unless otherwise specified. All experiments were repeated at least twice.

Different primary antibodies were assessed and diluted based on the manufacturer's instruction. The following are the antibodies used in this study, including the dilution and product code provided by cell signalling technology (Beverly, MA, USA): AKT (1:1000,

C67E7), Antirabbit-IgG, HRP-linked antibody (1:2000, 7074), Dvl2 (1:1000, 30D2), β-Catenin sampler kit (1:1000, 2951T), β-Catenin (1:1000, D10A8), β-Tubulin (1:1000, 9F3), GAPDH (1:5000, D16H11), GSK-3β (1:1000, 27C10), Lamin B1 (1:100, D4Q4Z), LRP6 (1:100, C47E12), mTOR (1:1000, 7C10), PDK1 (1:1000, 5662S), Phospho-c-Raf (Ser259) (1:1000, 9421T), Phspho-GSK-3β (Ser9) (1:1000, D85E12), Phospho-PDK1 (Ser241) (1:1000, C49H2), PTEN (1:1000, 138G6), N-Cadherin (1:100, D4R1H), and non-phospho (Active) β-Catenin (Ser33/37/Thr41) (1:1000, D13A1).

Table 2.4. Western blot buffers.

Buffer	**Component**
Running buffer	190 mM glycine, 25 mM Tris-base and 34.6 mM SDS
Transfer buffer	39 mM glycine,48 mM Tris-base and 20% (v/v) methanol
Blocking buffer	5% (w/v) non-fat dry milk dissolved in TBST
Washing buffer -TBST	150 mM NaCl, 50 mM Tris-base (pH=8.3) and 0.2% (v/v) Tween-20
NP40 lysis buffer	1% (v/v) NP40, 50 mM Tris-HCl (pH= 7.5), 1 mM EGTA, 1 mM EDTA, 1 mM Na orthovanadate, 50mM Na fluoride, 5 mM Na pyrophosphate and 0.27M sucrose
Protease inhibitors	0.1 mM PMSF, 1 mM Benzamidine and 0.1% (v/v) 2-mercaptoethanol
Cytoplasmic buffer	10 mM HEPES, 6o mM KCl, 1mM EDTA, 0.075% (v/v) NP40, 1 mM DTT and 1 mM PMSF
Cytoplasmic buffer without detergent	10 mM HEPES, 6o mM KCl, 1mM EDTA, 1 mM DTT and 1 mM PMSF
Nuclear buffer	50 mM HEPS, 250 mM KCl, 0.1 mM EDTA, 0.1 mM EGTA, 0.1% (v/v) NP40, 0.1% Glycerol, 10 mM Na fluoride, 10 mM Na orthovanadate, 1 mM DTT

Table 2.5. Resolving gel preparation (15 ml).

Component	10%	15%
1.5 M Tris (pH= 8.8)	5 ml	5 ml
30% acrylamide	4 ml	7.5 ml
Water	5.9 ml	2.4 ml
20% SDS	75 µl	75 µl
10% APS	75 µl	75 µl
TEMED	25 µl	25 µl

Table 2.6. Stacking gel preparation (5 ml).

Component	Amount
0.5 M Tris (pH= 6.8)	0.62 ml
30% acrylamide	0.833 ml
Water	3.82 ml
20% SDS	25 µl
10% APS	50 µl
TEMED	5 µl

2.2.4.2 Bradford assay: protein concentration measurement prior to western blotting

Cell lysates were loaded in a non-sterile 96-well plate in triplicate. Bovine serum albumin (BSA) was used as the protein standard at a concentration range of 0.125- 1 mg/ml. BSA standards were loaded at a volume of 5 µl/well, and cell lysate samples were loaded at a volume of 2 µl/well. Bradford reagent was then added to all wells (280 µl/well). The absorbance of 595 nm was detected on the plate reader and the sample was prepared at a concentration of 1 mg/ml in sodium dodecyl sulphate (SDS). Samples were heated at 90°C for 5 minutes to denature protein and stored at -20°C.

2.2.4.3 Cytoplasmic/nuclear localisation of β-catenin

The cytoplasmic and nuclear fractions of MRC-5 cells treated with Ag10 were separated to detect the β-catenin protein expressions present in both cytoplasm and nucleus. MRC-5 cells were seeded in T75 flask at a density of 4.5×10^6 cells per sample in 10 ml of cell culture medium. Cells were exposed to Ag10 at concentrations of 2.5, 5, and 10 µg/ml for 24 hours.

As illustrated in **Figure 2.1**, the media was aspirated and cold DPBS (10 ml) was added to the cells and gently detached using a scraper. Cell suspensions were centrifuged at 1,500 rpm for 10 minutes at 4°C. Cytoplasmic lysis buffer (250 µl) (**Table 2.4**), was added to cell pellets and incubated for 20 minutes on ice with periodic agitation. Cell lysates were centrifuged at 7,000 rpm for 10 minutes 4°C. The supernatants, cytoplasmic lysate, were transferred into a fresh cold microcentrifuge tube and kept on ice. Cell pellets were washed with cytoplasmic buffer without detergent (200 µl) (**Table 2.4**) and centrifuged at 7,000 rpm for 10 minutes at 4°C. Cell pellets containing cell nucleus were then lysed by adding nuclear lysis buffer (140 µl) (**Table 2.4**) and incubated on ice for 40 minutes with periodic agitation. Nuclear and cytoplasmic cell lysates were centrifuged at 13,000 rpm for 30 minutes at 4°C. The total protein concentration was measured by the Bradford assay as described in section 2.2.4.2. Western blot was performed as described in section 2.2.4.1, and three separate experiments were carried-out.

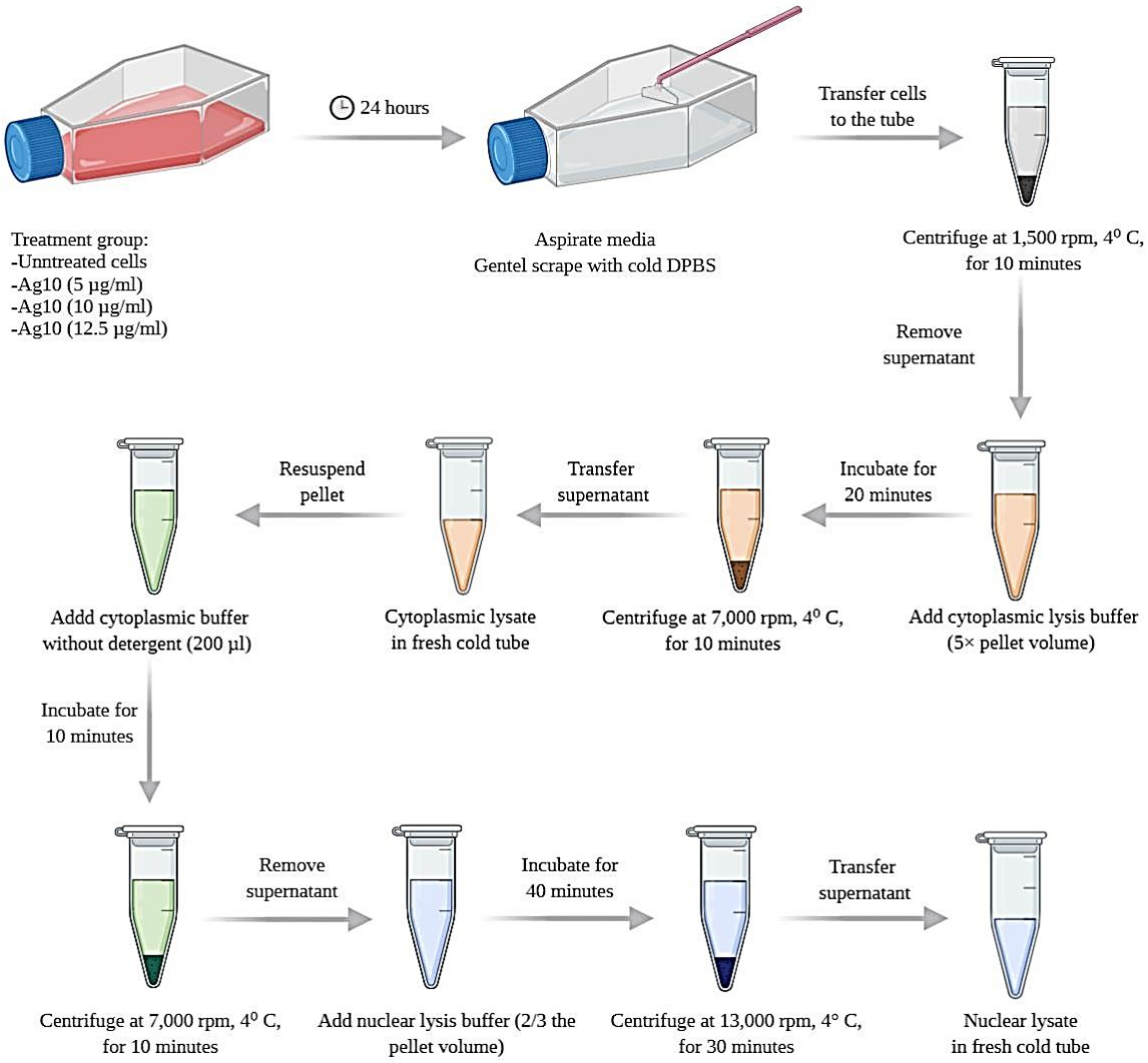


Figure 2.1. Schematic flow chart of cytoplasmic and nuclear fractions sample preparation. Scheme generated with BioRender.com.

2.2.4.4 Immunohistochemistry analysis (IHC) of β-catenin expression

MRC-5 cells were seeded in 8-well chambered slides at a density of 25×10^3 cells in 0.5 ml of cell culture medium and incubated overnight to adhere in 5% CO_2 at 37°C. Cells were treated with Ag10 at a concentration range of 2.5- 10 µg/ml for 24 hours. (4%) paraformaldehyde (500 µl) was used to fix the cells for 10 minutes at room temperature. Cells were then washed with DPBS three times for 10 minutes. (3%) BSA and (0.1%) Triton X-100 were used to block the cells for 10 minutes at room temperature. After three washes with DPBS for 10 minutes, cells were incubated with β-catenin antibody diluted in DPBS containing (3%) BSA (1:400) for 1 hour at room temperature. After three washes with DPBS for 10 minutes , the cells were incubated with Goat antirabbit conjugated to Alexa Fluor 594 (Molecular Probes, Eugene, OR, USA) diluted in DPBS containing (3%) BSA (1:400) for 1 hour at room temperature. The cells were then washed three times with DPBS for 10 minutes to remove unbound antibodies and mounted in vectashield with DAPI. The slides were imaged using a confocal laser microscope Zeiss LSM 780 at excitation and emission spectra of 360/460 nm for DAPI and 594/617 for labelled-β-catenin.

2.2.4.5 Wnt/β-catenin pathway activation by Lithium Chloride (LiCl)

LiCl activates Wnt/β-catenin pathway by the direct inhibition of GSK-3β activity (Xia et al., 2017a). In this experiment, Wnt/β-catenin pathway was activated in the cells by LiCl prior exposure to Ag10 in order to investigate the Ag10 potential to inhibit Wnt/β-catenin pathway. MRC-5 cells were seeded in 6-well plate at a density of 5×10^5 cells/well in 3 ml of cell culture medium and incubated overnight in 5% CO_2 at 37°C. Cells were treated with LiCl (20 mM), Ag10 (5, 10 and 12.5 µg/ml) for 24 hours (**Figure 2.2-A**). Other group of cells were exposed to LiCl and then to Ag10 as shown in **Figure 2.2-B**, in follows: cells treated with LiCl (20

mM) for 12 h then fresh media was added for 24 hours and cells treated with LiCl (20 mM) for 12 hours were exposed to Ag10 (5, 10 and 12.5 µg/ml) for 24 hours. Following the desired incubation, the cells were lysed using NP40 lysis buffer and western blot analysis was performed as previously described in section 2.2.4.1.

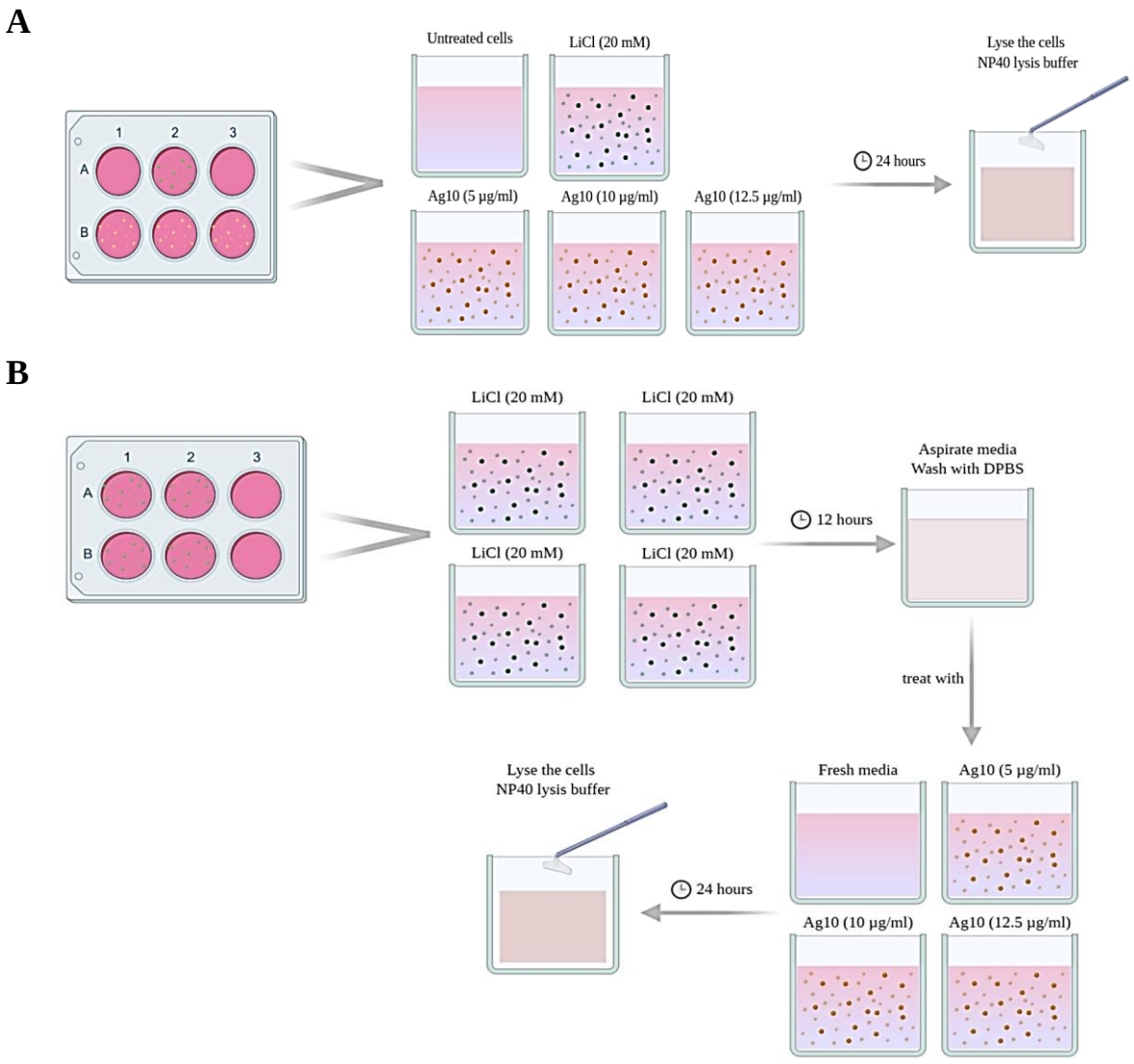


Figure 2.2. Schematic flow chart of cells treated with LiCl and Ag10. Scheme generated with BioRender.com.

2.2.4.6 Wnt/β-catenin pathway activation by Wnt agonist I

Wnt agonist I induces Wnt/β-catenin pathway without interfering with GSK-3β activity (Liu et al., 2005). In this experiment, Wnt/β-catenin pathway was activated in the cells by Wnt agonist I prior exposure to Ag10 in order to investigate the Ag10 potential to inhibit Wnt/β-catenin pathway. MRC-5 cells were seeded at in 6-well plate at a density of 5×10^5 cells/well in 3 ml of cell culture medium and allowed to adhere overnight in 5% CO_2 at 37°C. The cells were then treated for 24 hours with the following: Wnt agonist I (10 µM), Wnt agonist I (25 µM) and Ag10 (10 µg/ml) (**Figure 2.3-A**). Other cells were exposed to Wnt agonist I and then treated with Ag10 as shown in **Figure 2.3-B**, cells were exposed to Wnt agonist I (10 and 25 µM) for 12 hours were treated with Ag10 (10 µg/ml) for 24 hours. Following the desired incubation, the cells were lysed using NP40 lysis buffer and western blot analysis was performed as previously described in section 2.2.4.1.

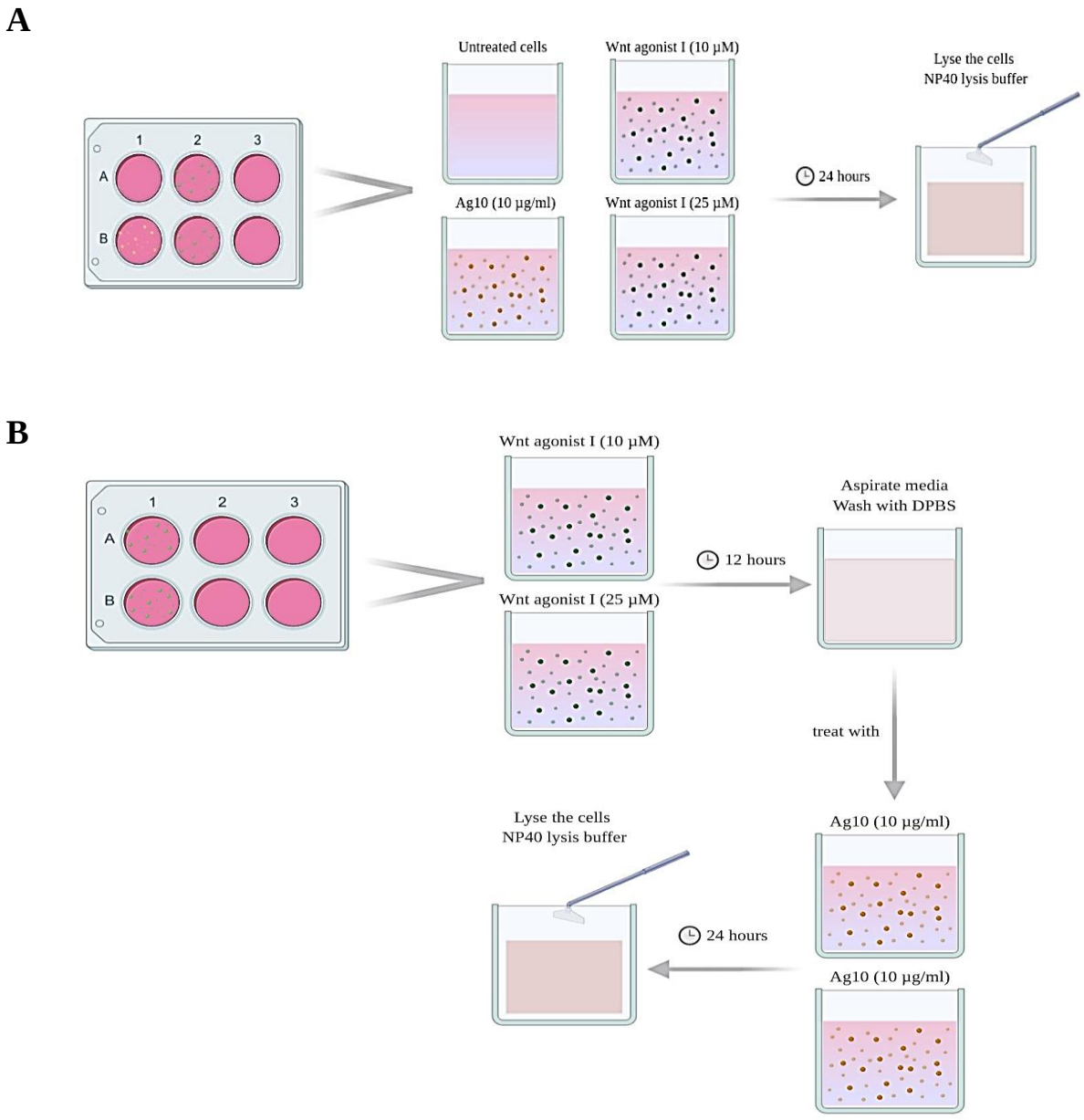


Figure 2.3. Schematic flow chart of cells treated with Wnt agonist I and Ag10. Scheme generated with BioRender.com.

2.2.5 Statistical data analysis

The data presented were analysed using GraphPad Prism software Version 8.1.2 (San Diego, CA, USA). All experiments were carried out at least for three independent times, unless otherwise specified, and displayed in all graphs as mean values ± standard deviation (SD). One-way and two-way ANOVA with Tukey's Post-Hoc test for multiple comparisons were used based on the type of data of multiple variances. Statistical significance differences between treatment group and untreated group were expressed as (*) $p < 0.05$; (**) $p < 0.002$; (***) $p < 0.0002$ and (****) $p < 0.0001$. Statistical significance differences between different treatments were expressed as a = $p < 0.05$ versus cells incubated with the same concentration of Ag10 or Au10; b = $p < 0.05$ versus cells incubated with the same concentration of Ag40 or Au40 and c = $p < 0.05$ versus cells incubated with the same concentration of Ag80 or Au80.

Chapter 3

Toxicological assessment of AgNPs of different sizes

3.1 Introduction

AgNPs are largely incorporated in many industrial products and intensively explored for various biomedical applications because of their powerful characteristics (Foss Hansen et al., 2016). However, safety concerns have been grown over the usage of AgNPs as they exhibit potential health risk (Chawla et al., 2018). The role of nanotoxicological studies is to examine NPs to determine their benefits versus their role in inducing cell injury and adverse signalling events. In this work, systematic assessments were performed to study the impact of AgNPs size in underlying toxicity in the lung cell culture model. It was crucial at the beginning to characterise the AgNPs using different methods including TEM and DLS to confirm the properties and more specifically the size of the purchased AgNPs. The next section of the chapter focuses on the toxicity assessments of AgNPs in the 2D monolayer cell culture model. Several toxicity assays were performed such as mLDH, MTT and Annexin V/PI assays to gain more understanding on the toxicity effect that can be associated with the size of AgNPs. It was also of interest to compare the influence of AgNPs size on the cytotoxicity in 2D monolayer and 3D multicellular spheroid cell culture models.

3.2 Characterisations of AgNPs of different sizes

Different NPs physiochemical properties can trigger diverse behaviours upon their interaction with cells (Sukhanova et al., 2018, Luyts et al., 2013). Therefore, to study the toxicity of the NPs, the key tool is to first determine the characteristic of the NPs. The aim of this subsection was to characterise the purchased AgNPs with size of 10, 40 and 80 nm using different approaches in order to assess their size, morphology, surface charge, and stability in cell culture medium.

3.2.1 Results and discussion

3.2.1.1 Size measurement

The size of the AgNPs were characterised using different techniques, including TEM, DLS, and ultraviolet-visible (UV-Vis) spectroscopy. TEM was used to determine the morphology and particle size distribution of the three AgNPs sizes. The microscopic images revealed the spherical shape of AgNPs (**Figure 3.1**). The size distribution was estimated by measuring the particles diameter and counting of at least 200 particles using Image J software (version 1.52a). As shown in **Figure 3.1 A-C**, the calculated average sizes of Ag10, Ag40 and Ag80 were corresponded to the measured size specified by the manufacture.

Next, the z-average particle size and polydispersity index (PDI) of the spherical AgNPs were analysed using DLS. The z-average size is assessed by measuring the hydrodynamic particle size of the entire population present in the sample. As presented in **Table 3.1**, the reported z-average sizes were within the primary size of AgNPs. The PDI represents the degree of particle heterogeneity in the sample and a PDI value greater than (> 0.7) indicates the heterogenous size distribution of a sample (Hughes et al., 2015, Danaei et al., 2018). Herein, the measured PDI values revealed that AgNPs were uniformly dispersed in the solution (**Table 3.1**).

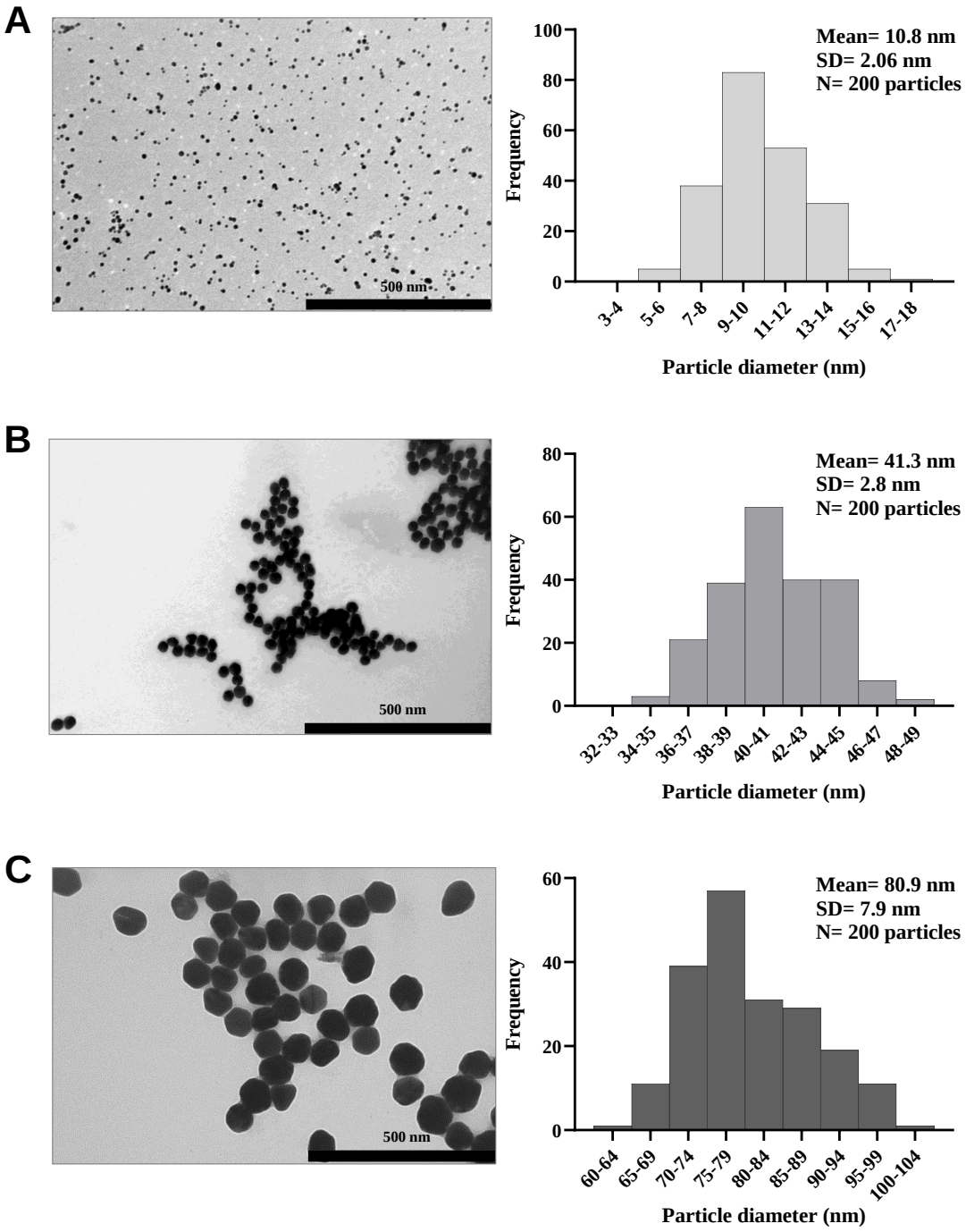


Figure 3.1. TEM micrographs and the size distributions of AgNPs of different sizes. Micrograph images with the size distribution of (**A**) Ag10; (**B**) Ag40 and (**C**) Ag80. The size distribution of AgNPs represents the mean average size ± SD (n= 200 particles) measured by using Image J software.

Table 3.1. Summary the characterisations of AgNPs.

Characterisation	Method	Ag10	Ag40	Ag80
Morphology	TEM	Spherical	Spherical	Spherical
Average size (nm)	TEM	11 ± 2	41 ± 2	81 ± 8
Z-average size (nm)	DLS	10 ± 5	43 ± 2	81 ± 1
PDI	DLS	0.4 ± 0	0.2 ± 0	0.1 ± 0
ζ-potential (mV)	DLS	-32 ± 5	-39 ± 3	-43 ± 6
λ max (nm)	UV-Vis	394	415	465

Symbol: PDI (Poly dispersity index), ζ-potential (zeta potential), λ max (maximum absorption wavelength).

AgNPs exhibit optical properties which able them to interact with light at specific wavelength (Wei et al., 2015). Here, UV-Vis spectroscopy was used to detect the plasmon absorption peak of AgNPs. As demonstrated in **Table 3.1**, the maximum absorption wavelength (λ max) of the AgNPs was red-shifted along with an increase in AgNPs size. The red shift of the absorption spectra is an indication of increasing in the AgNPs sized (Dadosh, 2009). Taking all together, the reported size of AgNPs of three sizes indicated their size stability in dispersion and the sizes were corresponding to the primary size of Ag10, Ag40 and Ag80.

3.2.1.2 Surface charge analysis

The surface charge of AgNPs may impact their cellular internalisation as well as their biological response (Barbasz et al., 2017). The surface charge was analysed by measuring the zeta (ζ) potential. The recorded ζ-potential values were negatively charged for the three sizes of AgNPs (**Table 3.1**). Negative charge is attributed to the presence of sodium citrate coating on the particle surface. The results confirmed the stability of AgNPs dispersion against aggregation, as the ζ-potential values were within the optimal magnitude value, which is more than -30 mV (Lowry et al., 2016). The observed increases in the ζ-potential values with

increasing in AgNPs size can be explained as a result of the higher citrate density on the surface of the larger particles (Nandhakumar et al., 2017).

3.2.1.3 AgNPs stability in cell culture media

In general, the cell culture media consists of different components that provide nutrients to cells, including proteins, sugars, vitamins, and amino acids (Milić et al., 2015). Various factors can significantly influence the potential interaction of AgNPs with the cells, including protein corona and aggregates formation (Cohen et al., 2014). Therefore, it is essential to consider the interaction of AgNPs and cell culture media components to understand any consequence changes in AgNPs size. Herein, the differently sized AgNPs were incubated at 37°C in a cell culture media in the presence or absence of foetal bovine serum (FBS) at a concentration of 10 µg/ml for 30 minutes, 24 hours, and 48 hours.

The hydrodynamic size distributions of AgNPs of the three sizes in an EMEM and Ham's F-12 Nutrient Mixture with serum (10% FBS) were measured using DLS. As shown in **Table 3.2**, the z-average sizes were increased in all three sizes of AgNPs upon their incubation with EMEM including FBS (10%) for 30 minutes and 24 hours. The z-average sizes after 48 hours illustrated a decrease in the sizes, which returned to the primary size of AgNPs. The size measurements of the AgNPs incubated with Ham's F-12 Nutrient Mixture medium with serum (10% FBS) are presented in (**Table A1**), which demonstrated similar changes in the z-average size of AgNPs of different sizes as found in EMEM. The changes in AgNPs sizes could be indicated the development of AgNPs-protein complex. It was suggested that citrate-coated AgNPs can easily interact with the proteins and components of the cell culture media due to the weak binding of the citrate stabiliser with the AgNPs (Milić et al., 2015).

Table 3.2. The stability of AgNPs in EMEM with or without (10%) FBS by measuring the size using DLS.

Z-average sizes of AgNPs in EMEM with (10%) FBS						
AgNPs	**30 mins**		**24 hrs**		**48hrs**	
	Size	**PDI**	**Size**	**PDI**	**Size**	**PDI**
Ag10	55 ±1	0.4 ±0	40 ±3	0.7 ±0	14 ±0	0.5 ±0
Ag40	62 ±1	0.2 ±0	63 ±1	0.2 ±0	38 ±1	0.2 ±0
Ag80	121 ±3	0.1 ±0	132 ±1	0.1 ±0	82 ±0	0.07 ±0
Z-average sizes of AgNPs in EMEM without (10%) FBS						
AgNPs	**30 mins**		**24 hrs**		**48hrs**	
	Size	**PDI**	**Size**	**PDI**	**Size**	**PDI**
Ag10	1574 ±154	0.7 ±0	3090 ±512	0.5 ±0.3	9120 ±708	0.8 ±0
Ag40	1862 ±108	0.6 ±0	4120 ±99	0.5 ±0.3	2360±227	0.9 ±0
Ag80	1842 ±52	1 ±0	4814 ±137	0.6 ±0.5	4342 ±220	1 ±0

Furthermore, the z-average sizes of the AgNPs in the EMEM without serum (10% FBS) were measured. The reported average sizes of AgNPs of the three sizes were above 1,000 nm with high PDI values between 0.4-1 (**Table 3.2**). The precipitation and aggregation of the AgNPs were clearly observed after AgNPs incubation with EMEM media without serum. This could be due to the presence of ionic salts such as sodium pyruvate and sodium bicarbonate in high concentrations with low concentration of proteins and amino acids in the cell culture medium (Allouni et al., 2009). The presence of FBS in the cell culture medium helps to stabilise the AgNPs by formation of protein corona (Gliga et al., 2014). The stability of AgNPs-protein binding is dependent on the binding energies which may form soft or hard corona (Casals et al., 2010). Following characterisations of AgNPs, the next goal of this study was to investigate the impact of AgNPs size in a 2D *in vitro* cell culture model. The following section is devoted to studying and discussing the toxicity of AgNPs of different sizes.

3.3 Toxicological assessment of AgNPs of different sizes in a 2D in vitro cell culture model

The toxicity profile of AgNPs can be greatly influenced by their different sizes (Sukhanova et al., 2018). The aim of this section was to study the impact of AgNPs size in eliciting diverse biological responses and subsequent toxicity in 2D *in vitro* cell culture models. Systematic toxicity studies were conducted, beginning with a biocompatibility assessment that investigated the cytotoxicity effect of three different sizes of AgNPs in healthy and cancerous lung cells with measuring the 50% cytotoxic concentration (CC50) value of each size of AgNPs. Then, the underlying mechanisms of toxicity of AgNPs were investigated including the induction of apoptosis, mitochondrial dysfunction, oxidative stress, and cell cycle arrest.

3.3.1 Results and discussion

3.3.1.1 Cell viability assessment of sodium citrate stabiliser

The AgNPs dispersions used in this study were stabilised with sodium citrate (2 mM). Therefore, the potential cytotoxic effect of sodium citrate coating on cells needs to be considered. Herein, the toxic effect of sodium citrate was investigated to confirm that the observed toxicity induced by AgNPs themselves not the coating.

First, a cytotoxicity study was performed using a modified lactate dehydrogenase (mLDH) assay. Herein, the modified version of LDH assay was used as an indirect method to assess cytotoxicity instead of the conventional method to be consistent with the toxicity assay used in AgNPs and to easy correlate the observed toxicity of citrate to AgNPs toxicity in the next subsection. Both MRC-5 and A549 cells were treated with 1mM of sodium citrate which was equivalent to using 10 µg/ml of AgNPs in stabiliser. The results revealed no considerable toxicity can be associated with the exposure of sodium citrate at concentration of 1 mM to

both cell lines for 24 and 48 hours with cell viability detected between 98% to 88% (**Figure 3.2 A and B**).

Another cell viability method was conducted using a LIVE/DEAD™ assay. This assay was used as a direct method to assess the cytotoxicity of sodium citrate which measures the live and dead cells. Different concentrations of sodium citrate were tested for cytotoxicity to identify the maximum safe concentration of sodium citrate. MRC-5 cells were exposed for 24 hours to sodium citrate at concentrations of 1.25, 1.5, and 1.7 mM which were equivalent to using of 12.5, 15, and 17 µg/ml of AgNPs in stabiliser. The data showed a concentration-dependent toxicity of sodium citrate, in which 40% cell death was detected with the highest concentration of 1.7 mM (**Figure 3.2 C-G**). As can be seen, sodium citrate coating can demonstrate toxicity at certain concentrations. However, the concentrations tested here did not show potential toxicity in the literature (Xia et al., 2018, Lan et al., 1999, Nguyen et al., 2020). The observed reduction of cell viability in this study is most probably due to the use of high volume of sodium citrate to treat the cells, around 85% of total volume at a concentration of 1.7 mM, therefore, the amount of nutrient exposed to cells was limited and this may trigger the cell death. The present results were consistent with a study conducted by Freese et al. (2012), who assumed that cellular exposure to a high level of sodium citrate on AuNPs surface may potentiate the toxicity effect of the AuNPs without influencing the AuNPs uptake rate.

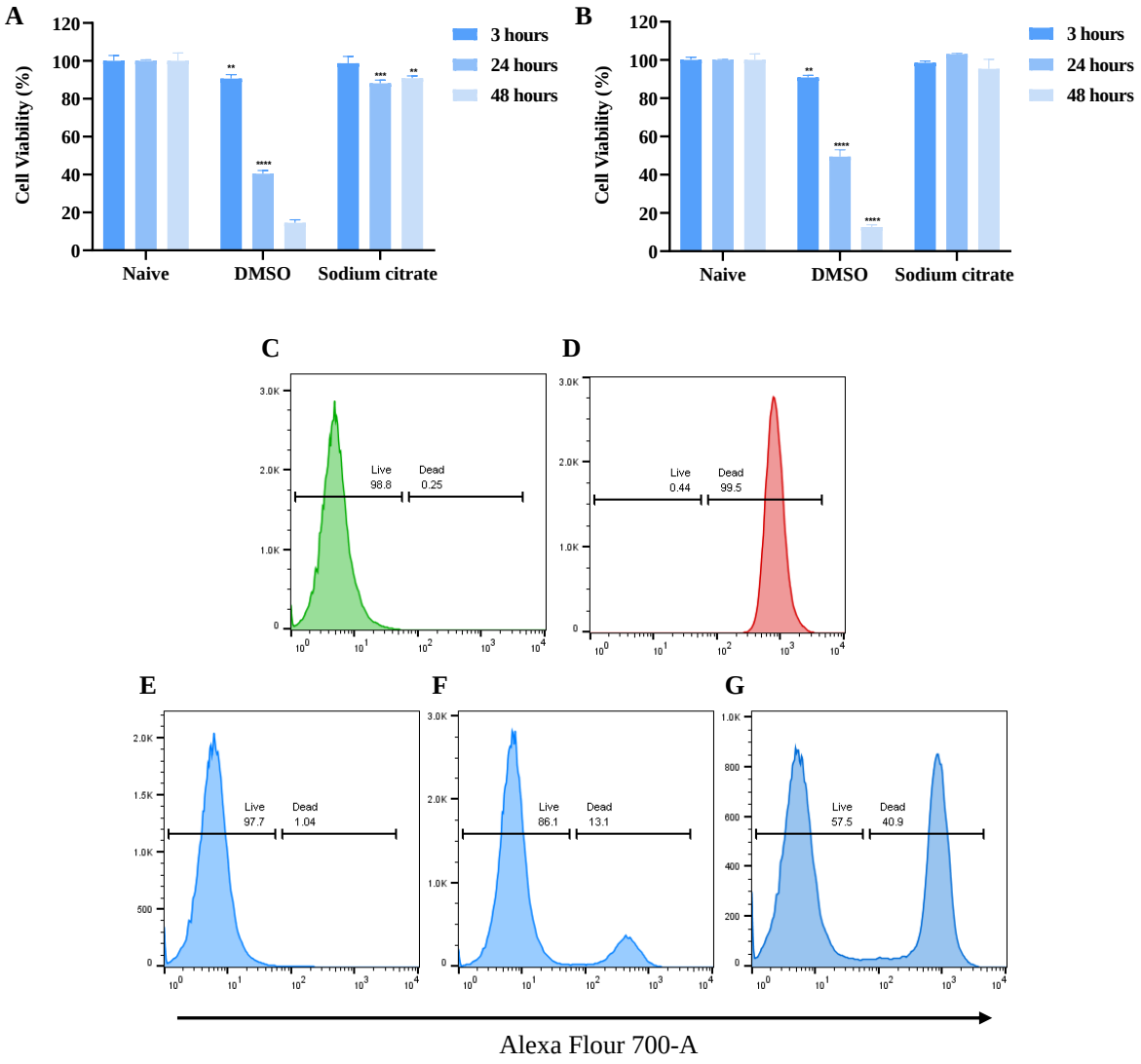


Figure 3.2. Cell viability assessment of MRC-5 and A549 cells treated with sodium citrate. Percentage of cell viability following sodium citrate treatment with concentration of 1 mM for 3, 24 and 48 hours on (**A**) MRC-5; and (**B**) A549 cells. DMSO (20%) used as positive control. Bars represent the mean ± SD (n=3). (**) $p < 0.002$; (***) $p < 0.0002$ and (****) $p < 0.0001$ versus untreated group by ANOVA test. The cell viability was measured using LIVE/DEAD Cell Stain Kit by flow cytometry after treating the MRC-5 cells for 24 hours with different concentrations of sodium citrates as follows: (**C**) untreated cells; (**D**) DMSO (20%) used as positive control; Sodium citrate (**E**) 1.25 mM; (**F**) 1.5mM and (**G**) 1.7 mM.

3.3.1.2 Cell viability assessment of AgNPs of different sizes

The cell viability and metabolic activity were assessed using mLDH and MTT assays to measure the cell viability of AgNPs and to identify their size-, time-, and concentration-dependent toxicity. First the amount of LDH in healthy cells was measured using mLDH assay. The total amount of LDH was expressed as a percentage of the viable cells corresponding to the untreated group. Both MRC-5 and A549 cells were exposed to AgNPs of different sizes with a concentration range between 0.625 to 15 µg/ml for 3, 24, and 48 hours. As illustrated in **Figure 3.3 A and D**, there was no observable toxic effect after 3 hours of MRC-5 and A549 cells incubation with Ag10, Ag40, and Ag80. After longer incubation times (24 and 48 hours), no significant reduction in cell viability was observed at low concentrations (0.625 to 5 µg/ml) of AgNPs of different size exposed to both healthy and cancerous lung cells. The cytotoxicity was relatively increased over longer time of incubations with high concentrations (7.5 to 15 µg/ml) of the three AgNPs sizes (**Figure 3.3**). The cell viability findings indicated that the cytotoxicity effect was dependent on the AgNPs size, concentration and exposure time. Around 30% cell viability was observed at 24 hours of exposure with high concentration of Ag10 and Ag40, whereas 60-75% cell viability was reported with Ag80, demonstrating the higher biocompatibility of larger AgNPs size when compared to the smaller sizes in both cell lines.

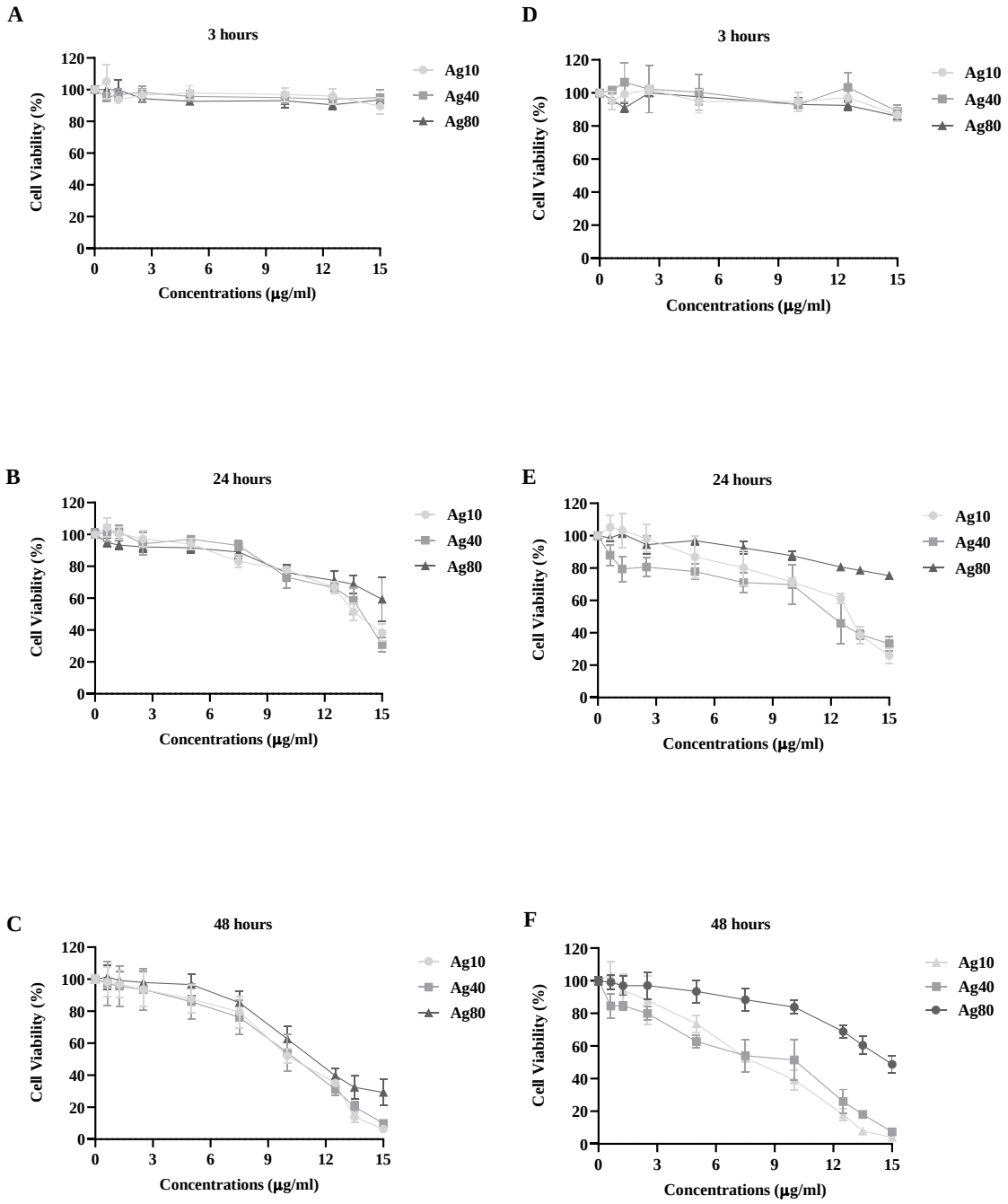


Figure 3.3. Cytotoxicity assessment of MRC-5 and A549 cells following exposure to AgNPs of different sizes using mLDH assay. Cell viability percentage of AgNPs of different sizes using a concentration range of (0.625– 15 µg/ml) after 3, 24 and 48 hours of incubation to (**A-C**) MRC-5 and (**D-F**) A549 cells. Data represent means ± SD (n=3).

The CC50 values were estimated according to the cell viability data from the mLDH assay using GraphPad prism 8 software. As shown in **Table 3.3**, both normal and cancerous lung cells demonstrated significantly low CC50 values for Ag10 and Ag40 when compared to Ag80 at 24 hours of exposure. A similar trend of size-dependent effect was reported from the CC50 values of A549 cell following 48 hours of incubation, whereas the three size illustrated similar toxicity pattern with MRC-5 cells.

It can be concluded that there was a positive correlation between AgNPs size and toxicity. Comparing the CC50 values between the healthy and cancerous lung cells, it was clear that the A549 cells were more sensitive to Ag10 and A40 than the MRC-5 cells. On the other hand, the larger particles (Ag80) demonstrated greater toxicity in the MRC-5 cells than A549 cells at both time points (**Table 3.3**). This can be due to a difference in the mechanism of AgNPs cellular internalisation between normal and cancerous lung cells. Cellular uptake of AgNPs was studied in the following subsection.

Table 3.3. The CC50 values of MRC-5 and A549 cells treated with AgNPs of different sizes. The estimated CC50 values from mLDH and MTT assays after 24 and 48 hours of MRC-5 and A549 cells exposure to AgNPs. The values are mean ± SD (n=3). (*) $p < 0.05$ versus other cell line by ANOVA test. c = $p < 0.05$ versus Ag80 of the same cell line and exposure time by ANOVA test.

AgNPs size	Exposure time (hours)	CC50 from mLDH (µg/ml)		CC50 from MTT (µg/ml)	
		MRC-5	A549	MRC-5	A549
Ag10	24	15.8 ± 0.8 ^{c}	12.4 ± 0.6 ^{*,c}	12.3 ± 0.8	10.1 ± 1 ^{c}
	48	10 ± 1	7.5 ± 0.2 ^{c}	13 ± 0.7	10.1 ± 1 *
Ag40	24	14.3 ± 1 ^{c}	11.9 ± 1.3 ^{c}	10.9 ± 1 ^{c}	9.2 ± 1 ^{c}
	48	10 ± 1.1	6.8 ± 1.5 $^{*, c}$	11.3 ± 1	8 ± 0.8
Ag80	24	20.4 ± 0.7 *	26.8 ± 1	14.2 ± 1.2	15 ± 1
	48	11.4 ± 1.1 *	15.3 ± 1	10.5 ± 0.8	11 ± 0.7

It is important to mention that the observed reduction in cell viability following exposure to high concentrations of AgNPs can be mediated by the presence of sodium citrate stabiliser and/or insufficient nutrient provided in the cell culture medium. Around 75% of total volume of AgNPs in cell culture medium was used at a concentration of 15 µg/ml. In this experiment, we intended to test high concentrations of AgNPs to be able to estimate the CC50 value. However, based on the previous toxicity findings of sodium citrate, a concentration of 1.25 mM of sodium citrate which was equal to the use of 12.5 µg/ml AgNPs was selected to be the highest AgNPs concentration can be used in this study to limit the potentially detrimental effect of sodium citrate stabiliser.

Then, the MTT assay was performed by quantifying the metabolic activity of the healthy cells. Both cells were treated with concentrations ranges of 1.25- 15 µg/ml for 24 and 48 hours. Concentration-dependent toxicity was detected for both the MRC-5 and A549 cells at both exposure times (**Figure 3.4**). The estimated CC50 values were measured based on the obtained data from the MTT assay, as shown in **Table 3.3**. It was noticed that the CC50 values of Ag10 and Ag40 were the lowest in both cell lines after 24 hours compared to the CC50 values of Ag80. However, the CC50 values revealed no size-dependent toxicity as well as no further toxicity was induced over longer exposure time (48 hours) in both cell lines. Moreover, the MTT data demonstrated that AgNPs of different sizes have induced similar cytotoxicity trends in both healthy and cancerous lung cells. Thus can be explained by AgNPs may not primarily target the mitochondrial metabolic function thereof no ultimate effect was observed with longer cellular exposure to AgNPs but it possibly there are other causes of AgNPs triggering toxicity.

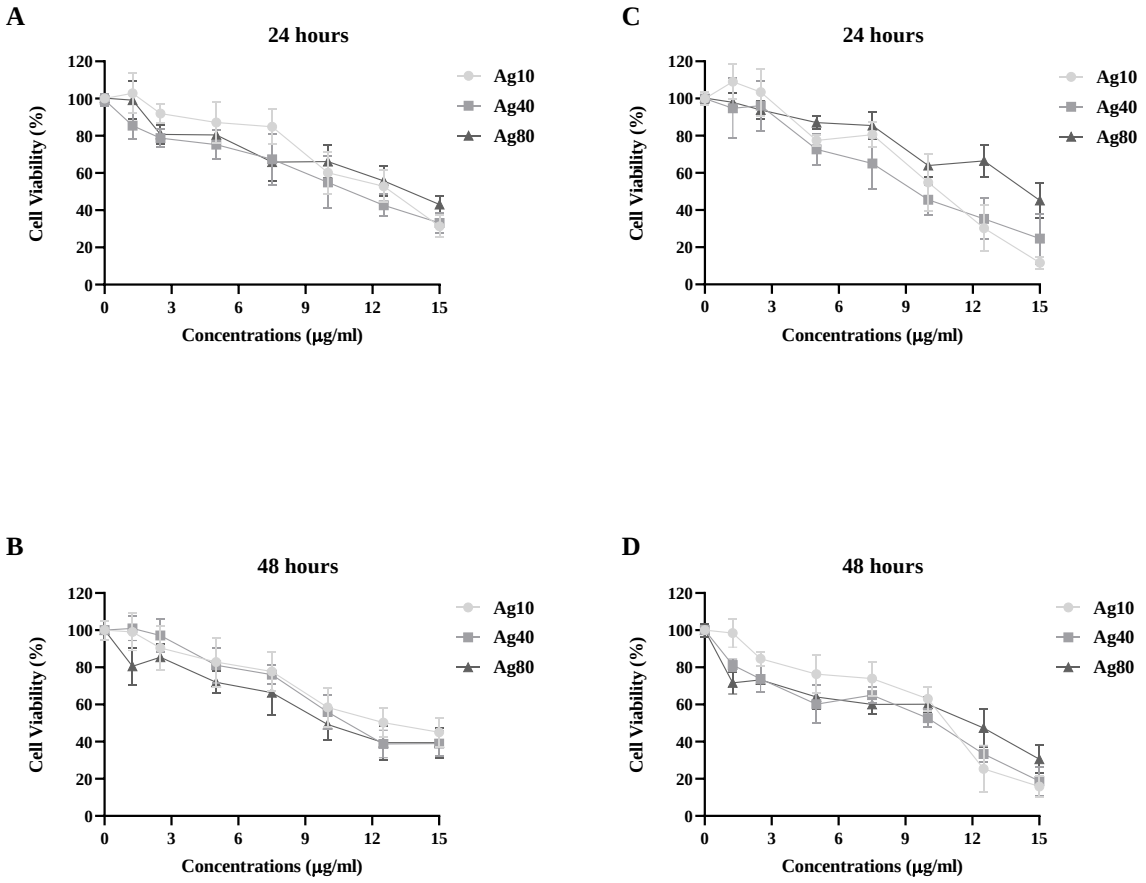


Figure 3.4. Cytotoxicity assessment of MRC-5 and A549 cells following the exposure to AgNPs of different sizes using MTT assay. Cell viability percentage of AgNPs of different sizes using a concentration range of (1.25– 15 µg/ml) after 24 and 48 hours of incubation in (**A-B**) MRC-5 and (**C-D**) A549 cells. Data represent means ±SD (n=3).

The cytotoxicity pattern of AgNPs obtained from both mLDH and MTT assays showed a size-dependent effect after 24 hours of exposure to different sizes of AgNPs. However, the cytotoxicity findings from mLDH assay showed that AgNPs were significantly reduced the cell viability compared to the cell viability detected in MTT assay after 48 hours of incubation. It is most likely that AgNPs did not directly affect the mitochondrial function and they possibly mediated cytotoxicity by other mechanisms. It should be noted that the findings from both assays can not be comparable as the MTT assay measured the metabolic activity as indirect

indication of viable cells whereas mLDH assay assessed the amount of LDH released from live cells that survived after AgNPs exposure (Ali-Boucetta et al., 2011).

The cell viability data from mLDH and MTT assays showed size-dependent toxicity at 24 hours in healthy and cancerous lung cells. Size-dependent toxicity effects detected in this study agrees with the findings by other researchers who used different AgNPs sizes and cell types including AgNPs sized 4.7 and 42 nm in human liver carcinoma and leukaemia cells (Avalos et al., 2014), citrate-coated AgNPs sized 5 and 50 nm in human bronchial epithelial cells (Lebedová et al., 2018), citrate-coated AgNPs sized 20 and 110 nm in human bronchial epithelial (Wang et al., 2014), and citrate-coated AgNPs sized 10, 20, 75, and 110 nm in human colorectal carcinoma cells (Williams et al., 2016). Several explanations have been suggested for the potency and drastic toxicity of smaller sized AgNPs compared to their larger counterparts. One suggestion is the dissolution of AgNPs into silver ions in the culture medium (Mcshan et al., 2014). The dissolution rate is expected to be higher for the smaller size of AgNPs because of their higher surface area, thereof tend to be more reactive. This observation was reported following PVP-coated AgNPs sized 5, 20, and 50 nm exposure to several types of cells including human lung adenocarcinoma epithelial cells (A549), human stomach cancer cells (SGC-7901), human hepatocellular carcinoma cells (HepG2) and human breast adenocarcinoma cells (MCF-7) (Liu et al., 2010, Mcshan et al., 2014). The extracellular released of silver ions in the cell culture medium have a high affinity for binding to the thiol moiety of the proteins in the cell membrane lead to compromised cell membrane (Chen and Schluesener, 2008, Liu et al., 2010). The second suggestion is the intracellular dissolution of AgNPs by Trojan-horse mechanism (Singh and Ramarao, 2012). It was suggested that the internalised smaller sized AgNPs can more easily dissolve and release high amount of silver ions inside the cells which lead to cell damage in human bronchial epithelial cells (BEAS-2B)

following exposure to PVP-coated AgNPs sized 5, 25, 50, and 110 nm (Gliga et al., 2014). The third suggestion is that the AgNPs cellular uptake mechanism and rate may vary based on AgNPs size which was observed in human astrocytoma (1321N1) and human lung adenocarcinoma epithelial cells (A549) (Liu et al., 2010, Varela et al., 2012).

AgNPs have shown much interest to be used as a cancer treatment. It was claimed by several studies the anticancer activity of AgNPs is due to their antiproliferative properties (Asharani et al., 2009a, Venugopal et al., 2017). Hence, the toxicity profile of AgNPs suggested as anticancer agent should be carefully considered toward their impact on healthy cells. Herein, AgNPs exhibited toxicity against both healthy and cancerous lung cells at the tested concentrations. Indeed, the preliminary data obtained from mLDH assay revealed the toxicity of AgNPs on each cell lines was dependent on size. The cancerous lung cells demonstrated high sensitivity toward Ag10 whereas the healthy lung cells were greatly affected by the larger size ones (Ag80). The present findings indicated the better use of small size AgNPs (10 nm) than larger counterparts to mitigate the toxic effect of AgNPs against healthy cells. However, further toxicity investigation is needed to be able to draw a broad conclusion on the toxicity profile of AgNPs on healthy cells. It worth mentioning that the differences in the estimated CC50 values between both cell lines were not substantial because of the low stock concentration of AgNPs used in this work which turned it difficult to determine the safety window of AgNPs.

Collectively, the cytotoxicity of AgNPs of different sizes was size, concentration- time and cell type-dependent. To further examine the AgNPs toxicity, the cell morphological changes induced by AgNPs were assessed. The next subsection demonstrates the findings.

3.3.1.3 Changes in cell morphology post AgNPs treatment

The cells may undergo certain morphological changes following their exposure to AgNPs. Microscopic images were captured using an optical microscope to observe cell morphology changes occurred following MRC-5 and A549 cells exposure to the three sizes of AgNPs for 24 hours. It was noticed morphological changes in both MRC-5 and A549 cells treated with AgNPs at high concentrations, in which the cells appeared unhealthy compared to the normal cell shape of the untreated cells (**Figure 3.5 and Figure 3.6**). Moreover, it was noticed a reduction in the cells number accompanied with presence of floating cells (dead cells) compared to untreated cells. The observable changes in the cells indicated the induction of toxicity by AgNPs.

The same observations have been found in previous studies which investigated the effect of AgNPs on human colon carcinoma (Caco-2) and A549 cells for 24 hours incubation, with a concentration range between 10 to 200 µg/ml (Lee et al., 2011, Böhmert et al., 2012, Chairuangkitti et al., 2013). The studies reported an alteration in the cells morphology due to AgNPs causing the inhibition of cell proliferation, ROS induction, and DNA damage. However, it was difficult to confirm the presence of AgNPs inside the cells using optical microscopy. Therefore, AgNPs cellular internalisation was investigated in this work, the next subsection presents and discusses the findings.

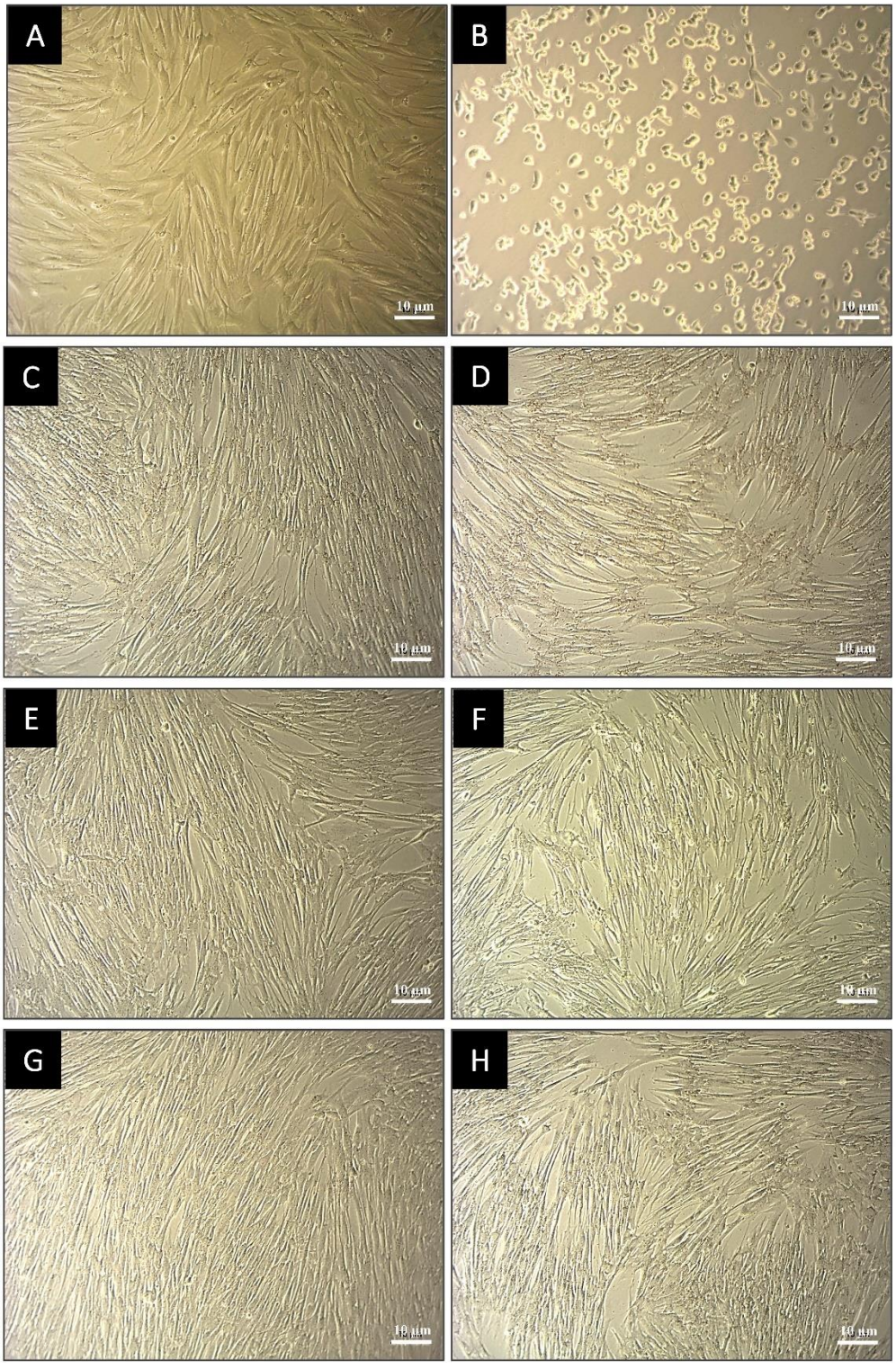


Figure 3.5. Cell morphological changes of MRC-5 cells treated with AgNPs of different sizes. Optical microscopic images of MRC-5 cells treated with AgNPs of different sizes for 24 hours. (**A**) untreated cells; (**B**) DMSO (20%) used as a positive control, Ag10 (**C**) 7.5 µg/ml and (**D**) 12.5 µg/ml; Ag40 (**E**) 7.5 µg/ml and (**F**) 12.5 µg/ml; Ag80 (**G**) 7.5 µg/ml and (**H**) 12.5 µg/ml. Scale bar 10 µm.

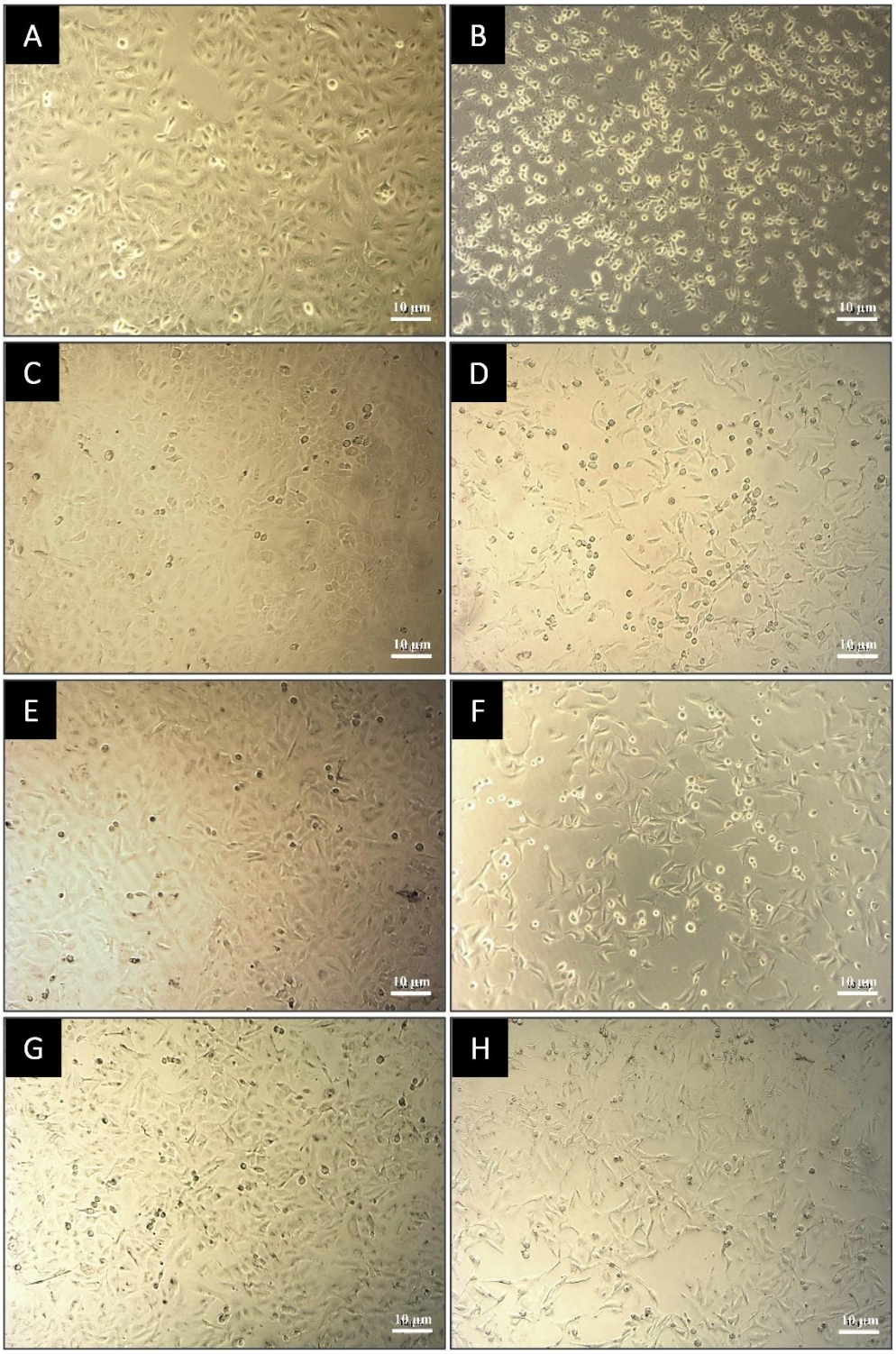


Figure 3.6. Cell morphological changes of A549 cells treated with AgNPs of different sizes. Optical microscopic images of A549 cells treated with AgNPs of different sizes for 24 hours. (**A**) untreated cells; (**B**) DMSO (20%) used as a positive control, Ag10 (**C**) 7.5 µg/ml and (**D**) 12.5 µg/ml; Ag40 (**E**) 7.5 µg/ml and (**F**) 12.5 µg/ml; Ag80 (**G**) 7.5 µg/ml and (**H**) 12.5 µg/ml. Scale bar 10 µm.

3.3.1.4 Cellular uptake of AgNPs

Previous studies postulated that the NPs size and net surface charge are the main factors altering NPs cellular interaction (Elsaesser and Howard, 2012, Toduka et al., 2012). AgNPs cellular uptake was investigated to understand whether the variation in the toxicity induced by different AgNPs sizes can be correlated with their cellular uptake differences. The cellular uptake of AgNPs was investigated in this work by measuring the side scattered (SSC) intensity using flow cytometry and quantifying the intracellular silver (Ag) ions using inductively coupled plasma mass spectrometry (ICP-MS).

3.3.1.4.1 Cell granularity assessment by flow cytometry

One of the methods that used to provide preliminary information about NPs cellular uptake is by measuring the SSC intensity which indicated the cell granularity. The cellular mass is enhanced with the internalisation of NPs inside the cells; however, this is considered a qualitative method as it is difficult to discriminate between whether the NPs are internalised in the cells or attached on the cell surface (Zucker et al., 2013, Jochums et al., 2017).

Both cell lines were treated with different concentrations of AgNPs sizes for 24 and 48 hours. The shift in the SSC light intensity of the treated cells was compared to the untreated cells. Both MRC-5 and A549 cells demonstrated an increase in the cell granularity following exposure to AgNPs of the three sizes at 24 and 48 hours (**Figure 3.7-A and Figure 3.8-A**).

The results showed that the increase in cell granularity was higher in the cells treated with Ag80 than Ag10 and Ag40 at the same concentration (**Figure 3.7 and Figure 3.8**). This somehow conflicts with the cytotoxicity finding of size-dependent toxicity. Similarly, a previous study reported a greater increase in the cell granularity of citrate-coated AgNPs sized 75 nm than the smaller size AgNPs sized 20 nm (Ortenzio et al., 2019). It was suggested that

the larger AgNPs being able to increase the inner density of the cells and scatter the light in higher quantities when compared to the smaller AgNPs. Moreover, Ortenzio and colleagues claimed that the side scatter is approximately proportional to the size of the AgNPs and may not be directly correlated to the numbers of AgNPs inside the cells or the uptake rate. It was presumed that single or aggregated AgNPs inside the cells can influence the side scatter intensity. Aggregation of AgNPs inside the cells could lead to an increase in the SSC intensity (Zucker et al., 2013). This could be the case in our observation in which the aggregation of the smaller size AgNPs inside the cells was required to generate greater light scattering. This implies that the use of this method could reflect a greater light scattering based on the size and the NPs aggregations inside the cells (Zucker et al., 2019). Another possible explanation can be associated with the rapid dissolution of the smaller size AgNPs to silver ions which did not increase in cellular mass, thereof scattering less amount of light (Beer et al., 2012). This could be also the reason for the toxicity of the smaller AgNPs size as reported in the cytotoxicity findings.

Moreover, it was noticed a decrease in the SSC signal with increasing concentration of Ag10 exposed to MRC-5 cells at both time points (**Figure 3.7 B and C**). This could be the result of a decrease in the cell viability with high concentration of Ag10. It was also observed a reduction in the SSC intensity after 48 hours of treatment with different concentration of Ag80 compared to 24 hours of treatment in MRC-5 cells (**Figure 3.7 B and C**). This could be due to a reduction in cell viability after longer incubation with Ag80 or the possibility of NPs redistribution between the cells during cell division (Jochums et al., 2017).

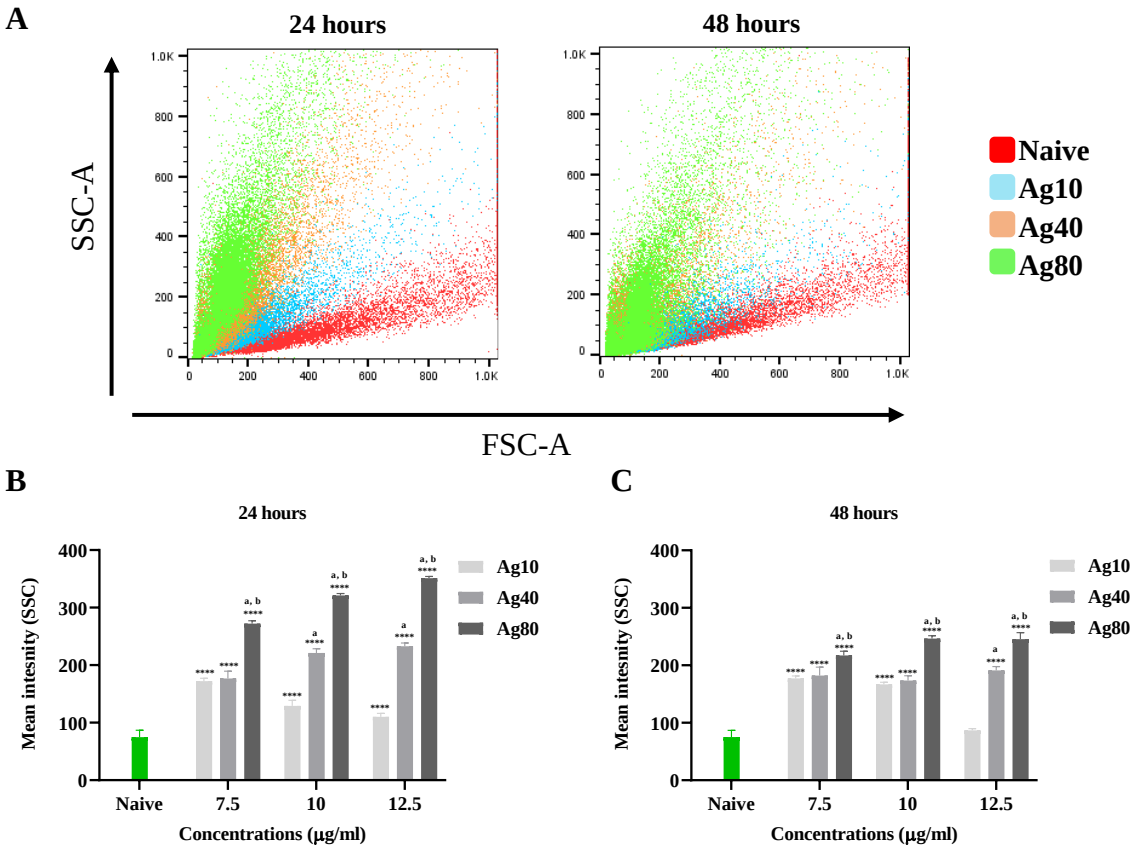


Figure 3.7. SSC light intensity analysis of cellular uptake of AgNPs in MRC-5 cells by flow cytometry. (**A**) Dot plots of side scatted intensity versus forward scattered intensity of MRC-5 cells treated with AgNPs of different sizes at concentration of 12.5 µg/ml for 24 and 48 hours. The mean intensity of the SSC light after (**B**) 24 and (**C**) 48 hours of exposure to AgNPs of different sizes at concentrations of 7.5, 10 and 12.5 µg/ml. Bars represent the mean ± SD (n=4). (****) $p < 0.0001$ versus untreated group by ANOVA test. a = $p < 0.05$ versus cells incubated with the same concentration of Ag10 and b = $p < 0.05$ versus cells incubated with the same concentration of Ag40 by ANOVA test.

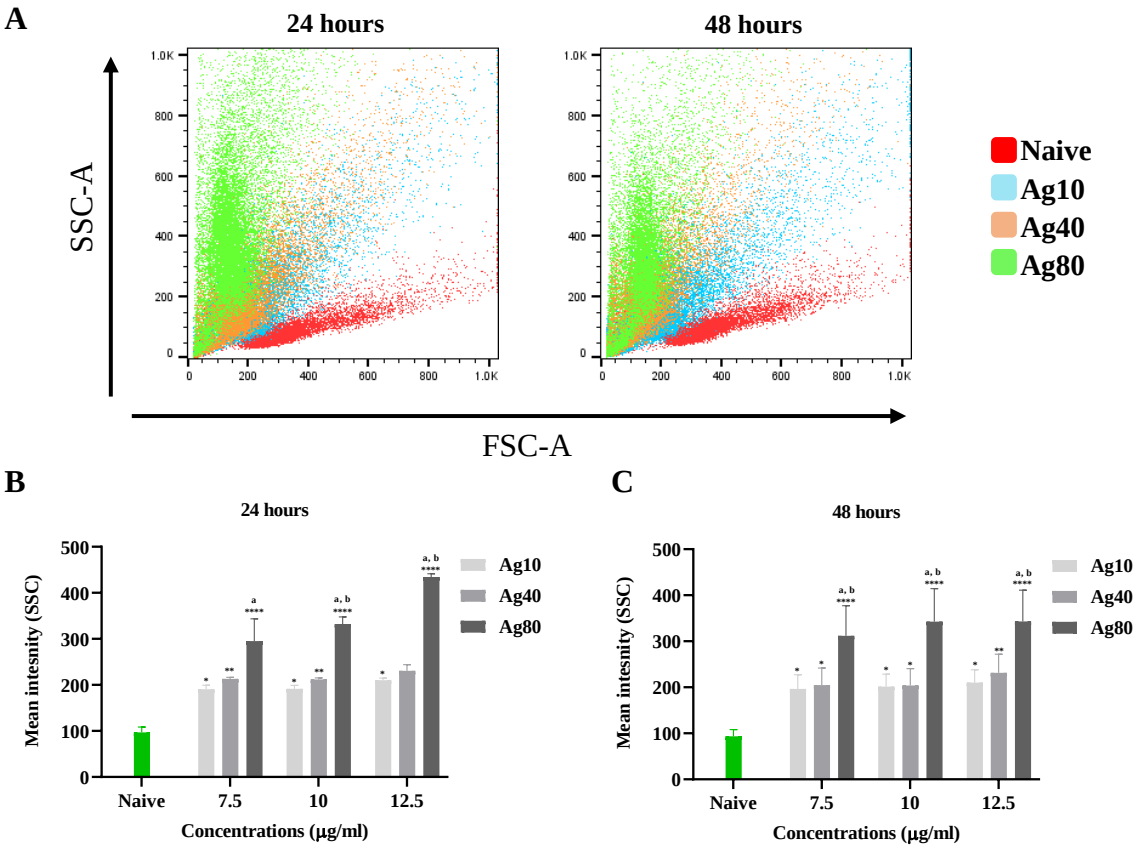


Figure 3.8. SSC light intensity analysis of cellular uptake of AgNPs in A549 cells by flow cytometry. (**A**) Dot plots of side scatted intensity versus forward scattered intensity of A549 cells treated with AgNPs of different sizes at concentration of 12.5 µg/ml for 24 and 48 hours. The mean intensity of the SSC light after (**B**) 24 and (**C**) 48 hours of exposure to AgNPs of different sizes at concentrations of 7.5, 10 and 12.5 µg/ml. Bars represent the mean ± SD (n=4). (*) $p < 0.05$; (**) $p < 0.002$ and (****) $p < 0.0001$ versus untreated group by ANOVA test. a = $p < 0.05$ versus cells incubated with the same concentration of Ag10 and b = $p < 0.05$ versus cells incubated with the same concentration of Ag40 by ANOVA test.

3.3.1.4.2 Intracellular Ag ions quantification by ICP-MS

The cellular uptake of Ag10 and Ag80 after 24 hours of exposure to MRC-5 and A549 cells was assessed. Both cell lines demonstrated concentration-dependent cellular internalisations of Ag10 and Ag80. The results showed that the cellular uptake of AgNPs was not dependent on their size (**Figure 3.9-A**).

In addition, the amount of Ag ions presented in cell culture media was measured (**Figure 3.9-B**). The amount of Ag ions in the cell culture medium was higher than the amount Ag ion detected inside the cells, thus was observed for different concentrations of Ag10 and Ag80 in both cell lines. However, the amount of Ag ions detected in MRC-5 cells exposed to highest concentration of Ag10 and Ag80 illustrated lower Ag amount remained in the media (4.8 and 5.7 µg/ml, respectively) compared to the Ag ions amount detected inside the cells (6.9 and 6.1 µg/ml, respectively). It was also noticed that the total silver mass concentration (cells and media) measured in A549 cells was higher than the total silver amount detected in MRC-5 cells (**Figure 3.9-B**). The variations in the ionic strength of the MRC-5 and A549 media may mediate the transformation of AgNPs at different levels. This indicated that the dissolution of AgNPs or their interaction with the organic/inorganic components can be strongly influenced by the composition of the surrounding cell culture medium as reported by (Kaiser et al., 2017). Also, the process of sample preparations represented technical challenges such as the tendency of AgNPs to deposit on the vial during sample digestion and on the ICP-MS probe during the analysis of the samples. Another issue, the possibility of acid mixture evaporation which may lead to slight changes in the base volume, thereof influence the final concentration of silver detected. These issues may interfere with accurate quantification of silver mass concentration measured by ICP-MS and lead to inconclusive results.

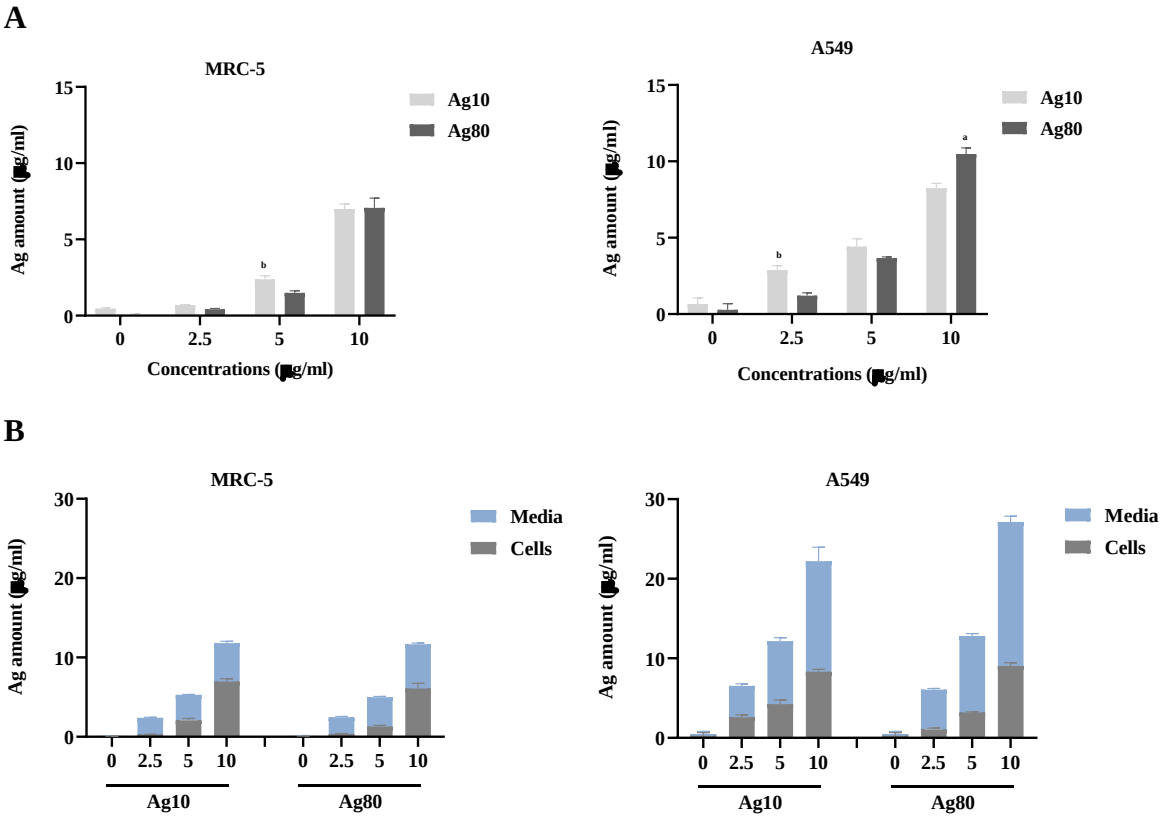


Figure 3.9. Cellular uptake of AgNPs in MRC-5 and A549 cells analysed by ICP-MS. (**A**) The amount of Ag (µg/ml) detected in the cells after 24 hours of exposure to Ag10 and Ag80 at concentrations of 2.5, 5 and 10 µg/ml in MRC-5 and A549 cells. Bars represent the mean ± SD (n=4). a = $p < 0.05$ versus cells incubated with the same concentration of Ag10; b= $p < 0.05$ versus cells incubated with the same concentration of Ag80 by ANOVA test. (**B**) The amount of Ag detected inside the cells and remained in the cell culture medium after 24 hours of exposure to Ag10 and Ag80 in both MRC-5 and A549 cells.

The reported intracellular accumulation of silver ions in MRC-5 was not significantly different from the silver ion amount detected in A549 cells. Moreover, the results indicated no differences in the level of silver ions detected between Ag10 and Ag80. This did not correlate with the reported toxicity profile of size-dependent effect. However, the induction of toxicity did not necessarily correlate with the intracellular amount of AgNPs. This observation was supported by previous investigators who explained that the detrimental impact of AgNPs can be mediated by AgNPs interaction with the cells membrane or AgNPs dissolution without AgNPs internalisation (Johnston et al., 2010). Therefore, the higher toxicity profile reported

for Ag10 than Ag80 can be caused by the direct interaction of Ag10 with cell membrane causing cellular damage or by faster dissolution of the smaller size AgNPs compared to the larger ones lead to induction of toxicity.

Apart from the advantage of the ICP-MS technique of being highly sensitive for the detection of silver and the measured silver amount can represent both cellular adsorption and uptake. However, the ICP-MS provides information as a mass concentration of silver regardless of the form of AgNPs (particles or ions) (Ortenzio et al., 2019). A previous study revealed that AgNPs cellular uptake measured by ICP-MS can be expressed as a mass concentration or calculated to the respective number of particles (Van Der Zande et al., 2016). It was reported that the amount of silver uptake was increased with increasing the AgNPs size when the AgNPs was expressed as a mass concentration, whereas the conversion of AgNPs mass concentration to particles number showed a size-dependent silver uptake in which the small size represented the maximum uptake. In the present work, the mass concentration of silver ions in Ag10 and Ag80 can not be comparable as the measured amount by ICP-MS did not reflect the number of particles. Moreover, the unit dose that used to treat the cells was in mass concentration and the number of the particles in Ag10 and Ag80 were not equal since the beginning. Therefore, the comparison between the effect of AgNPs size and cell types on the AgNPs cellular uptake can not be conclusive.

Collectively, The SSC light demonstrated the highest cellular uptake with Ag80 compared to the other sizes. The light from the SSC reflect the AgNPs only as the ionic silver did not scatter any light. In the case of ICP-MS, no pattern of size specific cellular uptake was noticed in the measured silver mass between Ag10 and Ag80. The silver mass determined by ICP-MS may indicate both the amount of particles and ions. However, the flow cytometry and ICP-MS findings were evident that the observed AgNPs size-dependent cytotoxicity was not influenced

by AgNPs cellular uptake. As mentioned earlier both techniques demonstrated some limitations, therefore, further investigations using advanced techniques are required to gain a clear understanding about the impact of AgNPs cellular uptake on their toxicity. To gain more insight about the AgNPs size impact on cellular toxicity, series of toxicity assessments were carried out to investigate oxidative stress, cell cycle arrest, mitochondrial disruption and apoptosis. The next subsection is devoted to present and explain the findings.

3.3.1.5 The mechanisms of AgNPs toxicity assessment

3.3.1.5.1 Oxidative stress detection

Oxidative stress is suggested to be the major toxicity mechanism of AgNPs by induction of ROS production (Flores-López et al., 2019, Barcińska et al., 2018). Due to the unpaired electron of ROS molecules, this turns the ROS to be highly reactive and increase their affinity to bind with other biomolecules (Manke et al., 2013). An abundance of ROS generation leads to disturbances of cellular redox haemostasis and triggers the DNA, lipid and protein oxidation (Khanna et al., 2015, Crisponi et al., 2017). Different cellular defence mechanisms are stimulated in the presence of high levels of ROS to mitigate the ROS damaging effect on cells. Lipophilic-based antioxidants such as vitamin E and hydrophilic-based antioxidants, such as vitamin C and glutathione can act to detoxify the ROS (He et al., 2017). However, the inability of the antioxidants to counteract the excess ROS may induce cell death. As the AgNPs toxic effect can be mainly triggered by oxidative stress, therefore, it is important to examine the potential ROS generation by AgNPs.

CellRox deep red reagent displays fluorescence signals only upon its oxidation by ROS. In the current work, this reagent was used to compare the extent of ROS induction of the differently sized AgNPs after 24h hours of incubation at concentrations of 7.5, 10, and 125 μg/ml in both

MRC-5 and A549 cells. This concentration range (7.5- 12.5 µg/ml) was selected as it has triggered low to high toxicity based on the earlier cell viability data. The data were presented and compared based on the median fluorescence intensity (MFI). A free- radical inducer, Menadione, was used as a positive control. The MFI was increased after 24 hours of exposure to the three AgNPs sizes, which indicated an increase in ROS generation in both MRC-5 and A549 cells (**Figure 3.10 A and B**).

In MRC-5 cells, a concentration-dependent induction of ROS was reported with cells exposed to Ag10 and Ag80 (**Figure 3.10-C**). Significant ROS generation was detected at the concentrations of 10 and 12.5 µg/ml ($p < 0.0002$) for Ag10 and only at 12.5 µg/ml for Ag80 ($p < 0.0002$). For MRC-5 cells treated with Ag40, the ROS generations recorded the highest MFI at concentrations of 7.5 and 10 µg/ml, with a MFI around 60 and 70 compared to 15 for the untreated group. However, a reduction in the MFI at the highest concentration of Ag40 was observed, this could be due to an increase in cell death.

In case of A549 cells, substantial increase in the ROS production following the exposure to the three sizes of AgNPs (**Figure 3.10-D**). The three sizes of AgNPs showed to increase ROS level to similar extent with no concentration-dependent effect. However, it was noticed that A549 cells incubated with low concentration of Ag40 (7.5 µg/ml) induced the highest level of ROS whereas Ag80 demonstrated pronounced increase in ROS at the highest concentration (12.5 µg/ml).

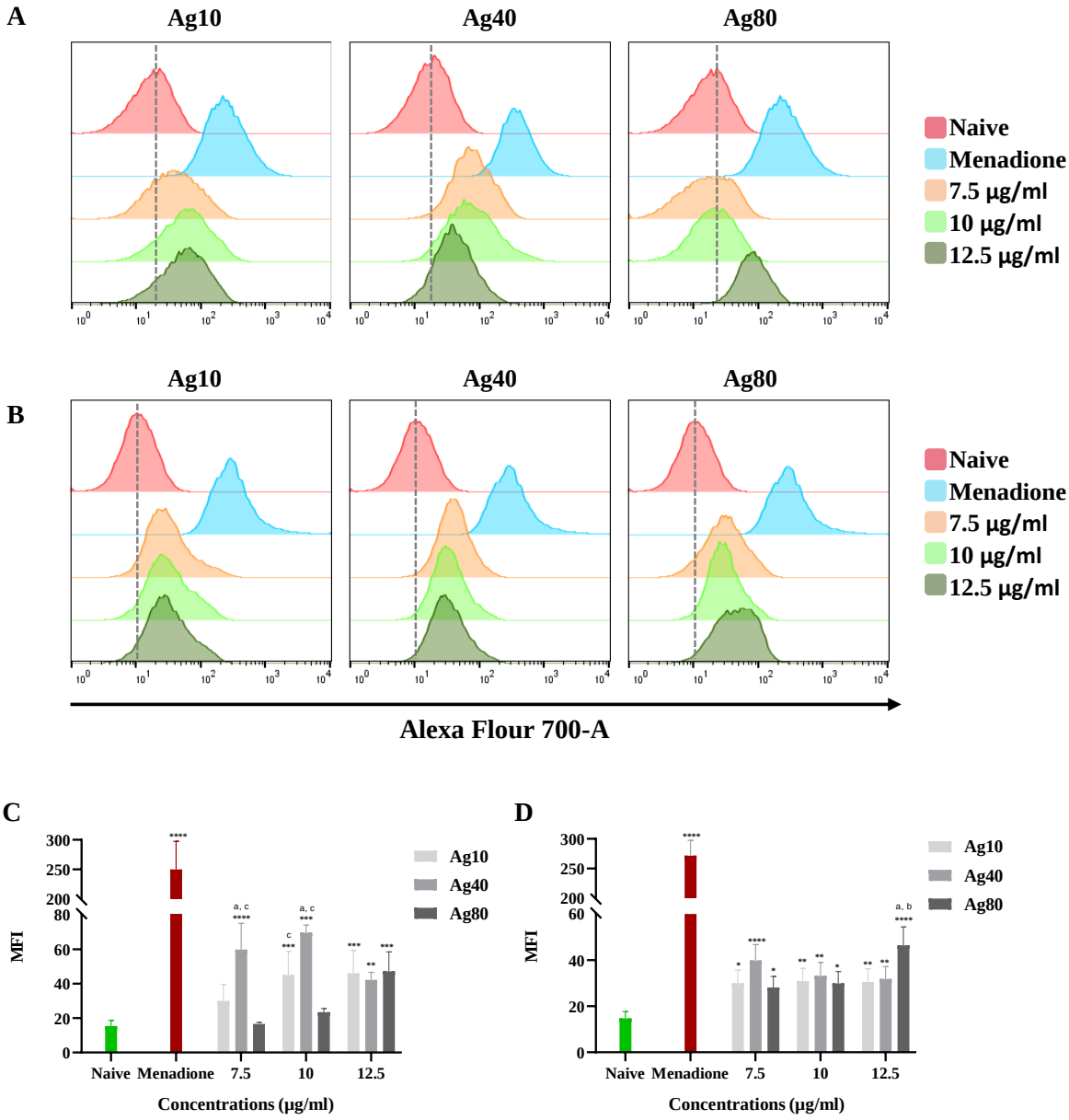


Figure 3.10. Oxidative stress detection in MRC-5 and A549 cells following the exposure to AgNPs of different sizes using CellRox deep red reagent. Histogram of flow cytometry analysis of cells treated with Ag10,Ag40 and Ag80 at concentrations of 7.5, 10 and 12.5 µg/ml for 24 hours in (**A**) MRC-5 and (**B**) A549 cells. Bar graphs represent the median fluorescence intensity (MFI) versus different concentration of AgNPs in (**C**) MRC-5 and (**D**) A549 cells. Menadione (50 µM) used as a positive control. Bars represent the mean ± SD (n=4). (*) $p < 0.05$; (**) $p < 0.002$; (***) $p < 0.0002$ and (****) $p < 0.0001$ versus untreated group by ANOVA test. a = $p < 0.05$ versus cells incubated with the same concentration of Ag10; b = $p < 0.05$ versus cells incubated with the same concentration of Ag40 and c = $p < 0.05$ versus cells incubated with the same concentration of Ag80 by ANOVA test.

The present data indicated that AgNPs mediated oxidative stress by increasing ROS generation which can be the primary mechanism under AgNPs cytotoxicity and cell damage induction as evident by several studies (Asharani et al., 2009b, Kim et al., 2009, Nowrouzi et al., 2010, Mortezaee et al., 2019). Several suggestions were elicited regarding the mechanism of AgNPs promoted ROS production. The possible generation of ROS can be either by the direct AgNPs induction of ROS via a Fenton-like reaction or an indirect reaction between the released silver ions and a thiol moiety on the respiratory chain enzyme inside the mitochondria, thus initiating ROS production in the mitochondria (Völker et al., 2013, Alkawareek et al., 2019). It was proposed that mitochondrial dysfunction can be mainly associated with ROS generation, leading to an imbalance in redox stability (Dasgupta et al., 2018, Sharma et al., 2019). Another study evident that the induction of cellular oxidative stress is due to silver ions dissolution from AgNPs (Maurer and Meyer, 2016). Silver ions have been found to significantly elevate ROS levels and deplete glutathione more than citrate-coated AgNPs themselves in human liver carcinoma cells (Vrček et al., 2016).

The current results illustrated no pattern of size-dependent formation of ROS which was in contrary to other investigators outcomes of AgNPs size-dependent induction of oxidative stress (Miethling-Graff et al., 2014, Avalos et al., 2014, Gopisetty et al., 2019). These studies have explained that the smaller AgNPs size is more reactive and potent which resulted in the induction of high amount of free radicals. Herein, it was observed significant production of ROS in MRC-5 cells exposed to Ag40 whereas AgNPs of different sizes induced similar increases in the ROS level in A549 cells. The pronounced cytotoxicity demonstrated the toxicity of Ag10 and Ag40 in both cell lines thus can be a consequence of ROS induction by Ag40 but ROS increases were not evident with Ag10. However, it was noticed in both cell lines that Ag80 mediated ROS induction in a concentration-dependent manner. Ag80 elicited

the lowest cytotoxicity compared to other sizes which confirmed here by triggering ROS production only at highest concentration of Ag80.

As function of cell-type dependent effect, AgNPs showed to trigger oxidative stress in both MRC-5 cell than A549 cells. An increase in ROS generation was pronounced in MRC-5 cells when exposed to Ag40 at concentration of 7.5 and 10 µg/ml ($p < 0.002$ and $p < 0.0001$) and at highest concentration of Ag10 ($p < 0.05$) compared to A549 cells. The data illustrated a pronounced induction of ROS in MRC-5 than A549 cells with smaller sizes (Ag10 and Ag40), but cytotoxicity observation illustrated the smaller size Ag10 elicited high potency to A549 cells than MRC-5 cells. These findings indicate the cytotoxicity of AgNPs can be mediated by ROS induction but there is possible other mechanisms of AgNPs mediated cytotoxicity.

The present findings demonstrated no concentration or size-dependent production of ROS which was conflicted with the cytotoxicity conclusion. This observation was presumed to be associated with induction of cell death at the tested exposure time. Moreover, the produced ROS are very reactive, unstable and have a relatively short life span which renders them difficult to measure (Forkink et al., 2010). It is thereof recommended to run a kinetic experiment to investigate ROS increases and also multiplex this experiment with another reagent to measure the dead cells to gain a better idea on the AgNPs size mediated oxidative stress. Furthermore, the CellRox deep red reagent used in this experiment revealed some limitations which were designated to measure superoxide anion and hydroxyl radical only and it is not suitable for detecting other free radicals like hydrogen peroxide (Cameron et al., 2018). Also, this reagent measures intracellular ROS that exist mainly in the cytoplasm but still, there is a possibility in the presence of ROS inside the mitochondria and nucleus that not detected in this experiment. To further confirm the induction of oxidative stress by cells exposure to

AgNPs, the glutathione, one of the hallmarks of ROS generation in cells was measured. The next subsection presents the findings.

3.3.1.5.2 Glutathione measurement

Under normal cellular conditions, the reduced glutathione (GSH) exists in higher amounts inside the cells. The reduced GSH acts as an antioxidant that oxidised and transformed into oxidised glutathione (GSSG) by the free radical as a defence mechanism to maintain the cellular redox homeostasis. The cells under stress may generate an immense amount of ROS in which the cells may not able to counteract, thus leads to deplete glutathione and initiate cellular death (Manke et al., 2013).

The present study determined the GSH/GSSG ratio as evidence of redox stability in the cell. In this experiment, cellular GSH and GSSG were quantified after treating MRC-5 and A549 cells with AgNPs for 24 hours at concentrations of 7.5, 10, and 125 µg/ml. Menadione was used as a positive control. In the MRC-5 cells, no changes in the GSH/GSSG ratio as compared to the untreated group were detected after treatment with the differently sized AgNPs at a concentration of 7.5 µg/ml. However, a reduction in the GSH/GSSG ratio was observed at concentrations of 10 and 12.5 µg/ml in a concentration- and size-dependent manner **(Figure 3.11-A**). In case of A549 cells, concentration- and size-dependent decrease in the GSH/GSSG ratio were reported after 24 hours of incubation with the differently sized AgNPs. Ag80 demonstrated no significant effect at the low concentration of 7.5 µg/ml (**Figure 3.11-B**).

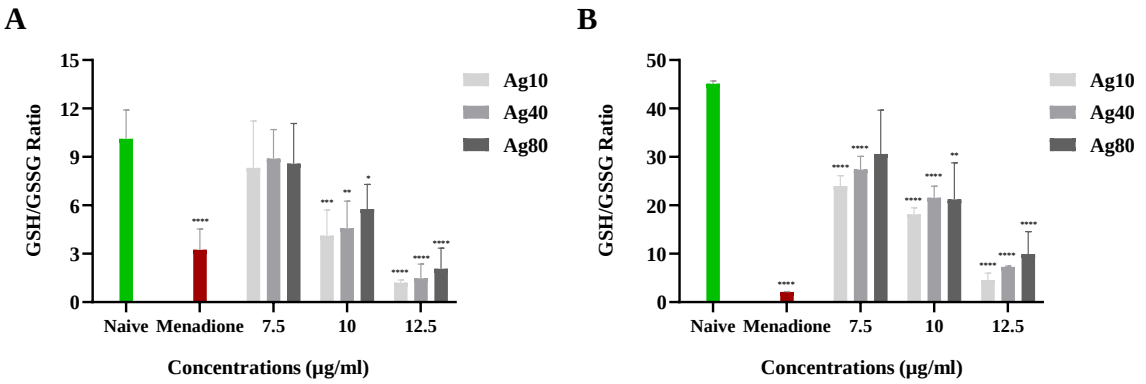


Figure 3.11. GSH/GSSG ratio quantification of MRC-5 and A549 cells following the exposure to AgNPs of different sizes using GSH/GSSG-Glo™ Assay. Both cells were treated with AgNPs at concentrations of 7.5, 10 and 12.5 µg/ml for 24 hours in (**A**) MRC-5 and (**B**) A549 cells. Menadione (50 µM) used as a positive control. Bars represent the mean ± SD (n=4). (*) $p < 0.05$; (**) $p < 0.002$; (***) $p < 0.0002$ and (****) $p < 0.0001$ versus untreated group by ANOVA test.

Our findings illustrated that AgNPs of different sizes promoted oxidative stress via induction of ROS level in the cells along with reduction of GSH level in both cell lines which was in agreement with previous studies that used different sizes of AgNPs and cell types including human hepatocyte carcinoma and human lung epithelial carcinoma exposed to AgNPs (13–43 nm) (Xin et al., 2016), human ovarian carcinoma exposed to PVP-coated AgNPs (24.1 nm) (Fahrenholtz et al., 2017) and human colon carcinoma exposed to AgNPs (60 nm) (Dasgupta et al., 2018). It was also reported a size-dependent depletion of GSH level in both cell lines which was previously claimed in human liver carcinoma and leukaemia cells exposed to AgNPs (4.7 and 42 nm) (Avalos et al., 2014) and normal human dermal fibroblasts exposed to AgNPs (4.7 and 42 nm) (Avalos et al., 2016).

The significant reduction of GSH/GSSG ratio reported in both cell lines did not directly correlate to the observed increases in the ROS level. Due to the short half-lives of the ROS, it is possible that AgNPs triggered high level of ROS formations earlier than the investigated exposure time (24 hours) and resulted in activation of antioxidant cellular response leading to

GSH reduction. Also, the evaluated ROS in this study was limited to superoxide anion and hydroxyl radical as described earlier and AgNPs may promote the formation of other ROS that was not investigated. Moreover, GSH is primarily detoxified hydrogen peroxide which is the final intermediate of other formed free radicals, however, hydrogen peroxide was not measured here in this work (Lushchak, 2012). Another possible reason is the dissolved silver ions may form a complex with the thiol group in GSH lead to substantial depletion of GSH level (Lebedová et al., 2018). The depletion of GSH level can cause a disruption in redox haemostasis leading to oxidation of protein and DNA and eventually cell damage (Asharani et al., 2009a). Moreover, Dasgupta et al. (2018) reported a disruption in GSH level can be accompanied with mitochondrial dysfunction, DNA damage and apoptosis in human colon carcinoma cells exposed to AgNPs. As the apoptosis can be triggered by AgNPs, the next subsection was devoted to analysis the mechanism of AgNPs in inducing cellular death.

3.3.1.5.3 Apoptosis detection

Apoptosis and necrosis are two cell death mechanisms can occur in the mammalian cell. Apoptosis is programmed cell death that occurs via intrinsic or extrinsic pathways as a normal physiological process (Pfeffer and Singh, 2018). The apoptosis process is regulated by different proteins, including pro-apoptotic, anti-apoptotic, and caspases proteins. The extrinsic pathway of apoptosis is stimulated by death receptors and death ligands, i.e., FAS and TNFα (Zaman et al., 2014). On the other hand, the intrinsic pathway of apoptosis can be mitochondrial-dependent and activated by cellular stress, DNA damage, and abnormal cell proliferation (Pfeffer and Singh, 2018). Necrotic cell death is stimulated by external signals, such as infection and toxic agents (Jog and Caricchio, 2014). The diversity in the mechanisms causing cell death stimulated by NPs is considerably dependent on NPs type, concentrations, exposure time, and cell type (Hussain et al., 2010, Foldbjerg et al., 2009, Harhaji et al., 2007).

Apoptosis and necrosis can occur in the cell through two distinct morphological changes. Annexin V conjugated to Alexa Flour and Propidium Iodide (PI) are two fluorescent markers used to discriminate between two pathways based on the cell membrane condition. Phosphatidylserine (PS) is normally located in the inner layer of the plasma membrane, and it shifts to the outer layer as cells undergo early apoptosis (Vermes et al., 2000). Annexin V stain is a membrane-binding protein that emits fluorescence upon it is binding to the PS in the outer layer of the plasma membrane. On the other hand, PI marker is a cell-impermeable for live cells and it intercalates DNA of the compromised cell membranes emitting red fluorescence in necrotic or late apoptotic cells (Vermes et al., 2000).

The extent and mechanisms of cell death were investigated in both MRC-5 and A549 cells after 24 and 48 hours of treatment using three concentrations (7.5, 10, and 12.5 μg/ml) of the differently sized AgNPs. Staurosporine and DMSO were used as positive controls for apoptosis and necrosis, respectively. As illustrated in **Figure 3.12**, depending on each stain intensity, the cells were divided into four quadrants and quantified as percentages, each quadrant corresponds to: Q4 (AnnexinV-/PI-) living cells; Q3 (AnnexinV+/PI-) early apoptosis, Q2 (AnnexinV+/PI+) late apoptosis and necrosis, and Q1 (AnnexinV-/PI+) cell fragments. Late apoptosis/necrosis populations were detected in MRC-5 and A549 cells following exposure to AgNPs for 24 and 48 hours (**Figure 3.12 and Figure 3.13 A-B**).

In the MRC-5 cells, an increase in the late apoptotic and necrotic population was observed after 24 hours for Ag10 and Ag40 and was accompanied by an increase in the cell fragment population with increasing the concentrations **(Figure 3.12-D**). A profound increase in the late apoptosis and necrosis populations was found after 48 hours, with around 20%, 13%, and 11% for Ag10, Ag40, and Ag80, respectively. However, Ag80 did not show any sign of toxicity at 24 hours, which confirmed the size- and time-dependent toxic effect of AgNPs. Cell fragment

population was substantially increased with increasing Ag10 and Ag40 concentrations (around 36% and 22%, respectively) after 48 hours of incubation **(Figure 3.12-D**).

For the A549 cells, the result indicated late apoptosis/necrosis induction in both a concentration- and size-dependent pattern (**Figure 3.13 A and B**). A noticeable statistically significant increases in the late apoptosis/necrosis population was found after 48 hours for Ag10, Ag40, and Ag80 (18%, 11% and 7%, respectively) **(Figure 3.13-D**). The data from this experiment revealed a size dependency of smaller size AgNPs indicating a more pronounced toxic effect induced. This finding is in agreement with Liu et al. (2010) work who reported size-dependent apoptosis mediated in human lung epithelial carcinoma cells (A549), human stomach cancer cells (SGC-7901), human breast cancer cells (MCF-7) and human hepatoblastoma cells (HepG2) following exposure to AgNPs sized 5, 20 and 50 nm at concentration of 0.5 μg/ml for 24 hours. The latter study explained that smaller sized AgNPs showed to easily internalised the cells and stimulated signalling cascade resulted in ROS-dependent apoptosis.

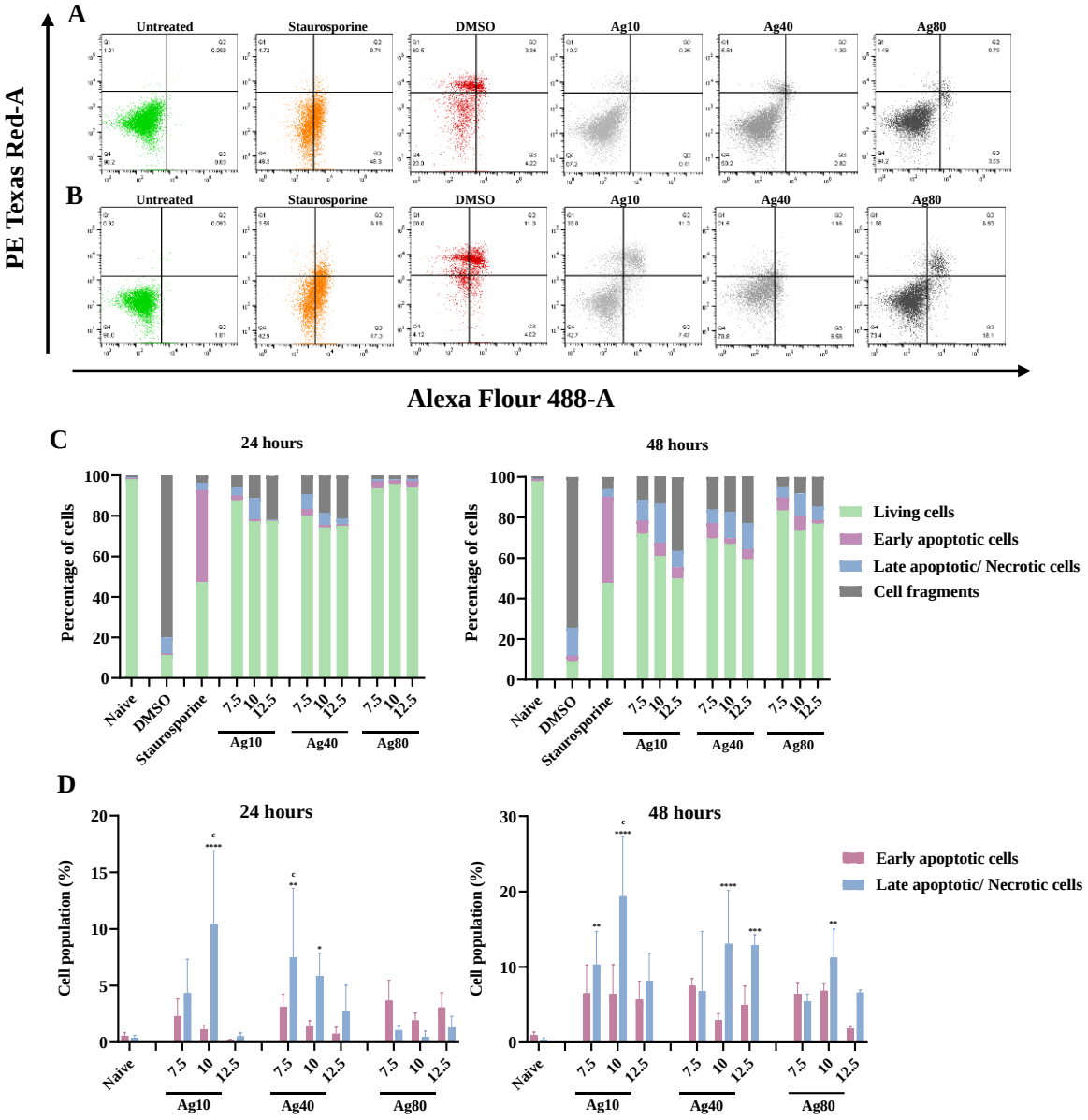


Figure 3.12. Apoptosis cell death analysis of MRC-5 cells following the exposure to AgNPs of different sizes using Annexin V and PI by flow cytometry. Dot plots of flow cytometry analysis of MRC-5 cells treated with AgNPs at concentrations of 12.5 µg/ml for (**A**) 24 and (**B**) 48 hours. Each dot plot divided into 4 quadrants of total 100% which correspond to: (Q4) living cells; (Q3) early apoptosis; (Q2) late apoptosis and necrosis; and (Q1) cell fragments. Staurosporine (1 µM) and DMSO (10%) were used as positive control for cell apoptosis and necrosis, respectively. (**C**) Stack graphs represent the cells percentage in each quadrant after 24 and 48 hours of exposure to AgNPs at concentration of 7.5, 10 and 12.5 µg/ml. (**D**) Bar graphs of early apoptotic and late apoptotic and necrotic populations after 24 and 48 hours of exposure to AgNPs of different sizes. Bars represent the mean ± SD (n=4). (*) $p < 0.05$, (**) $p < 0.002$, (***) $p < 0.0002$ and (****) $p < 0.0001$ versus untreated group by ANOVA test. c = $p < 0.05$ versus cells incubated with the same concentration of Ag80 by ANOVA test.

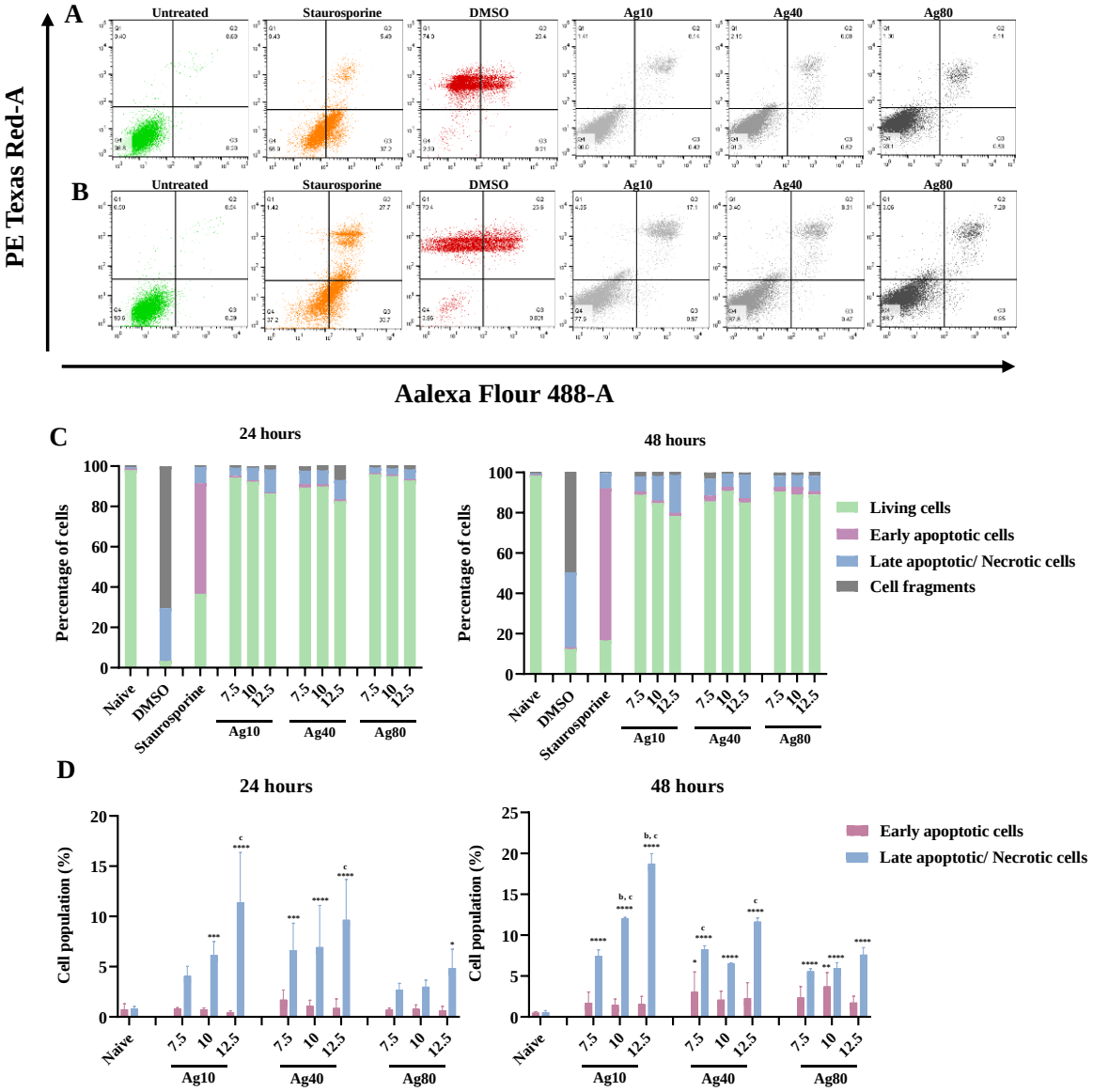


Figure 3.13. Apoptosis cell death analysis in A549 cells following the exposure to AgNPs of different sizes using Annexin V and PI by flow cytometry. Dot plots of flow cytometry analysis of A549 cells treated with AgNPs at concentrations of 12.5 µg/ml for (**A**) 24 and (**B**) 48 hours. Each dot plot divided into 4 quadrants of total 100% which correspond to: (Q4) living cells; (Q3) early apoptosis; (Q2) late apoptosis and necrosis; and (Q1) cell fragments. Staurosporine (1 µM) and DMSO (10%) were used as positive control for cell apoptosis and necrosis, respectively. (**C**) Stack graphs represent the cells percentage in each quadrant after 24 and 48 hours of exposure to AgNPs at concentration of 7.5, 10 and 12.5 µg/ml. (**D**) Bar graphs of early apoptotic and late apoptotic and necrotic populations after 24 and 48 hours of exposure to AgNPs of different sizes. Bars represent the mean ± SD (n=4). (*) $p < 0.05$, (**) $p < 0.002$, (***) $p < 0.0002$ and (****) $p < 0.0001$ versus untreated group by ANOVA test). b = $p < 0.05$ versus cells incubated with the same concentration of Ag40 and c = $p < 0.05$ versus cells incubated with the same concentration of Ag80 by ANOVA test.

Moreover, the present findings from both cell lines reported time-dependent increase in late apoptosis/necrosis cells. The highest concentration (12.5 μg/ml) of the three sizes of AgNPs induced substantial late apoptosis/necrosis cell death in A549 cells compared to MRC-5 cells at 24 hours of exposure with $p < 0.0001$ in Ag10, Ag40 and $p < 0.05$ in Ag80. However, MRC-5 demonstrated a significant increases in late apoptosis/necrosis population after longer incubation (48 hours) to AgNPs of different sizes at concentration of (10 μg/ml) compared to A549 cells with $p < 0.0002$ in Ag10, $p < 0.002$ in Ag40 and $p < 0.05$ in Ag80. These results indicated that 48 hours of exposure was sufficient to induce significant apoptosis in MRC-5 cell compared to A549 cells. As can be seen, AgNPs can affect normal lung cells more than cancerous cells and this raises concern regarding the use of AgNPs as an anticancer agent as the molecular toxicity and cell death extent can be more significant in the healthy than cancer cells.

Herein, AgNPs triggered early apoptosis/ necrosis cell death in both cell lines. The activation of apoptosis by AgNPs has been reported to be triggered by extrinsic or intrinsic pathways. Apoptosis-related gene changes have been observed in lung epithelial cells (A549), in which the AgNPs sized (40 nm) interfere with the proapoptotic factors such as Bax and Bid at the transcriptional level (Lee et al., 2011). Another study revealed an induction of apoptosis triggered by ROS-dependent pathway in hepatocyte carcinoma cells exposed to AgNPs sized (2 nm) (Zhu et al., 2016). Citrate-coated AgNPs with both 5 and 35 nm in size were found to promote apoptosis by targeting the mitochondria without the activation of the p53 pathway on osteosarcoma cells (Kovács et al., 2016).

Unexpectedly, neither cell lines demonstrated significant toxicity at both exposure durations which was not consistent with the cytotoxicity observations even when cells exposed to high concentration of AgNPs (12.5 μg/ml) in which the cell survival percentages in MRC-5 were

35%, 31% and 40% for Ag10, Ag40 and Ag80 and in A549 cells were 18%, 26% and 69% for Ag10, Ag40 and Ag80. It was presumed that AgNPs could interfere with the fluorescent markers due to their light scattering properties (Kumar et al., 2015, Riaz Ahmed et al., 2017). However, this can not be considered an issue as most of AgNPs were gently removed during sample preparation, also an appropriate gating was performed during sample analysis to exclude AgNPs and to limit any possible interference. Moreover, no interference was observed when AgNPs mixed with positive controls as shown in **Figure A3**. Nevertheless, the most possible reason for the unexpected low toxicity results detected in this experiment is that the dead cells could be detached and lead to unreliable estimation of cell death.

Taking together, AgNPs showed potential to increase ROS formation which was more pronounced in MRC-5 cells than A549 cells. Regardless that no size-dependent induction of ROS was detected, the cellular protective glutathione was depleted in a size-dependent pattern and can indicate the presence of excessive amount of ROS. In consequence of the oxidative stress triggered by AgNPs, the results shown that AgNPs induced late apoptosis/necrosis cell death in a size-dependent manner. In agreement with the present observations, previous studies found that AgNPs can mediate oxidative stress that leads to damaging of cell machinery and apoptosis in human epithelial lung cancer (A549) and human hepatocellular carcinoma HePG-2 cells (Zhu et al., 2016, Chairuangkitti et al., 2013). It was also evident that AgNPs can trigger apoptosis by targeting the mitochondrial function (Kanipandian et al., 2019). As ROS production showed a potential to promote apoptosis thus can be mediated via mitochondrial-dependent pathway, therefore, the mitochondrial membrane potential health was assessed in the next subsection.

3.3.1.5.4 Mitochondrial membrane potential health assessment

Mitochondria play essential roles in regulating cellular respiration to create energy, cellular metabolism, and cell death (Brand et al., 2013). The mitochondria is considered one of the main regulators of the cell fate, particularly the intrinsic pathway of cells undergoing programmed cell death. Moreover, the mitochondria has a role in the regulation of redox haemostasis in cells; therefore, the presence of a high level of ROS in cells may alter the normal mitochondrial function and result in mitochondrial-dependent cell death (Teodoro et al., 2011). Alterations in mitochondrial function may lead to mitochondria membrane depolarisation which is the first stage of cell death via the intrinsic pathway that resulted in mitochondrial expansion, loss of the cellular respiratory chain, translocation of cytochrome C, and activation of caspase-3 and -7 proteins in the cytoplasm (Maurer and Meyer, 2016).

The impairment of mitochondrial function was investigated by measuring the mitochondrial electrochemical gradient in MRC-5 and A549 cells treated with AgNPs at concentrations of (7.5, 10, and 12.5 µg/ml) for 24 hours. Carbonyl cyanide 3-chlorophenylhydrazone (CCCP) was used as a positive control. The data were presented and compared based on the MFI.

In the MRC-5 cells, significant decreases in MFI values were reported at concentration of 12.5 µg/ml in Ag10, Ag40, and Ag80, indicating a loss of MMP (**Figure 3.14 A and C**). A size-dependent effect was also identified in which MMP distribution was more pronounced for the small-sized Ag10 and Ag40. In case of A549 cells, an alteration in the MMP was detected after 24 hours of treatment with the three AgNPs sizes (**Figure 3.14 B and D**). A size-dependent loss of MMP was detected, in which Ag10 demonstrated the most potent effect.

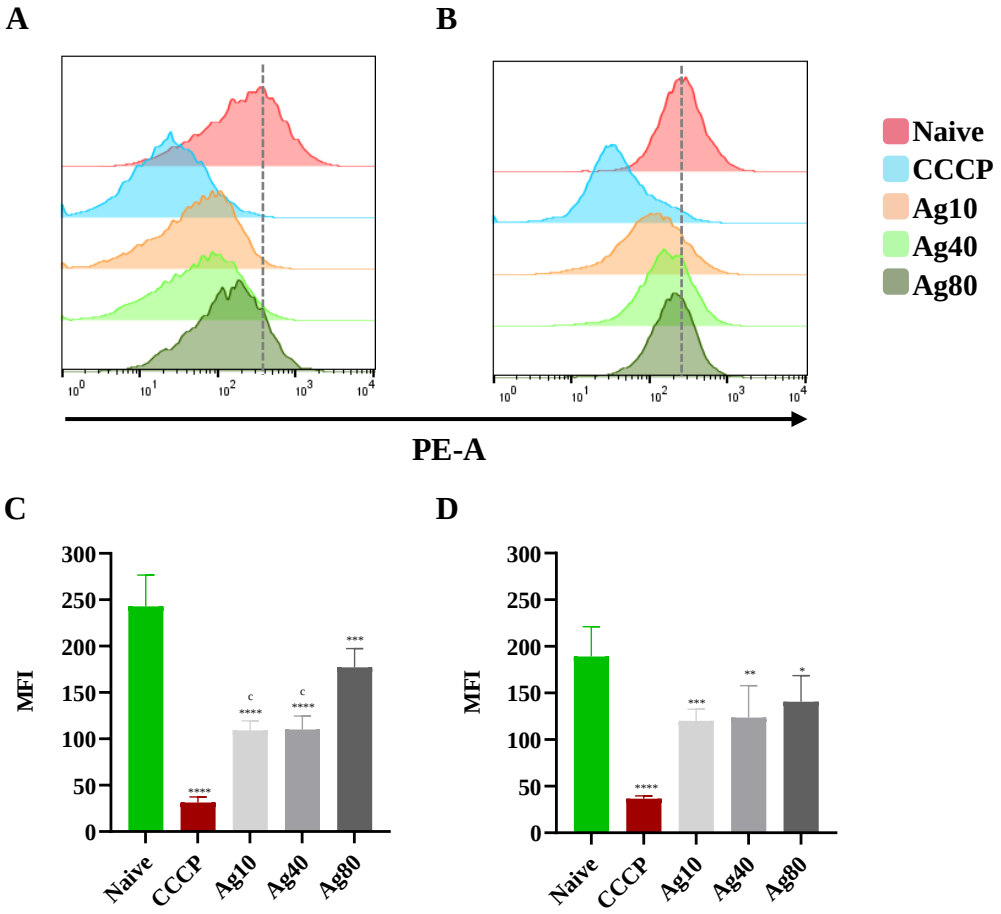


Figure 3.14. Detection of mitochondrial membrane potential state in MRC-5 and A549 cells following the exposure to AgNPs of different sizes using MitoProbe, TMRM assay by flow cytometry. Histogram of flow cytometry analysis of cells treated with AgNPs of different sizes at concentrations of 12.5 µg/ml for 24 hours in (**A**) MRC-5 and (**B**) A549 cells. The median fluorescence intensity (MFI) versus AgNPs of different sizes in (**C**) MRC-5 and (**D**) A549 cells. Carbonyl cyanide 3-chlorophenylhydrazone (CCCP) (50 mM) used as positive control. Bars represent the mean ± SD (n=4). (*) $p < 0.05$; (**) $p < 0.002$; (***) $p < 0.0002$ and (****) $p < 0.0001$ versus untreated group by ANOVA test. c = $p < 0.05$ versus cells incubated with the same concentration of Ag80 by ANOVA test.

Both MRC-5 and A549 cells demonstrated a disruption in the MMP. It was reported that ROS formation can mediated changes in the MMP to initiate apoptosis and was AgNPs size-dependent mitochondrial effect in macrophages exposed to AgNPs sized 15, 30, and 55 nm and in human breast adenocarcinoma exposed to AgNPs sized 15 and 75 nm (Carlson et al., 2008, Gopisetty et al., 2019). At the protein level, a study by Gurunathan et al. (2018) detected a release of cytochrome C in the cytoplasm along with the upregulation of proapoptotic proteins such as Bax and Bad, and the downregulation of antiapoptotic proteins including Bcl-2 and Bcl-xl in lung epithelial cancer cells (A549) exposed to AgNPs. However, the mechanism of AgNPs affecting the mitochondria is still unclear in terms of whether AgNPs influence the mitochondria directly or is mediated by the induction of ROS (Akter et al., 2018). The present study demonstrated that AgNPs can directly target the mitochondrial function as evident here by the loss of MMP and the disruption of the metabolic activity by MTT assay, thus can be a mechanism of AgNPs induced toxicity. Similar findings were previously postulated on the AgNPs toxic effects by targeting the mitochondria activity (Chairuangkitti et al., 2013, Kovács et al., 2016, Zhang and Gurunathan, 2016).

In this work, AgNPs demonstrated to influence cellular health and proliferation based on the detected cell viability. An oxidative stress induction by AgNPs was reported due to the overproduction of ROS and glutathione depletion. The mitochondria are considered as one of the primary sources of ROS formation under mitochondrial stress, however, the measured ROS in this study were mainly in the cytoplasm. AgNPs illustrated to mediate ultimate loss of MMP in both cell lines and this process is supposed to happen during the early stage of apoptosis and resulted in activation of caspase cascade. As consequence, the PS of the plasma membrane flip-flop occurred in the late stage of apoptosis which was confirmed earlier by the presence of late apoptosis/necrotic cells population. The cellular growth and division can be

also affected by cellular exposure to AgNPs. In order to further understand the toxic mechanism of AgNPs, the cell cycle progression was analysed in the next subsection.

3.3.1.5.5 Cell cycle progression analysis

The cellular exposure to NPs can lead to a biologically damaging response and cell injury. With an increase in the ROS level, cells under oxidative stress may potentiate the DNA damage, trigger cell cycle arrest and, eventually, induce cell death (Huang et al., 2017b). Therefore, AgNPs may interfere with cell cycle progression by suppressing different phases of the cell cycle: G0/G1, S and G2/M. The potential of AgNPs to supress the cell cycle at specific phases can be dependent on cell type and AgNPs characteristics (Eom and Choi, 2010, Chairuangkitti et al., 2013, Rosário et al., 2018). However, discontinuing exposure to toxic NPs can help cells to proliferate again. The inability of cells to recover and repair the damage may result in cell death through either apoptosis or necrosis (Huang et al., 2017b). As previously evident in the current study, the reduction in cell viability was observed in both lung cell lines following exposure to the three AgNPs sizes which indicated the cells ceased to proliferate. It was of interest to investigate if the AgNPs caused any disturbance in the cell cycle progression.

In this experiment, MRC-5 and A549 cells were treated for 24 and 48 hours with AgNPs of different sizes at concentrations of 7.5, 10, and 12.5 µg/ml. Topotecan and Etoposide were used as positive controls which induce G1/S and G2/M phase cell cycle arrests, respectively. For the MRC-5 cells, AgNPs of different sizes demonstrated potential arrest the cell cycle at the G2/M phase after 24 hours of exposure. Ag10 showed a pronounced accumulations of cells at G2/M phase with 34% at the highest concentration compared to 14% in the untreated group (**Figure 3.15 A and C**). At 48 hours of exposure, no sign of cell cycle arrest was detected

following exposure to AgNPs of different sizes. However, there was an increase in the population of subG1 phase, indicting the presence of apoptotic cell death in all AgNPs sizes and it was more noticeable with highest concentration. Concentration and size-dependent cell cycle arrest were noticed, in which Ag10 illustrated the pronounced effect on cell cycle progression of MRC-5 cells compared to other sizes.

In A549 cells, an increase in phase G2/M population was detected after 24 hours of exposure to the three AgNPs sizes in a concentration-dependent manner (**Figure 3.15 B and D**). It was also noticed the presence of apoptotic cells by increasing in the SubG cells which was more pronounced with Ag10 and Ag40. Moreover, no changes in the cell cycle progression after 48 hours of treatment, however, a substantial increase in the subG1 population were detected in a concentration-dependent patten for the three different AgNPs sizes. The highest accumulation of SubG1 population at concentration of 12.5 µg/ml with 24%, 28% and 20% in Ag10, Ag40 and Ag80, respectively, compared to 2% in untreated group. The induction of subG1 population by AgNPs was drastic in A549 cells than MRC-5 cells.

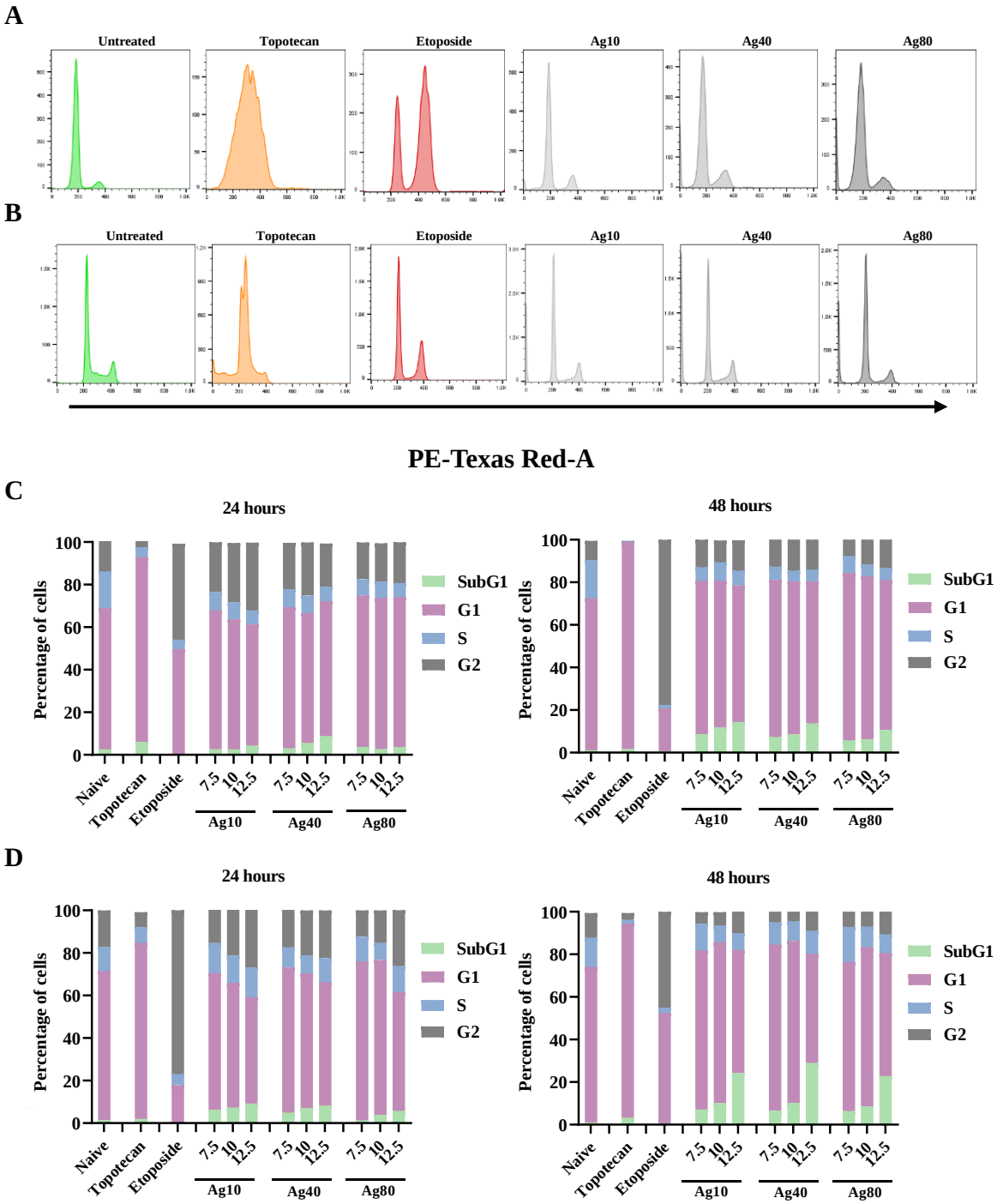


Figure 3.15. Cell Cycle progression analysis in MRC-5 and A549 cells following the exposure to AgNPs of different sizes using FxCycle™ PI/RNase Staining by flow cytometry. Histogram of flow cytometry analysis of cells treated with AgNPs of different sizes at high concentration (12.5 µg/ml) for 48 hours in (**A**) MRC-5 and (**B**) A549 cells. The stack graphs represent the cell percentage on each phase of the cell cycle after 24 and 48 hours of exposure to different concentration of AgNPs in (**C**) MRC-5 and (**D**) A549 cells. Bars represent the mean (n=4).

In agreement to our findings, several studies had reported cell cycle arrest in the G2/M phase triggered by AgNPs with concurrent increase in subG1 population in human lung epithelial cancer (A549) cells at concentration of 50- 100 µg/ml for 24 hours (Lee et al., 2011), in normal human lung fibroblast cells exposed to starch-coated AgNPs sized 6-20 nm at concentration of 25- 400 µg/ml for 48 hours (Asharani et al., 2009b) and nm in human lung epithelial cancer (A549) cells exposed to citrate-coated AgNPs (15 nm) at concentration of 12.1 µg/ml for 24 hours (Foldbjerg et al., 2012). Furthermore, a study indicated that AgNPs influence the toxicity in which G2/M phase cell cycle arrest with downregulation of cyclin B1 related gene in human keratinocytes cells treated with citrate-coated AgNPs for 48 hours (Bastos et al., 2016).

The present data demonstrated disturbance in cell cycle progression at G2/M phase, more specifically after 24 hours of incubation to AgNPs of different sizes in both cell lines. The G2/M transition phase is the point where the cell is preparing for mitosis to separate into two daughter cells. Blocking the cells cycle at this phase by AgNPs is most likely due to DNA damage and thereof prevent the cells to enter mitosis. Therefore, an increase in G2/M phase indicated an increase in the cell numbers at G2 growth phase for DNA repairing. Similarly, a study observed G2/M cell cycle arrest by AgNPs and it was reported an increase in the p21 and p53 expressions, which are essential proteins correlated with the regulation of cell cycle (Lee et al., 2011). At 48 hours, no changes in the cell cycle progression were observed, however, a substantial increase in apoptotic populations were detected in both cell lines in a concentration- and size-dependent manner. It could be the cells failed to repair the severe DNA damage at G2/M phase thereof, the cells undergo apoptosis. The current results supported the earlier evidence of late apoptosis/necrosis cell death measured by Annexin-V/PI assay in both cell lines. The induction of cell cycle arrest and halting the proliferation process under AgNPs influence can be reversible effects. It is possible for the cell to recover again and start the

proliferation process. The next subsection investigated the ability of cells to recover following AgNPs exposure.

3.3.1.5.6 Cells recovery post AgNPs treatment

It was of interest to examine the cell capability to recover after acute exposure to AgNPs. AgNPs may continue to induce an effect even after exposure cessation. Inability of cells to recover has been previously demonstrated for AgNPs (Dalzon et al., 2019). The ability of MRC-5 and A549 cells to survive and proliferate following exposure to toxic concentrations of Ag10, Ag40, and Ag80 were evaluated in the current study. Both cells were treated with the three AgNPs sizes in a concentration range of 5-12.5 µg/ml, which were selected based on the previous cytotoxicity results. After one day of treatment, the cells were allowed to recover for two, three, and four days by adding a fresh cell culture media. The cell viability was assessed at each time point using a mLDH assay.

In the MRC-5 cells, continuous decreases in cell viability were noticed after one day of removing the Ag10 and Ag40 at different concentrations (**Figure 3.16 A and B**). At days 3 and 4, the MRC-5 cells appeared to resume cell proliferation after exposure to Ag10 and Ag40. However, it was observed that the MRC-5 cells was not able to recover over time at the highest concentration (12.5 µg/ml) of Ag10 . In case of Ag80, a substantial recovery of the MRC-5 cells was observed over time after exposure to Ag80 at different concentrations (**Figure 3.16-C**). For the A549 cells, Ag10 showed a reduction in cell viability at days 2 and 3 with the lower concentrations. Meanwhile, the cells remained affected from the exposure to highest concentrations of Ag10 (10 and 12.5 µg/ml) and demonstrated no changes in cell viability at days 2 and 3 but cells started to recover after four days (**Figure 3.16-D**).

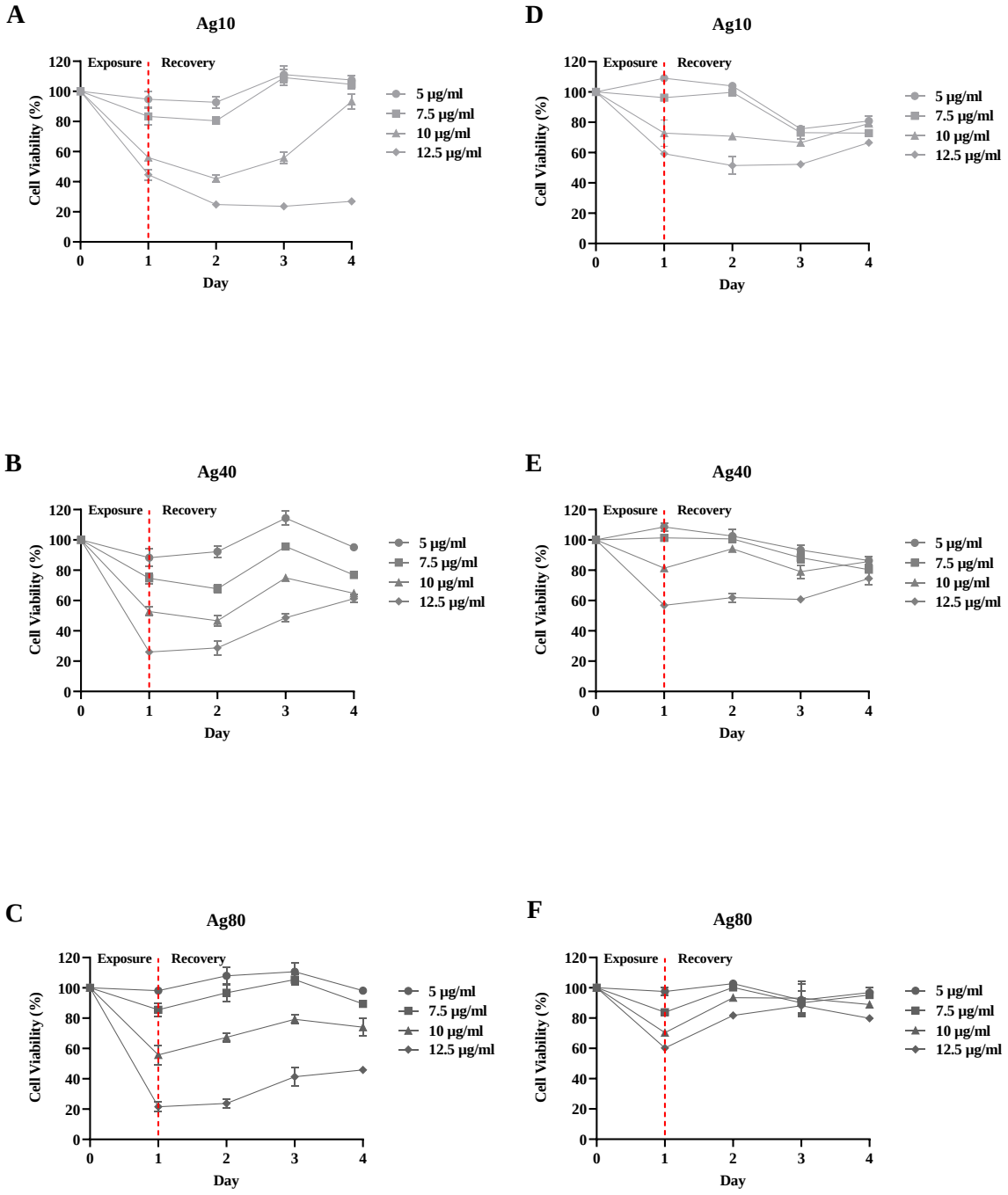


Figure 3.16. Recovery of MRC-5 and A549 cells following the exposure to AgNPs of different sizes. Both cell lines treated with AgNPs of different sizes in a concentration range of (5-12.5 µg/ml) for 1 day. Then the cells allowed to recover by adding fresh cell culture media for 2, 3 and 4 days. The cells recovery was detected by measuring the cell viability after MRC-5 cells exposure to (**A**) Ag10, (**B**) Ag40 and (**C**) Ag80 and A549 cells exposure to (**D**) Ag10, (**E**) Ag40 and (**F**) Ag80. Data represent the mean ± SD (n=4).

For A549 cells treated with Ag40, it was reported a consistent decrease in viability percentage at the lower concentrations over time. The A549 cells demonstrated positive cell proliferation after four days with Ag40 at the higher concentrations (10 and 12.5 µg/ml) (**Figure 3.16-E**). An increase in A549 cell proliferation was observed over time with different concentrations of Ag80 **(Figure 3.16-F**).

The cells recovery from the toxic effect of AgNPs was suggested to be concentration-dependent, as the cells showed slow or no recovery at the highest concentration of AgNPs with all sizes in both cell lines. Moreover, A549 cells demonstrated a reduction in cell viability with low concentrations of AgNPs. One possible suggestion of this observation is that AgNPs may return inside the cells, and the toxic effect of AgNPs continued after removal of AgNPs. However, the cells ability to proliferate was time-dependent and occurred in a slow pattern, which indicated a possible long-term consequence following AgNPs exposure in both healthy and canoes lung cell lines. Thereby, AgNPs biocompatibility must be considered when using AgNPs for cancer treatment. The slow recovery of MRC-5 cells following exposure to high concentrations of AgNPs and more specifically with Ag10 has revealed the impact of AgNPs physicochemical properties on their cellular behaviour.

The results of the current work were in accordance with those of previous study. A study conducted on human retinal epithelial cells reported the potential recovery of the cells at high concentration, up to 75 µg/ ml following cells treatment for one day and left for two to three days to recover (Garcia et al., 2019). Nevertheless, cell death was detected at the recovery stage with G2/M phase cell cycle arrest. Moreover, the same study examined the repeated exposure of AgNPs on the cells and identified the possible accumulation of AgNPs with long incubation time, causing an impairment of cell division due to a DNA damage (Garcia et al., 2019). Another study by Dalzon et al. (2019) exposed the macrophages to PVP-coated AgNPs

for 24 hours and then allowed to recover for 72 hours. The mitochondrial impairment, and decrease in the glutathione level which were observed after 24 hours of the AgNPs treatment, returned to their normal activity after 72 hours of recovery thus indicated the cell process were able to recover from AgNPs detrimental effect. The AgNPs potential to interfere with toxicity assays used in this work was considered. The next subsection demonstrates the investigation and procedure were conducted in this study to avoid the possibility of AgNPs-assay interference.

3.3.1.5.7 NPs- assay interference

In vitro assessments of NPs need some consideration when using standard toxicity assays. Because of certain NPs intrinsic features, like their optical properties of absorption or scattering light, electrical and catalytic activity. Possible NPs interference with different readout systems, such as absorbance, luminescence and fluorescence assays can result in false positive or negative outcomes (Guadagnini et al., 2015). NPs interaction with a fluorescent probe may result in NPs interference with light intensity emitted from the fluorescent probe (Riaz Ahmed et al., 2017). This work has considered the potential AgNPs interference with the assays used. Different procedures were performed while running the experiment to ensure the reliability of the results especially with the AgNPs concentrations used in this study Therefore, modified LDH assay was used instead of the original LDH assay in which the sample centrifugation step was performed after lysing the cells to avoid including any AgNPs residues in the testing sample. Moreover, in MTT and GSH/GSSG-Glo assays the cells were washed with DPBS after aspiration of the cell culture media to ensure washing the cells from AgNPs traces. AgNP interference with fluorescent assays were investigated. No AgNPs interference was observed with the fluorescent assays as shown for CellRox™ deep red assay

in (**Figure A2**), Alexa Fluor® 488 Annexin V/Dead cell apoptosis assay in (**Figure A3)**, MitoProbe™,TMRM assay in (**Figure A4**) and FxCycle™ PI/RNase staining in (**Figure A5**).

Based on our findings in this section about the AgNPs size-dependent effect on cellular toxicity in 2D monolayer cell culture model, however, it was of interest to further investigate the AgNPs size impact on 3D cell culture model. The next section illustrates and discusses the findings.

3.4 Toxicological assessment of AgNPs of different sizes in a 3D in vitro cell culture model

Different methods are used to create a 3D culture model which can be divided into two types; scaffold-based and scaffold-free culture models. The first type is formed by polymeric biomaterials, such as collagen and chitosan. The scaffold-free culture forms spheroids, in which the cells compact togethers (Costa et al., 2018). The 3D multicellular tumour spheroids of the scaffold-free method can be generated using a liquid overlay, which promote cell aggregation and avoid the adhesion of the cell on the well-plate surface. The 3D multicellular spheroids exemplify the physiological microenvironment of the *in vivo* features, such as cell-cell signalling, hypoxia and the extracellular matrix (Costa et al., 2016). The aim of this section was to investigate the influence of AgNPs size on the toxicity of lung tumour A549 spheroids and to compare the potency of AgNPs toxic effect between the 3D spheroids and the 2D monolayer models.

3.4.1 Results and discussion

3.4.1.1 Spheroids preparation

The 3D lung multicellular tumour spheroids (A549) in this work were prepared using a liquid overlay method. The growth curve was initially established and the spheroids growth were

imaged over seven days (**Figure 3.17-A**). The spheroids created a sphere-like shape and their circumference sizes were measured using ImageJ software. As illustrated in **Figure 3.17-B**, the spheroid circumference size on the first two days was around 20,000 µm. The size then gradually decreased over time, as the spheroids appeared denser. From days 5 to 7, the spheroid circumference size reached a plateau, with the smallest size of 1,200 µm reported along with the presence of dissociated cells around the spheroids borders (**Figure 3.17-A**).

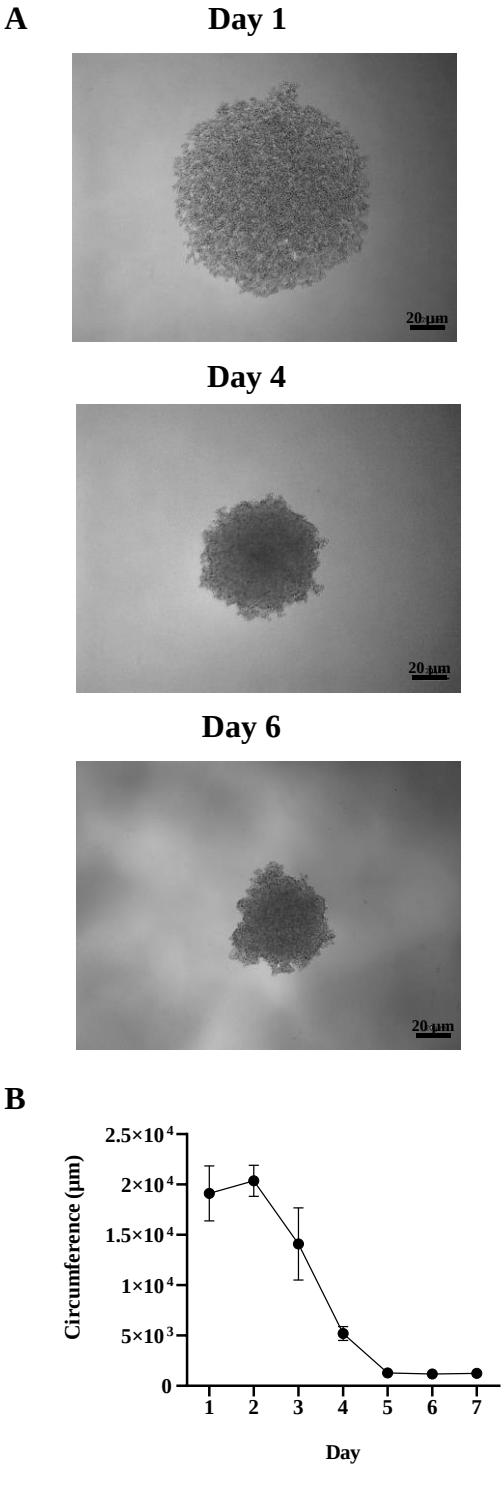


Figure 3.17. Growth curve of A549 spheroids. (**A**) Optical microscope images of A549 spheroids formation on day 1,4 and 6. The cells seeded at density of 8000 cells/well. Scale bar (20 µm). (**B**) A549 spheroid growth curve represents the circumference size changes in (µm) over 7 days. Data represent mean ± SD (n=20).

The spheroids demonstrated appropriately compact structure with denser core and well defined boarder (rim) at day 4 which was the day selected to treat the spheroid with AgNPs. The changes in spheroids morphology were assessed following their exposure to AgNPs in the next subsection.

3.4.1.2 Spheroids morphology and size changes

The A549 spheroids were treated at day 4 with Ag10 and Ag80 at concentration of (5 and 12.5 µg/ml) for 24 and 48 hours. Those concentrations were selected to investigate the potency of AgNPs and the sensitivity of A549 spheroids by their exposure to low and high concentration of AgNPs. DMSO (20%) was used as a positive control. At each time point, the spheroids were imaged with optical microscope. The changes in spheroid size were calculated by measuring the spheroid circumference. The spheroids treated with Ag10 revealed a concentration- and time-dependent effect **(Figure 3.18 A and B**). No changes in the spheroids integrity was reported at the low concentration of Ag10 at either time point with spheroid sizes of 1620 and 1670 µm, respectively compared to untreated spheroids (1570 µm). However, disruption of the spheroids compaction and dissociation of the cells were observed with the circumference size increased with time at high concentration (12.5 µg/ml) by 1.8- and 2.7-fold increases at 24 and 48 hours, respectively when compared to the size before treatment (**Figure 3.18-C**). For the spheroids treated with Ag80, an increase in the spheroid circumference was noted only after 48 hours of exposure to the both concentrations of Ag80 (**Figure 3.19-C**). Moreover, it was observed at 48 hours of spheroids treatment with high concentration of Ag80, an adsorption and accumulation of Ag80 on the spheroids, particularly on the spheroids border at the proliferating zone (**Figure 3.19-B**).

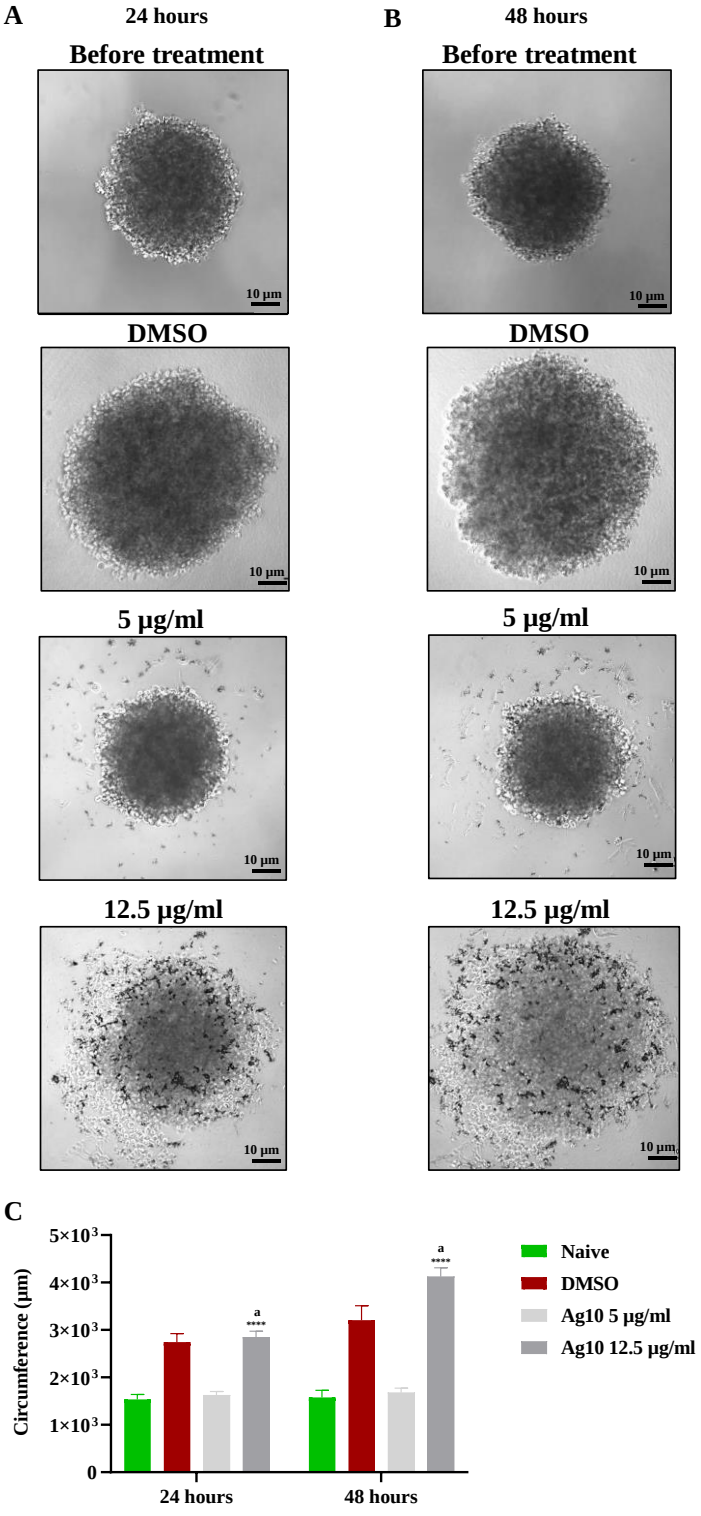


Figure 3.18. A549 spheroids morphological changes following the exposure to Ag10. Optical microscope images of A549 spheroids treated with Ag10 for (**A**) 24 and (**B**) 48 hours at concentrations of 5 and 12.5 µg/ml. Scale bar (10 µm). DMSO (20%) used as positive control. (**C**) Bar graph represents the circumference size of A549 spheroids after treatment with Ag10 for 24 and 48 hours. Bars represent the mean ± SD (n=20). (****) $p < 0.0001$ versus untreated group by ANOVA test. a = $p < 0.05$ versus cells incubated with 5 µg/ml of Ag10 by ANOVA test.

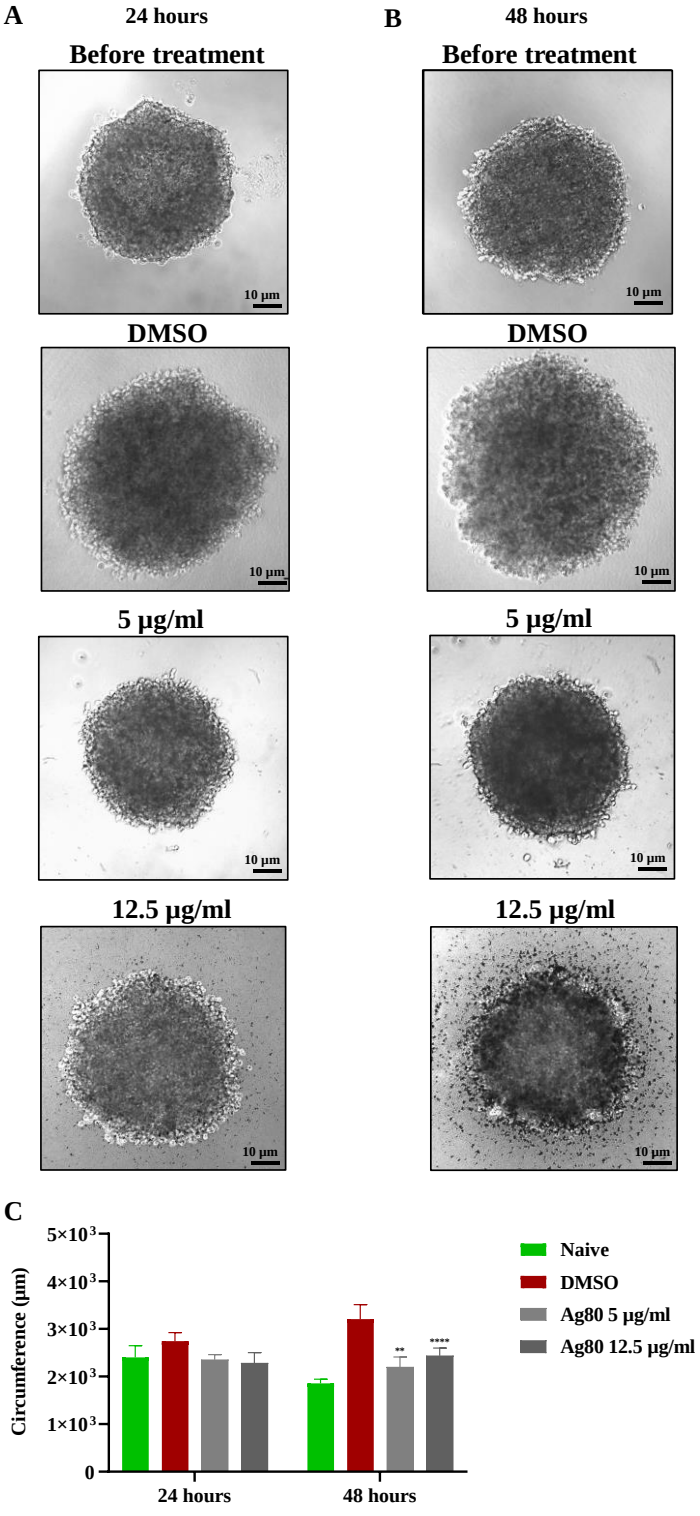


Figure 3.19. A549 spheroids morphological changes following the exposure to Ag80. Optical microscope images of A549 spheroids treated with Ag80 for (**A**) 24 and (**B**) 48 hours at concentrations of 5 and 12.5 µg/ml. Scale bar (10 µm). DMSO (20%) used as positive control. (**C**) Bar graph represents the circumference size of A549 spheroids after treatment with Ag80 for 24 and 48 hours. Bars represent the mean ± SD (n=20). (**) $p < 0.002$; (****) $p < 0.0001$ versus untreated group by ANOVA test.

The spheroid integrity was altered upon exposure to high AgNPs concentrations, particularly with Ag10. A possible explanation for the significant changes observed in the spheroid structures after the treatment with smaller sized AgNPs compared to larger ones that the smaller sized AgNPs can diffuse more easily between the cells (Senyavina et al., 2016). A study reported that the toxicity effect of AgNPs on spheroids model was dependent on AgNPs concentration. A reduction in cell viability by disruption of the membrane permeability was reported in concentration-dependent manner with AgNPs sized 10 nm exposed to primary human hepatocytes spheroids models at concentration range of 5- 50 µg/ml for 24 hours (Senyavina et al., 2016). To further understand the influence of AgNPs on A549 spheroids, a cytotoxicity assessment was conducted to evaluate the viability of the cells after AgNPs exposure.

3.4.1.3 Spheroids cytotoxicity assessment

Cell viability was measured using the LIVE/DEAD™ Cell Imaging Kit to distinguish between the live and dead cells. The spheroids were imaged following 48 hours of treatment with Ag10 and Ag80 at concentrations of 5 and 12.5 µg/ml. As shown in **Figure 3.20**, the presence of dead cells (red signals) in the spheroids after 48 hours of exposure were observed in both sizes of AgNPs at high concentration (12.5 µg/ml) and it was more pronounced with Ag10. The spheroid treated with Ag10 caused a destruction in the spheroid compaction (**Figure 3.20-A**).

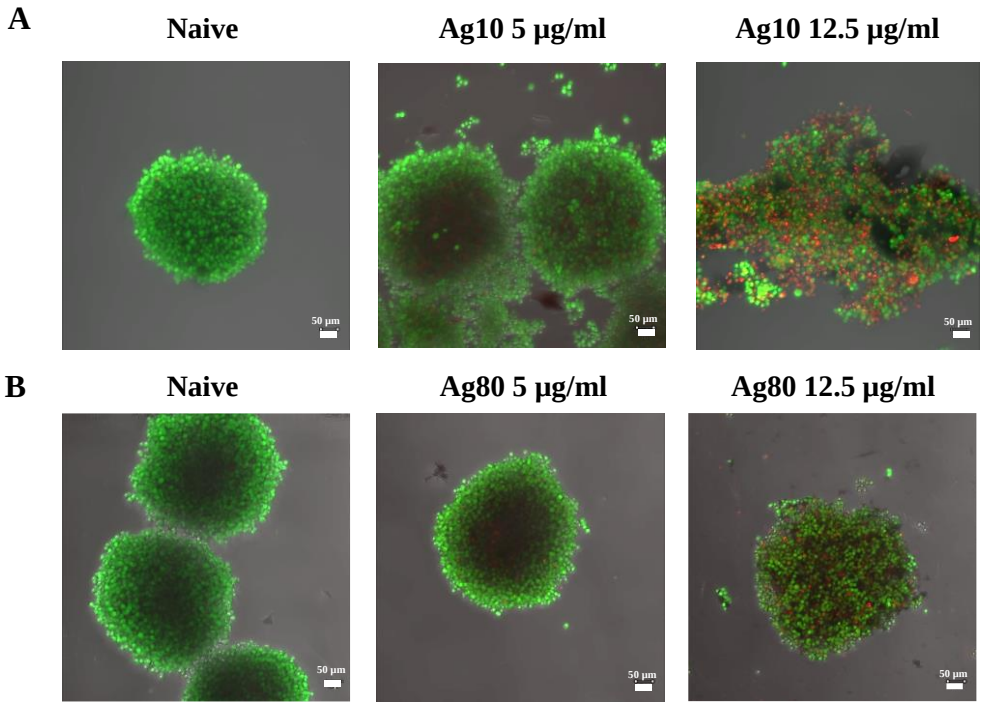


Figure 3.20. Cytotoxicity assessment of A549 spheroids following the exposure to Ag10 and Ag80. Confocal microscopy images of A549 spheroids treated for 48 hours with (**A**) untreated cells; Ag10 (5 and 12.5 µg/ml) and (**B**) untreated cells; Ag80 (5 and 12.5 µg/ml). Green signal corresponding to live cells and red signal corresponding to dead cells. Scale bar 50 µm.

The penetration of NPs into spheroids has been previously explained by many hypotheses, including NPs interaction with the outer surface of the spheroids via electrostatic attraction (Huang et al., 2017a). This suggestion is greatly influenced by protein corona, which might decrease the NPs affinity to internalise the cells. Moreover, the same author claimed that a negatively charge surface is the optimal surface charge gained by NPs to promote their interaction with cells because of the electric charge gradient displayed in spheroids of layer-like structure (Huang et al., 2017a). Another assumption is the dissolution of the metal NPs, in which Souza et al. (2019) presumed that the dissolved titanium ions from the titanium dioxide can form bio-complex with protein which facilitate their adsorption and internalisation into human osteoblast spheroids.

To conclude, AgNPs demonstrated size-, concentration- and time-dependent toxic effect upon their exposure to the healthy and cancerous lung cells. Late apoptosis/necrosis cell death is suggested to be induced via mitochondrial-dependent pathway. Moreover, an induction of ROS along with depletion of GSH level is an indication of AgNPs promoting oxidative stress. The findings from the AgNPs toxicity in 3D multicellular A549 spheroids model agreed with the 2D cell culture model results of AgNPs size-dependent toxicity effect. Moreover, smaller size of AgNPs demonstrated potential detrimental effect to the A549 spheroids which may consider for cancer treatment. However, A549 spheroids showed more resistance to AgNPs exposure compared to A549 cells in 2D monolayer model.

To further study the impact of NPs composition in associated toxicity which was one of the present study aims, the next chapter was devoted for AuNPs toxicity investigation using the same size of AgNPs (10, 40 and 80 nm) to compare the influence of NPs size as well as the NPs composition on toxicity.

Chapter 4

Toxicological assessment of AuNPs of different sizes

4.1 Introduction

Yet, to date, there is no consensus on the safety of AuNPs and their uses in medicine requires careful evaluation to understand the AuNPs potential adverse effects at a cellular level (Daraee et al., 2016). It is essential to consider biocompatibility and nanotoxicity studies of AuNPs prior to proceeding with biomedical applications. This chapter focuses on studying the relationship between AuNPs size and toxicity. As an initial step, the AuNPs were characterised to validate the size of the purchased AuNPs. Then, toxicity investigations were performed to assess the AuNPs potential to induce apoptosis, cell cycle arrest and oxidative stress in a 2D monolayer cell culture model. Finally, the cytotoxicity mediated by AuNPs in a 2D monolayer model was compared to toxicity induced by AuNPs in a 3D multicellular spheroid cell culture model.

4.2 Characterisations of AuNPs of different sizes

Different NPs can be manufactured with distinct characteristics. Defining NPs characteristics is an essential approach to assess their biological implications (Karakoçak et al., 2016). Strong evidence has been found for the relationship between specific NPs characteristics and their cellular adverse responses (Falagan-Lotsch et al., 2016, Surapaneni et al., 2018). The aim of this section was to characterise the purchased AuNPs with size of 10, 40 and 80 nm using several methods in order to examine AuNPs size, morphology, surface charge and stability in cell culture medium.

4.2.1 Results and discussion

4.2.1.1 Size measurement

The size of AuNPs can affect their cellular uptake and interaction with cellular components (Chithrani et al., 2006). Therefore, the size of the purchased AuNPs was examined as an initial step in this work using several approaches including TEM, DLS and UV-Vis spectroscopy. TEM micrographs were captured to determine the AuNPs size distribution and morphology. As shown in **Figure 4.1**, AuNPs of different sizes demonstrated a spherical shape. The AuNPs size distribution was also estimated by measuring the diameter of 200 individual particles using Image J software. The reported mean particle sizes of the AuNPs were within the manufacturer-proposed sizes (**Figure 4.1**). DLS was the second method used to analyse the hydrodynamic sizes of the AuNPs. The reported z-average sizes were within the primary sizes of AuNPs (**Table 4.1**). The recorded PDI values revealed the monodispersity of the samples (**Table 4.1**). The results represented the averages of three samples analysed from different AuNPs batches.

AuNPs demonstrate extraordinary optical properties which are highly dependent on their size. The UV spectrum of AuNPs was detected using UV-Vis spectroscopy. It was noticeable that the absorption peak was red-shifted along with increasing AuNPs sizes (**Table 4.1**). An increase in the AuNPs diameters resulted in longer absorption wavelength (López-Muñoz et al., 2012). Taking together, AuNPs of the three sizes demonstrated good stability and the measured sizes for Au10 Au40 and Au80 were relevant to their primary sizes.

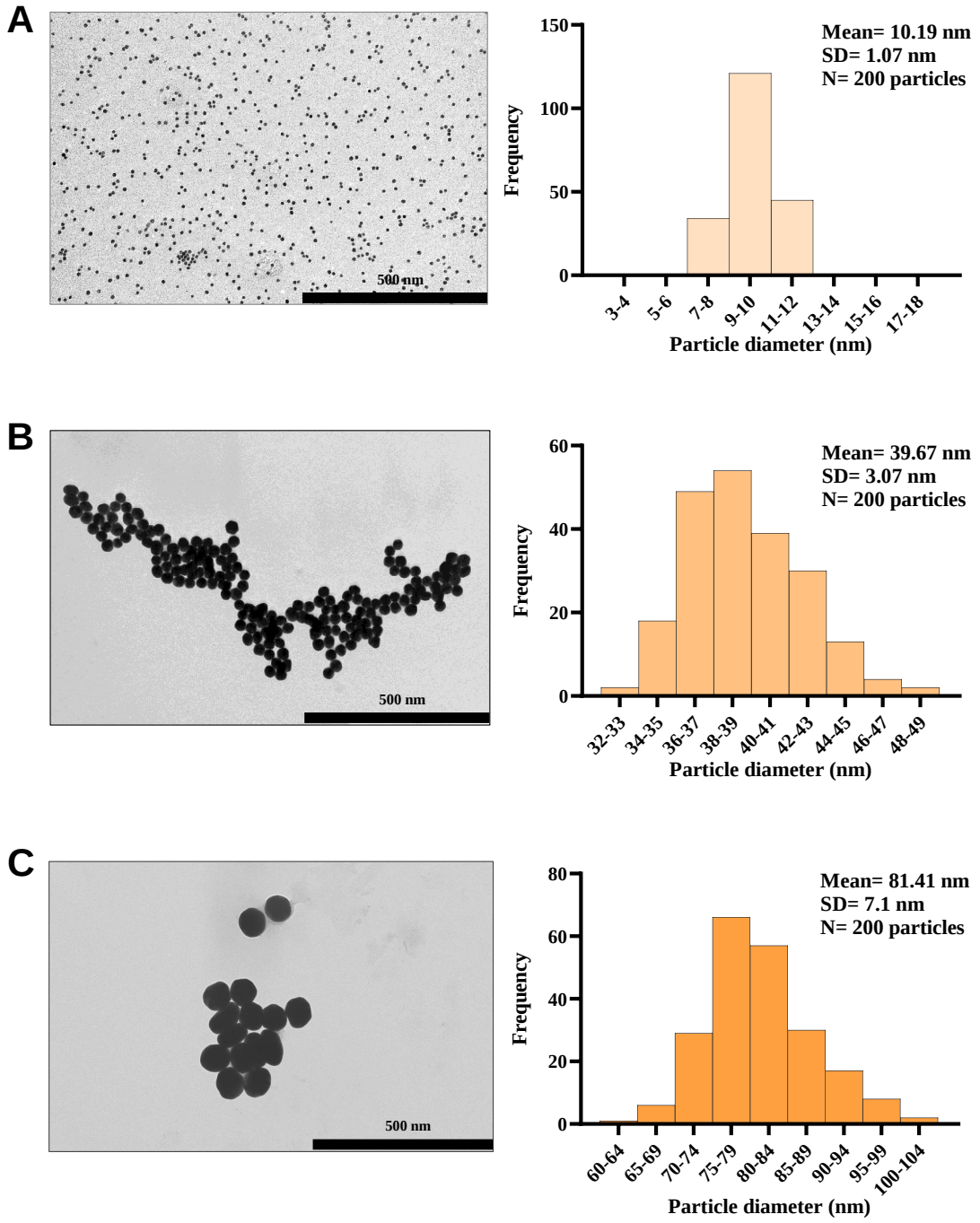


Figure 4.1. TEM micrographs and the size distributions of AuNPs of different sizes. Micrograph images with the size distribution of (**A**) Au10; (**B**) Au40 and (**C**) Au80. The size distribution of AuNPs represents the mean average size ± SD (n= 200 particles) measured by using Image J software.

Table 4.1. Summary of the characterisations of AuNPs.

Characterisation	Method	Au10	Au40	Au80
Morphology	TEM	Spherical	Spherical	Spherical
Average size (nm)	TEM	11 ± 1	40 ± 3	81 ± 7
Z-average size (nm)	DLS	15 ± 2	42 ± 1	78 ± 2
PDI	DLS	0.4 ± 0	0.3 ± 0	0.1 ± 0
ζ-potential (mV)	DLS	-31 ± 2	-37 ± 1	-38 ± 0
λ max (nm)	UV-Vis	517	526	551

Symbol: PDI (Poly dispersity index), ζ-potential (zeta potential), λ max: (maximum absorption wavelength).

4.2.1.2 Surface charge analysis

The surface charge of the AuNPs can provide information about their stability in the colloids. The measured ζ-potential demonstrated the negative surface of AuNPs of different sizes (**Table 4.1**). The negative charge detected was corresponding to the presence of sodium citrate on the AuNPs surfaces. The obtained ζ-potential values were within the optimal level (> -30 mV), indicating the stability of AuNPs of different sizes (Sikora et al., 2015).

4.2.1.3 AuNPs stability in cell culture media

The interaction of cell culture media composition primarily serum proteins by adsorption into the NPs surface can mediate the NPs properties including size and aggregation state (Strojan et al., 2017). In this work, the stability of AuNPs of different sizes was assessed by incubating AuNPs at a concentration of 26 µg/ml in a cell culture medium in the presence or absence of (10%) FBS for 30 minutes, 24 hours and 48 hours at 37°C.

The measured z-average sizes of Au10, Au40 and Au80 in EMEM with (10%) FBS were increased after incubation at three different exposure times (**Table 4.2**), thus could be the result of protein corona formation. Similar findings were observed with AuNPs in Ham's F-12

medium with (10%) FBS (**Table A2**). The adsorption of protein into the surface of AuNPs is probably due to the weak binding of the sodium citrate coating with AuNPs and this process is suggested to occur immediately following the interaction of the AuNPs with the cell culture medium (Strojan et al., 2017).

Table 4.2. The stability of AuNPs in EMEM with or without (10%) FBS by measuring the size using DLS.

Z-average sizes of AgNPs in EMEM with (10%) FBS						
AuNPs	**30 mins**		**24 hrs**		**48 hrs**	
	Size	**PDI**	**Size**	**PDI**	**Size**	**PDI**
Au10	23 ±1	0.4 ±0	41 ±3	0.6 ±0	55 ±0	0.5 ±0
Au40	60 ±1	0.2 ±0	89 ±1	0.2 ±0	56 ±1	0.1 ±0
Au80	111 ±2	0.08 ±0	121 ±1	0.1 ±0	120 ±4	0.09 ±0
Z-average sizes of AgNPs in EMEM without (10%) FBS						
AuNPs	**30 mins**		**24 hrs**		**48 hrs**	
	Size	**PDI**	**Size**	**PDI**	**Size**	**PDI**
Au10	2250 ±204	0.8 ±0	6630 ±178	1 ±0	2060 ±221	1 ±0
Au40	2367 ±253	1 ±0	2730 ±205	0.5 ±0	5470 ±799	1 ±0
Au80	2551 ±15	0.4 ±0	2850 ±199	1 ±0	2479 ±732	1 ±0

The z-average sizes of AuNPsv in EMEM without serum (10% FBS) were also assessed. The z-average sizes of AuNPs of different sizes detected were above 2000 nm with high PDI values (**Table 4.2**). Moreover, it was observed an aggregation and precipitation of AuNPs over time which can be a result of the presence of high salt concentration in the media (Sun et al., 2016).

In conclusion, the data demonstrated an alteration in the AuNPs sizes in cell culture media with FBS due to protein corona formation. Insights about AuNPs characteristics were generated in this section. The next step was to investigate the cytotoxicity profile of the AuNPs of different sizes in a 2D cell culture model. The following section presents the toxicity results.

4.3 Toxicological assessment of AuNPs of different sizes in a 2D in vitro cell culture model

AuNPs size is one factor that can drive different adverse cellular effects (Liu et al., 2014). Moreover, AuNPs concentration and exposure time are also fundamental factors that may affect NPs toxicity profiles (Lopez-Chaves et al., 2018). The aim of this section was to investigate the influence of AuNPs of different sizes in inducing distinct cellular adverse events in a 2D cell culture model. The toxicity assessments were performed systematically to investigate the cytotoxicity of AuNPs of different sizes after 3, 24 and 48 hours of exposure in healthy lung cells (MRC-5) and cancerous lung cells (A549). Following that, the mechanisms of AuNPs toxicity including, oxidative stress, cell cycle arrest and apoptosis were studied.

4.3.1 Results and discussion

4.3.1.1 Cell viability assessment of sodium citrate stabiliser

The sodium citrate stabiliser maintains the stability of AuNPs by reducing the tendency of AuNPs to form aggregates (Morais et al., 2012). However, the amount of stabilising agent used may negatively affect the cells (Freese et al., 2012). The potential toxicity of sodium citrate stabiliser was previously assessed in chapter 3 (section 3.3.1.1). Therefore, the highest concentration of the three AuNPs sizes used in this study was 41 µg/ml which was equal to using 1.3 mM of sodium citrate to ensure the minimum toxicity potential induced by stabiliser. The following step was to assess the cell viability of AuNPs of different sizes on both MRC-5 and A549 cells.

4.3.1.2 Cell viability assessment of AuNPs of different sizes

The cell viability assessment of the AuNPs was performed to evaluate the toxic effect of AuNPs exposure to the healthy and cancerous lung cells and to investigate the AuNPs potential to induce size-, concentration- and time-dependent toxicity. Two cell viability assays were used in this work: mLDH and MTT assays.

In the mLDH assay, the percentage of cell viability was assessed by quantification of LDH enzyme of the viable cells. The amount of LDH enzyme of the treated group was calculated to the relative amount of the untreated group. The MRC-5 and A549 cells were exposed to AuNPs of different sizes at a concentration range of 19-55 µg/ml for 3, 24 and 48 hours. Both MRC-5 and A549 cells demonstrated no significant reduction in cell viability following 3 hours of incubation with AuNPs of different sizes (**Figure 4.2 A and D**). However, a decrease in cell viability up to 70% with the highest concentration (55 µg/ml) at 3 hours of treatment. Concentration- and time-dependent toxicity was observed in both MRC-5 and A549 cells following 24 and 48 hours of incubation (**Figure 4.2**).

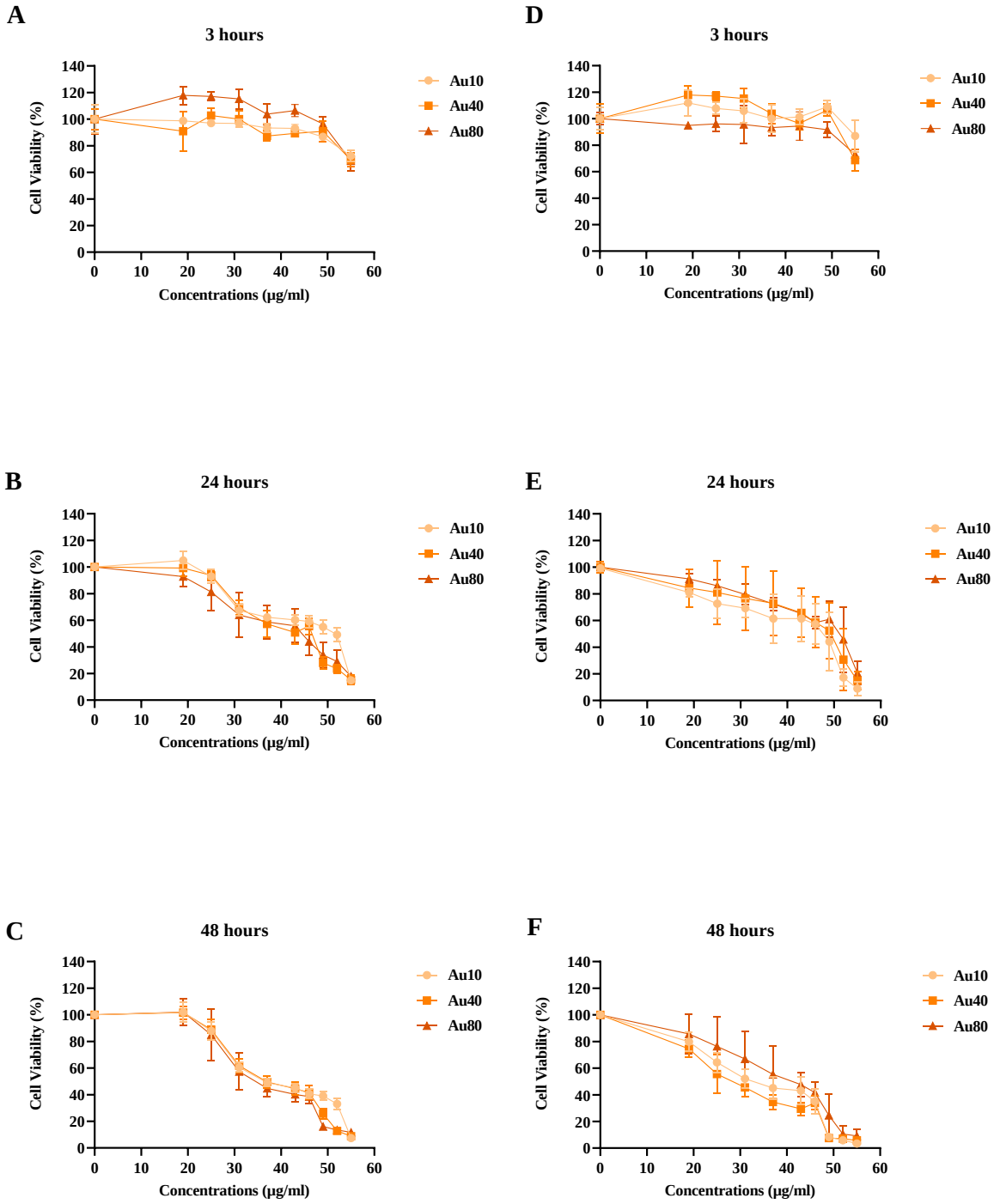


Figure 4.2. Cytotoxicity assessment of MRC-5 and A549 cells following the exposure to AuNPs of different sizes using mLDH assay. Cell viability percentage of AuNPs of different sizes using a concentration range of (19– 55 µg/ml) after 3, 24 and 48 hours of incubation in (**A-C**) MRC-5 and (**D-F**) A549 cells. Data represent means ±SD (n=3).

Next, the MTT assay was conducted to measure the metabolic activity of the cells. The MRC-5 and A549 cells were treated with AuNPs of three sizes for 24 and 48 hours at a concentration range of 19-55 µg/ml. The results revealed the potential of AuNPs to directly affect mitochondrial function and interrupt the mitochondrial metabolism state. AuNPs of the three sizes were able to decrease the cell viability in a concentration- and time-dependent pattern in both MRC-5 and A549 cells (**Figure 4.3**). Nevertheless, no further reduction were observed in the cell viability at concentrations between 49- 55 µg/ml after 48 hours of exposure to the three sizes of AuNPs in both MRC-5 and A549 cells (**Figure 4.3**). No size-dependent toxicity pattern was observed.

Based on mLDH and MTT cell viability findings, the CC50 values were calculated using GraphPad Prism 8 software. It worth mentioning that the cytotoxicity of AuNPs detected by reduction of cell viability at high concentrations (> 41 µg/ml) can be potentiated by the presence of sodium citrate and inadequate amount of nutrient exposed to the cells. In the present experiment, high concentrations of AuNPs were used only to calculate the CC50 value and based on the cytotoxicity of sodium citrate assessed earlier in this study, a concentration of 41 µg/ml was chosen to be the highest AuNPs concentration can be used in this study to minimise the possible detrimental effect of sodium citrate stabiliser.

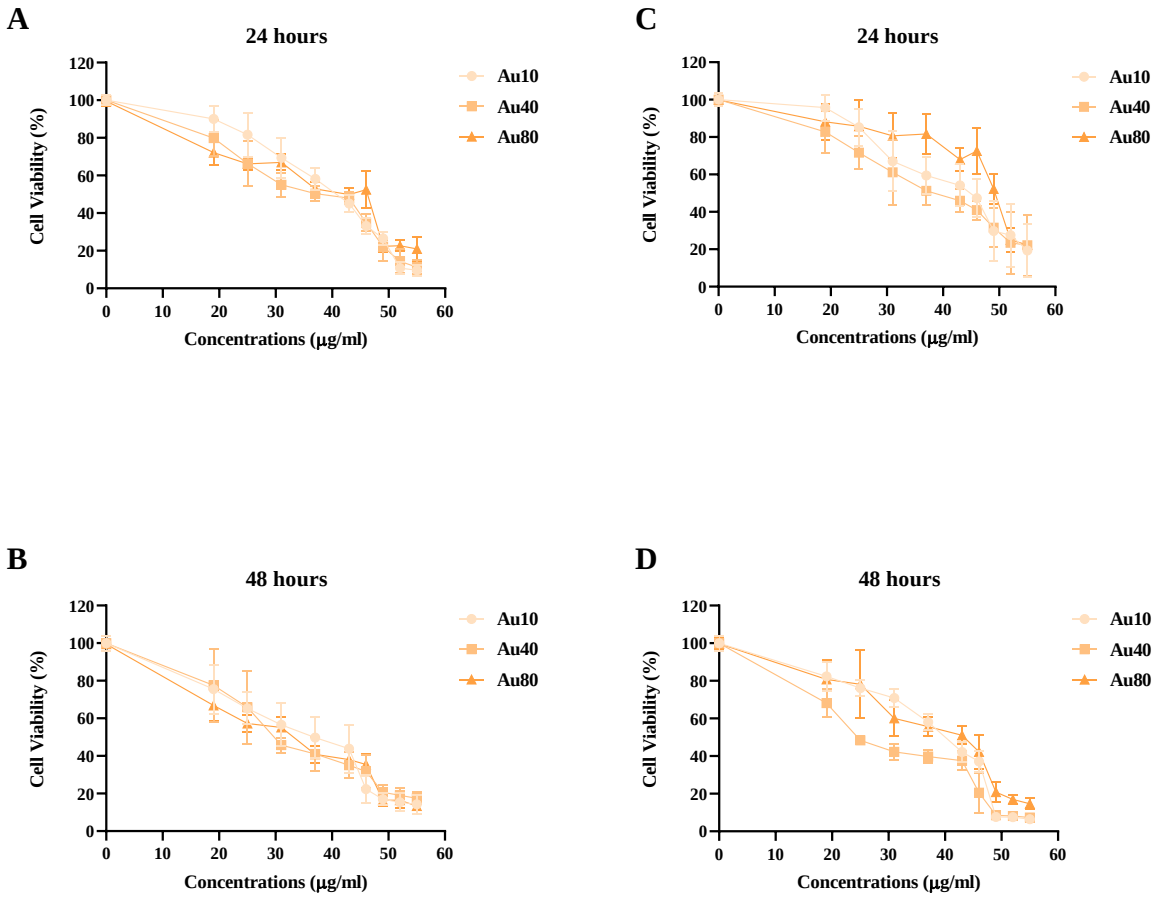


Figure 4.3. Cytotoxicity assessment of MRC-5 and A549 cells following the exposure to AuNPs of different sizes using MTT assay. Cell viability percentage of AuNPs of different sizes using a concentration range of (19–55 µg/ml) after 24 and 48 hours of incubation in (**A-B**) MRC-5 and (**C-D**) A549 cells. Data represent means ±SD (n=3).

The CC50 values estimated from mLDH revealed that MRC-5 cells were more sensitive to Au40 and Au80 compared to Au10 at 24 and 48 hours (**Table 4.3**). On the other hand, A549 cells exhibited more sensitivity toward smaller size AuNPs: Au10 > Au40 > Au80 at 24 hours. Similar to our findings in A549 cells, a study in human pulmonary fibroblasts exposed for 24 hours to water-based AuNPs sizes of different sizes was reported a size-dependent toxicity. The 50% cell viability was found at concentrations of 15.3, 17.8 and 18.9 µg/ml for AuNPs sizes of 30, 50 and 90 nm respectively (Ávalos et al., 2015). The measured CC50 values from the MTT assay illustrated that Au40 exhibited the most potent effect after 24 hours of exposure to both MRC-5 and A549 cells (**Table 4.3**). Interestingly, A549 cells implied high sensitivity to Au40 than other sizes in both assays after 48 hours.

Table 4.3. The CC50 values of MRC-5 and A549 cells treated with AuNPs of different sizes. The estimated CC50 values from mLDH and MTT assays after 24 and 48 hours of MRC-5 and A549 cells exposure to AuNPs. The values are mean ± SD (n=3). (*) $p < 0.05$ versus other cell line by ANOVA test. a = $p < 0.05$ versus Au10 at the same cell line and exposure time; b = $p < 0.05$ versus Au40 at the same cell line and exposure time the same exposure time and c = $p < 0.05$ versus Au80 at the same cell line and exposure time by ANOVA test.

AuNPs size	Exposure time (hours)	CC50 from mLDH (µg/ml)		CC50 from MTT (µg/ml)	
		MRC-5	A549	MRC-5	A549
Au10	**24**	46.4 ± 1.5	41 ± 1.2 *, b, c	38.2 ± 1	41 ± 1.4 c
	48	39.2 ± 1.3	32 ± 1 *, c	32.6 ± 1.2 *	37 ± 1.4
Au40	**24**	41.4 ± 1 *, a	45.7 ± 1.8	34 ± 1 a	37 ± 2 a, c
	48	38 ± 1.4	28.4 ± 0.8 *, a, c	31.3 ± 0.7	26.6 ± 0.6 *, a, c
Au80	**24**	40.5 ± 1.4 *, a	48.5 ± 1	36.6 ± 0.5 *	47.7 ± 1.2
	48	36.3 ± 1.1	37.5 ± 1.2	29.8 ± 0.5 *, a	37.1 ± 1

Moreover, the detected CC50 from both assays illustrated a cell-type specific effect toward exposure to different sizes of AuNPs. Au80 showed high toxicity against healthy lung cells than cancerous cells. On contrary, the smaller size Au10 showed more potency toward their exposure to A549 cells compared to MRC-5 cells (**Table 4.3**). The current results indicate that there was a difference in the toxicity response between MRC-5 and A549 cells towards their exposure to the same sizes of AuNPs. Hence, there was cell-type-dependent toxicity noted. This can be the result of distinct cellular uptake affinities of each cell type to different AuNPs sizes.

Several hypotheses were generated regarding the relationship between AuNPs size and toxicity. One suggestion deduced that AuNPs with sizes ranging between 25-50 nm can be internalised more efficiently due to the membrane wrapping effect that determines the amount and the rate of NPs uptake and toxicity (Chithrani and Chan, 2007, Wang et al., 2010). AuNPs membrane wrapping phenomena is dependent on AuNPs size and occurred by AuNPs cross the plasma membrane via ligand-receptor interaction and membrane diffusion (Chithrani and Chan, 2007). Previous studies exposed human cervical cancer cells and non small lung cancer cells to citrate-coated AuNPs with size range between 14- 100 nm indicated that AuNPs with size of 45-50 nm induced the highest cellular uptake (Chithrani et al., 2006, Wang et al., 2010). In another study, carboxylic-acid-coated AuNPs sized 30 and 50 nm were internalised to greater extent than AuNPs sized 90 nm in human prostate cancer cells (Malugin and Ghandehari, 2010). Similarly, a study by Mironava et al. (2010) demonstrated the presence of variations in the uptake mechanisms affinity for different NPs sizes. The citrate-coated, 45 nm AuNPs illustrated higher toxicity than the 13 nm size in human dermal fibroblasts after 72 hours of exposure because AuNPs sized 45 nm were internalised via clathrin-mediated endocytosis as a primary uptake mechanism and 13 nm AuNPs were taken up by phagocytosis.

Another suggestion revealed the size-dependent toxicity of AuNPs following exposure to several sizes of AuNPs to different types of cells. Size-dependent toxicity was reported in human colorectal adenocarcinoma and human hepatoblastoma cells exposed to citrate-coated AuNPs sized 10, 30, 60 nm (Lopez-Chaves et al., 2018), retinal pigment epithelial cells and human embryonic kidney cells exposed to cetyltrimethylammonium chloride (CTAC)-coated AuNPs sized 5, 10, 20, 30, 50, 100 nm (Karakoçak et al., 2016) and human lung cancer cells exposed to citrate-coated AuNPs 5, 10, 20, 40 nm (Liu et al., 2014). However, the evidence of AuNPs toxicity still shows divergent conclusions as some studies confirmed the biocompatibility or low potential toxicity of AuNPs (Qu and Lü, 2009, Cheng et al., 2015). It was suggested that AuNPs mitigated the ROS production in cells, causing no severe cytotoxicity. This was observed with a human prostate cancer cells exposed to carboxylic-acid-coated AuNPs sized 30 and 50 nm, which were internalised to a greater extent than AuNPs sized 90 nm (Malugin and Ghandehari, 2010).

AuNPs have shown anticancer bioactivity by inhibiting cell proliferation and inducing apoptosis (Rajeshkumar, 2016, Huang et al., 2014). However, AuNPs may also induce detrimental effect against healthy cells. The present study indicated the potential reduction of cell proliferation in both MRC-5 and A549 cells when exposed to AuNPs. The cytotoxicity findings illustrated cell-type dependent effect toward their exposure to different sizes of AuNPs. AuNPs with a size of 80 nm demonstrated high potency against healthy MRC-5 cells than cancerous A549 cells. On the other hand, A549 cells elicited high sensitivity to the smaller size Au10. These results imply a positive effect to further investigate the anticancer activity of AuNPs with consideration of size impact on healthy cells. As AuNPs interaction with cells can cause alterations in cell morphology and growth. The next experiment was devoted to observe the cell morphology changes.

4.3.1.3 Changes in cell morphology post AuNPs treatment

Morphological images for both MRC-5 and A549 cells were captured with an optical microscope following exposure to the AuNPs for 24 hours. As shown in **Figure 4.4**, no significant changes in the growth pattern of MRC-5 cells after incubation with AuNPs of different sizes at concentrations of 26 and 41 µg/ml were observed. However, shrinkage of the cells size was apparent at both concentrations of all AuNPs sizes. The presence of floating cells (dead cells) at high concentration of AuNPs were also noticed.

In A549 cells, the cells treated with Au10 and Au40 demonstrated changes in cell morphology (spindle-shape), mainly at high concentration with the presence of dead cells (**Figure 4.5 D and F**). In case of A549 cells treated with Au80, no changes in the cells morphology were observed compared to the untreated cells (**Figure 4.5 G and H**). A study was reported changes in cells morphology which was correlated to apoptosis cell death mediated by mitochondrial dysfunction and oxidative stress in human lung cancer cells exposed to AuNPs sized 37 nm for 24 hours (Ramalingam et al., 2016). In order to obtain a clear evidence about AuNPs internalisation, the next subsection represents the cellular uptake assessments.

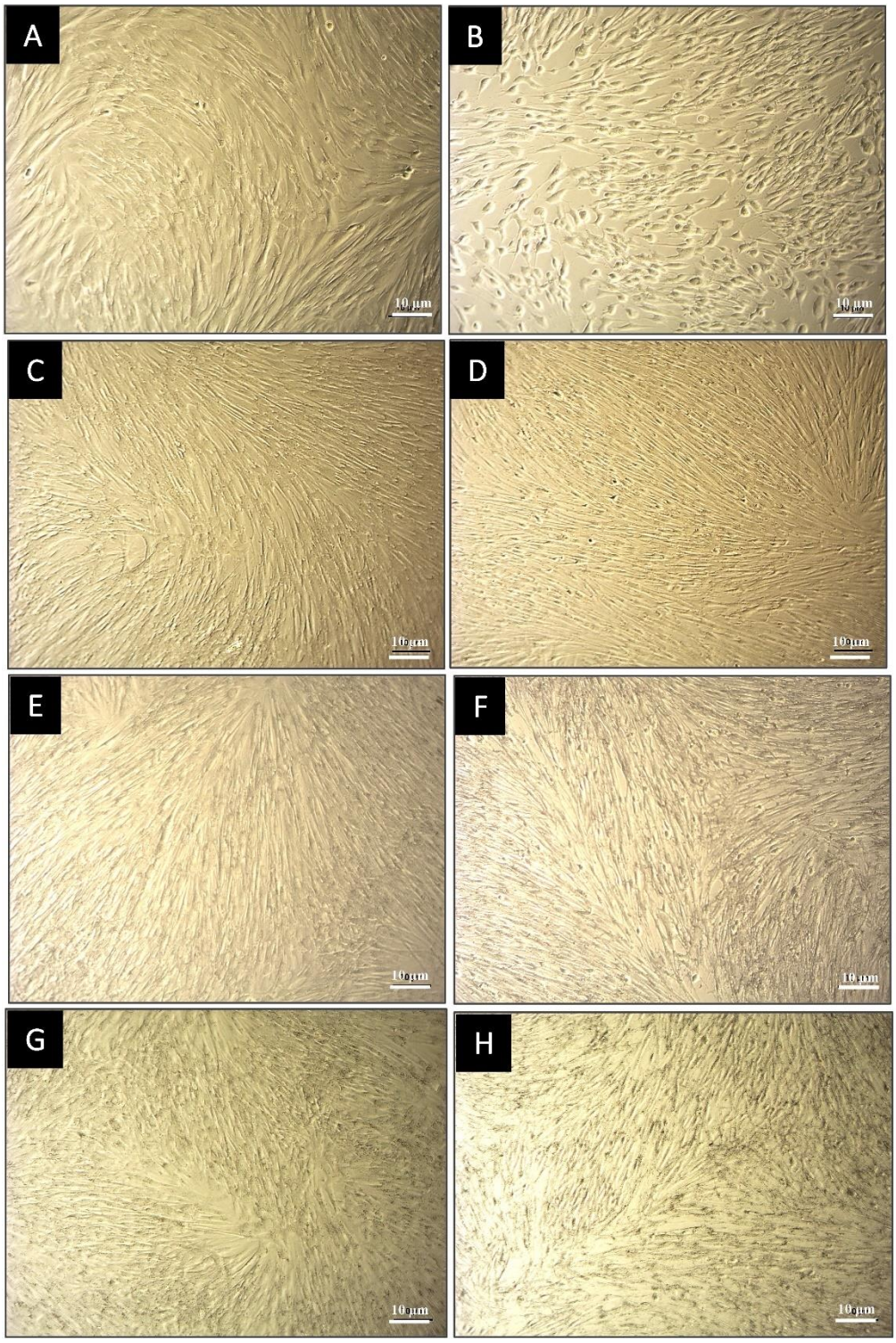


Figure 4.4. Cell morphological changes of MRC-5 cells treated with AuNPs of different sizes. Optical microscope images of MRC-5 cells treated with AuNPs of different sizes for 24 hours. (**A**) untreated cells; (**B**) DMSO (20%) used as a positive control, Au10 (**C**) 26 µg/ml and (**D**) 41µg/ml; Au40 (**E**) 26 µg/ml and (**F**) 41 µg/ml; Au80 (**G**) 26 µg/ml and (**H**) 41 µg/ml. Scale bar 10 µm.

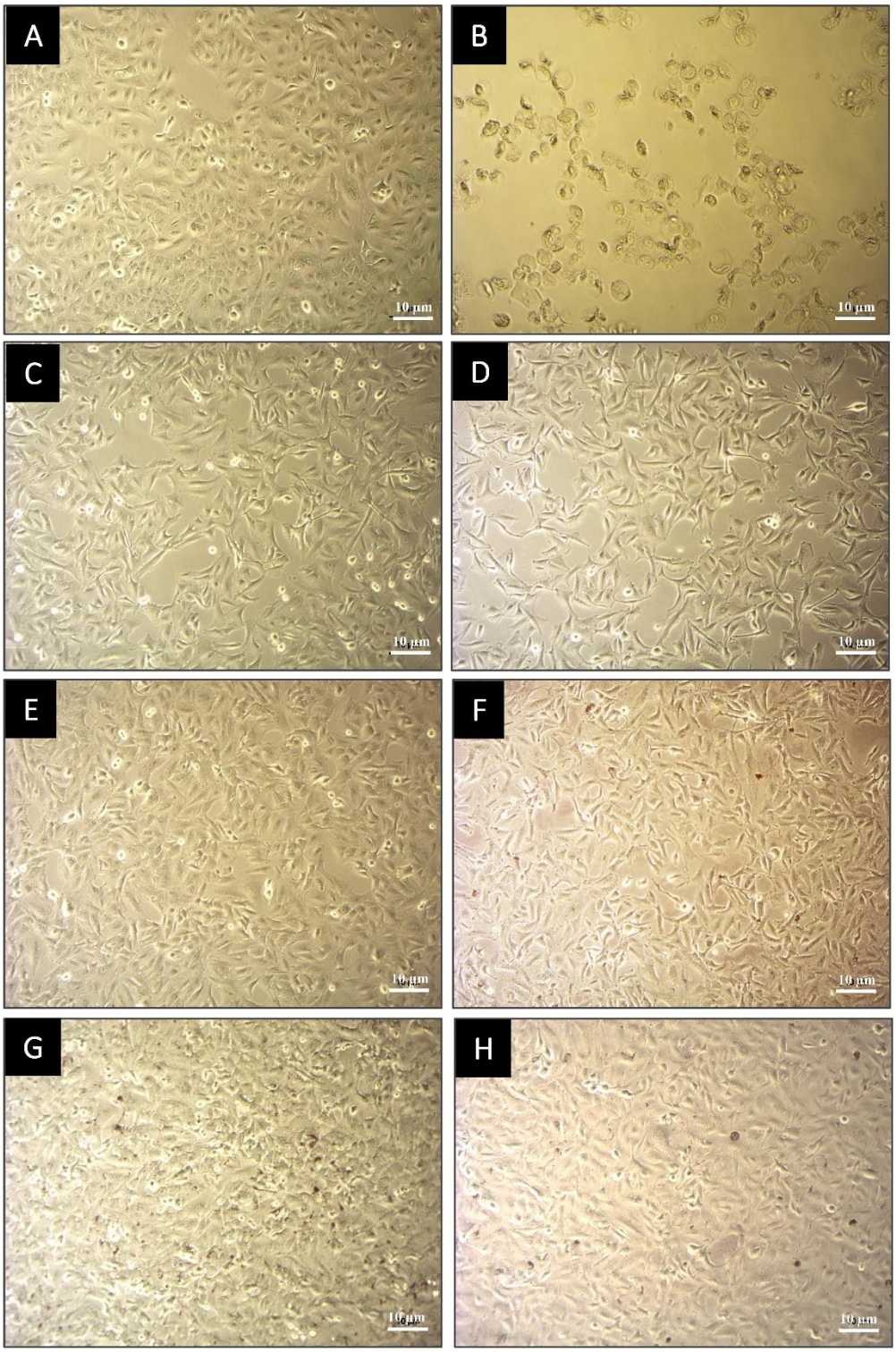


Figure 4.5. Cell morphological changes of A549 cells treated with AuNPs of different sizes. Optical microscope images of A549 cells treated with AuNPs of different sizes for 24 hours. (**A**) untreated cells; (**B**) DMSO (20%) used as a positive control, Au10 (**C**) 26 µg/ml and (**D**) 41µg/ml; Au40 (**E**) 26 µg/ml and (**F**) 41 µg/ml; Au80 (**G**) 26 µg/ml and (**H**) 41 µg/ml. Scale bar 10 µm.

4.3.1.4 Cellular uptake of AuNPs

Several factors can influence the NPs cellular uptake including NPs size, shape and surface charge (Panzarini et al., 2018). Herein, tow different methods were used to investigate the AuNPs cellular uptake; cell granularity assessment by flow cytometry and Au ion quantification by ICP-MS.

4.3.1.4.1 Cell granularity assessment by flow cytometry

The SSC light measured by flow cytometry corresponds to the granularity of the cells. An increase in SSC (cell granularity) compared to the untreated cell may indicate the cellular uptake of NPs (Ibuki and Toyooka, 2012). In this work, both MRC-5 and A549 cells were treated with AuNPs of different sizes for 24 and 48 hours.

In MRC-5 cells, no significant changes in the side scatter after 24 hours of incubation was detected except when the cells treated with Au40 and Au80, at low concentration (26 µg/ml) (**Figure 4.6-B**). At 48 hours of incubation, a substantial increase in the cell granularity was noticed with the three sizes of AuNPs. Both Au40 and Au80 showed an increase in cell granularity at concentrations of 36 and 41 µg/ml compared to Au10 (**Figure 4.6-C**). The results revealed a time-dependent uptake towards MRC-5 cells exposure to the AuNPs. This indicated the longer the incubation the greater NPs interaction with the cells, which can mediates the potential AuNPs toxicity. In case of A549 cells, Au10 showed significant shift in the SSC at 36 and 41 µg/ml than Au40 and Au80 at 24 hours of exposure (**Figure 4.7**). After 48 hours of incubation, Au10 demonstrated the highest uptake compared to Au40 and Au80 with the three different concentrations (**Figure 4.7-C**). Concentration-dependent uptake was detected with the three AuNP sizes at 48 hours of treatment. The cellular uptake of AuNPs was time-dependent with each size of AuNPs.

The present results illustrated that the toxicity of AuNPs of different sizes was correlated to their cellular uptake. MRC-5 cells demonstrated a noticeable increase in Au40 and Au80 cellular uptake and attachment on cell surfaces, which supported the observed toxicity in the previous cytotoxicity assessment following 24 hours of exposure. In contrast, A549 cells showed preferential uptake to the smaller size, Au10, which also consistent to the earlier cytotoxicity findings at 24 hours of incubation. The current observations elicited the interaction of AuNPs with cells can be dependent on the NPs size and the cell-type. The results were in agreement with other investigators who used different sizes of AuNPs on cancer cells (Park et al., 2017, Zhou et al., 2017). MRC-5 and A549 cells are non-phagocytic cells and able to internalise small AuNPs via endocytosis mechanism (Ng et al., 2015, Vyas and Goswami, 2019). However, each cell line can express preferential cellular uptake pathways toward their exposure to different AuNPs sizes as demonstrated in our results. The current approach used to examine the cellular uptake is qualitative method and did not specifically represent the internalisation of the AuNPs but maybe the attachment of NPs on the cell membrane surface. For this reason, further assessments on the cellular uptake of AuNPs of different sizes are essential to understand the mechanisms of the AuNPs cellular internalisation. To gain further understanding of how AuNPs interfere with cellular function and ultimate cell damage several toxicity investigations were performed including oxidative stress, cell death mechanism and cell cycle arrest. The next subsection is dedicated to discussing the results.

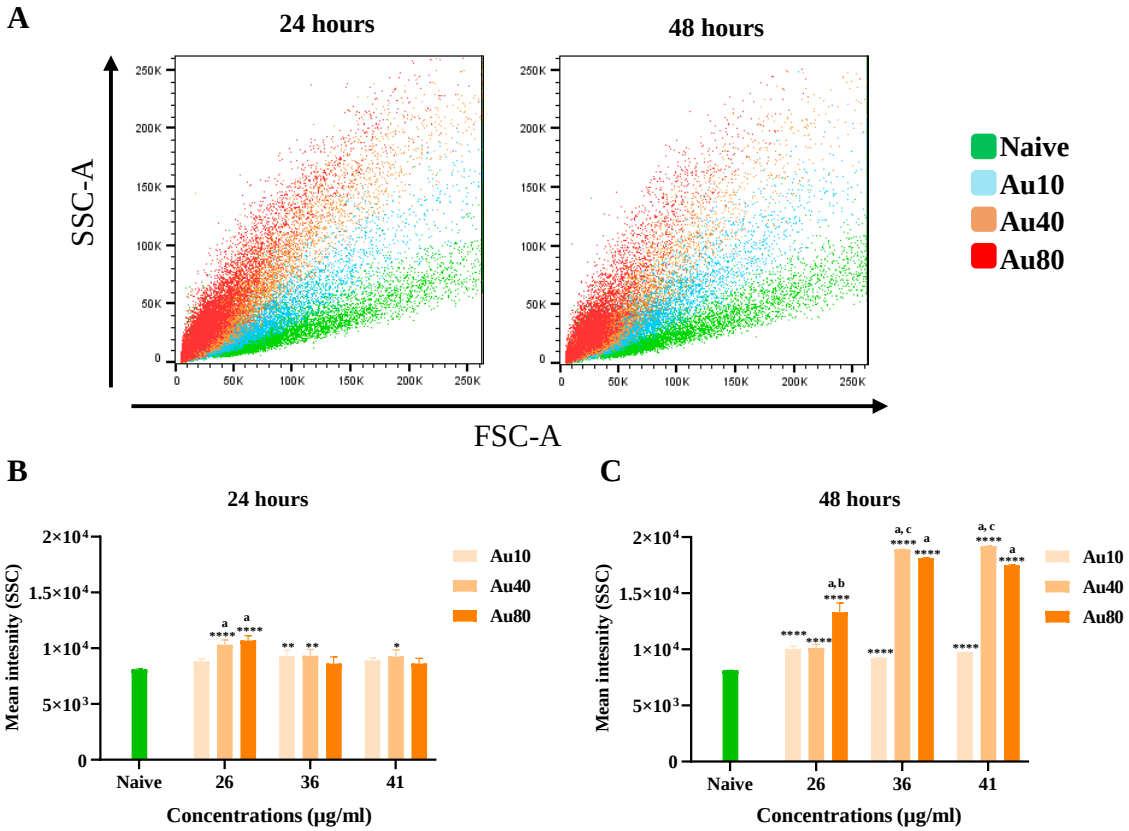


Figure 4.6. SSC light intensity analysis of cellular uptake of AuNPs in MRC-5 cells by flow cytometry. (**A**) Dot plots of side scatted intensity versus forward scattered intensity of MRC-5 cells treated with AuNPs of different sizes at concentration of 41 µg/ml for 24 and 48 hours. The mean intensity of the SSC light after (**B**) 24 and (**C**) 48 hours of exposure to AuNPs of different sizes at concentrations of 26, 36 and 41 µg/ml. Bars represent the mean ± SD (n=4). (*) $p < 0.05$; (**) $p < 0.002$ and (****) $p < 0.0001$ versus untreated group by ANOVA test. a = $p < 0.05$ versus cells incubated with the same concentration of Au10; b = $p < 0.05$ versus cells incubated with the same concentration of Au40 and c = $p < 0.05$ versus cells incubated with the same concentration of Au80 by ANOVA test.

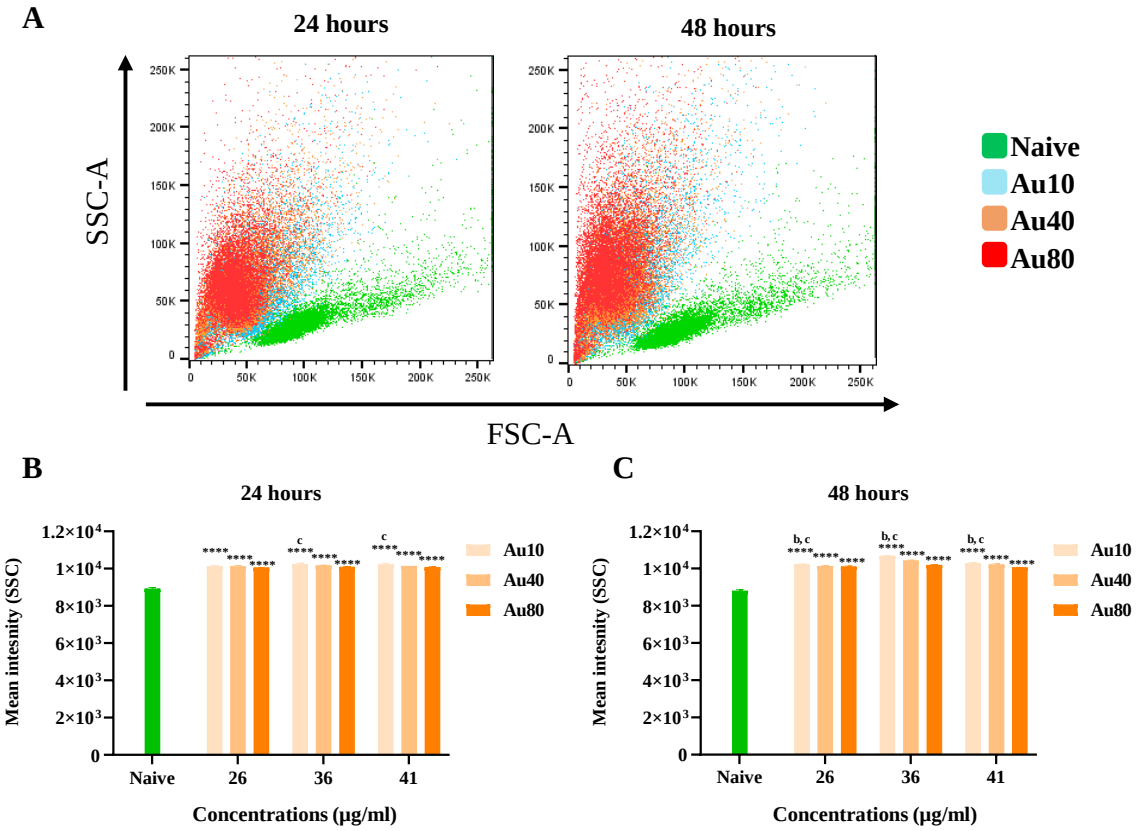


Figure 4.7. SSC light intensity analysis of cellular uptake of AuNPs in A549 cells by flow cytometry. (**A**) Dot plots of side scatted intensity versus forward scattered intensity of A549 cells treated with AuNPs of different sizes at concentration of 41 µg/ml for 24 and 48 hours. The mean intensity of the SSC light after (**B**) 24 and (**C**) 48 hours of exposure to AuNPs of different sizes at concentrations of 26, 36 and 41 µg/ml. Bars represent the mean ± SD (n=4). (****) $p < 0.0001$ versus untreated group by ANOVA test. b = $p < 0.05$ versus cells incubated with the same concentration of Au40 and c = $p < 0.05$ versus cells incubated with the same concentration of Au80 by ANOVA test.

4.3.1.5 The mechanisms of AuNPs toxicity assessment

4.3.1.5.1 Oxidative stress detection

It was previously claimed in the literature that oxidative stress mediated by the induction of ROS is the primary toxicity mechanism of AuNPs (Mateo et al., 2014, Rizwan et al., 2017, Pan et al., 2009, Li et al., 2010). AuNPs can initiate oxidative stress directly by ROS generation upon their interaction with the cells and suppress the antioxidant level such as glutathione (Abdal Dayem et al., 2017). The CellRox reagent was used to assess the oxidative stress following MRC-5 and A549 cells exposure to AuNPs of different sizes at concentrations of 26, 36 and 41 µg/ml for 24 hours. This concentration range (26- 41 µg/ml) was selected as it has mediated low to high cytotoxicity based on the earlier cell viability data. Menadione, an oxidative stress inducer, was used as a positive control.

The observed findings illustrated that no oxidative stress was induced in both cell lines following exposure to different concentration of AuNPs of the three sizes in comparison to untreated cells (**Figure 4.8**). Similar to the current findings, a study obtained no sign of oxidative stress for AuNPs sized lower than 100 nm exposed to colorectal adenocarcinoma cells (Aueviriyavit et al., 2014). However, oxidative stress was previously evident as the main mechanism mediating AuNPs toxicity in human leukaemia and human hepatoblastoma cells were exposed to water-based AuNPs sized 30, 50 and 90 nm at concentration range of (15 - 22 µg/ml) at 1 and 24 hours (Mateo et al., 2014). Another study found oxidative stress induced by citrate-coated AuNPs AuNPs at concentration range of (100- 500 µg/ml) after 30 minutes of exposure to human metastatic breast adenocarcinoma but not with human epithelial breast cancer cells (Surapaneni et al., 2018). As can be seen from the literature the results showed contradicting conclusion regarding AuNPs triggered ROS production in which the cell type, concentration and exposure time can influence the AuNPs induced oxidative stress.

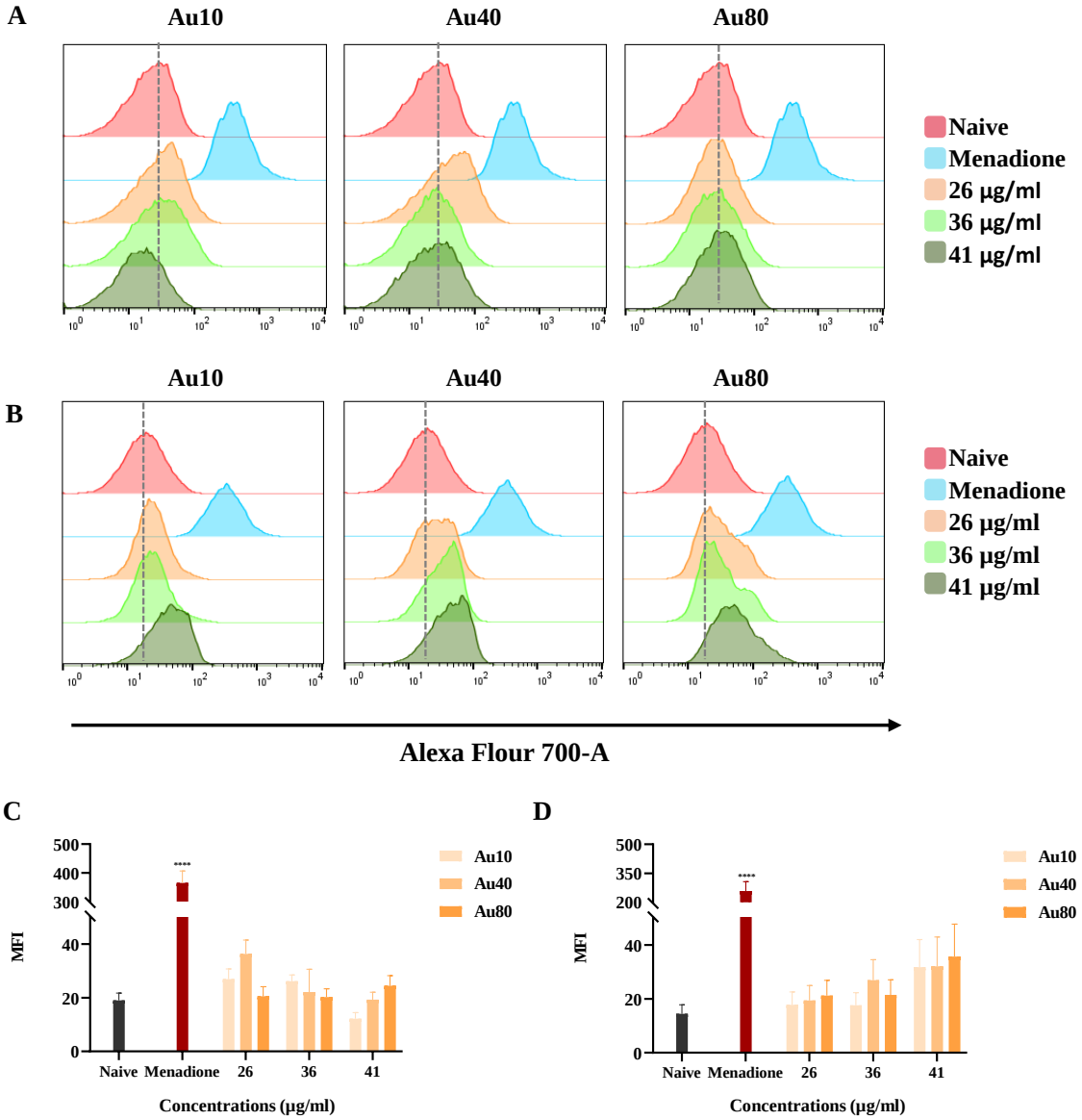


Figure 4.8. Oxidative stress detection of MRC-5 and A549 cells following the exposure to AuNPs of different sizes using CellRox deep red reagent. Histogram of flow cytometry analysis of cells treated with Au10, Au40 and Au80 at concentrations of 26, 36 and 41 µg/ml for 24 hours in (**A**) MRC-5 and (**B**) A549 cells. Bar graphs represent the median fluorescence intensity (MFI) versus different concentration of AuNP in (**C**) MRC-5 and (**D**) A549 cells. Menadione (50 µM) used as a positive control. Bars represent the mean ± SD (n=4). (****) p <0.0001 versus untreated group by ANOVA test.

The present findings revealed the cytotoxicity of AuNPs was not mediated by ROS formation and it could be another mechanism that triggered the toxicity of AuNPs. However, it was difficult to conclude if oxidative stress is one of the toxic mechanisms for AuNPs at the tested time point due to the short half-life of the produced ROS, which might be challenging to detect. ROS are very reactive and can be easily bound to and oxidise cellular elements (Prasad et al., 2019). It was observed that high ROS formation was triggered in human leukaemia cells after 24 hours of AuNPs incubation whereas AuNPs induced ROS production in human hepatoblastoma cells after 1 hour (Mateo et al., 2014). This reveals the ROS production is dependent on the exposure time and cell type. In order to further clarify our current findings of AuNPs induce oxidative stress, the level of cellular glutathione was quantified in the next step.

4.3.1.5.2 Glutathione measurement

Glutathione is a potent cellular antioxidant that counters the high level of ROS inside the cells. Free radicals promote the oxidation of GSH (reduced form) to GSSG (oxidised form) (Manke et al., 2013). Herein, the levels of GSH and GSSG were measured following 24 hours incubation of AuNPs of different sizes at concentrations of 26, 36 and 41 µg/ml in both normal and cancerous lung cells. Menadione was used as a positive control. Interestingly, the MRC-5 and A549 cells treated with AuNPs of different sizes illustrated an increase in the GSH/GSSG ratio at concentrations of 26 and 36 µg/ml compared to the untreated group (**Figure 4.9**). Whereas a substantial reduction of the GSH/GSSG ratio was noticed in both cell lines at a high concentration (41 µg/ml) with the three different sizes of AuNPs (p-value < 0.0001) (**Figure 4.9**). No trend of size-dependent effect was detected.

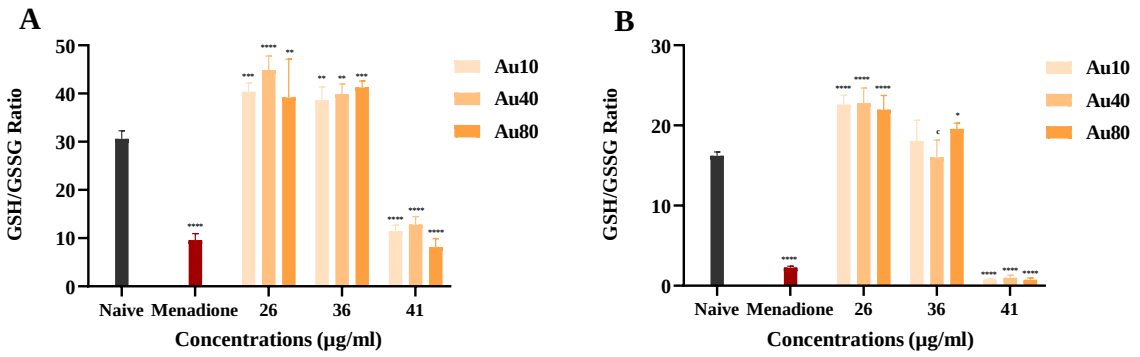


Figure 4.9. GSH/GSSG ratio quantification of MRC-5 and A549 cells following the exposure to AuNPs of different sizes using GSH/GSSG-Glo Assay. Both cells were treated with AuNPs of different sizes at concentrations of 26, 36 and 41 µg/ml for 24 hours in (**A**) MRC-5 and (**B**) A549 cells. Menadione (50 µM) used as a positive control. Bars represent the mean ± SD (n=4). (*) $p < 0.05$; (**) $p < 0.002$; (***) $p < 0.0002$ and (****) $p < 0.0001$ versus untreated group by ANOVA test. c = $p < 0.05$ versus cells incubated with the same concentration of Au80 by ANOVA test.

The present findings demonstrated an increase in GSH level, this could be the result of AuNPs triggered GSH production in the mitochondria It was suggested that AuNPs can mediate antioxidant activity in the cells (Barathmanikanth et al., 2010). Furthermore, the drastic reduction of GSH levels at high concentration of AuNPs of different sizes can be due to the overproduction of ROS at an earlier time that was not detectable after 24 hours of exposure. Previous studies claimed that an alteration in the glutathione level mediated by the induction of ROS is a major cause of AuNPs toxicity in human leukaemia cells, human hepatoblastoma cells and human pulmonary fibroblasts following exposure to AuNPs sized 30, 50 and 90 nm for 24-72 hours (Mateo et al., 2014, Ávalos et al., 2015). However, it was evident that the depletion of GSH is an early indicator for apoptosis induction despite the absence of ROS formation (Franco et al., 2007) and this could be the reason for AuNPs cytotoxicity at high concentration. As the AuNPs caused intracellular GSH depletion at high concentration, the next step of this work was to investigate the apoptosis cell death mediated by cellular exposure to AuNPs.

4.3.1.5.3 Apoptosis detection

The interaction of AuNPs with cells can induce cell death. It was reported in the literature that AuNPs might triggers apoptosis, necrosis or autophagy as a primary cell death mode promoted by the AuNPs cellular exposure (Sun et al., 2018). However, AuNPs can behave differently in cells depending on AuNPs properties, exposure time and cell types (Bhamidipati and Fabris, 2017). In this study, the cells were stained to discriminate between apoptotic and necrotic cells using Annexin V conjugated to Alexa Flour and PI markers. Both MRC-5 and A549 cells were incubated with three concentrations (26, 36 and 41 µg/ml) of AuNPs of the three sizes for 24 and 48 hours. Staurosporine and DMSO were used as apoptotic and necrotic positive control inducers, respectively.

In the MRC-5 cells, no sign of cell death was detected after 24 hours of exposure to the AuNPs of the three sizes (**Figure 4.10 C and D**). Nevertheless, an increase in the cell fragment population was observed at the highest concentration of AuNPs of different sizes. After 48 hours of exposure and at a low concentration of 26 µg/ml, the early apoptotic population was reported around 6%, 7.5% and 3.7% in Au10, Au40 and Au80, respectively, compared to 0.8% in the untreated control (**Figure 4.10-D**). The results were statistically significant with ($p < 0.0001$) in Au10 and Au40 and ($p < 0.01$) in Au80. However, no cell death was detected with the higher concentration of AuNPs of the three sizes. Moreover, late apoptosis/necrotic population was recorded at low concentrations, which was only significant with Au40 and Au80 (8% and 3.4%, respectively). No size- or concentration-dependent cell death was noticed with AuNPs treatment.

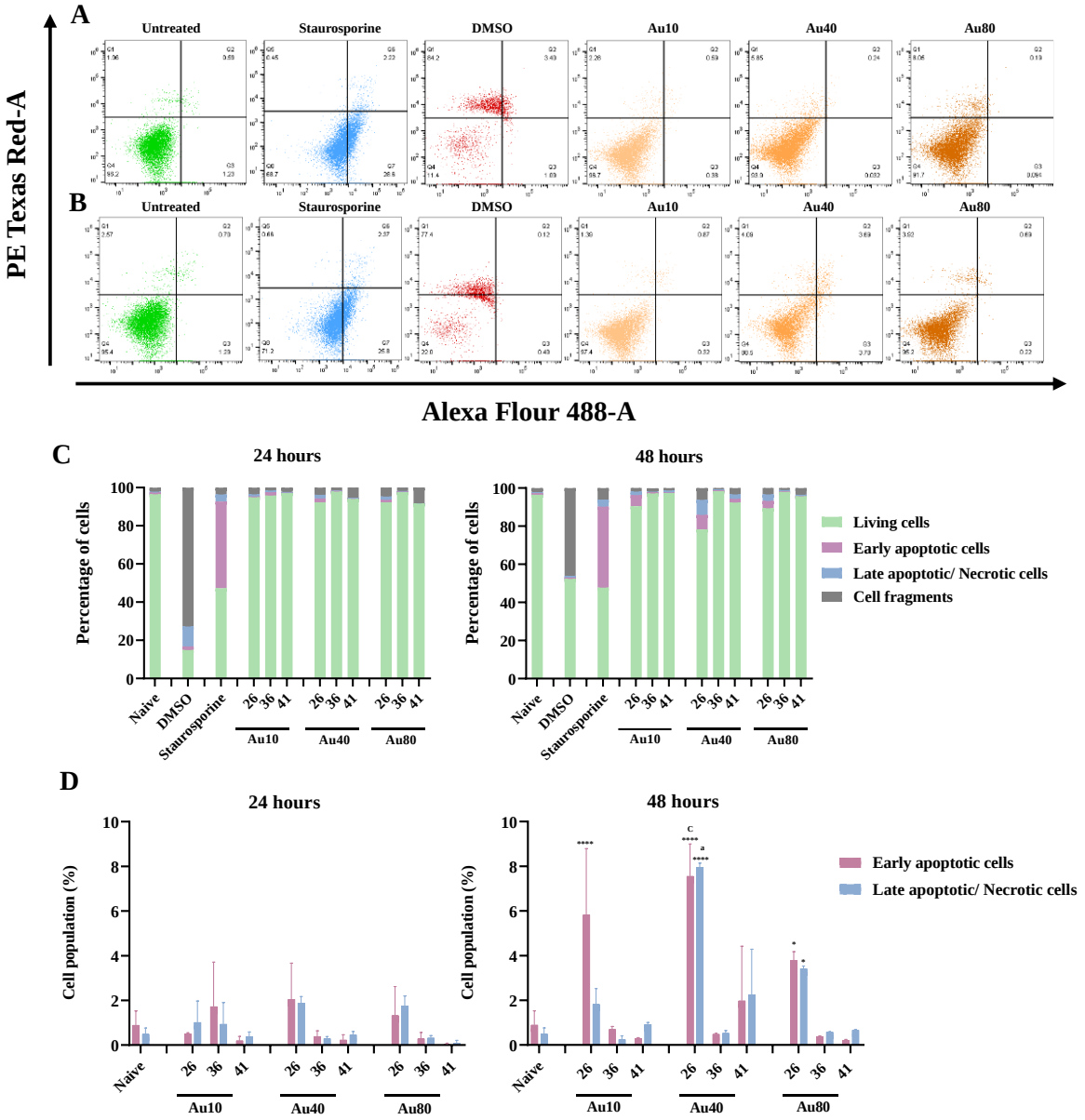


Figure 4.10. Apoptosis cell death analysis of MRC-5 cells following the exposure to AuNPs of different sizes using Annexin V and PI by flow cytometry. Dot plots of flow cytometry analysis of MRC-5 cells treated with AuNPs at concentrations of 41 µg/ml for (**A**) 24 and (**B**) 48 hours. Each dot plot divided into 4 quadrants of total 100% which correspond to: (Q4) living cells; (Q3) early apoptosis; (Q2) late apoptosis and necrosis; and (Q1) cell fragments. Staurosporine (1 µM) and DMSO (10%) were used as positive control for cell apoptosis and necrosis, respectively. (**C**) Stack graphs represent the cells percentage in each quadrant after 24 and 48 hours of exposure to AuNPs at concentration of 26, 36 and 41 µg/ml. (**D**) Bar graphs of early apoptotic and late apoptotic and necrotic populations after 24 and 48 hours of exposure to AuNPs of different sizes. Bars represent the mean ± SD (n=4). (*) $p < 0.05$ and (****) $p < 0.0001$ versus untreated group by ANOVA test. a = $p < 0.05$ versus cells incubated with the same concentration of Au10 and c = $p < 0.05$ versus cells incubated with the same concentration of Au80 by ANOVA test.

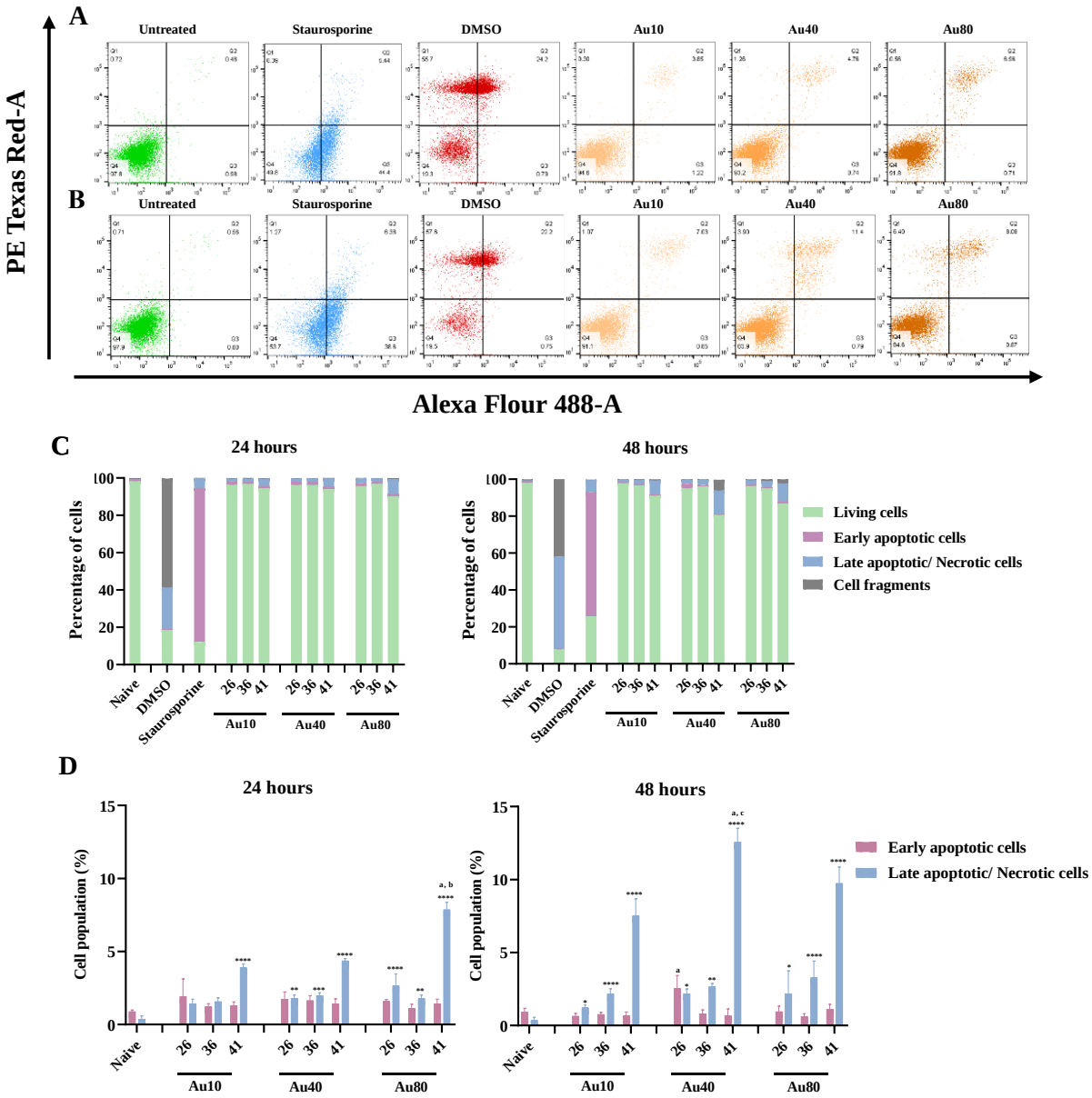


Figure 4.11. Apoptosis cell death analysis of A549 cells following the exposure to AuNPs of different sizes using Annexin V and PI by flow cytometry. Dot plots of flow cytometry analysis of A549 cells treated at concentrations of 41 µg/ml for (**A**) 24 and (**B**) 48 hours. Each dot plot divided into 4 quadrants of total 100% which correspond to: (Q4) living cells; (Q3) early apoptosis; (Q2) late apoptosis and necrosis; and (Q1) cell fragments. Staurosporine (1 µM) and DMSO (10%) were used as positive control for cell apoptosis and necrosis, respectively. (**C**) Stack graphs represent the cells percentage in each quadrant after 24 and 48 hours of exposure to AuNPs at concentration of 26, 36 and 41 µg/ml. (**D**) Bar graphs of early apoptotic and late apoptotic and necrotic populations after 24 and 48 hours of exposure to AuNPs of different sizes. Bars represent the mean ± SD (n=4). (*) $p < 0.05$, (**) $p < 0.002$, (***) $p < 0.0002$ and (****) $p < 0.0001$ versus untreated group by ANOVA test. a = $p < 0.05$ versus cells incubated with the same concentration of Au10; b = $p < 0.05$ versus cells incubated with the same concentration of Au40 and c = $p < 0.05$ versus cells incubated with the same concentration of Au80 by ANOVA test.

For A549 cells, the late apoptosis/necrosis cell population was detected with the three concentrations of Au40 and Au80 after 24 hours of incubation (**Figure 4.11**). Au10 demonstrated a late apoptosis/necrosis cell population at the highest concentration only. After longer incubation, 48 hours, an increase in the late apoptosis/necrosis cell population in a concentration-dependent pattern was observed with three AuNPs sizes (**Figure 4.11-D**). The maximum population of late apoptosis/necrosis percentage was reported with Au40 (12%). Time- and concentration-dependent cell death was detected with A549 cells.

In agreement to the present results, several investigations have demonstrated the potential of AuNPs to trigger apoptosis cell death in human lung cancer and human colorectal cancer cells (Ramalingam et al., 2017, Mironava et al., 2010, Ramalingam et al., 2016). One study reported a high level of apoptotic population with citrate-coated AuNPs sized 45 nm compared to 13 nm in human dermal fibroblasts, confirming size-dependent cell death (Mironava et al., 2010). AuNPs can trigger apoptosis cell death by different mechanisms. Caspase-dependent apoptosis cell death induced by endoplasmic reticulum stress was elucidated as the primary cytotoxic mechanism of tannic-acid-coated AuNPs sized 20 and 70 nm in human neutrophils (Noël et al., 2016). Apoptosis and G0/G1 cell cycle arrest of citrate-coated AuNPs sized 20, 40 and 60 nm were observed in human lung cancer cells following 72 hours of incubation (Choudhury et al., 2013). Mitochondrial-dependent apoptosis mediated by oxidative stress generation has been shown with AuNPs sized 37 nm in human lung cancer cells (Ramalingam et al., 2016).

The data showed that the early apoptosis population was triggered in MRC-5 cells when exposed to low concentration of AuNPs for 48 hours, whereas the late apoptosis/necrosis cell population was detected in A549 cells exposed AuNPs for 24 and 48 hours. Both cell lines did not show substantial cell death induction following their exposure to AuNPs. The potential

AuNPs interference with the stains was considered in this experiment. However, this can not be an issue as an appropriate gating to exclude AuNPs was performed during the sample analysis. Also, no interference was detected when AuNPs mixed with positive controls (**Figure A3)**. The most probable reason of reporting low percentage of cell death is that the dead cells could be detached. Nevertheless, as evident earlier, no oxidative stress was observed by AuNPs and this could the reason of not detecting significant induction of cell death. So far, the results revealed the safety profile of AuNPs which did not mediate severe toxicity at tested concentrations and time points. Hence, apoptosis can be mediated by mitochondrial dysfunction. The next step was to examine the health state of the mitochondria.

4.3.1.5.4 Mitochondrial membrane potential health assessment

Mitochondria are responsible for cellular metabolism, cell fate and maintaining the intracellular redox state (Brand et al., 2013). The MMP is the central regulator to generate energy (ATP) (Zorova et al., 2018). Therefore, the mitochondria act as a vulnerable target contributing to NPs cytotoxicity (Wu et al., 2020). The state of MMP after cell exposure to AuNPs was tested using a TMRM probe to determine mitochondrial activity. Both the healthy and cancerous lung cells were incubated with AuNPs at concentrations of 41 µg/ml for 24 hours. The CCCP was used as positive control that inhibits oxidative phosphorylation.

In MRC-5 cells, a loss of MMP was reported with three sizes of AuNPs with compared to the untreated cells of healthy mitochondria (**Figure 4.12 A and C**). Moreover, Au40 and Au80 demonstrated a significant reduction in the mitochondrial activity in comparison to Au10 of the same concentration. The same observation was found with A549 cells, significant loss of MMP was observed following exposure to AuNPs of the three sizes (**Figure 4.12 B and D**). The lowest MFI was recorded with Au80. Together with previous reported MTT results,

AuNPs may interfere with mitochondrial function after their exposure to MRC-5 and A549 cells.

As aforementioned, apoptosis cell death is the mode of cell death triggered by cellular AuNPs exposure, particularly after 48 hours. However, the current results may indicate a mitochondria-mediated apoptosis pathway as a toxicity mechanism of AuNPs. Mitochondria-mediated apoptosis was previously reported in human lung cancer cells exposed to sodium borohydride-coated AuNPs sized 20-37 nm with cell cycle arrest at the G2/M phase after 24 hours of treatment (Ramalingam et al., 2017) and human leukaemia cells exposed to pegylated-AuNPs sized 6.1 nm that altered the mitochondria membrane potential after 48 and 72 hours of exposure (Huang et al., 2014). It was also reported that human lung cancer cells treated with citrate-coated AuNPs sized 20, 40 and 60 nm resulted in upregulation of proapoptotic proteins following 72 hours of incubation (Choudhury et al., 2013). However, in this study, AuNPs illustrated reduction in mitochondrial activity at 24 hours of incubation and triggered apoptosis after 48 hours of exposure. To gain further evidence regarding AuNPs toxicity, it was of interest to investigate the AuNPs potential to interfere with cell cycle progression as the next step.

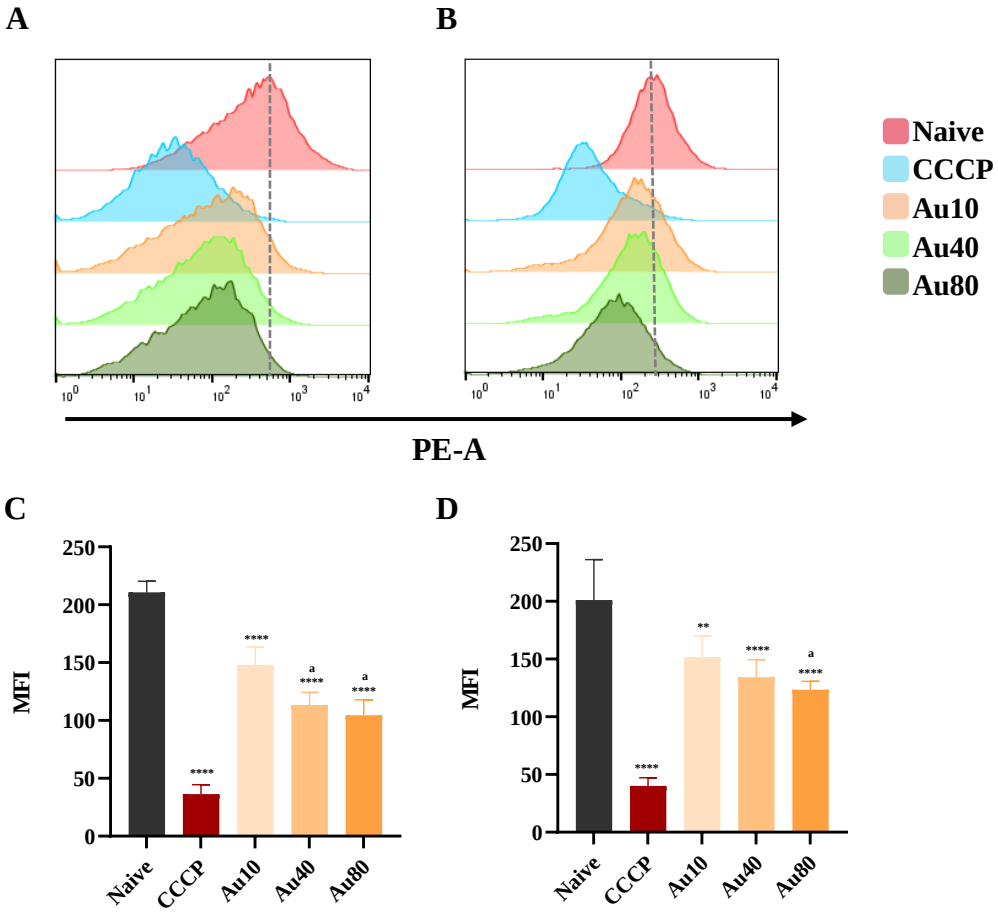


Figure 4.12. Detection of mitochondrial membrane potential state of MRC-5 and A549 cells following the exposure to AuNPs of different sizes using MitoProbe, TMRM assay by flow cytometry. Histogram of flow cytometry analysis of cells treated with AuNPs of different sizes at concentrations of 41 µg/ml for 24 hours in (**A**) MRC-5 and (**B**) A549 cells. The median fluorescence intensity (MFI) versus AuNPs of different sizes in (**C**) MRC-5 and (**D**) A549 cells. Carbonyl cyanide 3-chlorophenylhydrazone (CCCP) (50 mM) used as positive control. Bars represent the mean ± SD (n=4). (**) $p < 0.002$ and (****) $p < 0.0001$ versus untreated group by ANOVA test. a = $p < 0.05$ versus cells incubated with the same concentration of Au10 by ANOVA test.

4.3.1.5.5 Cell cycle progression analysis

AuNPs may suppress the proliferation of cells by aborting cell cycle progression (Ramalingam et al., 2016). The PI/RNase stain was used to investigate the cell cycle stage. Both MRC-5 and A549 cells were treated with 26, 36 and 41 µg/ml of AuNPs of the three sizes for 24 and 48 hours. Topotecan and Etoposide were used as positive controls which induced G1/S phase and G2/M phase arrest, respectively.

MRC-5 cells treated for 24 hours with Au10 and Au80 exhibited a concentration-dependent arrest at G2/M phase. Around 20% and 22% cells accumulation at G2/M phases were recorded at highest the concentrations of Au10 and Au80 compared to 10% in the untreated group (**Figure 4.13-C**). For Au40, an increase in the subG1 population was only detected with 36 and 41 µg/ml. Following 48 hours, the AuNPs of the three sizes mediated cells accumulation at the G2/M phase accompanied with increasing the subG1 population in a concentration-dependent pattern indicating apoptosis (**Figure 4.13-C**). In A549 cells, no observed changes were detected at the low concentration (26 µg/ml) with the three sizes of AuNPs. However, cell cycle arrest at the G2/M phase was reported after 24 hours of exposure to AuNPs of the three sizes at 36 and 41 µg/ml (**Figure 4.13-D**). After 48 hours of incubation of the cells at a concentration of 36 µg/ml, an arrest of the cells at G2/M was obtained with the three sizes of AuNPs. Moreover, a concentration-dependent increase in cell accumulation at subG1 was observed with the AuNPs of different sizes after 48 hours of exposure (**Figure 4.13-D**). No size-dependent effect was detected in A549 and MRC-5 cells.

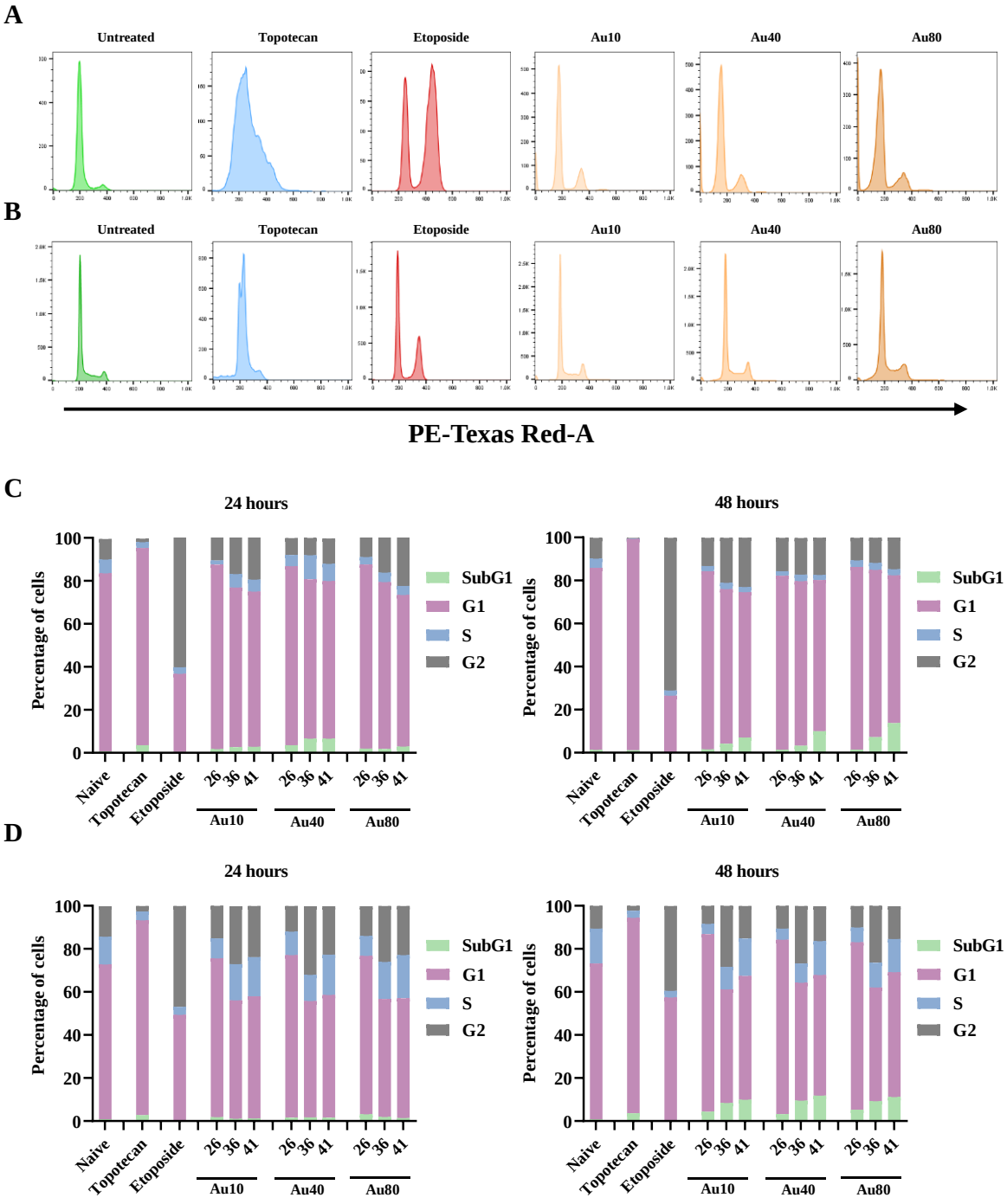


Figure 4.13. Cell Cycle progression analysis of MRC-5 and A549 cells following the exposure to AuNPs of different sizes using FxCycle™ PI/RNase Staining by flow cytometry. Histogram of flow cytometry analysis of cells treated with AuNPs of different sizes at high concentration (41 µg/ml) for 48 hours in (**A**) MRC-5 and (**B**) A549 cells. The stack graphs represent the cell percentage on each phase of cell cycle after 24 and 48 hours of exposure to different concentration of AuNPs in (**C**) MRC-5 and (**D**) A549 cells. Bars represent the mean (n=4).

In agreement with these findings, human lung cancer cells exposed to sodium borohydride-coated AuNPs sized 20- 37 nm were found to arrest the cell cycle at the G2/M phase after 24 hours (Ramalingam et al., 2017). The same study also found an increase in the apoptotic subG1 population secondary to oxidative stress induction and mitochondrial membrane dysfunction. Another study found that pegylated-AuNPs sized 6.1 nm exposed to human leukaemia cells increased the subG1 apoptosis cell death accompanied with mitochondrial damage after 48 and 72 hours of exposure (Huang et al., 2014). Citrate-coated AuNPs sized 20, 40 and 60 nm used to treat human lung cancer cells were found to accumulate the cells on SubG1, indicating cell apoptosis along with increasing the protein expression of proapoptotic proteins following 72 hours incubation (Choudhury et al., 2013).

As presented earlier, a decrease in cell viability was in a concentration-dependent manner after incubation with the AuNPs of the three sizes. In addition, an arrest of the cell cycle at the G2/M phase was reported after 24 hours of exposure with an induction of apoptosis after a prolonged incubation time with the AuNPs of three sizes in both cells. It most likely the cells could not repair the DNA damage lead to accumulation of cells in G2/M phase then the cells failed to reach G1 phase which resulted in the induction of apoptosis. These findings supported the previous observation of late apoptosis/necrosis cell death. However, the question was addressed in the ability of the cells to recover and regain the cell cycle progression and proliferation after cessation of AuNPs exposure to the cells. The next step demonstrates and discusses the findings.

4.3.1.5.6 Cells recovery post AuNPs treatment

It was of interest to identify the cells ability to recover following the exposure to AuNPs. Both MRC-5 and A549 cells were exposed for 1 day to the AuNPs of different sizes. The concentration range of (26- 41 µg/ml) were used to treat the cells based on the previous cell viability results. After one day of exposure, the AuNPs were removed, and fresh media were added for 2, 3 and 4 days. Cell viability was measured after each time point using the mLDH assay to determine the possible cell recovery from AuNPs and the ability to counteract the toxic effects of AuNPs.

In MRC-5 cells, the cell viability showed a continuous decrease at day 2 after cessation of AuNPs exposure in all concentrations of Au10 and Au40 (**Figure 4.14 A and B**). At day 3, an increase in the cell viability was observed with low concentrations (26 and 31 µg/ml) of Au10 and Au40. On the other hand, cells exposed to high concentrations (36 and 41 µg/ml) of Au10 and Au40 showed continues decreases in cell viability (23% and 27%). At day 4, the cell viability increased after exposure to different concentrations of Au10 and Au40 with higher than 50% cell viability. In the cells treated with Au80, the toxic effect was continued even after treatment removal at days 2 and 3 with cell viability 30% and 24%, respectively, at highest concentrations. The cell viability showed a gradual increase at day 4 with the different concentrations of Au80 (**Figure 4.14-C**). The AuNPs of different sizes demonstrated almost the same pattern of potential recovery after AuNPs exposure in MRC-5 cells.

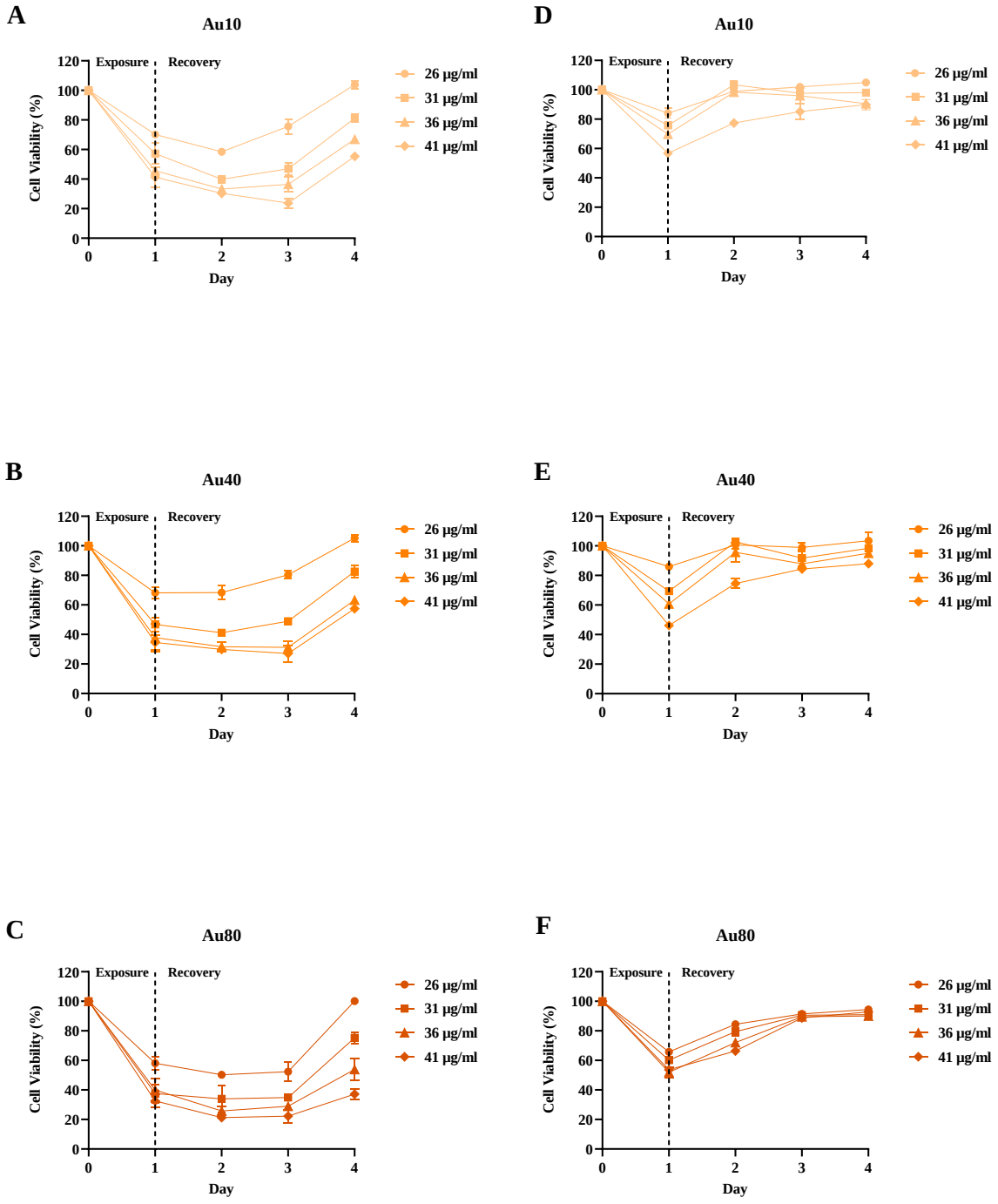


Figure 4.14. Recovery of MRC-5 and A549 cells following the exposure to AuNPs of different sizes. Both cell lines treated with AuNPs of different sizes at a concentration range of (26- 41 µg/ml) for 1 day. Then the cells allowed to recover by adding fresh cell culture media for 2, 3 and 4 days. The cells recovery was detected by measuring the cell viability after MRC-5 cells exposure to (**A**) Au10, (**B**) Au40 and (**C**) Au80 and A549 cells exposure to (**D**) Au10, (**E**) Au40 and (**F**) Au80. Data represent the mean ±SD (n=4).

In case of A549 cells, the cells exposed to AuNPs of different sizes illustrated a gradual increase in cell viability with the different concentrations from day 2 to day 4 (**Figure 4.14 D-F**). The cell viability after 1 day of exposure to a high concentration (41 µg/ml) of AuNPs was 57%, 46% and 54% for Au10, Au40 and Au80, respectively. At day 4, the detected cell viability percentages were 90%, 88% and 93% for Au10, Au 40 and Au80. There was no size-dependent recovery detected from the obtained findings.

After comparing the possible cell recovery between the healthy MRC-5 and the cancerous A549 cells, it was apparent that the A549 cells were able to overcome the toxic effect of the AuNPs after 1 day of exposure with an immediate increase in cell viability compared to the MRC-5 cells, which remained influenced by the presence of the AuNPs inside the cells. It most likely that AuNPs retained inside the cells even after removing the AuNPs from the cell culture medium, therefore AuNPs continued to interfere with cell proliferation. The present findings demonstrated the impact of AuNPs being dependent on the cell type. The observed detrimental effect of AuNPs on MRC-5 raises concern regarding the use of AuNPs for cancer treatment and different biomedical applications. Similar to our findings, a study reported that human dermal fibroblast cells were exposed to citrate-coated AuNPs with sizes 13 and 45 nm for 3 days and then allowed to recover for 5 days. However, the study revealed a size-dependent response in which a slow recovery rate of AuNPs sized 45 nm was noticed compared to the smaller size AuNPs (13 nm) (Mironava et al., 2010).

4.3.1.5.7 NPs- assay interference

AuNPs display optical characteristics, thereof the interference of AuNPs with the reagent or fluorescent probe is highly possible. The AuNPs interaction with the assay may lead to inaccurate or misleading results. In this work, the interaction of AuNPs with fluorescent probes was tested. No AuNPs interreference was noticed with the fluorescent assays as demonstrated for CellRox™ deep red assay in (**Figure A2**), Alexa Fluor® 488 Annexin V/Dead Cell Apoptosis assay in (**Figure A3)**, MitoProbe™,TMRM assay in (**Figure A4**) and FxCycle™ PI/RNase staining in (**Figure A5**). For mLDH, MTT and GSH/GSSG-Glo assays, same steps were followed as mentioned previously in chapter 3 (section 3.3.1.5.7).

Although the 2D monolayer is the most used cell culture model in preclinical studies for drug investigation and development, the 3D multicellular model are a promising approach since this model resembles the physiological environment to the human tissue. The next section demonstrates and discusses the toxicity of AuNPs in a 3D cell culture model.

4.4 Toxicological assessment of AuNPs of different sizes in a 3D in vitro cell culture model

The 3D cell culture model used as a representative model to the *in vivo* solid tumour (Nunes et al., 2019). The 3D model has been found to mimic the microenvironment of the solid tumour compared to the 2D model (Menshykau, 2017). Herein, the 3D scaffold-free cell culture model (spheroids) was prepared for A549 cells using a liquid overlay technique. The aim of this section was to examine the impact of AuNPs size in inducing toxicity in A549 spheroids model and to compare the cytotoxicity findings with the relevant results from the 2D monolayer model.

4.4.1 Results and discussion

4.4.1.1 Spheroids morphology and size changes

A549 spheroids were exposed to AuNPs for 24 and 48 hours. Low and high concentrations (26 and 41 µg/ml) of Au10 and Au80 were selected to treat the A549 spheroids to assess the spheroids sensitivity toward the exposure to AuNPs. DMSO (20%) was used as a positive control. The spheroids were imaged after each time point of treatment using optical microscopy. As demonstrated in **Figure 4.15 and Figure 4.16**, the spheroids maintained the compact structure following the exposure to Au10 and Au80 at both time points. For spheroids treated with Au80, the accumulation of NPs around the spheroids at a concentration of 26 µg/ml was clearly observed (**Figure 4.16**). The spheroids circumference changes were also measured. There were no significant changes detected between the circumferences sizes of spheroids treated with Au10 and Au80 and the ones before treatment at either 24 or 48 hours of incubation (**Figure 4.15-C and Figure 4.16-C**). These observations indicated that AuNPs did not mediate toxicity in the A549 spheroidal model. To further investigate the AuNPs effect on A549 spheroids, the cytotoxicity assessment was performed in the next subsection.

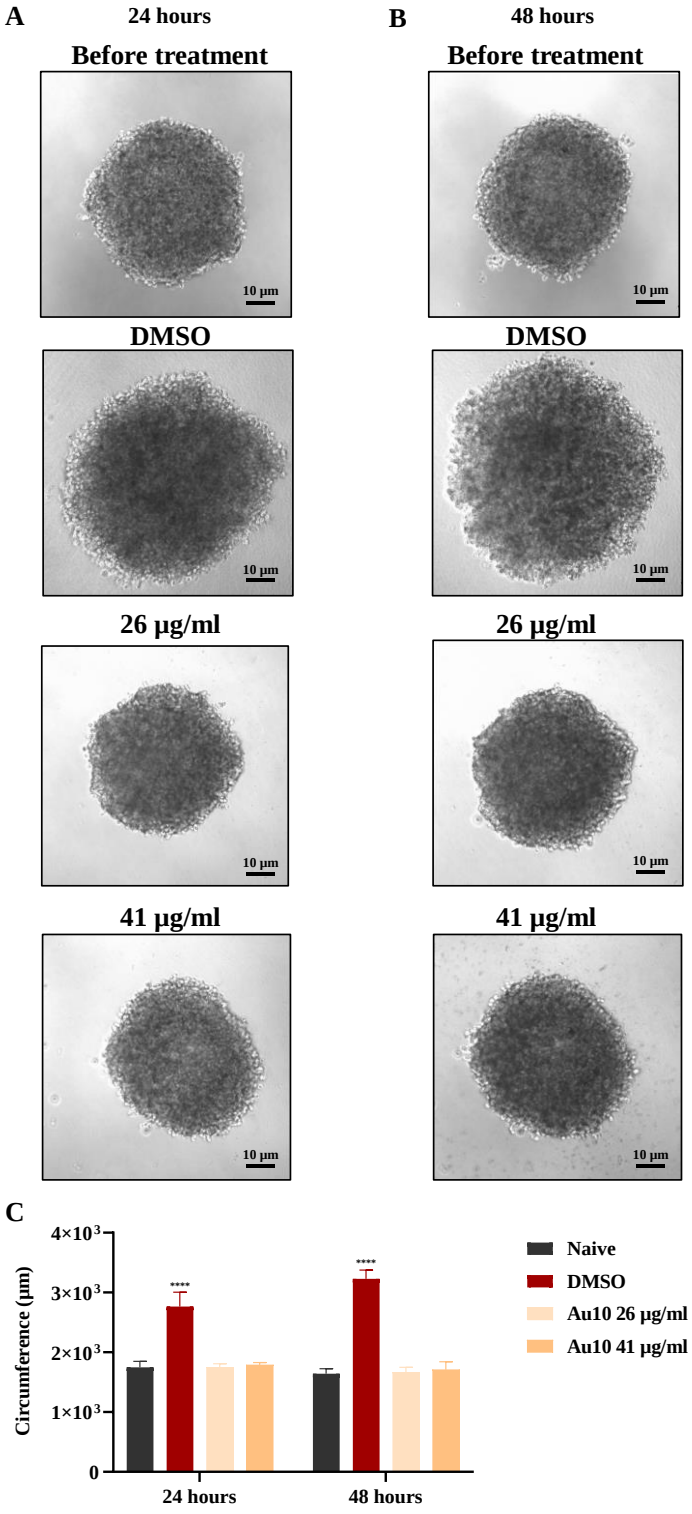


Figure 4.15. A549 spheroids morphological changes following the exposure to Au10. Optical microscope images of A549 spheroids treated with Au10 for (**A**) 24 and (**B**) 48 hours at concentrations of 26 and 41 µg/ml. Scale bar (10 µm). DMSO (20%) used as positive control. (**C**) Bar graph represents the circumference size of A549 spheroids after treatment with Au10 for 24 and 48 hours. Bars represent the mean ± SD (n=10). (****) p <0.0001 versus untreated group by ANOVA test.

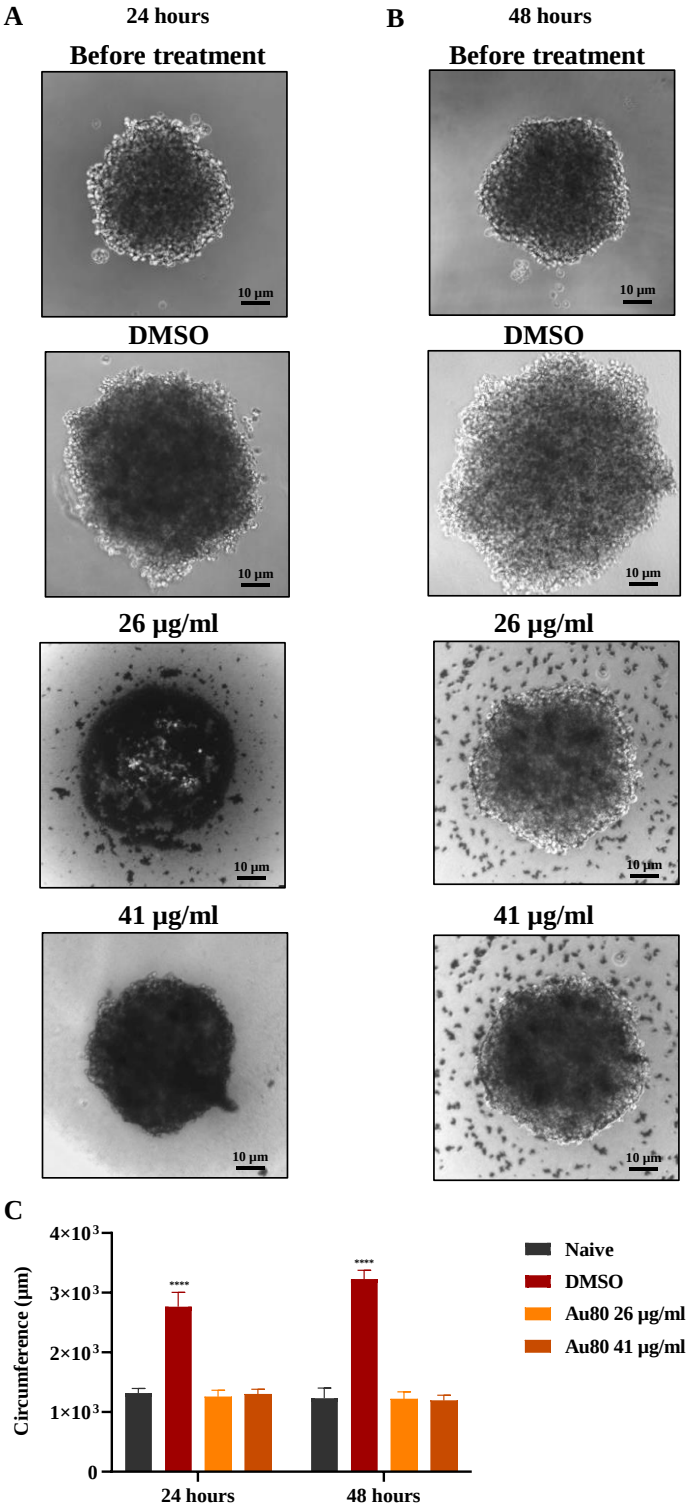


Figure 4.16. A549 spheroids morphological changes following the exposure to Au80. Optical microscope images of A549 spheroids treated with Au80 for (**A**) 24 and (**B**) 48 hours at concentrations of 26 and 41 µg/ml. Scale bar (10 µm). DMSO (20%) used as positive control. (**C**) Bar graph represents the circumference size of A549 spheroids after treatment with Au80 for 24 and 48 hours. Bars represent the mean ± SD (n=10). (****) p <0.0001 versus untreated group by ANOVA test.

4.4.1.2 Spheroids cytotoxicity assessment

The cell viability in the spheroids was assessed using a Live/Dead cell imaging kit by confocal microscopy. A549 spheroids were treated for 48 hours with Au10 and Au80 at concentrations of 26 and 41 µg/ml. As showed in **Figure 4.17**, the spheroids remained viable after exposure to Au10 and Au80 at both concentrations. However, the presence of the red signal in spheroids treated with Au10 at a concentration of 41 µg/ml indicated the presence of dead cells. In all treatment samples of both AuNPs sizes, the spheroids maintained their packed integrity.

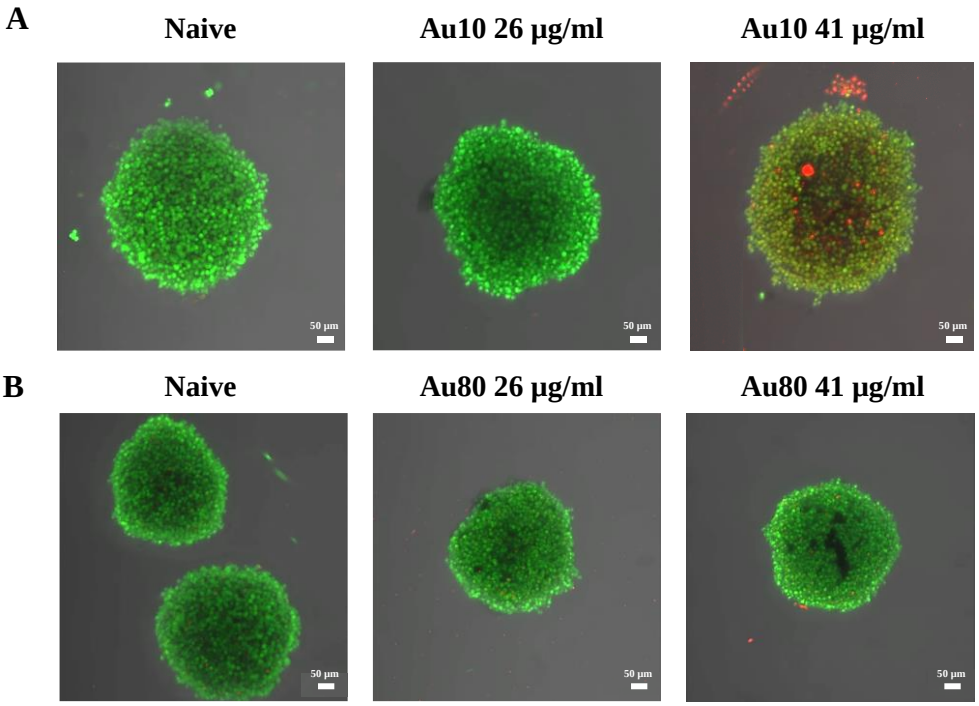


Figure 4.17. Cytotoxicity assessment of A549 spheroids following exposure to Au10 and Au80. Confocal microscopy images of A549 spheroids treated for 48 hours with; (**A**) untreated cells, Au10 (26 and 41 µg/ml) and (**B**) untreated cells; Au80 (26 and 41 µg/ml). Green signal corresponding to live cells and red signal corresponding to dead cells. Scale bar 50 µm.

The present findings demonstrated no sign of size-dependent toxicity following A549 spheroids exposure to Au10 and Au80. In contrast to the current results, previous studies have shown the size-dependent cellular uptake and toxicity of AuNPs on 3D spheroids (England et al., 2015, Huang et al., 2012). This rather contradictory result may be due to the uses of different properties of AuNPs. The spheroids treated with both Au10 and Au80 at a concentration of 41 µg/ml demonstrated low or no red signal as an indication of cell death. However, the same concentration of Au10 and Au80 showed reduction in cell viability with more than 50% when exposed to A549 cells in the 2D monolayer for 48 hours. Thus indicates that the A549 spheroids model is less sensitive to AuNPs than the 2D monolayer model. A study investigated the toxicity effect of zinc oxide NPs in a 2D and 3D models of human epithelial colorectal adenocarcinoma revealed that the cytotoxicity of the NPs was overestimated in the 2D model, whereas the 3D model demonstrated more reliable outcomes to study NPs cellular behaviours and toxicity (Wu et al., 2017).

In conclusion, the AuNPs of the three sizes demonstrated reductions in cell viability in concentration- and time-dependent manners in the 2D monolayer model. The sensitivity toward each size of AuNPs was different between the normal and cancerous lung cells. No oxidative stress was detected. However, mitochondrial-dependent apoptosis cell death was the possible mechanism of AuNPs toxicity. The A549 spheroids model showed more resistant to AuNPs exposure compared to A549 cells in 2D monolayer model.

One approach of NPs to induce adverse cellular events is by modulating cell signalling pathways. The ability of NPs to target specific cell signalling pathways can explain the causes of the observed toxicity (Rauch et al., 2013). The following chapter explores the impact of both AgNPs and AuNPs in two cell signalling pathways, PI3K/AKT and Wnt/β-catenin cell signalling pathways.

Chapter 5

Impacts of AuNPs and AgNPs on PI3K/AKT and Wnt/β-catenin cell signalling pathways

5.1 Introduction

Growing attention is being paid to the biological responses triggered by AuNPs and AgNPs on specific cell signalling pathways through their interaction with the cells (Yang and Wong, 2016, Rauch et al., 2013). The effect of AuNPs and AgNPs can be highly influenced by their different characteristics, resulting in discrete cellular responses (Ajdary et al., 2018). PI3K/AKT and Wnt/ β-catenin pathways are two crucial cell signalling pathways that control different cellular processes including; cell growth, cell adhesion and cell survival (Logan and Nusse, 2004, Manning and Toker, 2017). PI3K/AKT signalling pathway controls several downstream cascades which found to be dysregulated in different human diseases, such as cancer (Cristiano et al., 2006), neurodegenerative (Ksiezak-Reding et al., 2003) and cardiovascular (Condorelli et al., 2002) diseases. This renders the PI3K/AKT pathway a potential therapeutics target. In Wnt/ β-catenin pathway, the overactivation of Wnt can lead to uncontrolled cell proliferation which found to be associated in the progression of several cancer types such as gastric cancer (Dong et al., 2015), breast cancer (Khramtsov et al., 2010), lung cancer (Mazieres et al., 2005) and colorectal cancer (Kobayashi et al., 2000). Thus, the deactivation of Wnt/β-catenin pathway can contribute to apoptosis and reduce cell proliferation (Pu et al., 2009). The behaviour of nanoparticles toward these cell signalling pathways is not well explored.

Moreover, PI3K/AKT pathway crosstalk with Wnt/ β-catenin pathways in several ways and it was found to be correlated with multidrug resistance in cancers (Liu et al., 2020, Zhu et al., 2021). Thereof, both pathways are subjected to intensive research for therapeutic targeting approaches more specifically for cancer treatments. Hence, the present study was interested to explore the influence of AuNPs and AgNPs on modulating the PI3K/AKT and Wnt/β-catenin cell signalling pathways which may help to identify a novel candidate to target cancer cells.

Also, the available evidence on the effects of AuNPs and AgNPs on both pathways were limited in the literature as demonstrated in section 1.5. This work aimed to explore the impact of metal-based NPs composition (AuNPs and AgNPs) and size (10 and 80 nm) in modulating the proteins expression in healthy and cancerous lung cells.

5.2 The influences of AuNPs and AgNPs of different sizes on the PI3K/AKT cell signalling pathway

The PI3K/AKT signalling pathway plays a role in the regulation of several cellular processes, including cell proliferation, cell survival, cell migration, cytoskeletal reorganisation and energy metabolism (Franke et al., 1997, Shi et al., 2019). The activation of the PI3K/AKT pathway occurs via extracellular signal transduction such as growth and survival ligands bind to the receptor tyrosine kinase (RTK) (Burgering and Coffer, 1995, Manning and Toker, 2017). This promotes the production of phosphatidylinositol trisphosphates (PIP3) in the plasma membrane (**Figure 5.1**). AKT is the key downstream protein of the PI3K pathway (Toulany et al., 2017). Activation of the PI3K/AKT pathway is dependent on the phosphoinositide-dependent kinase 1 (PDK1) recruitment into cell membranes leading to AKT activation via its phosphorylation at Threonine 308 (Ther308) residue. For full AKT activation, the mammalian target of rapamycin complex (mTORC2) triggers the phosphorylation of AKT at Serine 473 (Ser473) site (Guo et al., 2015). Thereafter, downstream cascades are activated which regulated several biological functions (**Figure 5.1**).

Apoptosis is prevented by AKT, AKT is responsible for the inactivation and phosphorylation of several proteins, including c-RAF (proto-oncogene), Bad and caspase 9, which are the main proteins involved in apoptosis (Cardone et al., 1998, Zimmermann and Moelling, 1999). Moreover, AKT phosphorylates the Glycogen synthase kinase-3 β (GSK-3β) protein, which has a role in glycogen synthesis in cells. AKT also regulates cell cycle progression through

inhibiting cyclin D1 proteolysis and triggering GSK-3β phosphorylation (Diehl et al., 1998, Porta et al., 2014). Phosphatase and tensin homolog (PTEN) is a tumour suppressor protein that negatively regulates the PI3K/AKT pathway via promoting the dephosphorylation of PIP3 to phosphatidylinositol bisphosphates (PIP2) (Cantley and Neel, 1999, Manning and Toker, 2017). Moreover, mTOR is also activated by its phosphorylation as a downstream cascade of the AKT activation, which enhances cell growth (Navé et al., 1999).

mTOR is a serine/threonine kinase involved in two different complexes called mTOR complex 1 (mTORC1) and mTOR complex 2 (mTORC2). mTORC1 plays a role in cellular growth and the autophagy process. The PI3K/AKT signalling pathway is the upstream controller of mTORC1 activity. mTORC2 mediates cell survival and proliferation through AKT activation (Nitulescu et al., 2018). It has been suggested that an impairment in the activity of PI3K/AKT and mTOR pathways is correlated with different diseases, including cardiovascular diseases, diabetes and several types of cancer, such as ovarian and cervical cancers (Shi et al., 2019).

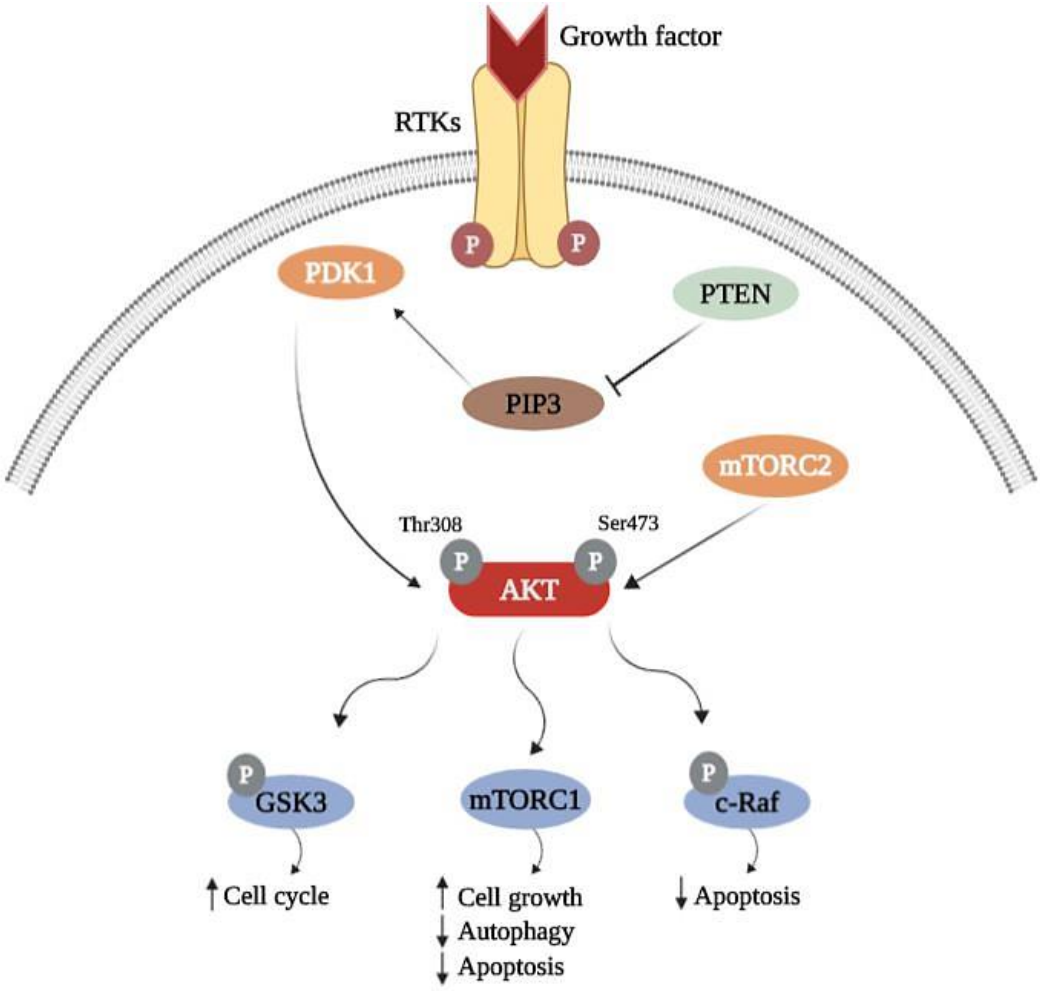


Figure 5.1. Schematic representation of PI3K/AKT pathway. The AKT pathway is activated by growth factors or survival ligands, which bind to the plasma membrane receptor, including RTKs. Upon the activation of the receptor, it triggers the production of PIP3. The full activation of AKT is mediated by its phosphorylation at Thr308 and Ser473 residues by PDK1 and mTORC2, respectively. As a consequence of AKT acitvation, it influences several biological functions, including phosphorylation of GSK-3β and c-Raf and activation of mTORC1 proteins. PTEN negatively regulates the PI3K/AKT pathway. Scheme generated with BioRender.com.

5.2.1 Results and discussion

5.2.1.1 The impacts of AuNPs on the PI3K/AKT cell signalling pathway

The impact of AuNPs sized 10 and 80 nm on the activity of the PI3K/AKT signalling pathway was studied. Several proteins were selected that are involved in the upstream and downstream of the PI3K/AKT signalling cascade. This work investigated the exposure of healthy and cancerous lung cells to Au10 and Au80 with different concentrations (16, 26, 36 and 41 µg/ml) for 24 hours. PDk1 was investigated first. PDK1 is the upstream protein that mediates AKT activity by its phosphorylation on Ther308 residue (Nitulescu et al., 2018).

In MRC-5 cells, no significant downregulation in the PDK1 protein expression was observed after exposure to different concentrations of Au10 and Au80 for 24 hours (**Figure 5.2**). For A549 cells, the PDK1 protein expression demonstrated a reduction in the protein level at high concentrations (36 and 41 µg/ml) was reported with Au10 and Au80 (**Figure 5.3**). However, the expression was significantly downregulated only at a concentration of 41 µg/ml in Au10 ($p < 0.002$).

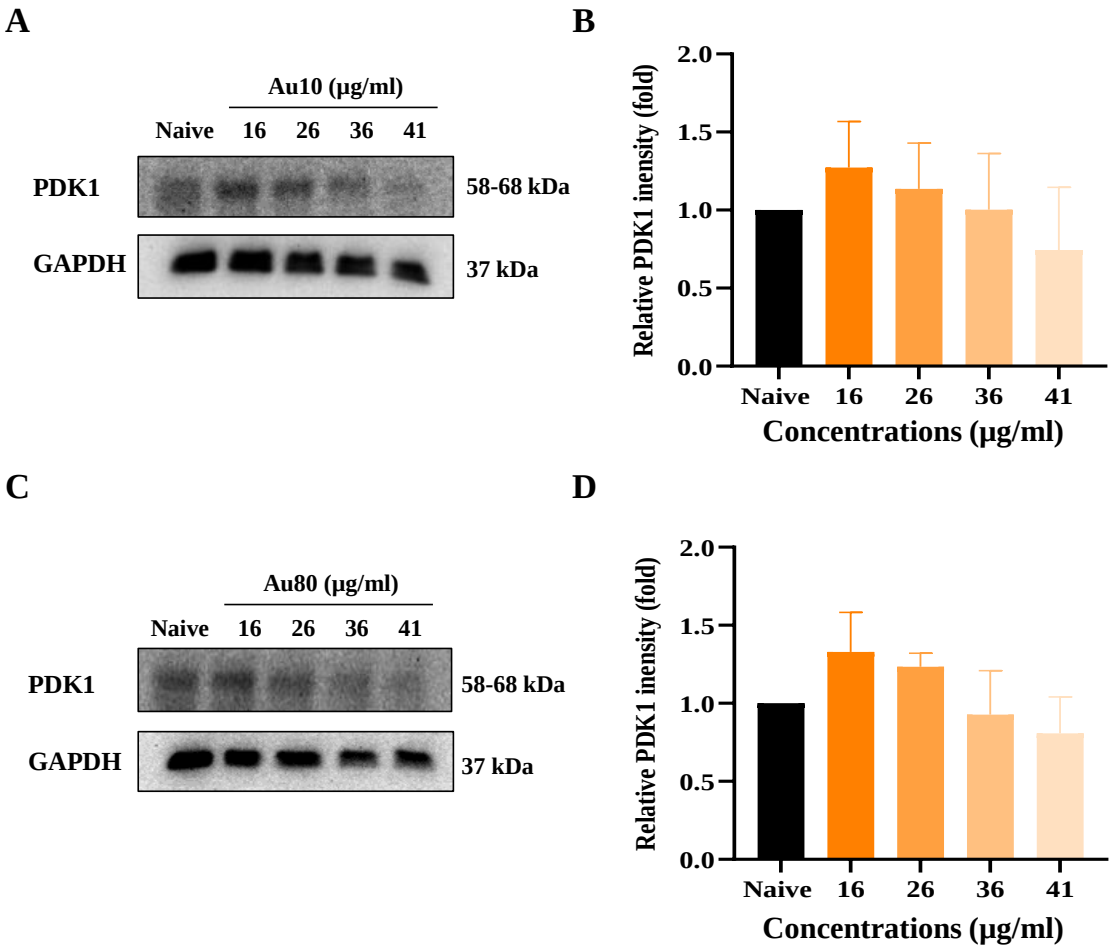


Figure 5.2. The protein expression analysis of PDK1 following MRC-5 cells exposure to Au10 and Au80 of different concentrations for 24 hours. The representative western blot showing the levels of PDK1 protein expression in MRC-5 cells treated with (**A**) Au10 and (**C**) Au80 at concentrations of 16, 26, 36 and 41 µg/ml for 24 hours. Naive represents the protein expression of untreated cells. Bar graphs represent the protein quantification of MRC-5 cells treated with (**B**) Au10 and (**D**) Au80. The protein expression was normalised to corresponding GAPDH (loading control). The protein level presented as a protein intensity ratio relative to naive (untreated group). The data expressed with fold unit, bars represent the mean ± SD (n=4).

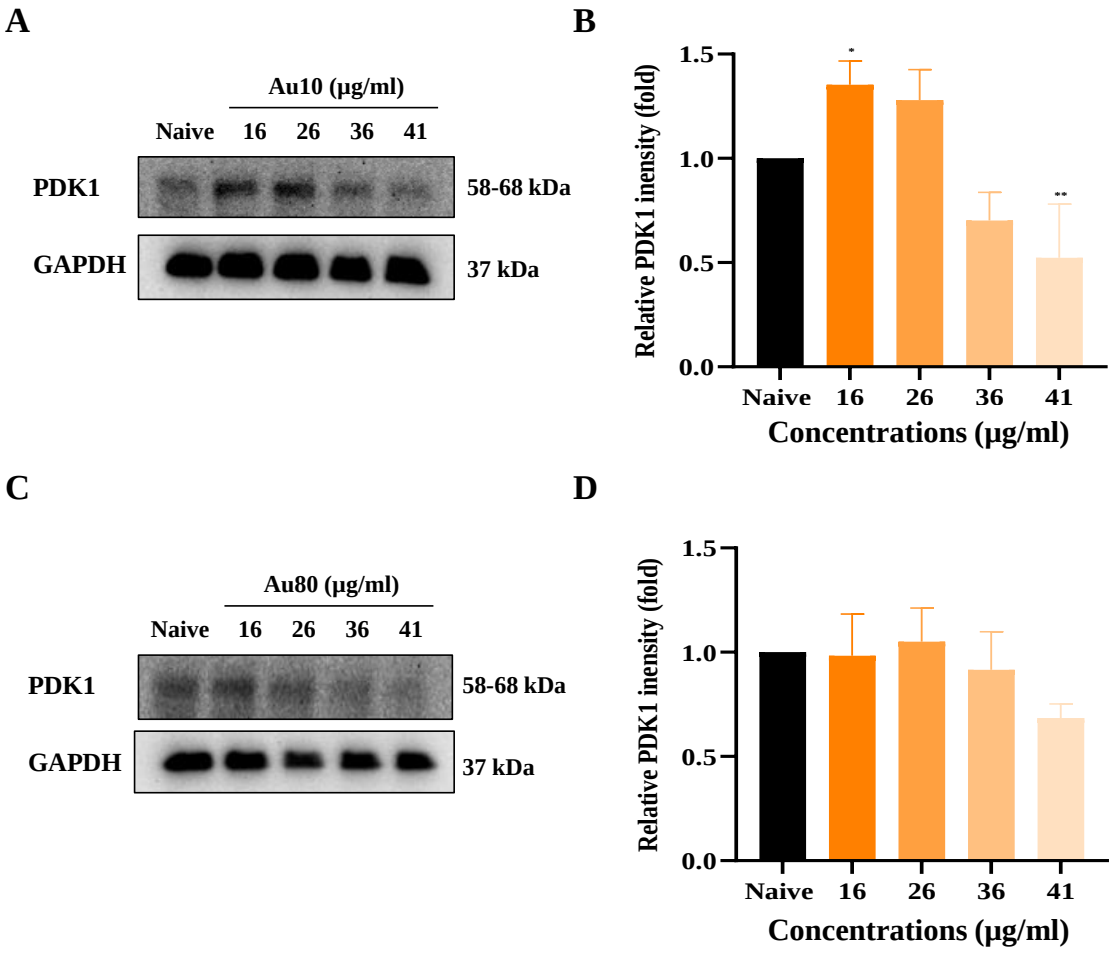


Figure 5.3. The protein expression analysis of PDK1 following A549 cells exposure to Au10 and Au80 of different concentrations for 24 hours. The representative western blot showing the levels of PDK1 protein expression in A549 cells treated with (**A**) Au10 and (**C**) Au80 at concentrations of 16, 26, 36 and 41 µg/ml for 24 hours. Naive represents the protein expression of untreated cells. Bar graphs represent the protein quantification of A549 cells treated with (**B**) Au10 and (**D**) Au80. The protein expression was normalised to corresponding GAPDH (loading control). The protein level presented as a protein intensity ratio relative to naive (untreated group). The data expressed with fold unit, bars represent the mean ± SD (n=4). (*) $p < 0.05$ and (**) versus untreated group by ANOVA test.

Next, mTOR was investigated. mTOR is another protein responsible for AKT activation by its phosphorylation at Ser473 residue (Porta et al., 2014). No changes in the mTOR expression were found following MRC-5 and A549 cells incubation with Au10 and Au80 of different concentrations (**Figure 5.4 and Figure 5.5**). The activity of the AKT domain through its phosphorylation by PDK1 and mTOR was not considerably influenced following treatment with Au10 and Au80 in normal and cancerous lung cells.

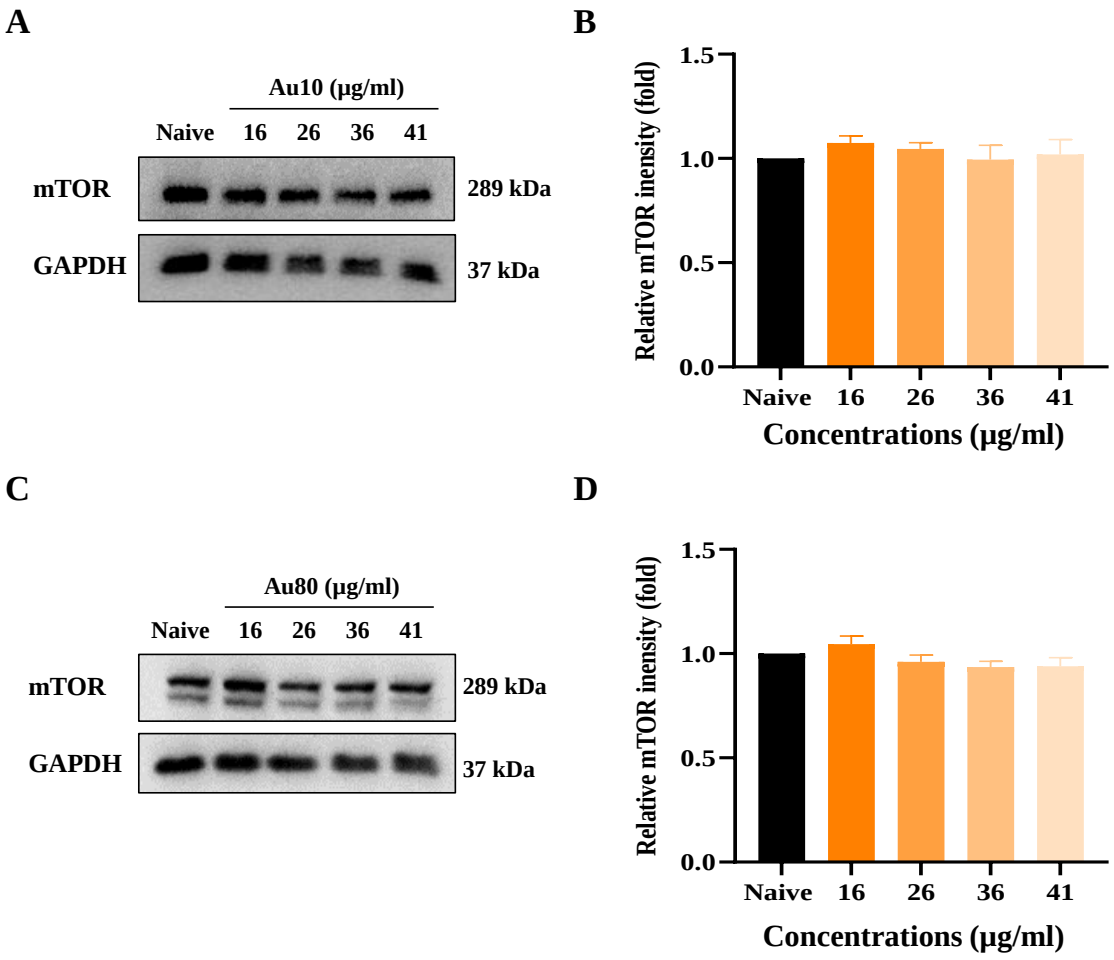


Figure 5.4. The protein expression analysis of mTOR following MRC-5 cells exposure to Au10 and Au80 of different concentrations for 24 hours. The representative western blot showing the levels of mTOR protein expression in MRC-5 cells treated with (**A**) Au10 and (**C**) Au80 at concentrations of 16, 26, 36 and 41 µg/ml for 24 hours. Naive represents the protein expression of untreated cells. Bar graphs represent the protein quantification of MRC-5 cells treated with (**B**) Au10 and (**D**) Au80. The protein expression was normalised to corresponding GAPDH (loading control). The protein level presented as a protein intensity ratio relative to naive (untreated group). The data expressed with fold unit, bars represent the mean ± SD (n=4).

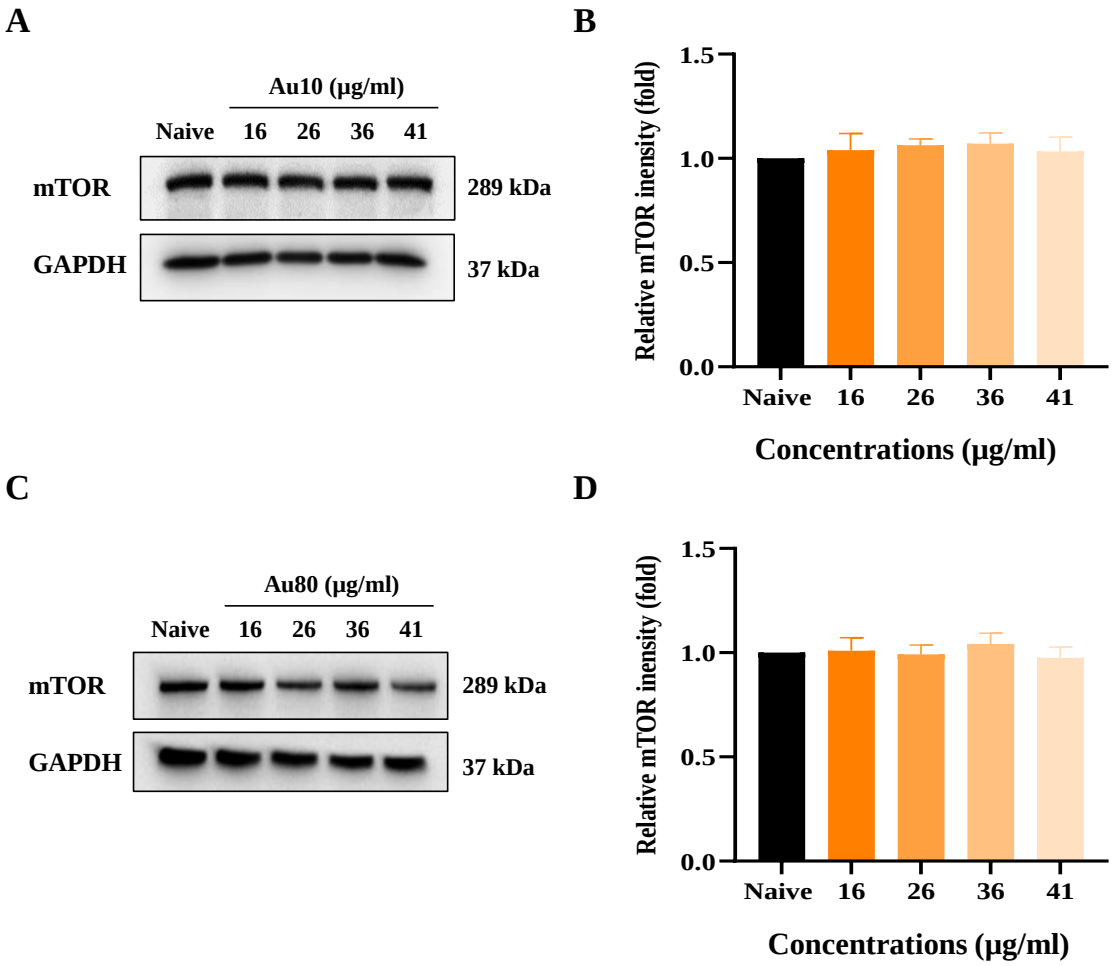


Figure 5.5. The protein expression analysis of mTOR following A549 cells exposure to Au10 and Au80 of different concentrations for 24 hours. The representative western blot showing the levels of mTOR protein expression in A549 cells treated with (**A**) Au10 and (**C**) Au80 at concentrations of 16, 26, 36 and 41 µg/ml for 24 hours. Naive represents the protein expression of untreated cells. Bar graphs represent the protein quantification of A549 cells treated with (**B**) Au10 and (**D**) Au80. The protein expression was normalised to corresponding GAPDH (loading control). The protein level presented as a protein intensity ratio relative to naive (untreated group). The data expressed with fold unit, bars represent the mean ± SD (n=4).

Following that, the tumour suppressor phosphatase (PTEN) protein level was assessed. PTEN is an upstream protein that opposes PI3K/AKT activity, which suppresses cell growth and triggers apoptosis in cells (Porta et al., 2014). No significant alterations in PTEN expression were observed in either MRC-5 or A549 cells treated with different concentrations of Au10 and Au80 (**Figure 5.6 and Figure 5.7**).

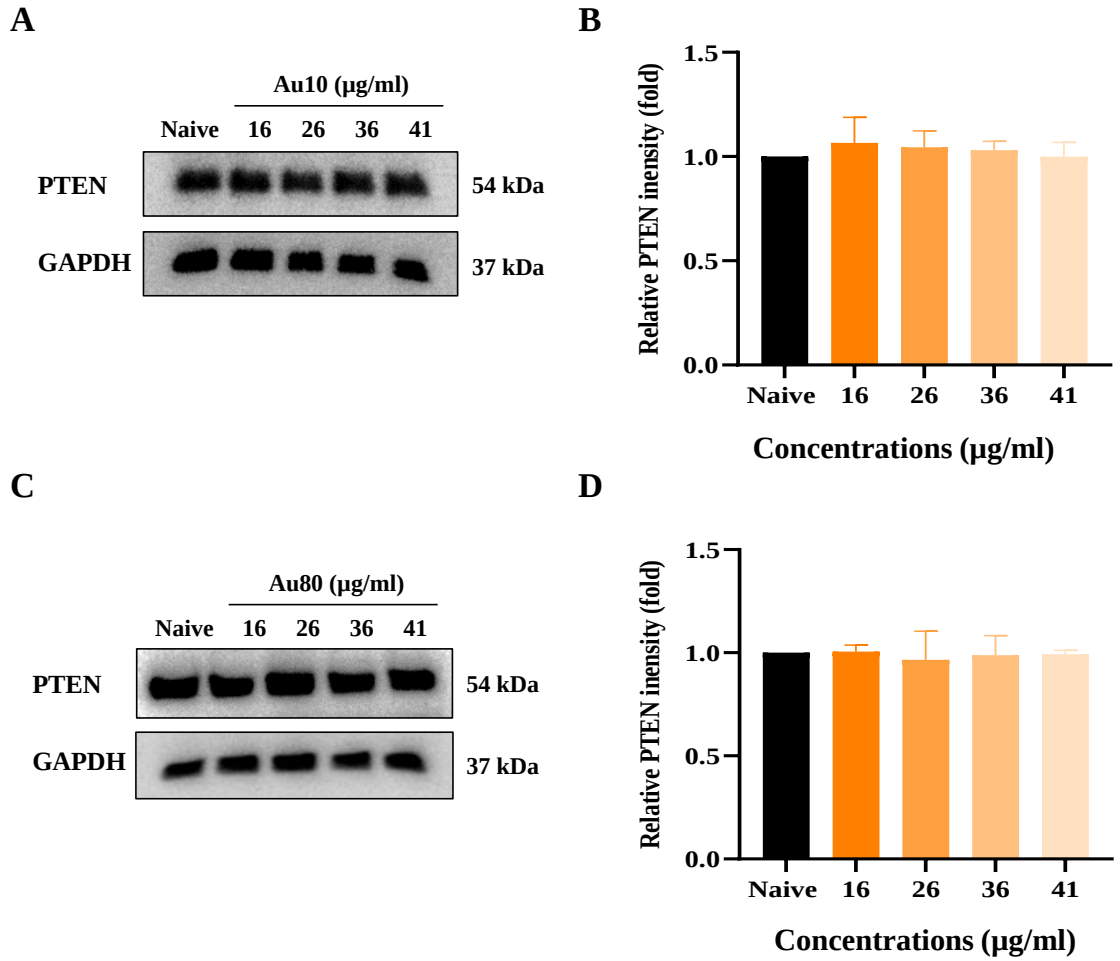


Figure 5.6. The protein expression analysis of PTEN following MRC-5 cells exposure to Au10 and Au80 of different concentrations for 24 hours. The representative western blot showing the levels of PTEN protein expression in MRC-5 cells treated with (**A**) Au10 and (**C**) Au80 at concentrations of 16, 26, 36 and 41 µg/ml for 24 hours. Naive represents the protein expression of untreated cells. Bar graphs represent the protein quantification of MRC-5 cells treated with (**B**) Au10 and (**D**) Au80. The protein expression was normalised to corresponding GAPDH (loading control). The protein level presented as a protein intensity ratio relative to naive (untreated group). The data expressed with fold unit, bars represent the mean ± SD (n=4).

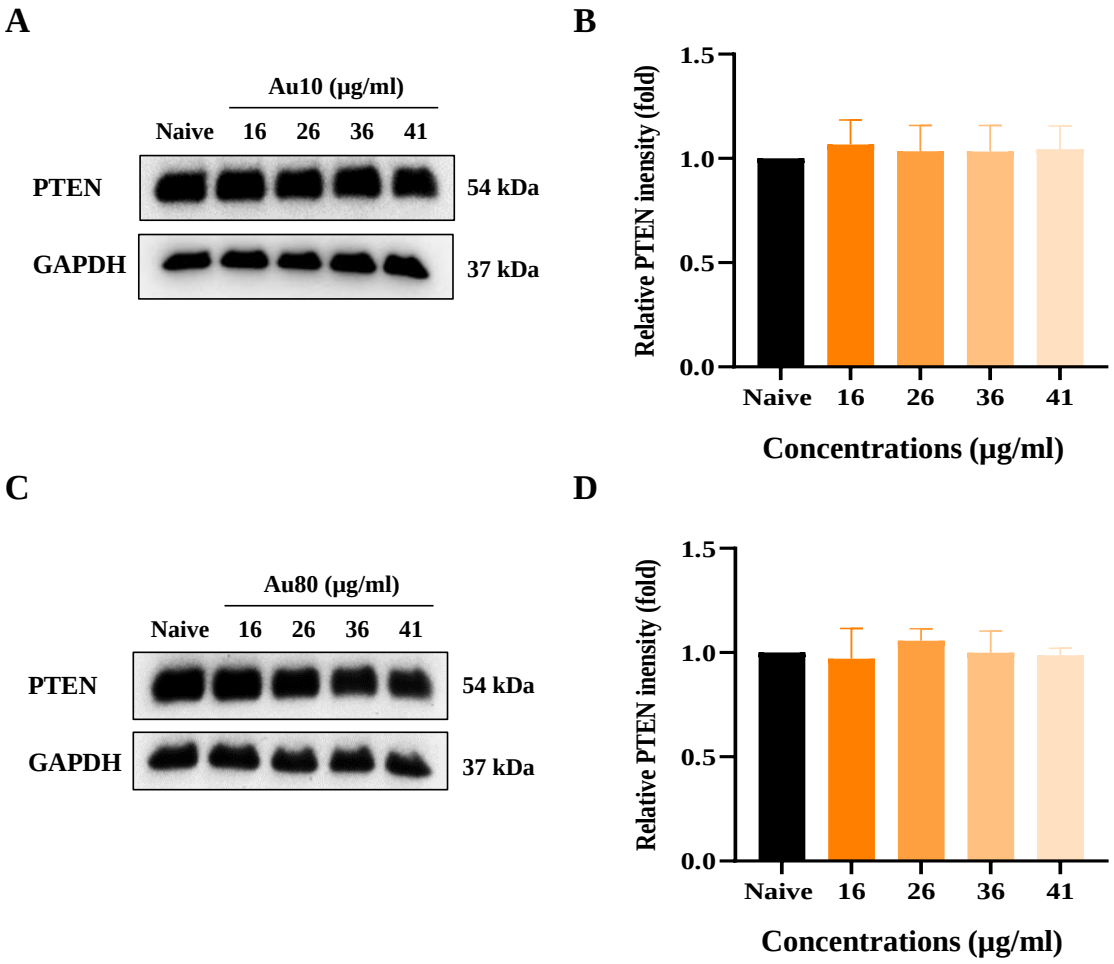


Figure 5.7. The protein expression analysis of PTEN following A549 cells exposure to Au10 and Au80 of different concentrations for 24 hours. The representative western blot showing the levels of PTEN protein expression in A549 cells treated with (**A**) Au10 and (**C**) Au80 at concentrations of 16, 26, 36 and 41 µg/ml for 24 hours. Naive represents the protein expression of untreated cells. Bar graphs represent the protein quantification of A549 cells treated with (**B**) Au10 and (**D**) Au80. The protein expression was normalised to corresponding GAPDH (loading control). The protein level presented as a protein intensity ratio relative to naive (untreated group). The data expressed with fold unit, bars represent the mean ± SD (n=4).

Then, the AKT protein level was assessed in both cell lines. The key function of AKT is to promote cell proliferation and suppress apoptosis machinery (Nitulescu et al., 2018). No alteration was detected on the AKT protein expression following MRC-5 or A549 cells exposure to Au10 and Au80 of different concentrations (**Figure 5.8 and Figure 5.9**). The downstream c-Raf protein which is regulated by AKT was investigated as the next step.

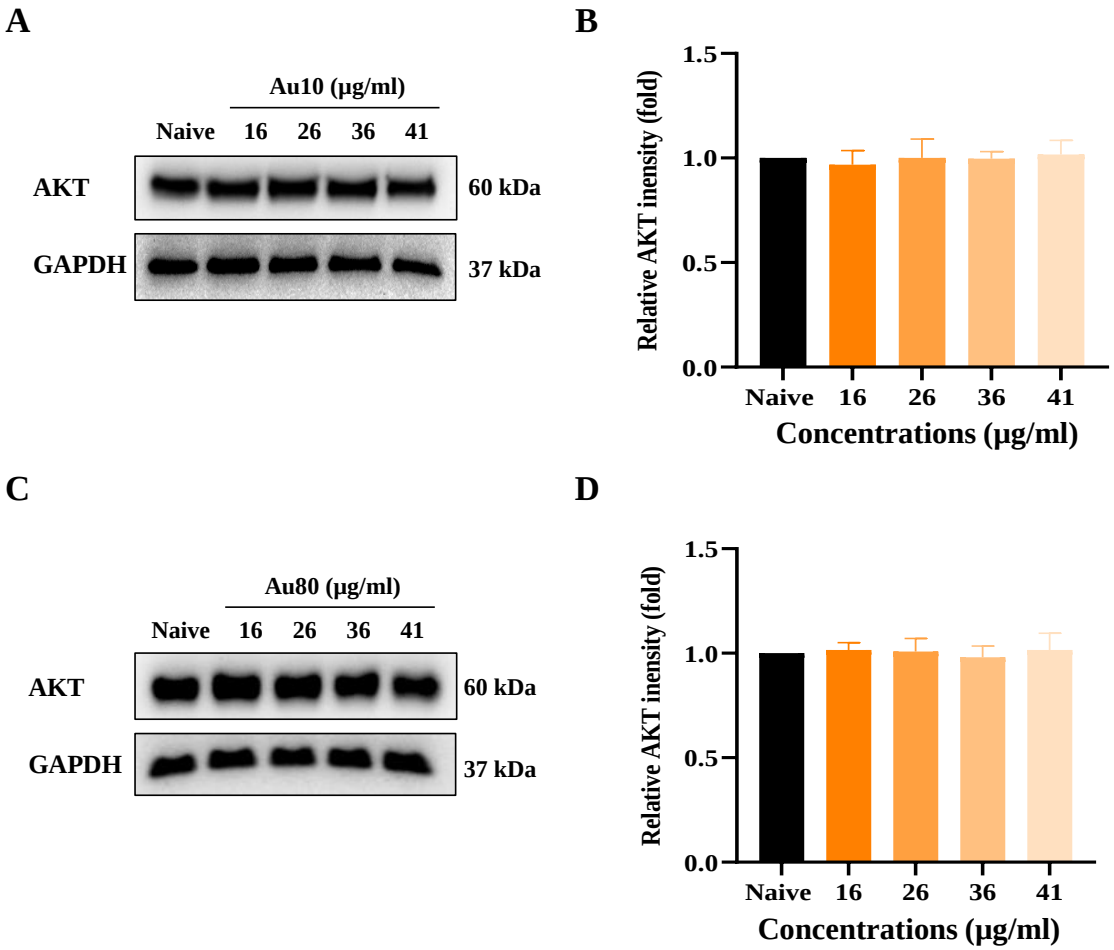


Figure 5.8. The protein expression analysis of AKT following MRC-5 cells exposure to Au10 and Au80 of different concentrations for 24 hours. The representative western blot showing the levels of AKT protein expression in MRC-5 cells treated with (**A**) Au10 and (**C**) Au80 at concentrations of 16, 26, 36 and 41 µg/ml for 24 hours. Naive represents the protein expression of untreated cells. Bar graphs represent the protein quantification of MRC-5 cells treated with (**B**) Au10 and (**D**) Au80. The protein expression was normalised to corresponding GAPDH (loading control). The protein level presented as a protein intensity ratio relative to naive (untreated group). The data expressed with fold unit, bars represent the mean ± SD (n=4).

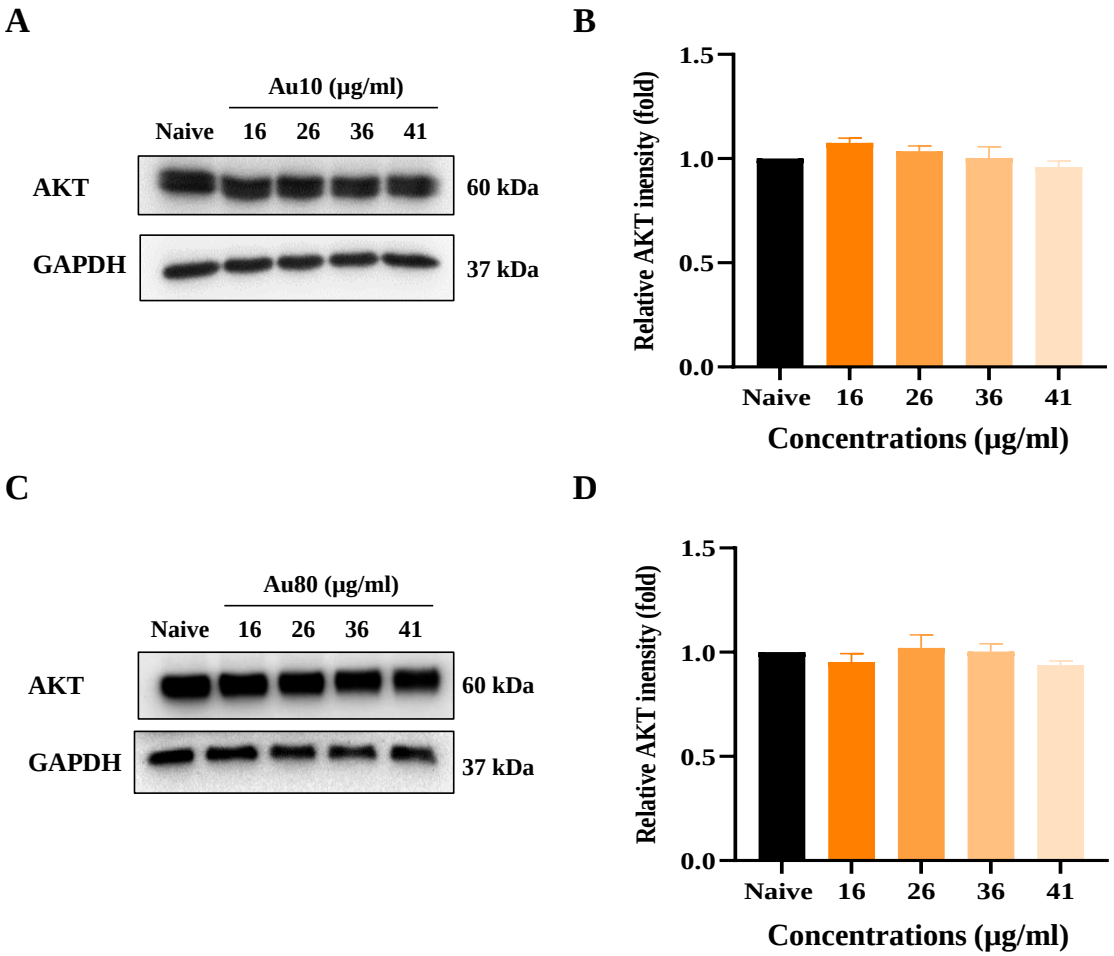


Figure 5.9. The protein expression analysis of AKT following A549 cells exposure to Au10 and Au80 of different concentrations for 24 hours. The representative western blot showing the levels of AKT protein expression in A549 cells treated with (**A**) Au10 and (**C**) Au80 at concentrations of 16, 26, 36 and 41 µg/ml for 24 hours. Naive represents the protein expression of untreated cells. Bar graphs represent the protein quantification of A549 cells treated with (**B**) Au10 and (**D**) Au80. The protein expression was normalised to corresponding GAPDH (loading control). The protein level presented as a protein intensity ratio relative to naive (untreated group). The data expressed with fold unit, bars represent the mean ± SD (n=4).

c-Raf protein activity can be activated or inhibited by its phosphorylation at different sites such as Ser338, Ser494, Ser259 and Tyrosine 341 (Tyr341) (Leicht et al., 2007). The AKT protein is responsible for the phosphorylation of c-Raf (phospho-c-Raf) at Ser259, resulting in decreased c-Raf activity (Manning and Toker, 2017). The level of phospho-c-Raf (Ser259) was significantly reduced in MRC-5 cells treated with Au10 and Au80 at high concentrations (36 and 41 µg/ml) compared to the control group (**Figure 5.10**). Moreover, no significant differences were found when comparing the intensity reduction between the two AuNPs sizes. The same observation was identified in A549 cells, in which a substantial decrease was found in the expression of phospho-c-Raf (Ser259) at a high concentration of Au10 and Au80 (**Figure 5.11**). However, no size-dependent response was reported in the downregulation of phospho-c-Raf (Ser259) protein, around 0.45- and 0.58-fold, in Au10 and Au80 of the highest concentration.

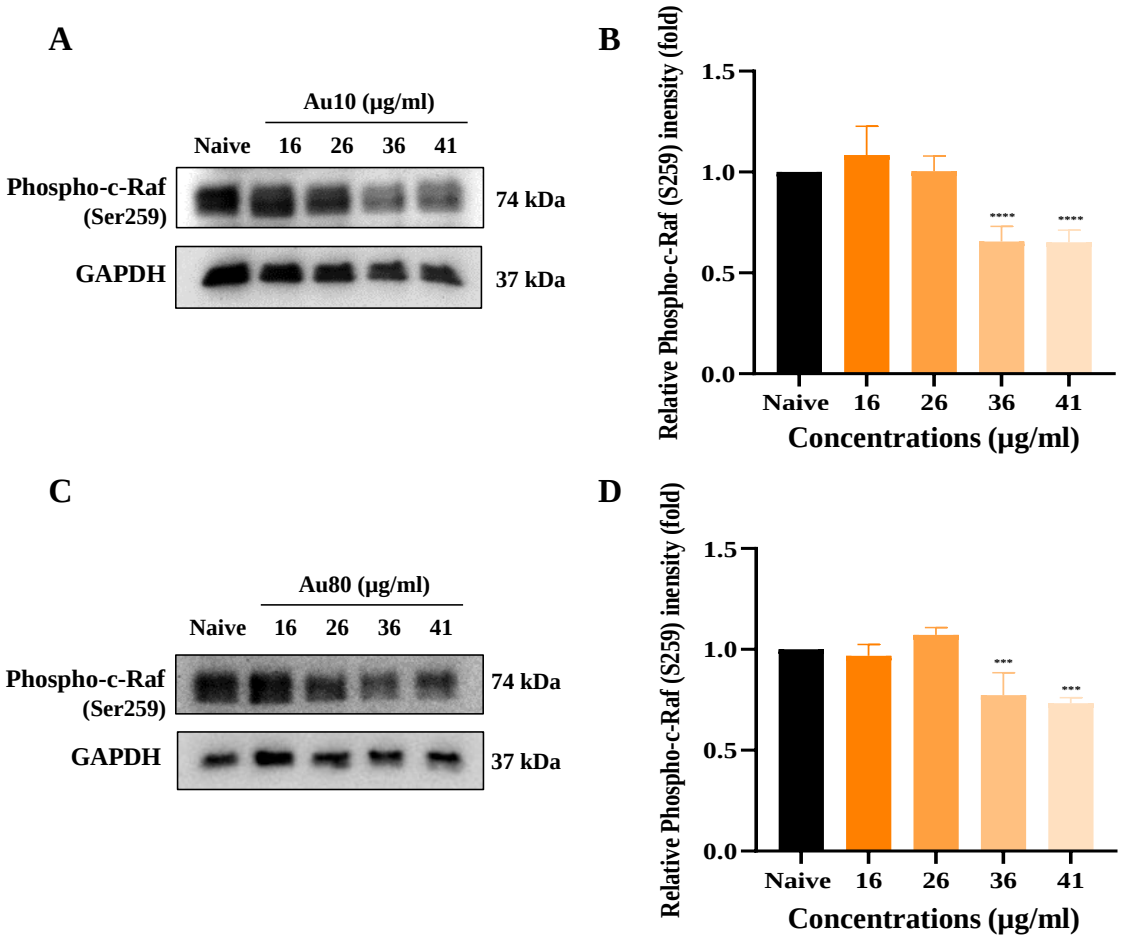


Figure 5.10. The protein expression analysis of phospho-c-Raf (Ser259) following MRC-5 cells exposure to Au10 and Au80 of different concentrations for 24 hours. The representative western blot showing the levels of phospho-c-Raf (Ser259) protein expression in MRC-5 cells treated with (**A**) Au10 and (**C**) Au80 at concentrations of 16, 26, 36 and 41 µg/ml for 24 hours. Naive represents the protein expression of untreated cells. Bar graphs represent the protein quantification of MRC-5 cells treated with (**B**) Au10 and (**D**) Au80. The protein expression was normalised to corresponding GAPDH (loading control). The protein level presented as a protein intensity ratio relative to naive (untreated group). The data expressed with fold unit, bars represent the mean ± SD (n=4). (***) $p < 0.0002$ and (****) $p < 0.0001$ versus untreated group by ANOVA test.

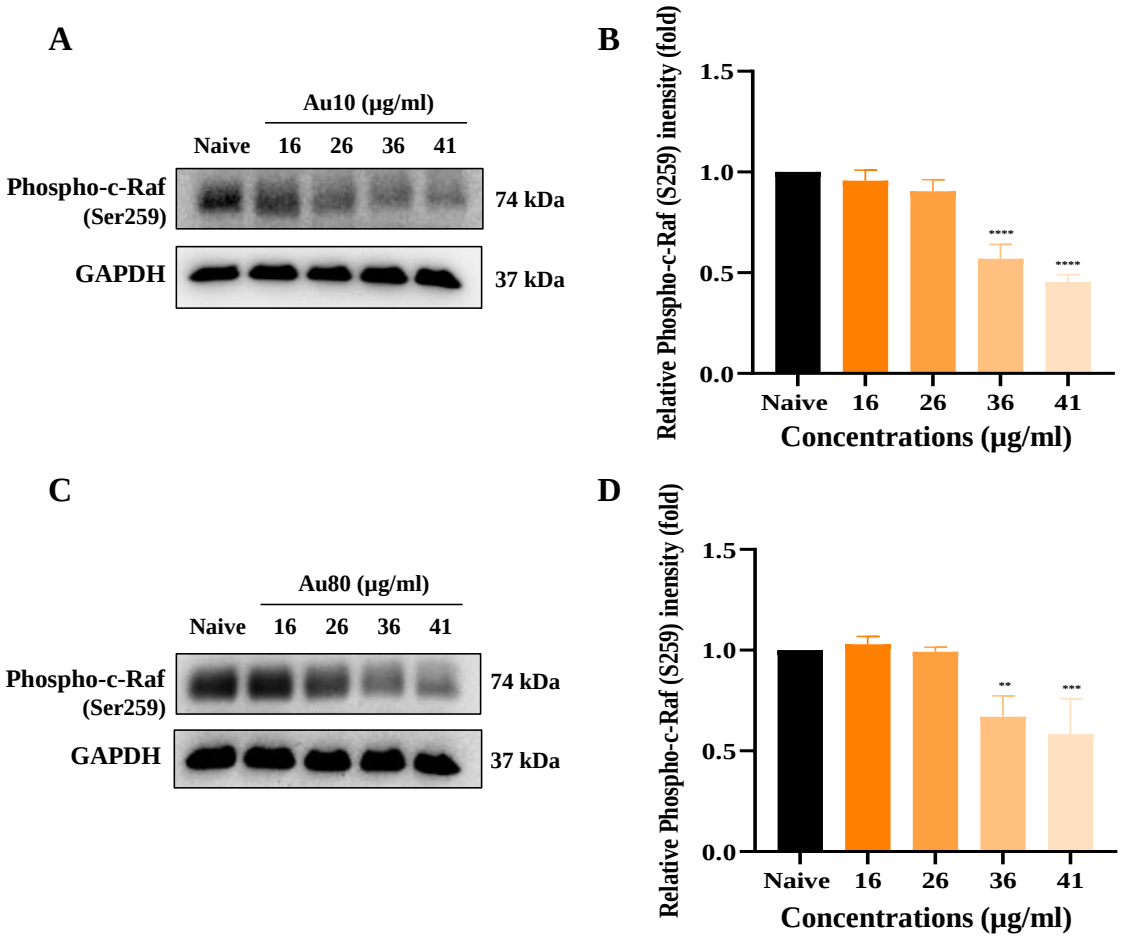


Figure 5.11. The protein expression analysis of phospho-c-Raf (Ser259) following A549 cells exposure to Au10 and Au80 of different concentrations for 24 hours. The representative western blot showing the levels of phospho-c-Raf (Ser259) protein expression in A549 cells treated with (**A**) Au10 and (**C**) Au80 at concentrations of 16, 26, 36 and 41 µg/ml for 24 hours. Naive represents the protein expression of untreated cells. Bar graphs represent the protein quantification of A549 cells treated with (**B**) Au10 and (**D**) Au80. The protein expression was normalised to corresponding GAPDH (loading control). The protein level presented as a protein intensity ratio relative to naive (untreated group). The data expressed with fold unit, bars represent the mean ± SD (n=4). (**) $p < 0.002$; (***) $p < 0.0002$ and (****) $p < 0.0001$ versus untreated group by ANOVA test.

The PI3K pathway activity is dependent on AKT protein activation in order to control several cellular functions (Manning and Toker, 2017). In cancer, AKT protein found to be predominantly overexpressed which mediates uncontrolled cell proliferation and suppresses apoptosis by inhibiting cytochrome C release from the mitochondria (Kennedy et al., 1999). Therefore, therapeutic targeting of AKT is one of the recent research focus to develop AKT inhibitors (Dumble et al., 2014, Crabb et al., 2017). Herein, high concentrations of Au10 and Au80 mediated a decrease in the PDK1 level in A549 cells which could result in attenuating AKT activity. As a consequence of reducing AKT activity, a downregulation in the phospho-c-Raf (Ser259) level was detected. The results indicated partial inhibition of AKT phosphorylation as there was no influence on mTOR activity which is the second regulator of AKT phosphorylation. These findings are in agreement with the literature (Pan et al., 2014, Chan et al., 2019, Comfort et al., 2011) which were evident an inhibitory effect of AuNPs on AKT activity by mediating AKT dephosphorylation resulted in inhibition of angiogenesis, cell migration and inflammatory response.

In the present work, AuNPs demonstrated no considerable effect in the PI3K/AKT signalling transduction based on the investigated proteins and this may further support the earlier evidence in chapter 4 of no significant toxicity and apoptosis were induced following cellular exposure to AuNPs. Nevertheless, further investigation is required by exploring others upstream and downstream cascades for better understating the possible toxicity mechanism of AuNPs by dysregulating PI3K/AKT signalling pathway. The impact of AgNPs on PI3K/AKT signalling pathway was also studied. The next subsection presents and discusses the findings.

5.2.1.2 The impacts of AgNPs on the PI3K/AKT cell signalling pathway

The impact of AgNPs sized 10 and 80 nm on the PI3K/AKT signalling cascade was investigated on MRC-5 and A549 cells. PDK1 protein is one of the regulators of AKT phosphorylation at the Ther308 domain. Substantial reduction in PDK1 expression was detected in MRC-5 cells treated with Ag10 and Ag80 only at a concentration of 10 µg/ml compared to the control group (**Figure 5.12**). Similarly, the PDk1 level was suppressed in A549 cells treated with Ag10 and Ag80 at high concentration (10 µg/ml) ($p < 0.05$) (**Figure 5.13**). However, the inhibition of PDK1 activity by Ag10 and Ag80 was more significant in MRC-5 cells compared to A549 cells. Based on this finding, it was of interest to investigate the active form of PDK1 which is the phosphorylated form of PDK1 (phospho-PDK1) at Ser241 residue.

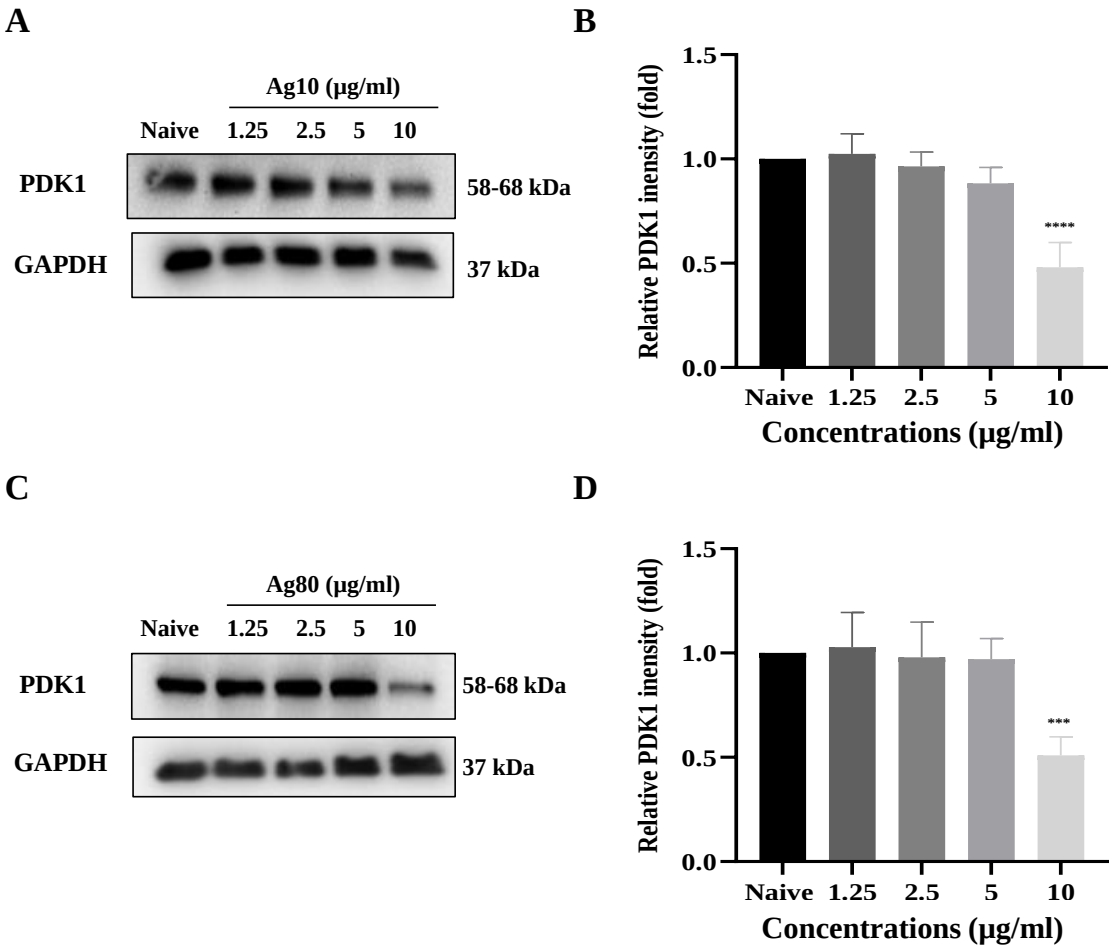


Figure 5.12. The protein expression analysis of PDK1 following MRC-5 cells exposure to Ag10 and Ag80 of different concentrations for 24 hours. The representative western blot showing the levels of PDK1 protein expression in MRC-5 cells treated with (**A**) Ag10 and (**C**) Ag80 at concentrations of 1.25, 2.5, 5 and 10 µg/ml for 24 hours. Naive represents the protein expression of untreated cells. Bar graphs represent the protein quantification of MRC-5 cells treated with (**B**) Ag10 and (**D**) Ag80. The protein expression was normalised to corresponding GAPDH (loading control). The protein level presented as a protein intensity ratio relative to naive (untreated group). The data expressed with fold unit, bars represent the mean ± SD (n=4). (***) $p < 0.0002$ and (****) $p < 0.0001$ versus untreated group by ANOVA test.

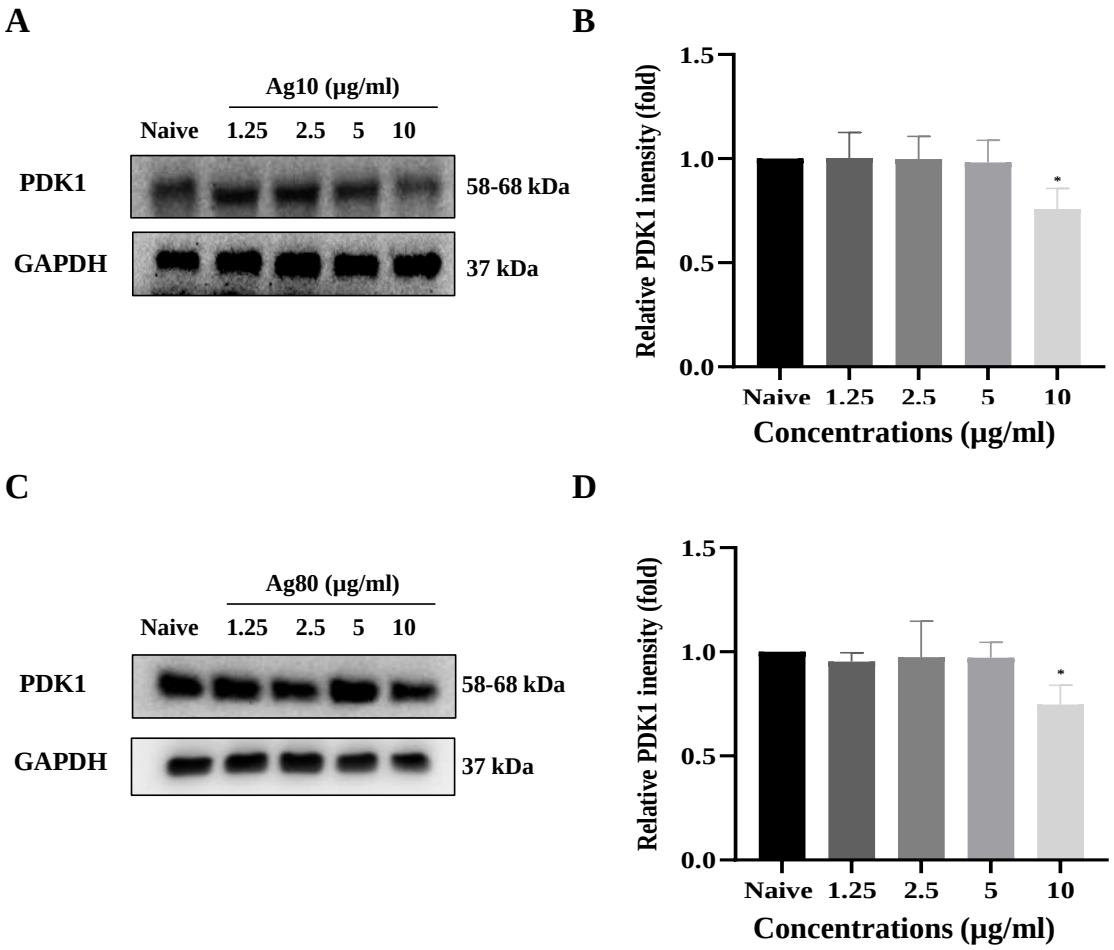


Figure 5.13. The protein expression analysis of PDK1 following A549 cells exposure to Ag10 and Ag80 of different concentrations for 24 hours. The representative western blot showing the levels of PDK1 protein expression in A549 cells treated with (**A**) Ag10 and (**C**) Ag80 at concentrations of 1.25, 2.5, 5 and 10 µg/ml for 24 hours. Naive represents the protein expression of untreated cells. Bar graphs represent the protein quantification of A549 cells treated with (**B**) Ag10 and (**D**) Ag80. The protein expression was normalised to corresponding GAPDH (loading control). The protein level presented as a protein intensity ratio relative to naive (untreated group). The data expressed with fold unit, bars represent the mean ± SD (n=4). (*) $p < 0.05$ versus untreated group by ANOVA test.

A decrease in PDK1 phosphorylation at Ser241 site was detected in MRC-5 cells incubated with Ag10 and Ag80 at a high concentration of 10 µg/ml (**Figure 5.14**). Similar observation found in A549 cells, the phospho-PDK1 level reduction was significant at high concentrations of Ag10 and Ag80 (**Figure 5.15**).

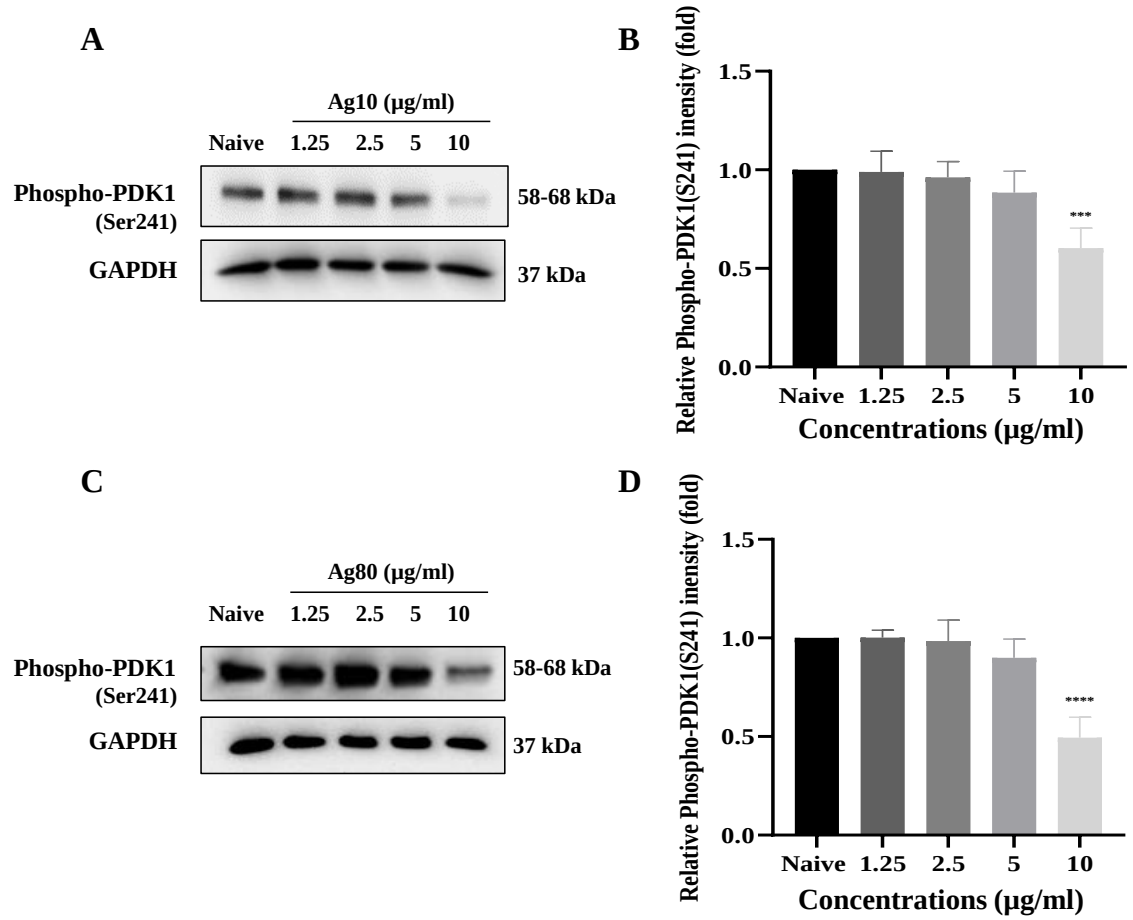


Figure 5.14. The protein expression analysis of phospho-PDK1 (Ser241) following MRC-5 cells exposure to Ag10 and Ag80 of different concentrations for 24 hours. The representative western blot showing the levels of phospho-PDK1 (Ser241) protein expression in MRC-5 cells treated with (**A**) Ag10 and (**C**) Ag80 at concentrations of 1.25, 2.5, 5 and 10 µg/ml for 24 hours. Naive represents the protein expression of untreated cells. Bar graphs represent the protein quantification of MRC-5 cells treated with (**B**) Ag10 and (**D**) Ag80. The protein expression was normalised to corresponding GAPDH (loading control). The protein level presented as a protein intensity ratio relative to naive (untreated group). The data expressed with fold unit, bars represent the mean ± SD (n=4).). (***) $p < 0.0002$ and (****) $p < 0.0001$ versus untreated group by ANOVA test.

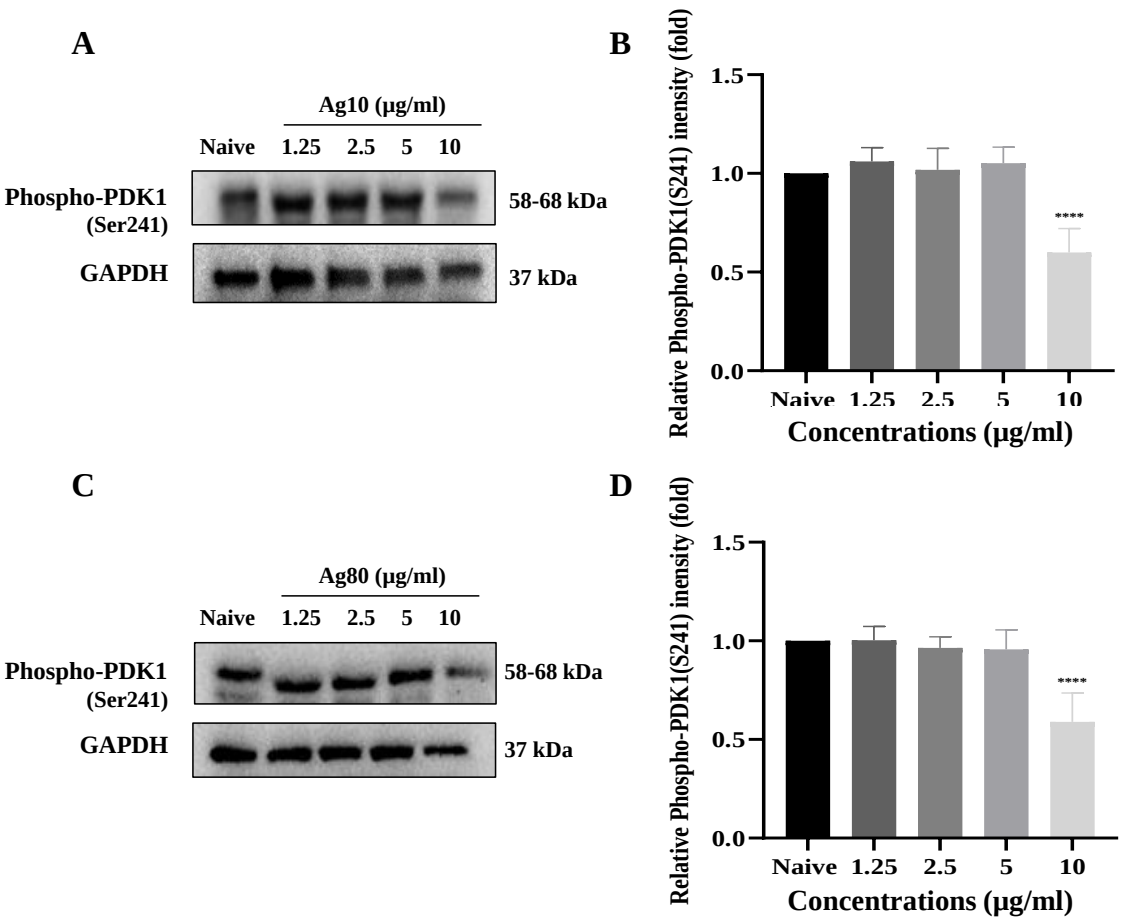


Figure 5.15. The protein expression analysis of phospho-PDK1 (Ser241) following A549 cells exposure to Ag10 and Ag80 of different concentrations for 24 hours. The representative western blot showing the levels of Phospho-PDK1 (Ser241) protein expression in A549 cells treated with (**A**) Ag10 and (**C**) Ag80 at concentrations of 1.25, 2.5, 5 and 10 µg/ml for 24 hours. Naive represents the protein expression of untreated cells. Bar graphs represent the protein quantification of A549 cells treated with (**B**) Ag10 and (**D**) Ag80. The protein expression was normalised to corresponding GAPDH (loading control). The protein level presented as a protein intensity ratio relative to naive (untreated group). The data expressed with fold unit, bars represent the mean ± SD (n=4). (****) $p < 0.0001$ versus untreated group by ANOVA test.

Next, the mTOR protein, the second regulator of AKT activity, was also tested. No observable interference in mTOR protein expression following 24 hours of incubation at different concentrations of Ag10 and Ag80 in either healthy or cancerous lung cells was found (**Figure 5.16 and Figure 5.17**).

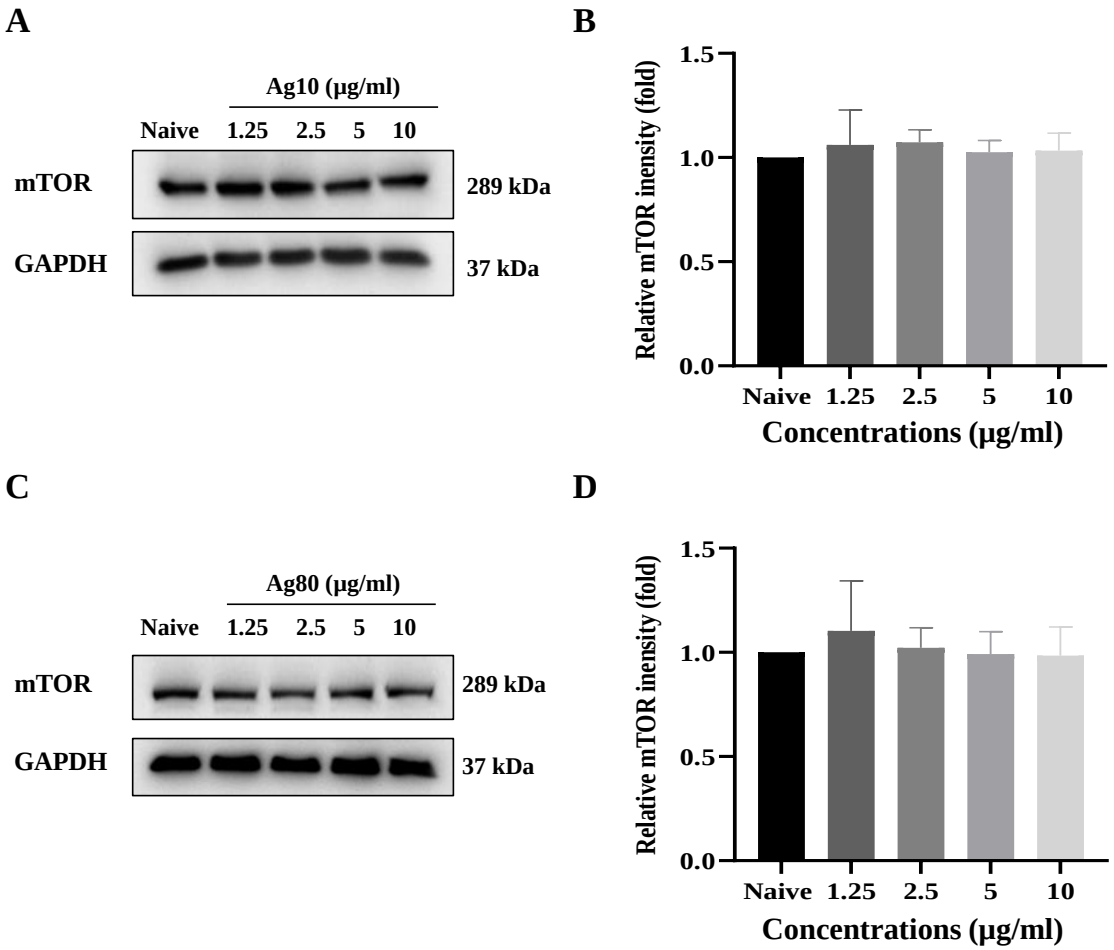


Figure 5.16. The protein expression analysis of mTOR following MRC-5 cells exposure to Ag10 and Ag80 of different concentrations for 24 hours. The representative western blot showing the levels of mTOR protein expression in MRC-5 cells treated with (**A**) Ag10 and (**C**) Ag80 at concentrations of 1.25, 2.5, 5 and 10 µg/ml for 24 hours. Naive represents the protein expression of untreated cells. Bar graphs represent the protein quantification of MRC-5 cells treated with (**B**) Ag10 and (**D**) Ag80. The protein expression was normalised to corresponding GAPDH (loading control). The protein level presented as a protein intensity ratio relative to naive (untreated group). The data expressed with fold unit, bars represent the mean ± SD (n=4).

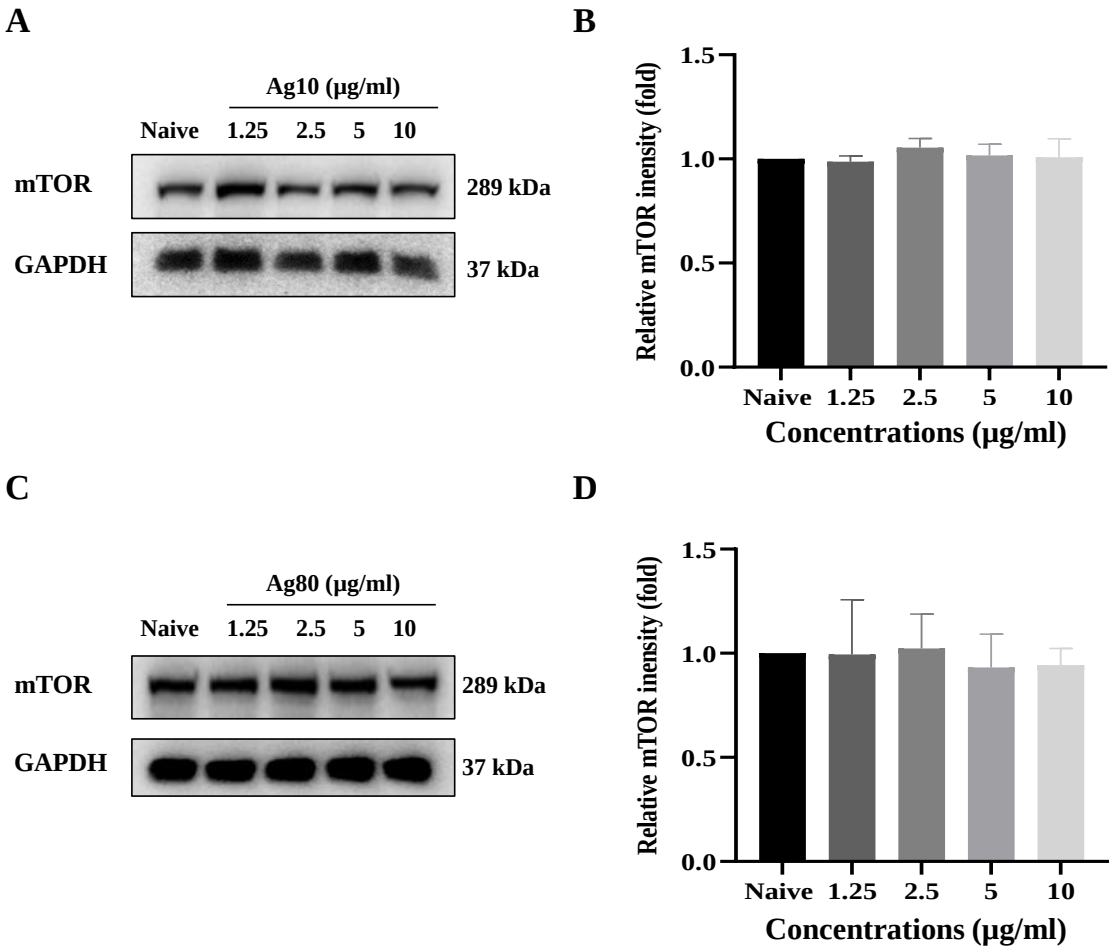


Figure 5.17. The protein expression analysis of mTOR following A549 cells exposure to Ag10 and Ag80 of different concentrations for 24 hours. The representative western blot showing the levels of mTOR protein expression in A549 cells treated with (**A**) Ag10 and (**C**) Ag80 at concentrations of 1.25, 2.5, 5 and 10 µg/ml for 24 hours. Naive represents the protein expression of untreated cells. Bar graphs represent the protein quantification of A549 cells treated with (**B**) Ag10 and (**D**) Ag80. The protein expression was normalised to corresponding GAPDH (loading control). The protein level presented as a protein intensity ratio relative to naive (untreated group). The data expressed with fold unit, bars represent the mean ± SD (n=4).

Following that, the negative regulator of the PI3K/AKT pathway, (PTEN), was assessed after cellular exposure to AgNPs. The MRC-5 and A549 cells exposed to Ag10 and Ag80 of varying concentrations demonstrated no changes in the PTEN protein level after 24 hours of exposure compared to the untreated group (**Figure 5.18 and Figure 5.19**).

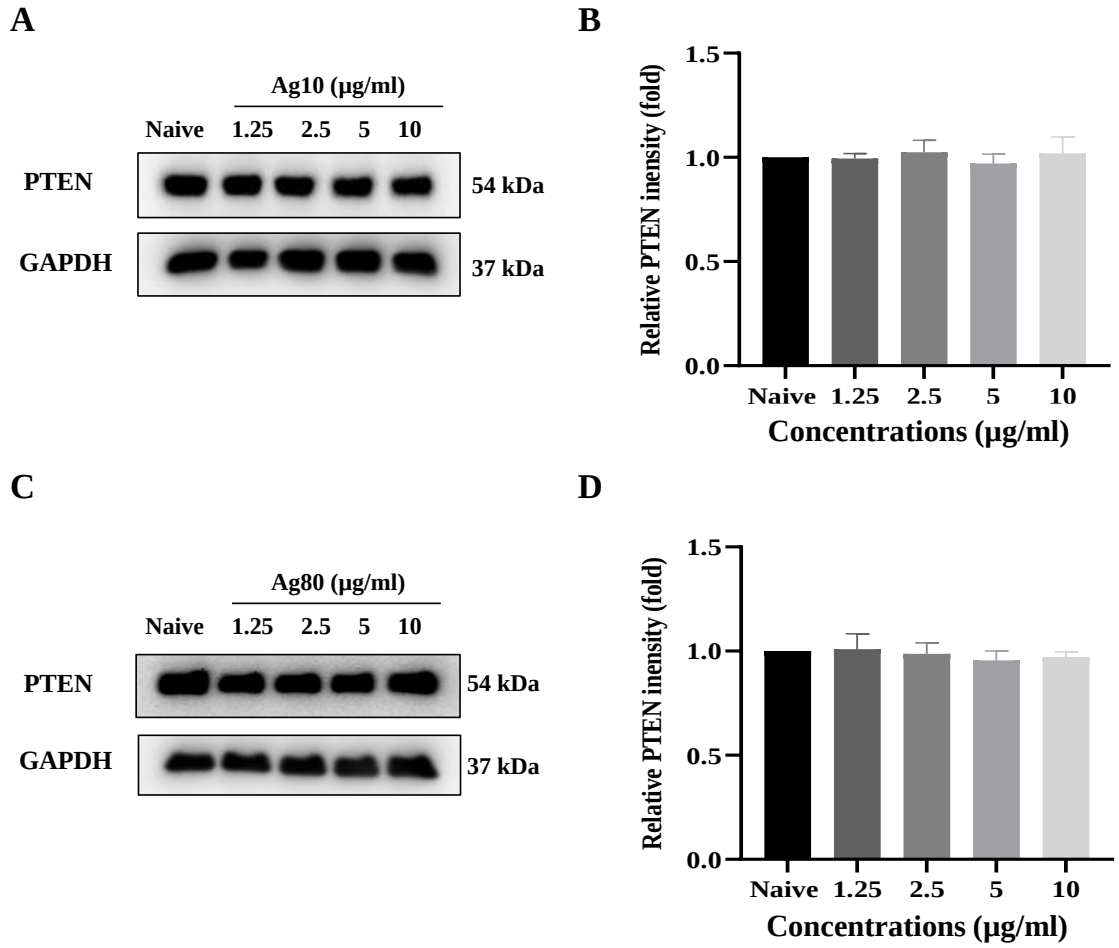


Figure 5.18. The protein expression analysis of PTEN following MRC-5 cells exposure to Ag10 and Ag80 of different concentrations for 24 hours. The representative western blot showing the levels of PTEN protein expression in MRC-5 cells treated with (**A**) Ag10 and (**C**) Ag80 at concentrations of 1.25, 2.5, 5 and 10 µg/ml for 24 hours. Naive represents the protein expression of untreated cells. Bar graphs represent the protein quantification of MRC-5 cells treated with (**B**) Ag10 and (**D**) Ag80. The protein expression was normalised to corresponding GAPDH (loading control). The protein level presented as a protein intensity ratio relative to naive (untreated group). The data expressed with fold unit, bars represent the mean ± SD (n=4).

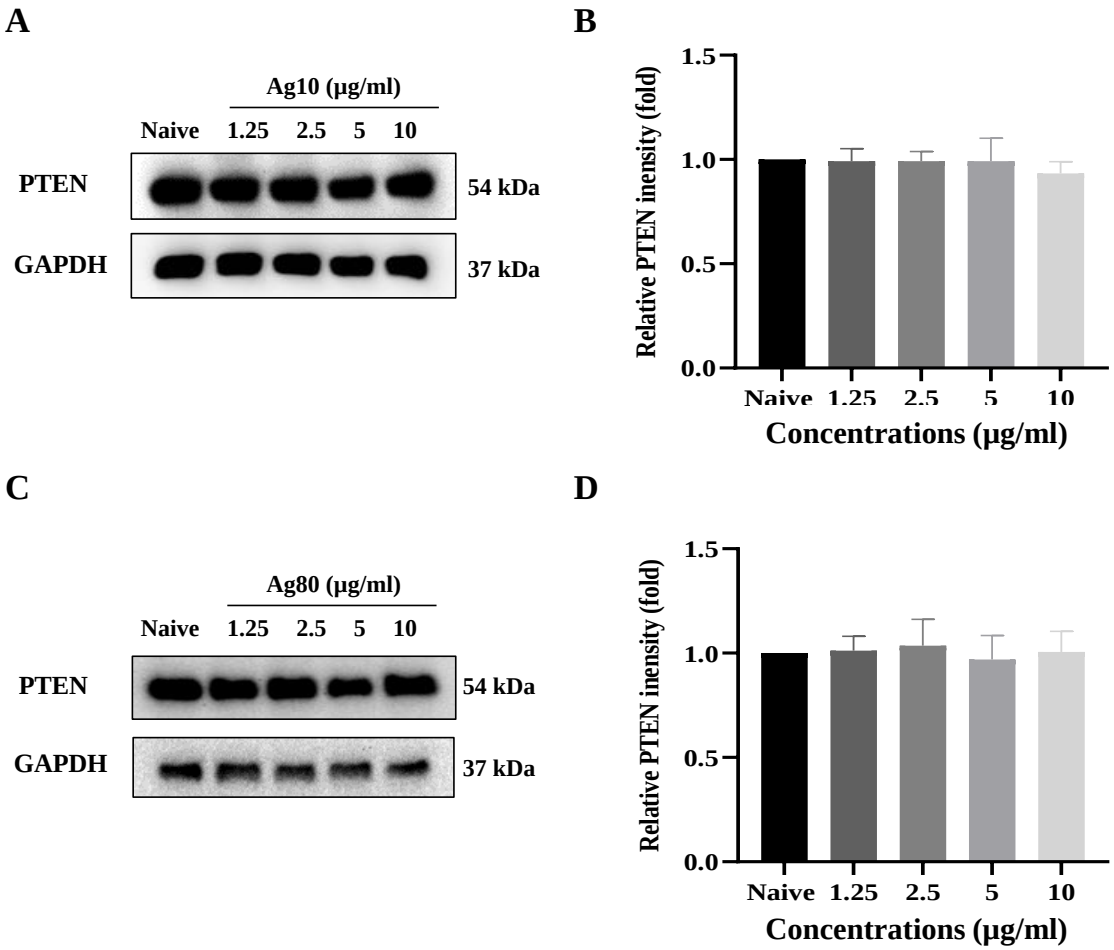


Figure 5.19. The protein expression analysis of PTEN following A549 cells exposure to Ag10 and Ag80 of different concentrations for 24 hours. The representative western blot showing the levels of PTEN protein expression in A549 cells treated with (**A**) Ag10 and (**C**) Ag80 at concentrations of 1.25, 2.5, 5 and 10 µg/ml for 24 hours. Naive represents the protein expression of untreated cells. Bar graphs represent the protein quantification of A549 cells treated with (**B**) Ag10 and (**D**) Ag80. The protein expression was normalised to corresponding GAPDH (loading control). The protein level presented as a protein intensity ratio relative to naive (untreated group). The data expressed with fold unit, bars represent the mean ± SD (n=4).

Then, the activity of AKT level was assessed. In treated MRC-5 cells, a decrease in the AKT level was noticed following exposure to high concentrations of Ag10 (10 µg/ml) and Ag80 (5 and 10 µg/ml) (**Figure 5.20**). Ag80 demonstrated more pronounced reduction in AKT level compared to Ag10. The same effect was observed in A549 cells treated with Ag10 and Ag80 at a high concentration (10 µg/ml), which demonstrated a significant reduction in AKT protein expression compared to the untreated group ($p < 0.05$) (**Figure 5.21**). However, the observed

effect on AKT level was more significant in the healthy lung cells than the cancerous lung cells.

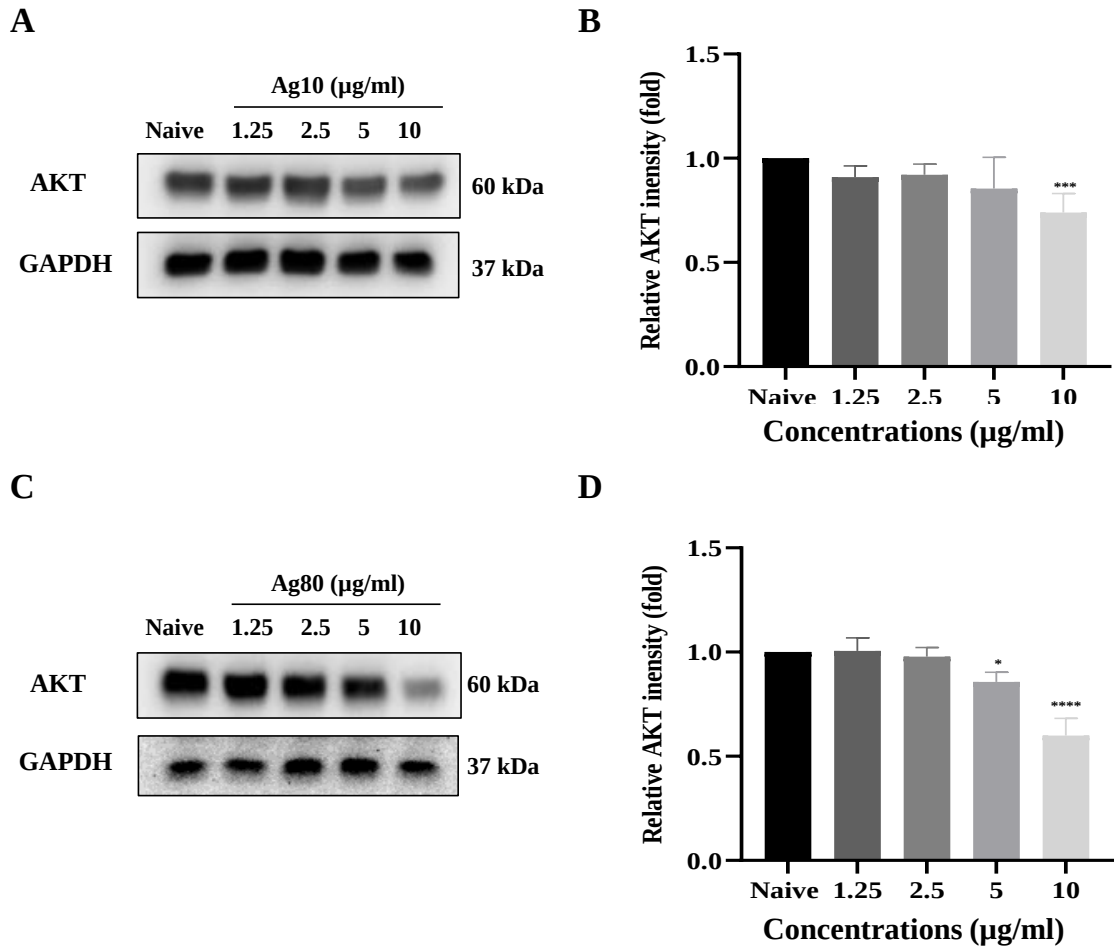


Figure 5.20. The protein expression analysis of AKT following MRC-5 cells exposure to Ag10 and Ag80 of different concentrations for 24 hours. The representative western blot showing the levels of AKT protein expression in MRC-5 cells treated with (**A**) Ag10 and (**C**) Ag80 at concentrations of 1.25, 2.5, 5 and 10 µg/ml for 24 hours. Naive represents the protein expression of untreated cells. Bar graphs represent the protein quantification of MRC-5 cells treated with (**B**) Ag10 and (**D**) Ag80. The protein expression was normalised to corresponding GAPDH (loading control). The protein level presented as a protein intensity ratio relative to naive (untreated group). The data expressed with fold unit, bars represent the mean ± SD (n=4). (*) $p < 0.05$; (***) $p < 0.0002$ and (****) $p < 0.0001$ versus untreated group by ANOVA test.

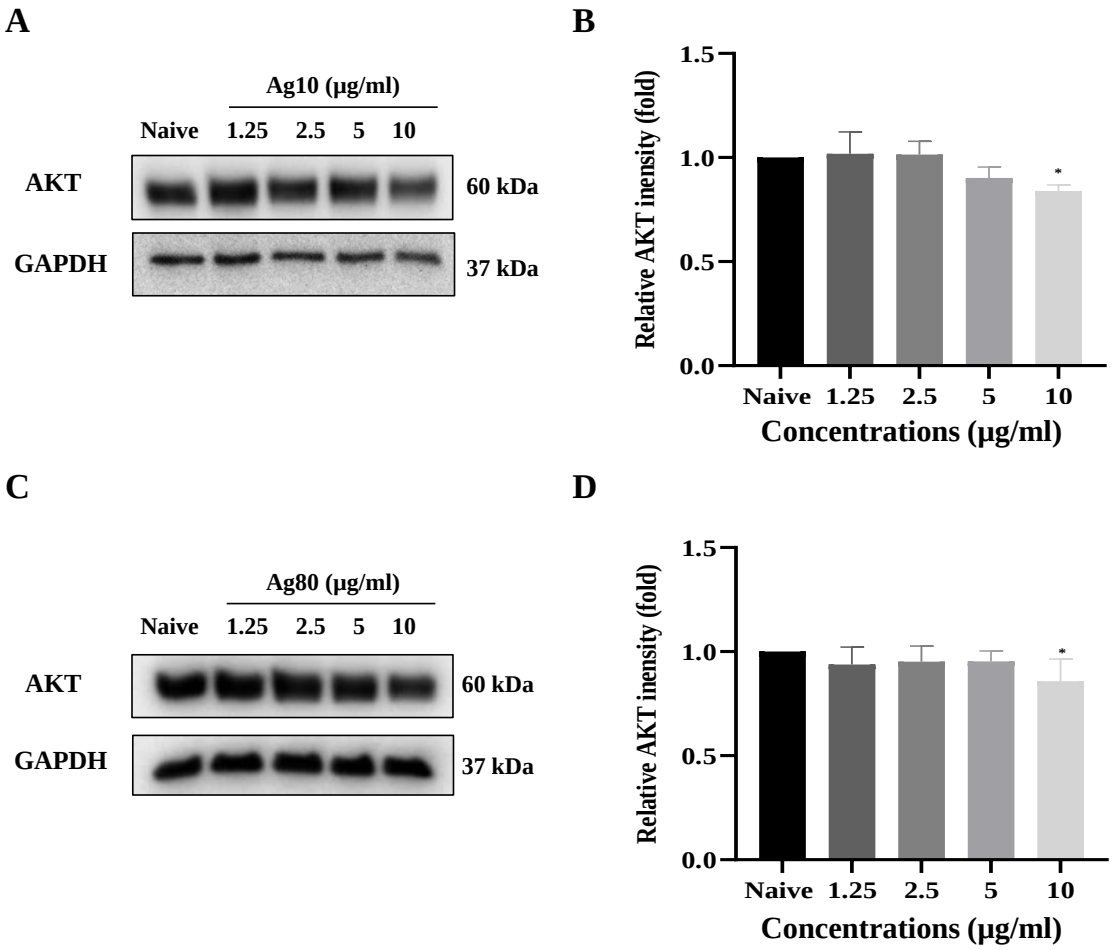


Figure 5.21. The protein expression analysis of AKT following A549 cells exposure to Ag10 and Ag80 of different concentrations for 24 hours. The representative western blot showing the levels of AKT protein expression in A549 cells treated with (**A**) Ag10 and (**C**) Ag80 at concentrations of 1.25, 2.5, 5 and 10 µg/ml for 24 hours. Naive represents the protein expression of untreated cells. Bar graphs represent the protein quantification of A549 cells treated with (**B**) Ag10 and (**D**) Ag80. The protein expression was normalised to corresponding GAPDH (loading control). The protein level presented as a protein intensity ratio relative to naive (untreated group). The data expressed with fold unit, bars represent the mean ± SD (n=4). (*) $p < 0.05$ versus untreated group by ANOVA test.

The c-Raf protein is the downstream cascade of AKT. The phosphorylation of c-Raf at Ser359 residue occurs upon AKT activation, leading to inactivation of the c-Raf protein that controls the apoptosis machinery. A statistically significant reduction in the protein level of phospho-c-Raf (Ser259) was detected at high concentrations of Ag10 and Ag80 in both MRC-5 and A549 cells (**Figure 5.22 and Figure 5.23**). No size effect differences were detected between Ag10 and Ag80 in the phospho-c-Raf (Ser259) expression level.

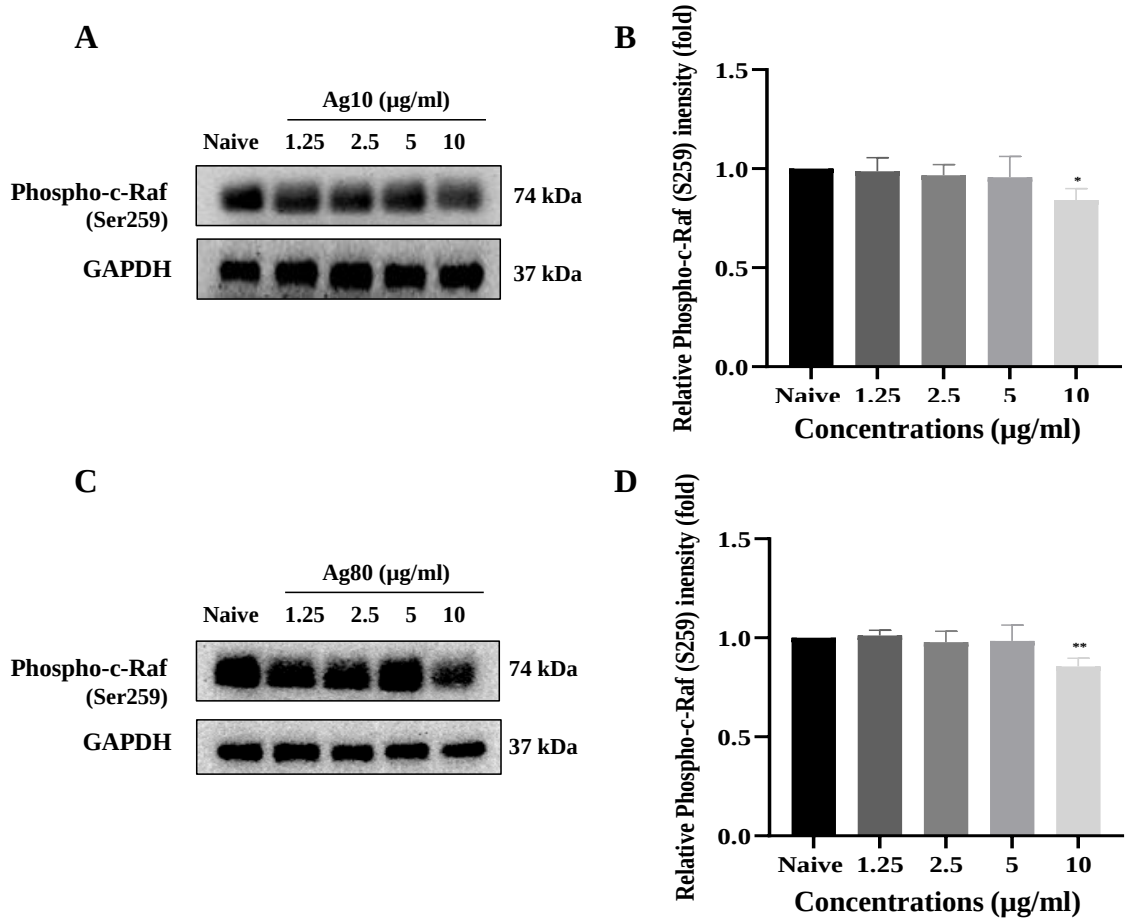


Figure 5.22. The protein expression analysis of phospho-c-Raf (Ser259) following MRC-5 cells exposure to Ag10 and Ag80 of different concentrations for 24 hours. The representative western blot showing the levels of phospho-c-Raf (Ser259) protein expression in MRC-5 cells treated with (**A**) Ag10 and (**C**) Ag80 at concentrations of 1.25, 2.5, 5 and 10 µg/ml for 24 hours. Naive represents the protein expression of untreated cells. Bar graphs represent the protein quantification of MRC-5 cells treated with (**B**) Ag10 and (**D**) Ag80. The protein expression was normalised to corresponding GAPDH (loading control). The protein level presented as a protein intensity ratio relative to naive (untreated group). The data expressed with fold unit, bars represent the mean ± SD (n=4). (*) $p < 0.05$ and (**) $p < 0.002$ versus untreated group by ANOVA test.

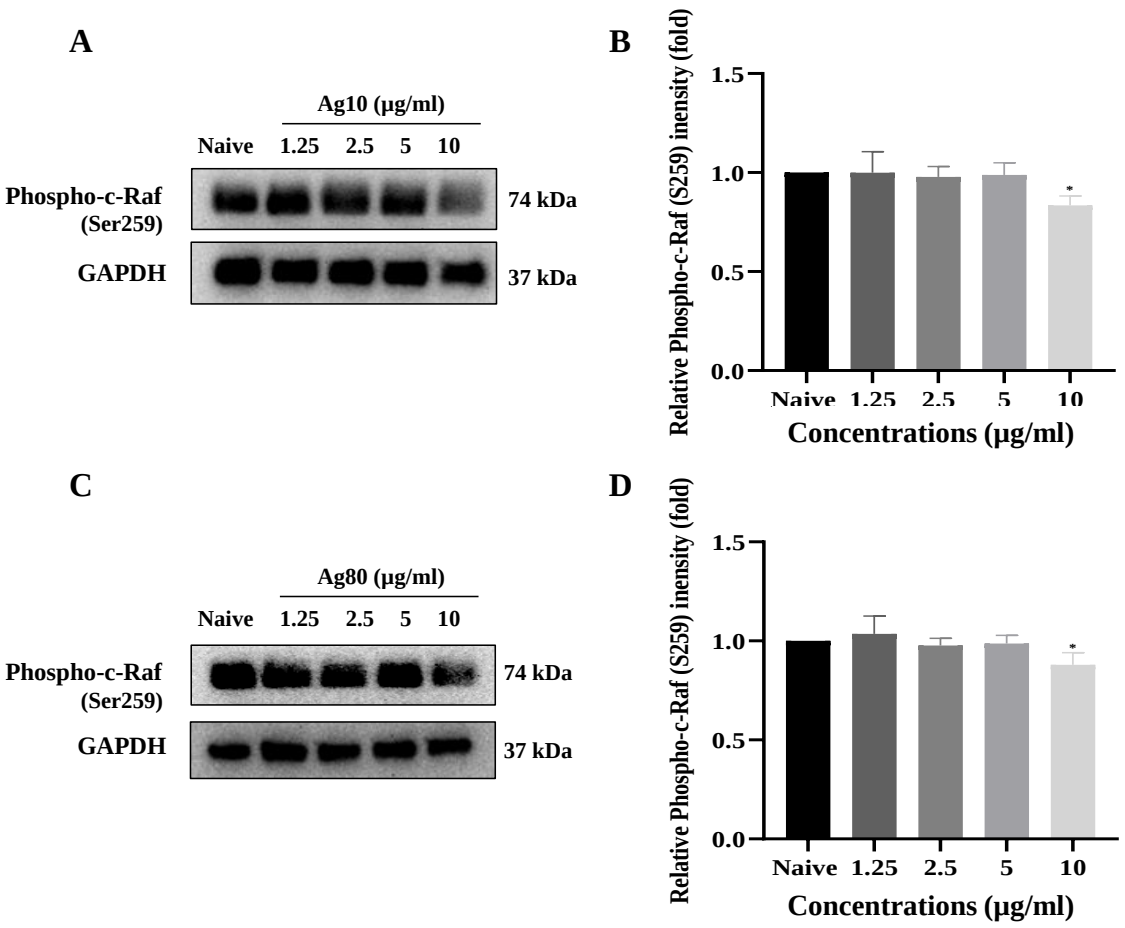


Figure 5.23. The protein expression analysis of phospho-c-Raf (Ser259) following A549 cells exposure to Ag10 and Ag80 of different concentrations for 24 hours. The representative western blot showing the levels of phospho-c-Raf (Ser259) protein expression in A549 cells treated with (**A**) Ag10 and (**C**) Ag80 at concentrations of 1.25, 2.5, 5 and 10 µg/ml for 24 hours. Naive represents the protein expression of untreated cells. Bar graphs represent the protein quantification of A549 cells treated with (**B**) Ag10 and (**D**) Ag80. The protein expression was normalised to corresponding GAPDH (loading control). The protein level presented as a protein intensity ratio relative to naive (untreated group). The data expressed with fold unit, bars represent the mean ± SD (n=4). (*) $p < 0.05$ versus untreated group by ANOVA test.

Taking together, the results demonstrated the potential of AgNPs to interfere with the PI3K/AKT signalling pathway activity. It was noted that high concentrations of Ag10 and Ag80 cause an inhibition in the AKT level. This could be a consequence of the suppression of PDK1 activity by AgNPs which is responsible for AKT phosphorylation. As shown in **Figure 5.1**, the activation of AKT protein is responsible for the activation/inhibition of several downstream cascades. As a result of AKT inhibition by AgNPs, the phosphorylated form of c-Raf was reduced, indicating a possible induction of cell death.

The dysregulation of AKT pathway by AgNPs leads to suppression of cell proliferation and this can be one of the causes associated to the observed AgNPs cytotoxicity in chapter 3. Moreover, toxicity data confirmed that AgNPs were mediated apoptosis which can be a result of the AKT pathway inhibition. Developing inhibitor molecules that target AKT is considered a promising strategy for cancer treatment (Manning and Toker, 2017). It was previously reported that AgNPs trigger apoptosis and attenuate cell proliferation via alteration of the PI3K/AKT signalling pathway was suggested as one mechanism of AgNPs induced toxicity in human hepatic cancer and human cervical cancer cells along with suppression of ERK/MAPK and p53 signalling pathways (Zhu et al., 2016, Yuan et al., 2018). However, the current evidence of this work was not sufficient to draw a full conclusion regarding the impact of AgNPs on PI3K/AKT pathway and the detected toxicity. Further studies are needed to better understand the underlying mechanism of AgNPs influence on cell signalling pathways.

The current work was also interested to investigate the impact of AuNPs and AgNPs on Wnt/β-catenin cell signalling pathway in both normal and cancerous lung cells. The following subsection represents and discusses the findings.

5.3 The influences of AuNPs and AgNPs of different sizes on the Wnt/β-catenin cell signalling pathway

Wnt signalling is classified into canonical and non-canonical pathways (Pai et al., 2017). The canonical pathway has been found to be involved in the growth of early embryos and to trigger tumour formation. Wnt/β-catenin signalling plays an essential role in the regulation of cell proliferation, cell death, cell differentiation and cell adhesion (Pai et al., 2017). β-catenin protein is the core component in the canonical pathway.

The activation of Wnt/β-catenin signalling (on-state) occurs via the interaction of extracellular Wnt ligands with frizzled receptors (Pai et al., 2017) (**Figure 5.24**). Consequently, low-density lipoprotein receptors related to protein 5/6 (LRP5/6) co-receptors are activated and bind to frizzled receptors, forming an active frizzled-LRP5/6 complex. This triggers the activation of Dishevelled (Dvl) protein by its phosphorylation. Dvl protein therefore sequesters GSK-3 protein together with Casein kinase 1 (CK1) and Axin complex, leading to stabilisation of β-catenin and promoting its accumulation in the cytoplasm. Then, β-catenin is translocated to the nucleus and binds to T-cell factor/Lymphocyte enhancer binding factor (TCF/Lef), which triggers cellular proliferation through activation of cyclin D1, c-myc, c-jun and CD44 (Clevers and Nusse, 2012).

On the other hand, in the absence of Wnt signalling (off-state) (**Figure 5.24**), the ubiquitination of β-catenin is targeted by the phosphorylation of β-catenin (Suryawanshi et al., 2016). Hence β-catenin undergoes proteasomal degradation. N-cadherin protein which coordinate cell-cell adhesion promotes the association of the Adenomatous polyposis Coli (APC), Axin and GSK-3β destruction complex. β-catenin phosphorylation at Ser45 first occurs by CK1 protein. Consequently, the phosphorylation of β-catenin at Ser33, Ser37 and Ther41 sites is promoted by GSK-3β. Phosphorylation of β-catenin leads to protein destabilisation, which tags the

protein for ubiquitination and proteasomal degradation (Valenta et al., 2012). The PI3K/AKT signalling pathway is cross-talked with the Wnt/β-catenin signalling pathway. AKT inhibits GSK-3β activity, which is the negative regulator of the Wnt signalling pathway. Impairment in Wnt/β-catenin pathway mainly by dysregulation of β-catenin and GSK-3β activities was reported in several types of tumours including colorectal, lung and breast tumours (Krishnamurthy and Kurzrock, 2018). The impact on Wnt/β-catenin following the exposure of healthy and cancerous lung cells to AuNPs and AgNPs of different sizes is explored next.

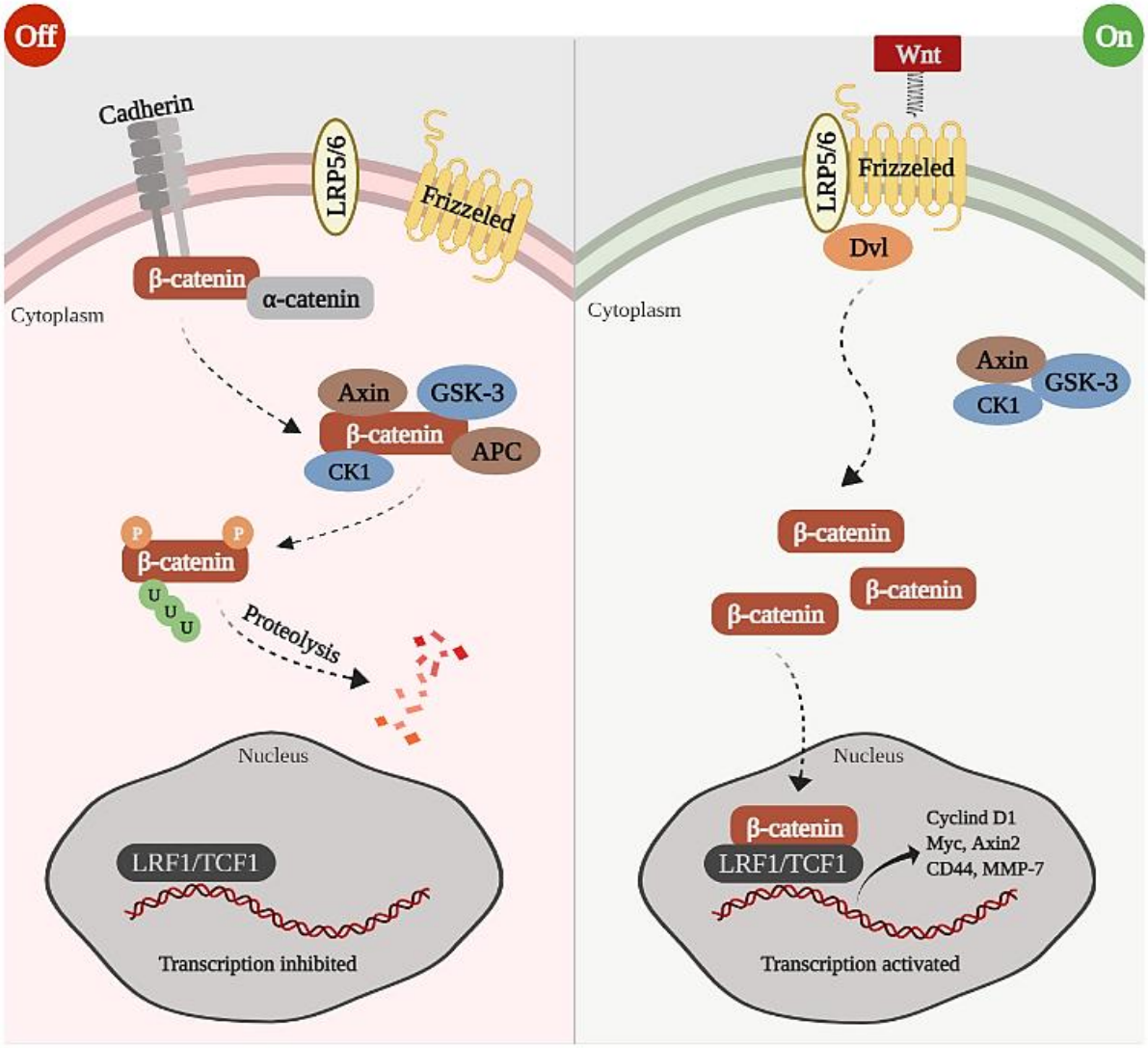


Figure 5.24. Schematic representation of Wnt/ β-catenin signalling pathway. On state: Wnt ligand binding to frizzled receptors triggers frizzeled-LRP5/6 complex formation, which leads to the activation of Dvl protein. Dvl protein deactivates the destruction complex (GSK-3/CK1/Axin) leading to the stabilisation and accumulation of β-catenin in the cytoplasm. The β-catenin is then translocated to the nucleus and binds to TCF/Lef which mediates the gene transcription and induces cell proliferation. Of state: In the absence of Wnt ligand, the of β-catenin is targeted by its phosphorylation and binds to the destruction complex (GSK-3/CK1/Axin) and APC results in the ubiquitination of β-catenin and subsequent proteasomal degradation. Scheme generated with BioRender.com.

5.3.1 Results and discussion

5.3.1.1 The impacts of AuNPs on the Wnt/β-catenin cell signalling pathway

Several protein expressions involved in the Wnt/β-catenin signalling cascade were analysed to investigate the AuNPs impact on MRC-5 and A549 cells. First, β-catenin protein expression was measured in both cell lines following incubation with Au10 and Au80 of different concentrations (16, 26, 36 and 41 µg/ml) for 24 hours. In MRC-5 cells, a significant reduction in β-catenin expression was noted only at a concentration of 41 µg/ml for both Au10 and Au80 (p-values < 0.0002 and < 0.002, respectively) (**Figure 5.25**). In case of A549 cells, the β-catenin intensity was substantially decreased among cells exposure to Au10 and Au80 at concentrations of 36 and 41 µg/ml (**Figure 5.26**). No size-dependent reduction in β-catenin intensity was noticed in either cell line.

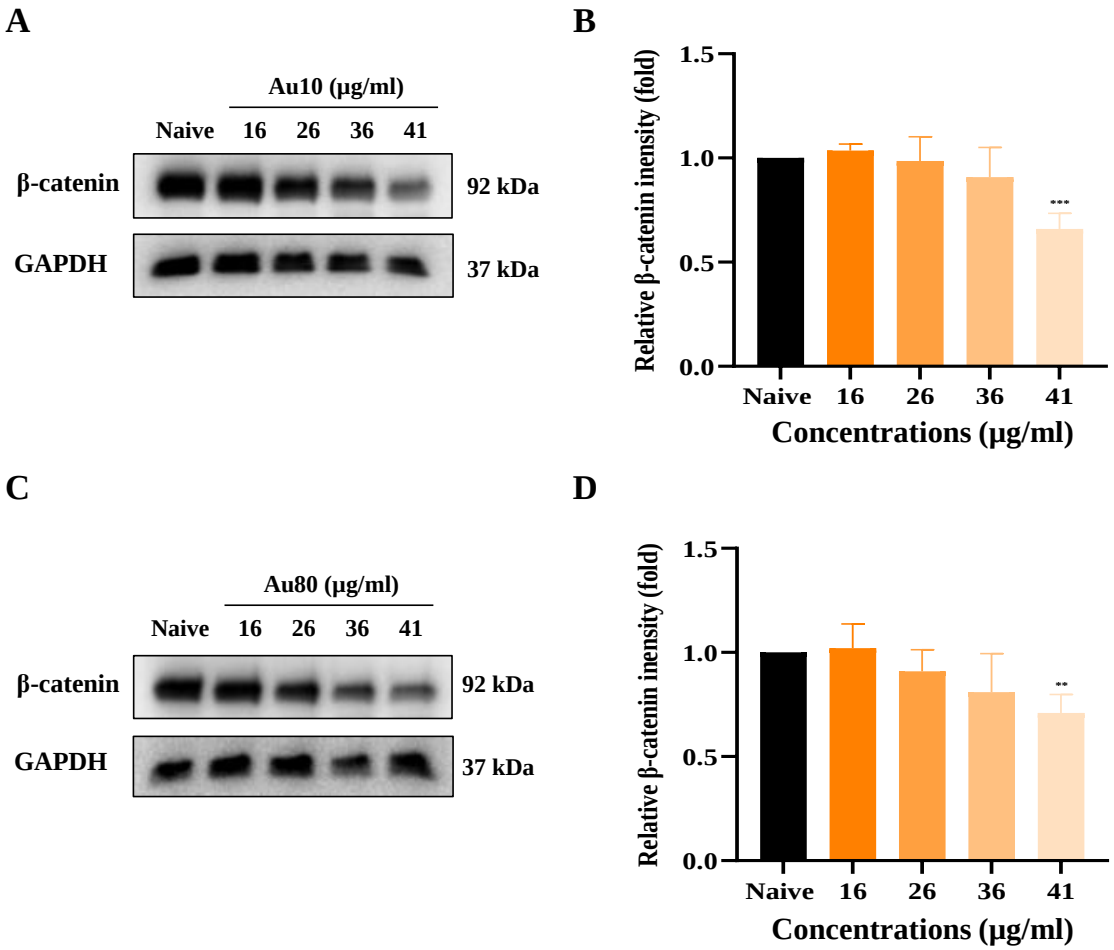


Figure 5.25. The protein expression analysis of β-catenin following MRC-5 cells exposure to Au10 and Au80 of different concentrations for 24 hours. The representative western blot showing the levels of β-catenin protein expression in MRC-5 cells treated with (**A**) Au10 and (**C**) Au80 at concentrations of 16, 26, 36 and 41 µg/ml for 24 hours. Naive represents the protein expression of untreated cells. Bar graphs represent the protein quantification of MRC-5 cells treated with (**B**) Au10 and (**D**) Au80. The protein expression was normalised to corresponding GAPDH (loading control). The protein level presented as a protein intensity ratio relative to naive (untreated group). The data expressed with fold unit, bars represent the mean ± SD (n=4). (**) $p < 0.002$ and (***) $p < 0.0002$ versus untreated group by ANOVA test.

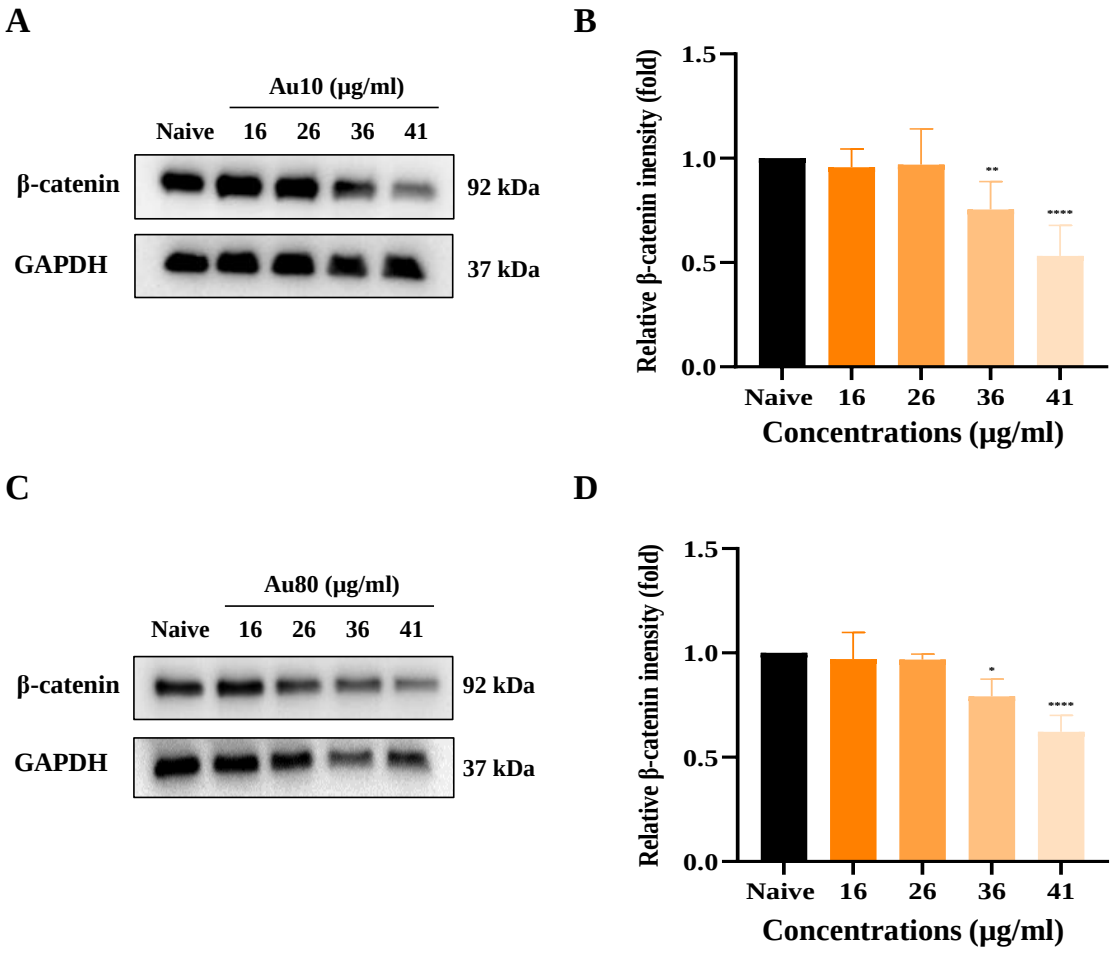


Figure 5.26. The protein expression analysis of β-catenin following A549 cells exposure to Au10 and Au80 of different concentrations for 24 hours. The representative western blot showing the levels of β-catenin protein expression in A549 cells treated with (**A**) Au10 and (**C**) Au80 at concentrations of 16, 26, 36 and 41 µg/ml for 24 hours. Naive represents the protein expression of untreated cells. Bar graphs represent the protein quantification of A549 cells treated with (**B**) Au10 and (**D**) Au80. The protein expression was normalised to corresponding GAPDH (loading control). The protein level presented as a protein intensity ratio relative to naive (untreated group). The data expressed with fold unit, bars represent the mean ± SD (n=4). (*) $p < 0.05$; (**) $p < 0.002$ and (****) $p < 0.0001$ versus untreated group by ANOVA test.

GSK-3β is another key protein in the Wnt/β-catenin signalling pathway which is analysed in this work. GSK-3β protein is part of the destruction complex that promotes β-catenin targeting for degradation. A significant downregulation was observed in GSK-3β protein expression in both MRC-5 and A549 cells exposed to high concentrations of Au10 and Au80 (36 and 41 µg/ml) (**Figure 5.27 and Figure 5.28**). Au10 demonstrated more pronounced reduction in GSK-3β than Au80 in both cell lines.

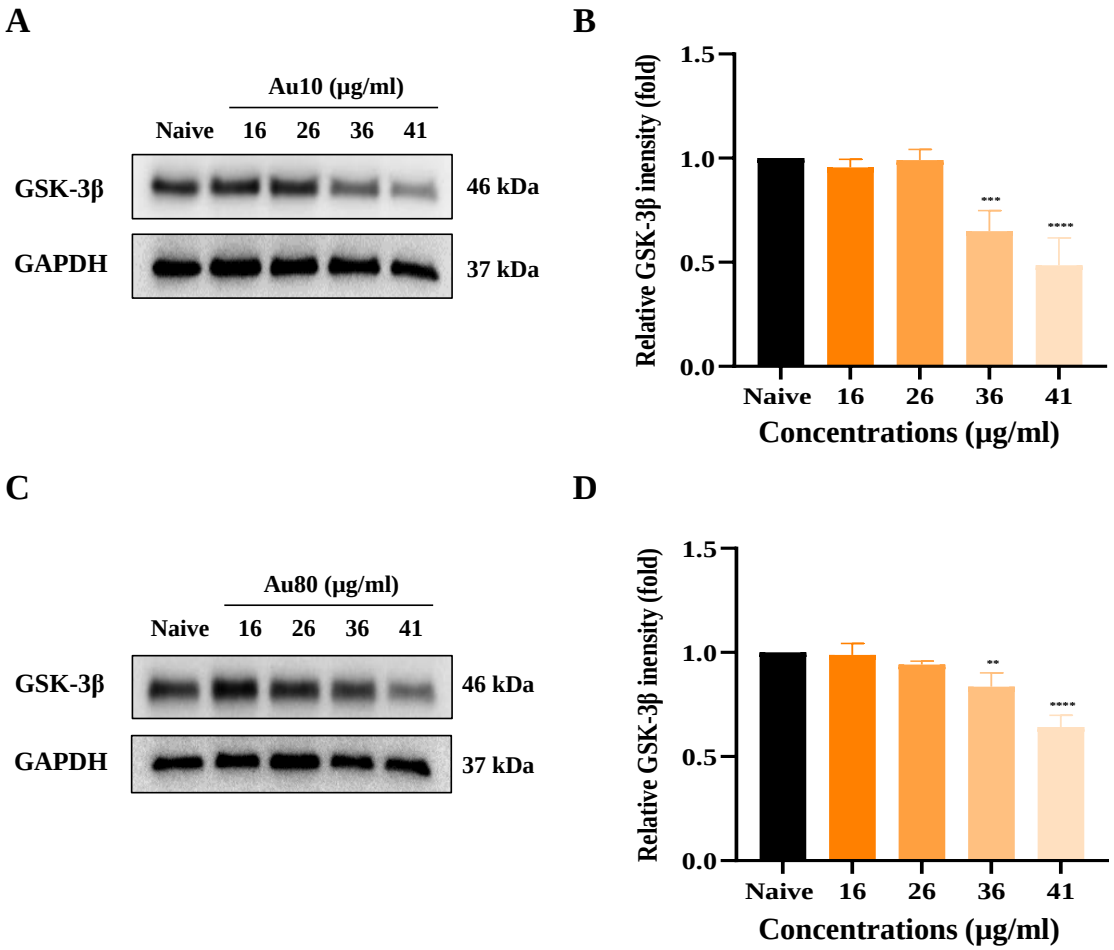


Figure 5.27. The protein expression analysis of GSK-3β following MRC-5 cells exposure to Au10 and Au80 of different concentrations for 24 hours. The representative western blot showing the levels of GSK-3β protein expression in MRC-5 cells treated with (**A**) Au10 and (**C**) Au80 at concentrations of 16, 26, 36 and 41 µg/ml for 24 hours. Naive represents the protein expression of untreated cells. Bar graphs represent the protein quantification of MRC-5 cells treated with (**B**) Au10 and (**D**) Au80. The protein expression was normalised to corresponding GAPDH (loading control). The protein level presented as a protein intensity ratio relative to naive (untreated group). The data expressed with fold unit, bars represent the mean ± SD (n=4). (**) $p < 0.002$; (***) $p < 0.0002$ and (****) $p < 0.0001$ versus untreated group by ANOVA test.

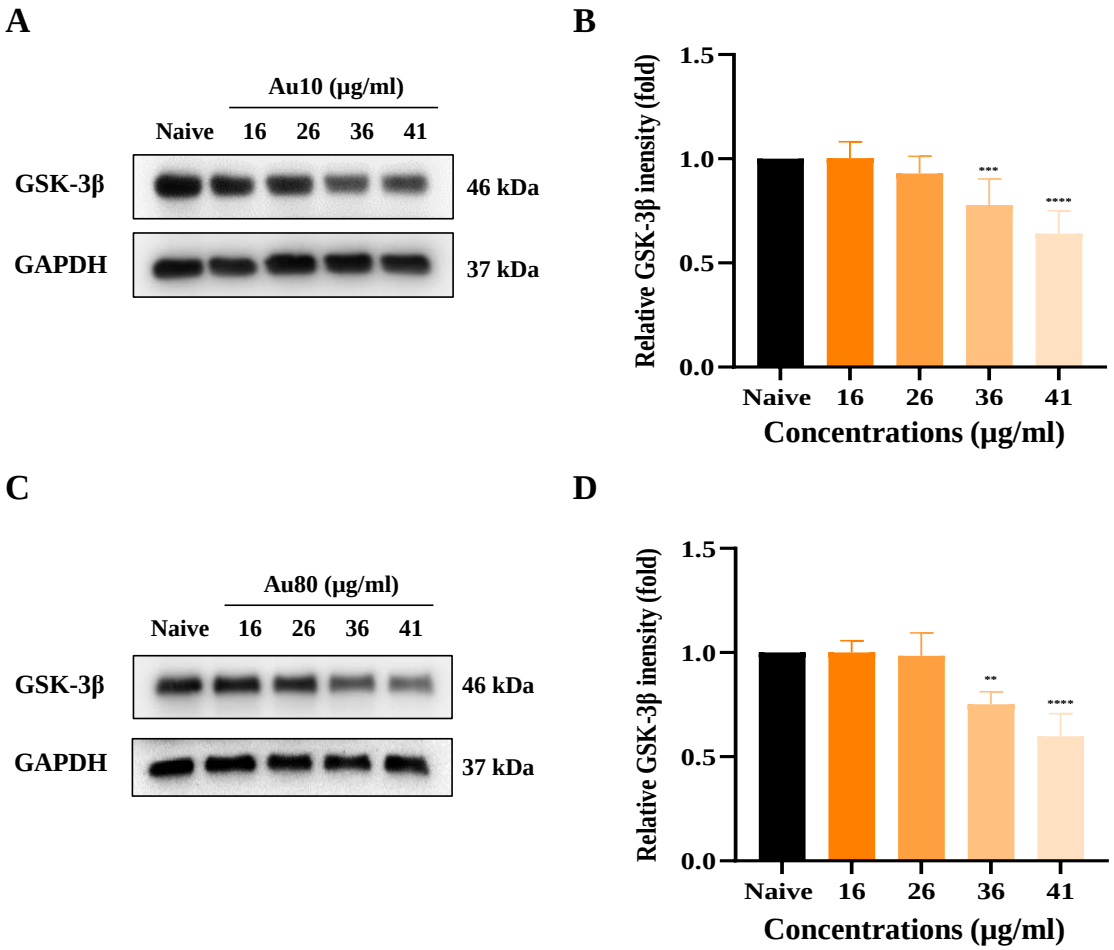


Figure 5.28. The protein expression analysis of GSK-3β following A549 cells exposure to Au10 and Au80 of different concentrations for 24 hours. The representative western blot showing the levels of GSK-3β protein expression in A549 cells treated with (**A**) Au10 and (**C**) Au80 at concentrations of 16, 26, 36 and 41 µg/ml for 24 hours. Naive represents the protein expression of untreated cells. Bar graphs represent the protein quantification of A549 cells treated with (**B**) Au10 and (**D**) Au80. The protein expression was normalised to corresponding GAPDH (loading control). The protein level presented as a protein intensity ratio relative to naive (untreated group). The data expressed with fold unit, bars represent the mean ± SD (n=4). (**) $p < 0.002$; (***) $p < 0.0002$ and (****) $p < 0.0001$ versus untreated group by ANOVA test.

Based on the this finding, it was of interest to study the phosphorylated form of GSK-3β (phospho-GSK-3β) at Ser9 residue. GSK-3β is a downstream target of AKT and is negatively regulated by AKT pathway. AKT phosphorylates and inactivates GSK-3β, which in turn promote cell proliferation and metabolism (Manning and Toker, 2017). Phospho-GSK-3β (Ser9) is the inactive form of GSK-3β found when Wnt signalling is activated. In MRC-5, an increase in the phospho-GSK-3β was detected with increasing concentrations of Au10 and

Au80 (**Figure 5.29**). Similar effects were observed with A549 cells, in which the phospho-GSK-3β intensity was significantly increased with varying concentrations of Au10 and Au80 except for 16 µg/ml of Au80, no alteration in phospho-GSK-3β was noticed (**Figure 5.30**). Thereof, AuNPs showed a potential to supress the GSK-3β activity in both lung cell lines.

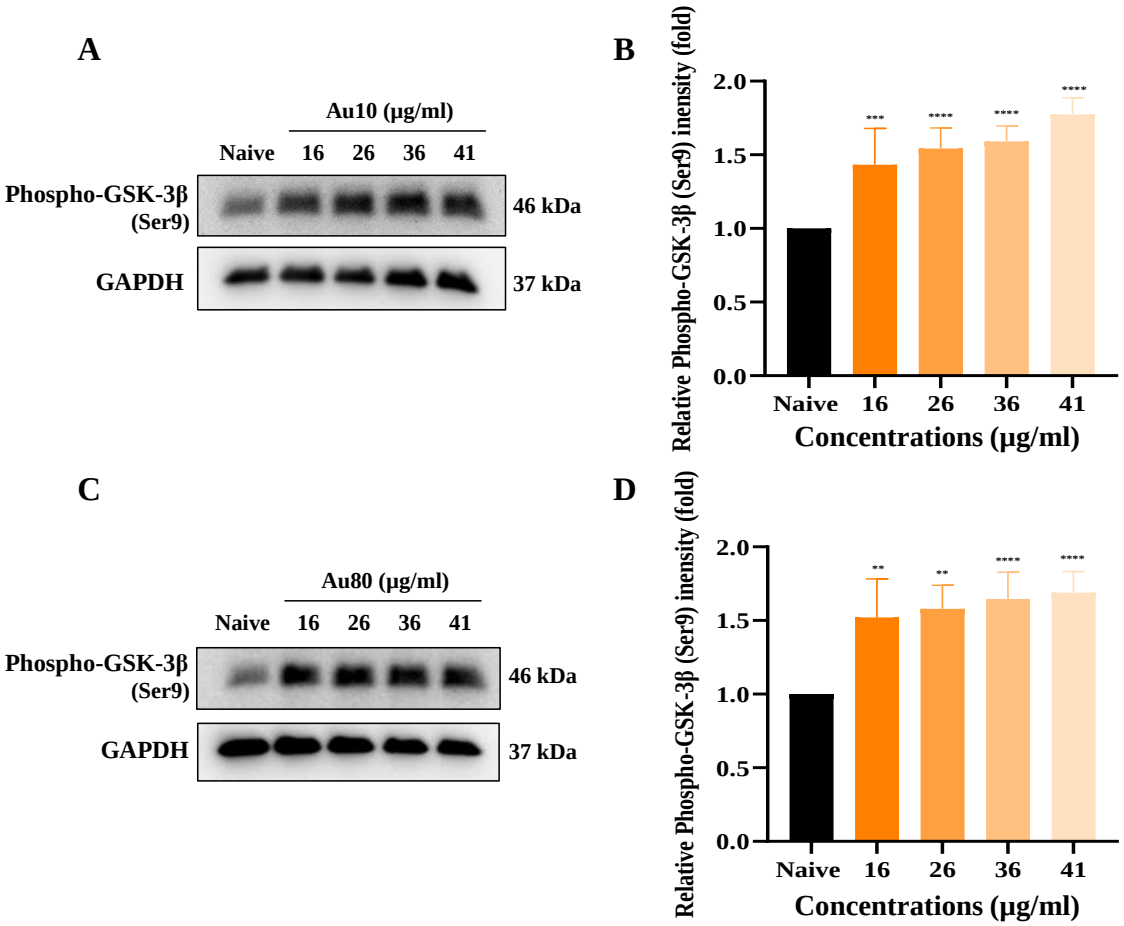


Figure 5.29. The protein expression analysis of phospho-GSK-3β (Ser9) following MRC-5 cells exposure to Au10 and Au80 of different concentrations for 24 hours. The representative western blot showing the levels of phospho-GSK-3β (Ser9) protein expression in MRC-5 cells treated with (**A**) Au10 and (**C**) Au80 at concentrations of 16, 26, 36 and 41 µg/ml for 24 hours. Naive represents the protein expression of untreated cells. Bar graphs represent the protein quantification of MRC-5 cells treated with (**B**) Au10 and (**D**) Au80. The protein expression was normalised to corresponding GAPDH (loading control). The protein level presented as a protein intensity ratio relative to naive (untreated group). The data expressed with fold unit, bars represent the mean ± SD (n=4). (**) $p < 0.002$; (***) $p < 0.0002$ and (****) $p < 0.0001$ versus untreated group by ANOVA test.

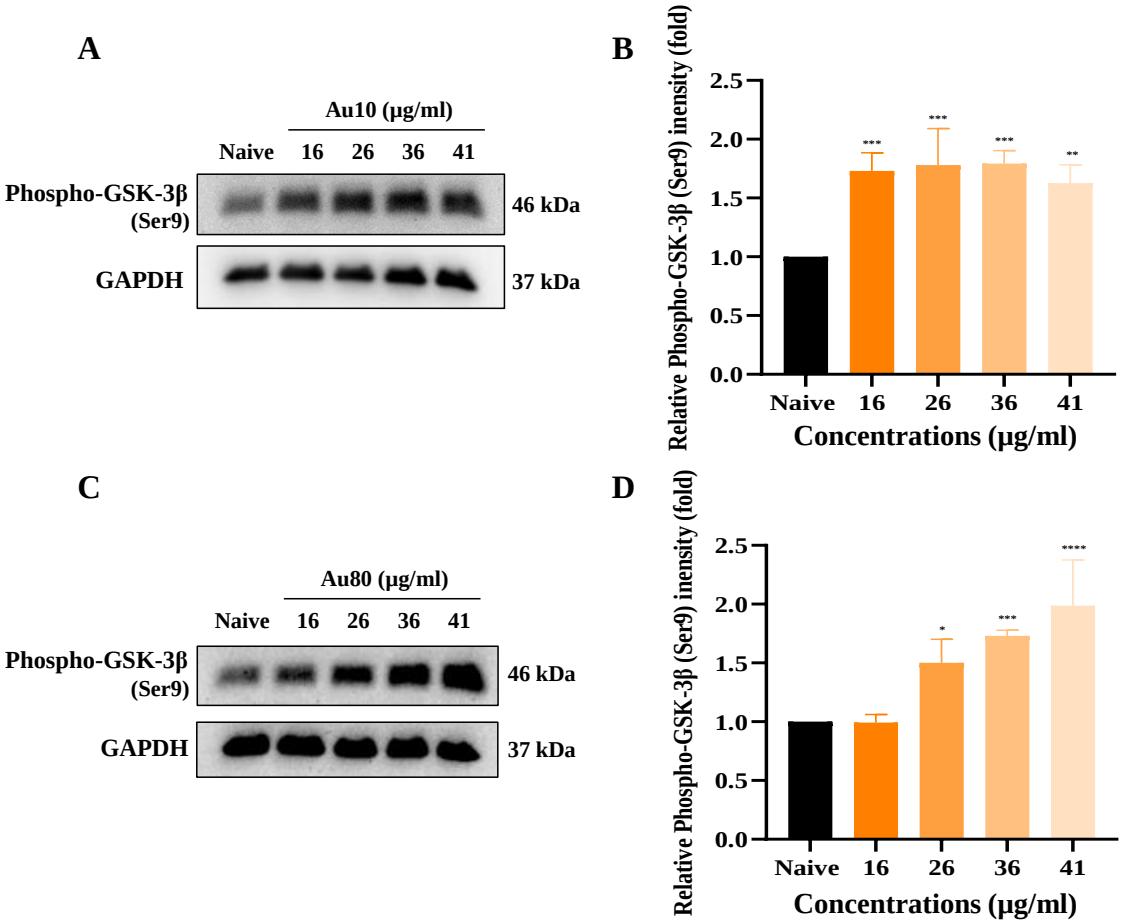


Figure 5.30. The protein expression analysis of phospho-GSK-3β (Ser9) following A549 cells exposure to Au10 and Au80 of different concentrations for 24 hours. The representative western blot showing the levels of phospho-GSK-3β (Ser9) protein expression in A549 cells treated with (**A**) Au10 and (**C**) Au80 at concentrations of 16, 26, 36 and 41 µg/ml for 24 hours. Naive represents the protein expression of untreated cells. Bar graphs represent the protein quantification of A549 cells treated with (**B**) Au10 and (**D**) Au80. The protein expression was normalised to corresponding GAPDH (loading control). The protein level presented as a protein intensity ratio relative to naive (untreated group). The data expressed with fold unit, bars represent the mean ± SD (n=4). (*) $p < 0.05$; (**) $p < 0.002$; (***) $p < 0.0002$ and (****) $p < 0.0001$ versus untreated group by ANOVA test.

β-catenin which is the core component mediated Wnt/β-catenin pathway activity which associated with cancer progression, recurrence and chemoresistance (Krishnamurthy and Kurzrock, 2018). Therefore, β-catenin inhibitor is a promising approach for Wnt/β-catenin pathway therapeutic targeting. In this work, AuNPs showed to interfere with the signalling transduction of the Wnt/β-catenin pathway. A decrease in β-catenin activity was observed following cellular exposure to Au10 and Au80. However, no size-dependent effect was reported in the reduction of β-catenin. A similar finding was detected in human breast adenocarcinoma following 24 hours of exposure to AuNPs resulted in induction of oxidative stress and cell death by attenuating Wnt/β-catenin pathway activity and MAPK signalling pathway activation (Surapaneni et al., 2018).

GSK-3β is a negative regulator of Wnt/β-catenin pathway and it shows much interest as a potential therapeutic target for several types of cancers (Sokolosky et al., 2014, Duda et al., 2020). In the current work, GSK-3β level was significantly inhibited and showed size-dependent effect following cellular exposure to Au10 and Au80. Also, upregulation of the inactive form of GSK-3β (phosphorylated GSK-3β) was reported. The dysregulation of both β-catenin and GSK-3β levels, the two essential components in Wnt/β-catenin pathway may result in AuNPs inducing toxicity. In agreement with the current findings, Surapaneni et al. (2018), reported inhibition of β-catenin along with triggering of GSK-3β phosphorylation in human breast adenocarcinoma. The latter study elucidated that the cysteamine-capped AuNPs (positively charged) showed significant alterations in the Wnt/β-catenin pathway compared to citrate-capped AuNPs (negatively charged). Regardless that the explanation of AuNPs coating-dependent effect was not justified in the study, however, this can highlight that AuNPs properties may induce distinct effects in the signalling pathways. The next subsection, presents and discusses the impact of AgNP on Wnt/β-catenin cell signalling pathway.

5.3.1.2 The impacts of AgNPs on the Wnt/β-catenin cell signalling pathway

The impact of AgNPs on the Wnt/β-catenin signalling transduction was investigated. First, the β-catenin protein expression was investigated following MRC-5 cells exposure to Ag10 and Ag80 for 24 hours. Downregulation of β-catenin level was observed in particular at high concentration (10 µg/ml) of Ag10 and Ag80 (**Figure 5.31**). The same was observed with A549 cells, suppression of β-catenin expression at highest concentration of Ag10 and Ag80 was reported (**Figure 5.32**). Size-dependent effects were noticed in which the smaller Ag10 demonstrated a higher reduction in the protein level than Ag80 in both cell lines.

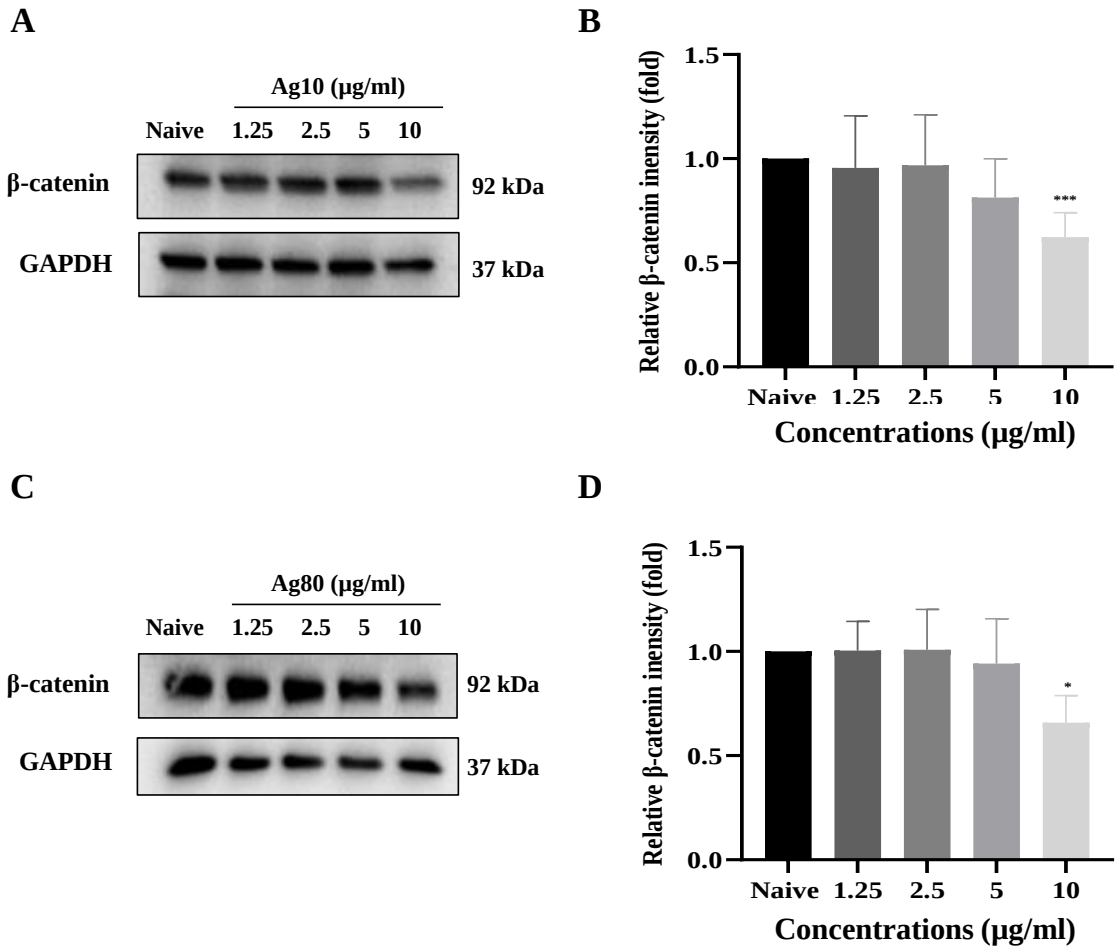


Figure 5.31. The protein expression analysis of β-catenin following MRC-5 cells exposure to Ag10 and Ag80 of different concentrations for 24 hours. The representative western blot showing the levels of β-catenin protein expression in MRC-5 cells treated with (**A**) Ag10 and (**C**) Ag80 at concentrations of 1.25, 2.5, 5 and 10 µg/ml for 24 hours. Naive represents the protein expression of untreated cells. Bar graphs represent the protein quantification of MRC-5 cells treated with (**B**) Ag10 and (**D**) Ag80. The protein expression was normalised to corresponding GAPDH (loading control). The protein level presented as a protein intensity ratio relative to naive (untreated group). The data expressed with fold unit, bars represent the mean ± SD (n=4). (*) $p < 0.05$ and (***) $p < 0.0002$ versus untreated group by ANOVA test.

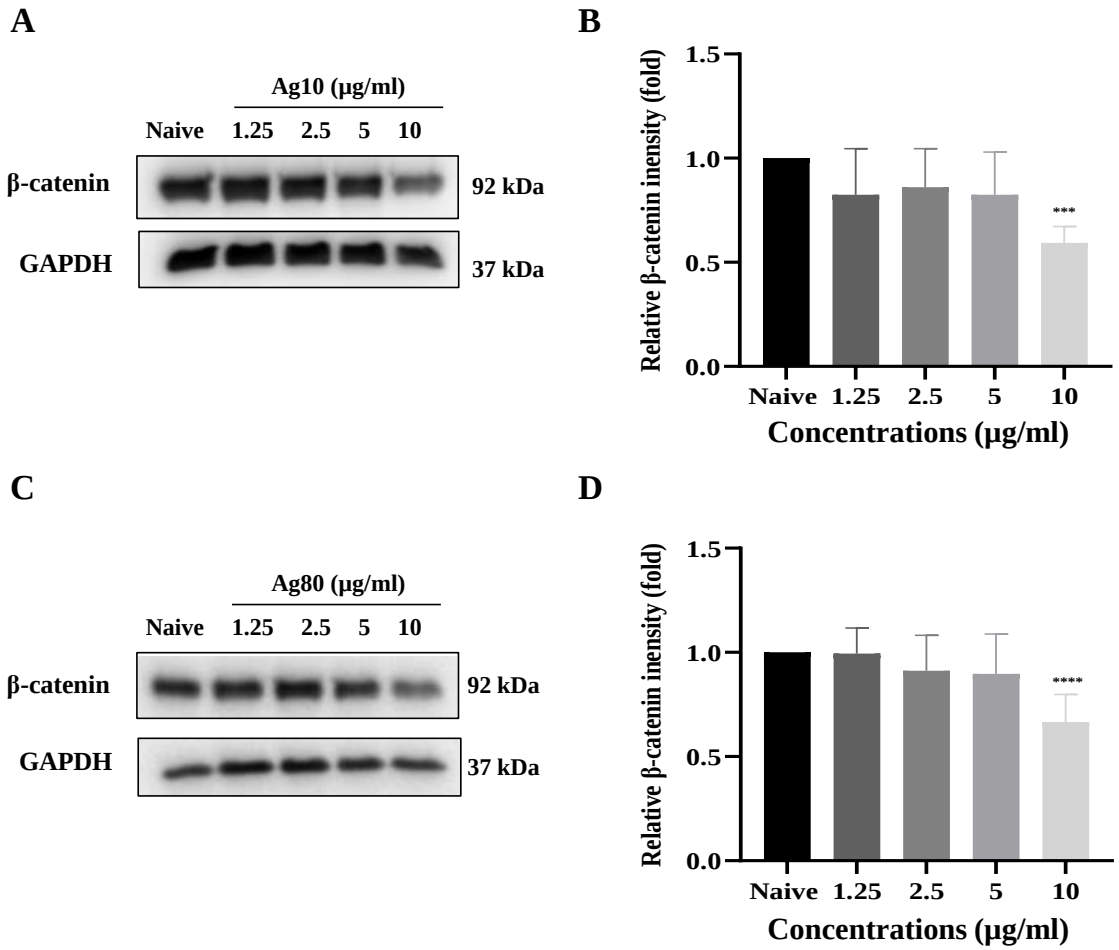


Figure 5.32. The protein expression analysis of β-catenin following A549 cells exposure to Ag10 and Ag80 of different concentrations for 24 hours. The representative western blot showing the levels of β-catenin protein expression in A549 cells treated with (**A**) Ag10 and (**C**) Ag80 at concentrations of 1.25, 2.5, 5 and 10 µg/ml for 24 hours. Naive represents the protein expression of untreated cells. Bar graphs represent the protein quantification of A549 cells treated with (**B**) Ag10 and (**D**) Ag80. The protein expression was normalised to corresponding GAPDH (loading control). The protein level presented as a protein intensity ratio relative to naive (untreated group). The data expressed with fold unit, bars represent the mean ± SD (n=4). (***) $p < 0.0002$ and (****) $p < 0.0001$ versus untreated group by ANOVA test.

Next, GSK-3β, another key component in Wnt/β-catenin signalling, was analysed. In MRC-5 cells, inhibition in GSK-3β level was detected at highest concentration of Ag10 and Ag80 (**Figure 5.33**). Similar identification was observed in A549 cells. A concentration-dependent reduction was detected following exposure to Ag10 (**Figure 5.34-A**), but a significant decrease in the protein level was reported only at high concentrations for cells treated with

Ag80 **(Figure 5.34-C**). Size-dependent inhibition of GSK-3β expression was observed with both cell lines.

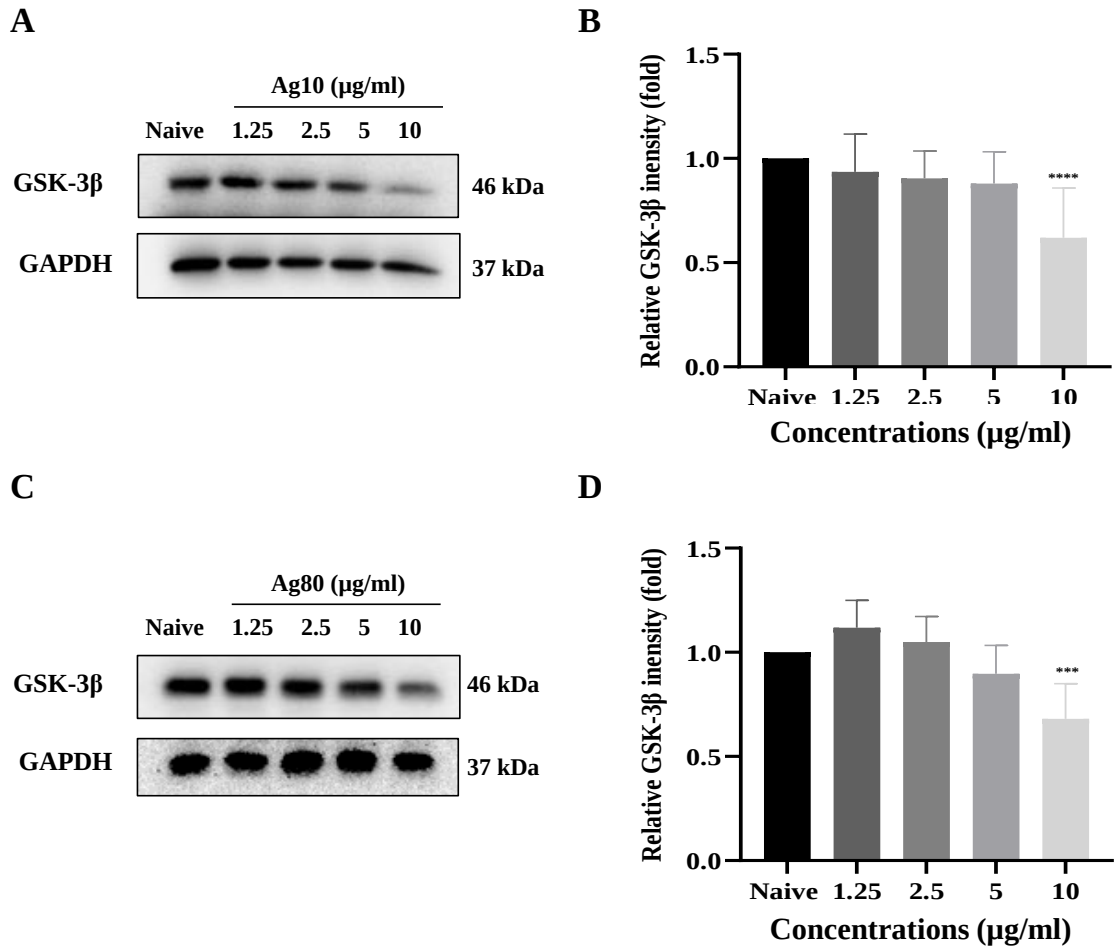


Figure 5.33. The protein expression analysis of GSK-3β following MRC-5 cells exposure to Ag10 and Ag80 of different concentrations for 24 hours. The representative western blot showing the levels of GSK-3β protein expression in MRC-5 cells treated with (**A**) Ag10 and (**C**) Ag80 at concentrations of 1.25, 2.5, 5 and 10 µg/ml for 24 hours. Naive represents the protein expression of untreated cells. Bar graphs represent the protein quantification of MRC-5 cells treated with (**B**) Ag10 and (**D**) Ag80. The protein expression was normalised to corresponding GAPDH (loading control). The protein level presented as a protein intensity ratio relative to naive (untreated group). The data expressed with fold unit, bars represent the mean ± SD (n=4). (***) $p < 0.0002$ and (****) $p < 0.0001$ versus untreated group by ANOVA test.

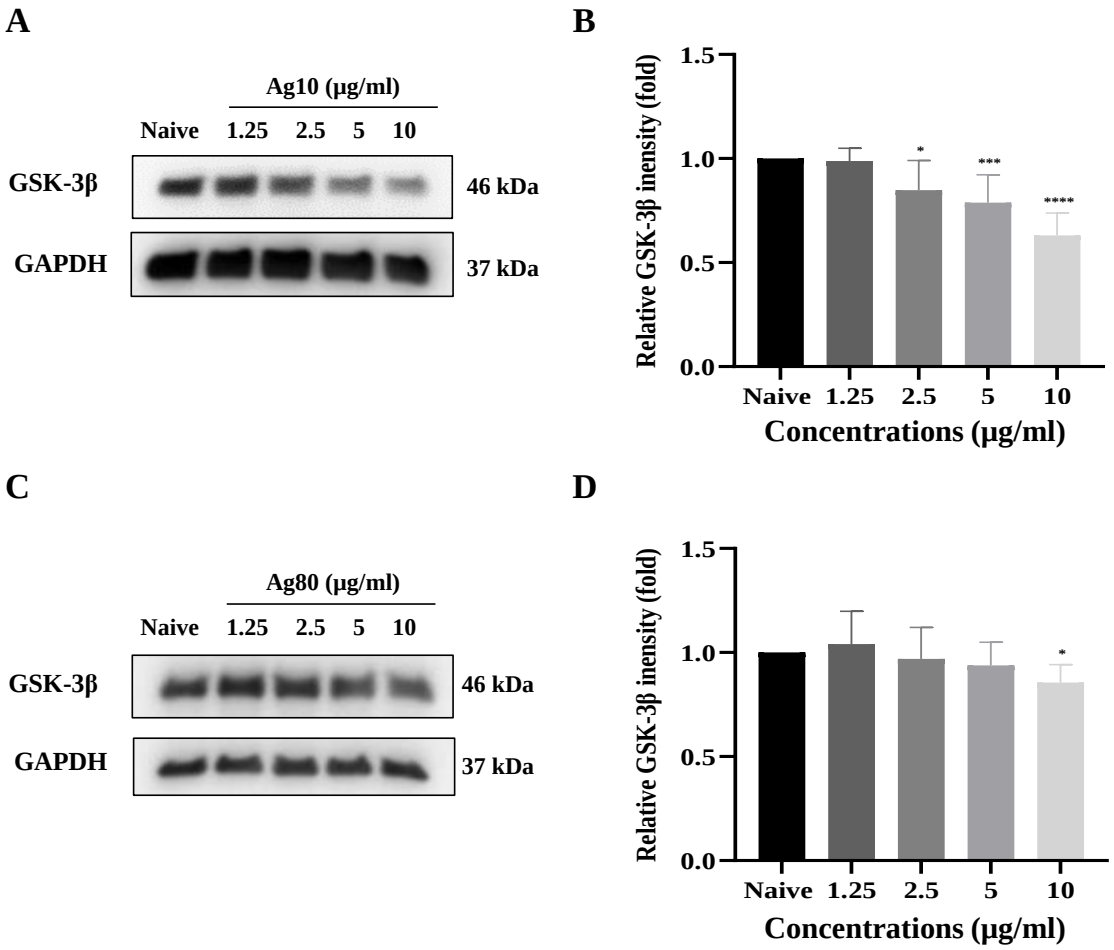


Figure 5.34. The protein expression analysis of GSK-3β following A549 cells exposure to Ag10 and Ag80 of different concentrations for 24 hours. The representative western blot showing the levels of GSK-3β protein expression in A549 cells treated with (**A**) Ag10 and (**C**) Ag80 at concentrations of 1.25, 2.5, 5 and 10 µg/ml for 24 hours. Naive represents the protein expression of untreated cells. Bar graphs represent the protein quantification of A549 cells treated with (**B**) Ag10 and (**D**) Ag80. The protein expression was normalised to corresponding GAPDH (loading control). The protein level presented as a protein intensity ratio relative to naive (untreated group). The data expressed with fold unit, bars represent the mean ± SD (n=4). (*) $p < 0.05$; (***) $p < 0.0002$ and (****) $p < 0.0001$ versus untreated group by ANOVA test.

5.3.1.2.1 The effects of AgNPs on β-catenin and GSK-3β proteins phosphorylation

The following step was to investigate the phosphorylation residues of both β-catenin and GSK-3β. β-catenin phosphorylation by CK1 at Ser45 and by GSK-3β at Ser33, 37 and Ther41 residues lead to β-catenin being tagged for proteasomal degradation (Verheyen and Gottardi, 2010). AKT and protein kinase A (PKA) regulate the phosphorylation of β-catenin at Ser552 and Ser675 residues, respectively, which results in high β-catenin translocation into the nucleus (Daugherty and Gottardi, 2007).

The MRC-5 cells treated with Ag10 illustrated a concentration-dependent decrease in the phosphorylated β-catenin (phospho-β-catenin) at Thr41/Ser45 residue, indicating a reduction in the activity of GSK-3β and CK1, which are responsible for the phosphorylation of β-catenin at Thr41/Ser45 sites (**Figure 5.35 A and B**). As mentioned previously, the GSK-3β phosphorylates the β-catenin at (Ser33/37/Thr41) residues. Herein, the non-phospho-β-catenin (Ser33/37/Thr41) which is the active form of β-catenin was investigated. As shown in (**Figure 5.35 C and D**), no changes in the active β-catenin protein expression was observed which indicated no phosphorylation in β-catenin mediated by GSK-3β took place.

The phosphorylation of β-catenin at Ser675 and Ser552 residues leads to β-catenin translocation into the nucleus. The MRC-5 cells treated with Ag10 demonstrated a reduction in protein expression in particular at a high concentration in both phospho-β-catenin (Ser675 and Ser552) residues (**Figure 5.36**). A reduction of phosphorylation can be related to the suppression of AKT activity by AgNPs, as previously evidenced.

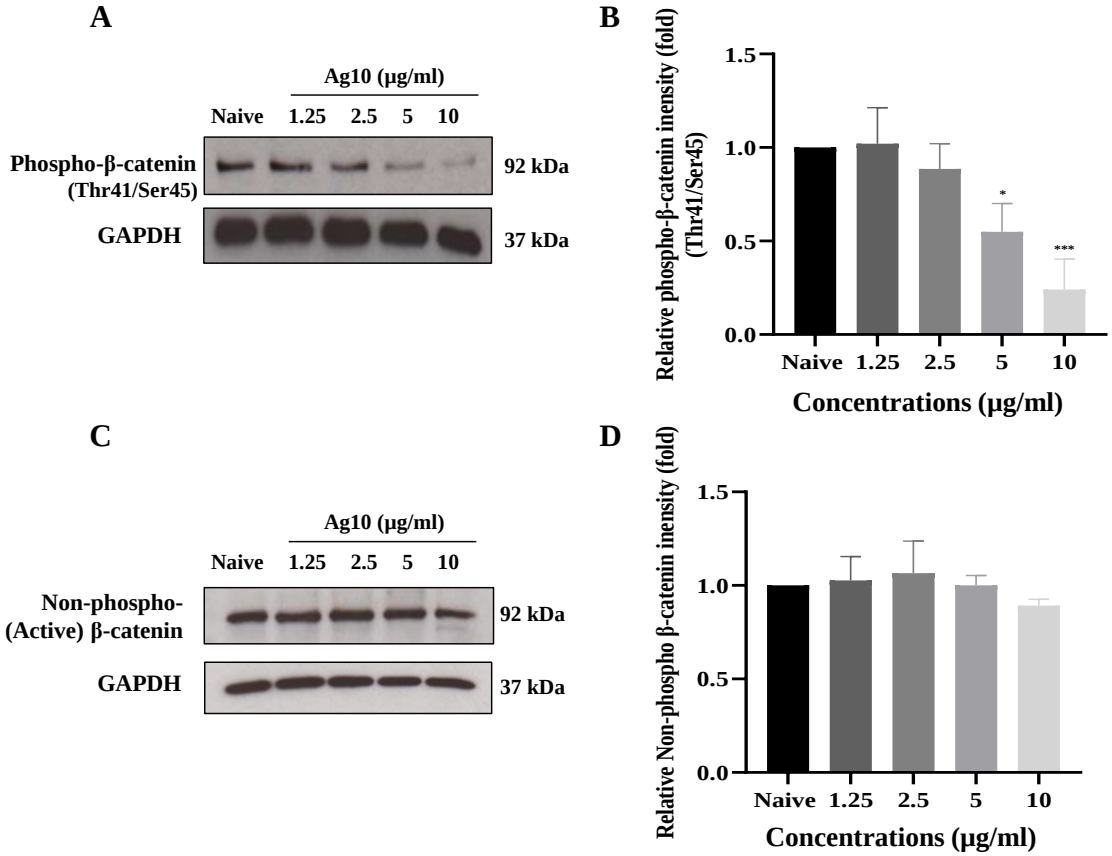


Figure 5.35. The protein expression analysis of phospho-β-catenin (Thr41/Ser45) and non-phospho- (Active) β-catenin (Ser33/37/Thr41) following MRC-5 cells exposure to Ag10 of different concentrations for 24 hours. The representative western blot showing the levels of (**A**) phospho-β-catenin (Thr41/Ser45) and (**C**) non-phospho- (Active) β-catenin (Ser33/37/Thr41) protein expressions in MRC-5 cells treated with Ag10 at concentrations of 1.25, 2.5, 5 and 10 µg/ml for 24 hours. Naive represents the protein expression of untreated cells. Bar graphs represent the protein quantification of (**B**) phospho-β-catenin (Thr41/Ser45) and (**D**) non-phospho- (Active) β-catenin (Ser33/37/Thr41). The protein expression was normalised to corresponding GAPDH (loading control). The protein level presented as a protein intensity ratio relative to naive (untreated group). The data expressed with fold unit, bars represent the mean ± SD (n=3). (*) $p < 0.05$ and (***) $p < 0.0002$ versus untreated group by ANOVA test.

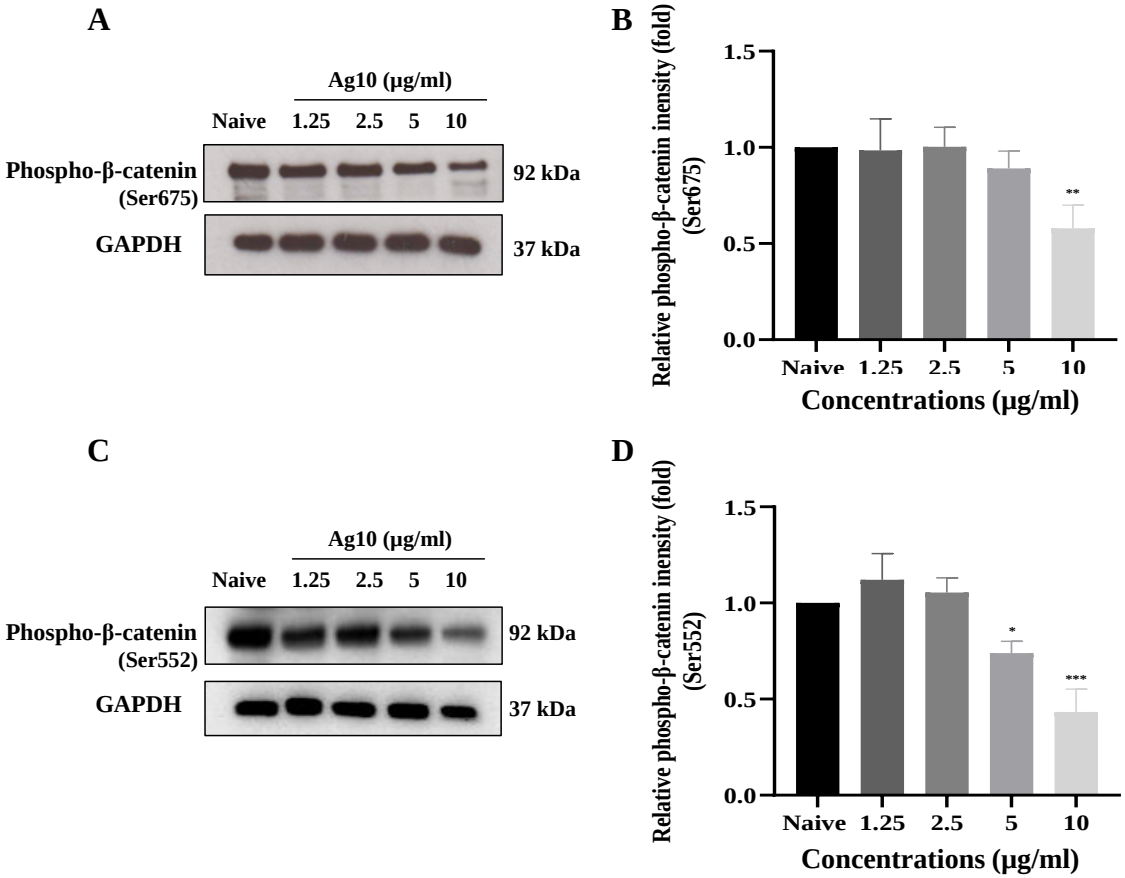


Figure 5.36. The protein expression analysis of phospho-β-catenin (Ser675) and phospho-β-catenin (Ser552) following MRC-5 cells exposure to Ag10 of different concentrations for 24 hours. The representative western blot showing the levels of (**A**) phospho-β-catenin (Ser675) and (**C**) phospho-β-catenin (Ser552) protein expressions in MRC-5 cells treated with Ag10 at concentrations of 1.25, 2.5, 5 and 10 µg/ml for 24 hours. Naive represents the protein expression of untreated cells. Bar graphs represent the protein quantification of (**B**) phospho-β-catenin (Ser675) and (**D**) phospho-β-catenin (Ser552). The protein expression was normalised to corresponding GAPDH (loading control). The protein level presented as a protein intensity ratio relative to naive (untreated group). The data expressed with fold unit, bars represent the mean ± SD (n=3). (*) $p < 0.05$; (**) $p < 0.002$ and (***) $p < 0.0002$ versus untreated group by ANOVA test.

Then, the phosphorylated GSk-3β at Ser9 residue was investigated. Both MRC-5 and A549 cells illustrated an upregulation of phospho-GSK-3β (Ser9) at different concentrations of Ag10 and Ag80 **(Figure 5.37 and Figure 5.38**). The phosphorylated form of GSK-3β is the inactive form that exists in the on-state of Wnt/β-catenin signalling.

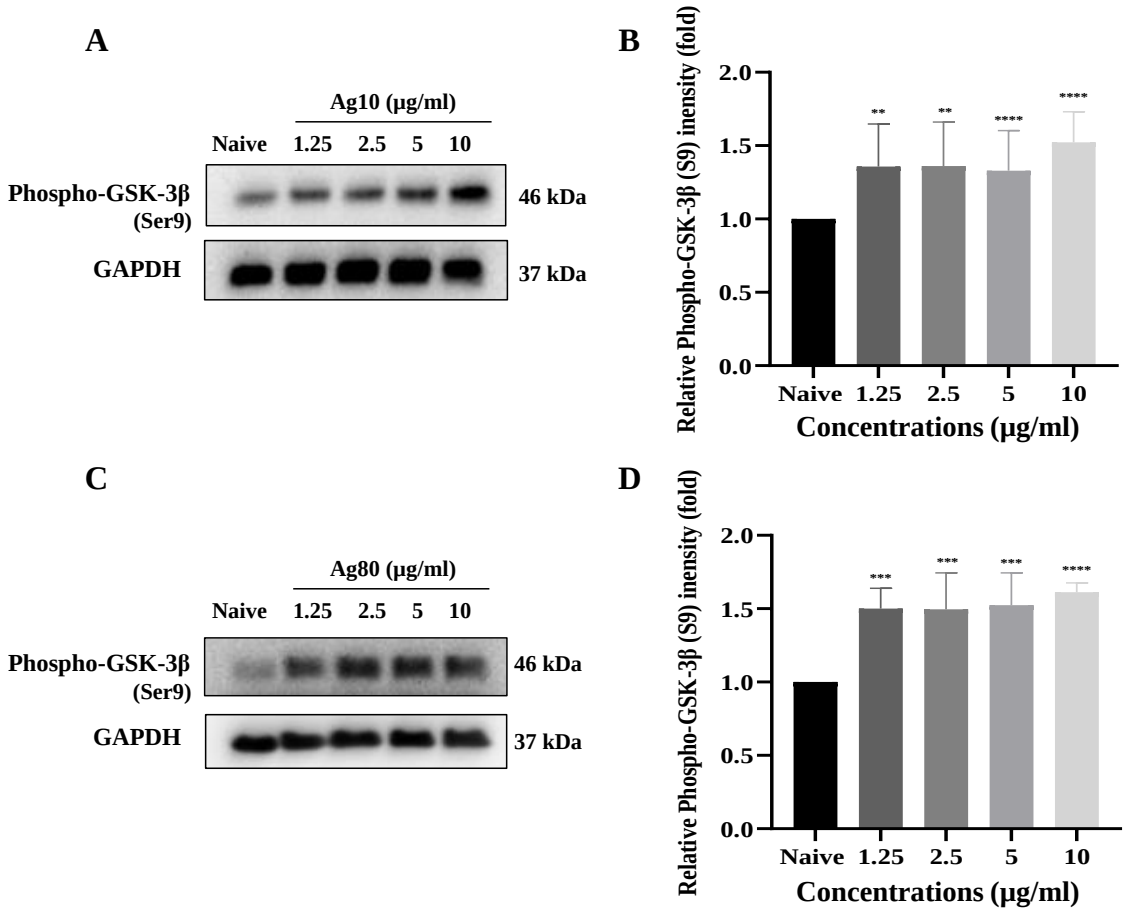


Figure 5.37. The protein expression analysis of phospho-GSK-3β (Ser9) following MRC-5 cells exposure to Ag10 and Ag80 of different concentrations for 24 hours. The representative western blot showing the levels of phospho-GSK-3β (Ser9) protein expression in MRC-5 cells treated with (**A**) Ag10 and (**C**) Ag80 at concentrations of 1.25, 2.5, 5 and 10 µg/ml for 24 hours. Naive represents the protein expression of untreated cells. Bar graphs represent the protein quantification of MRC-5 cells treated with (**B**) Ag10 and (**D**) Ag80. The protein expression was normalised to corresponding GAPDH (loading control). The protein level presented as a protein intensity ratio relative to naive (untreated group). The data expressed with fold unit, bars represent the mean ± SD (n=4). (**) $p < 0.002$; (***) $p < 0.0002$ and (****) $p < 0.0001$ versus untreated group by ANOVA test.

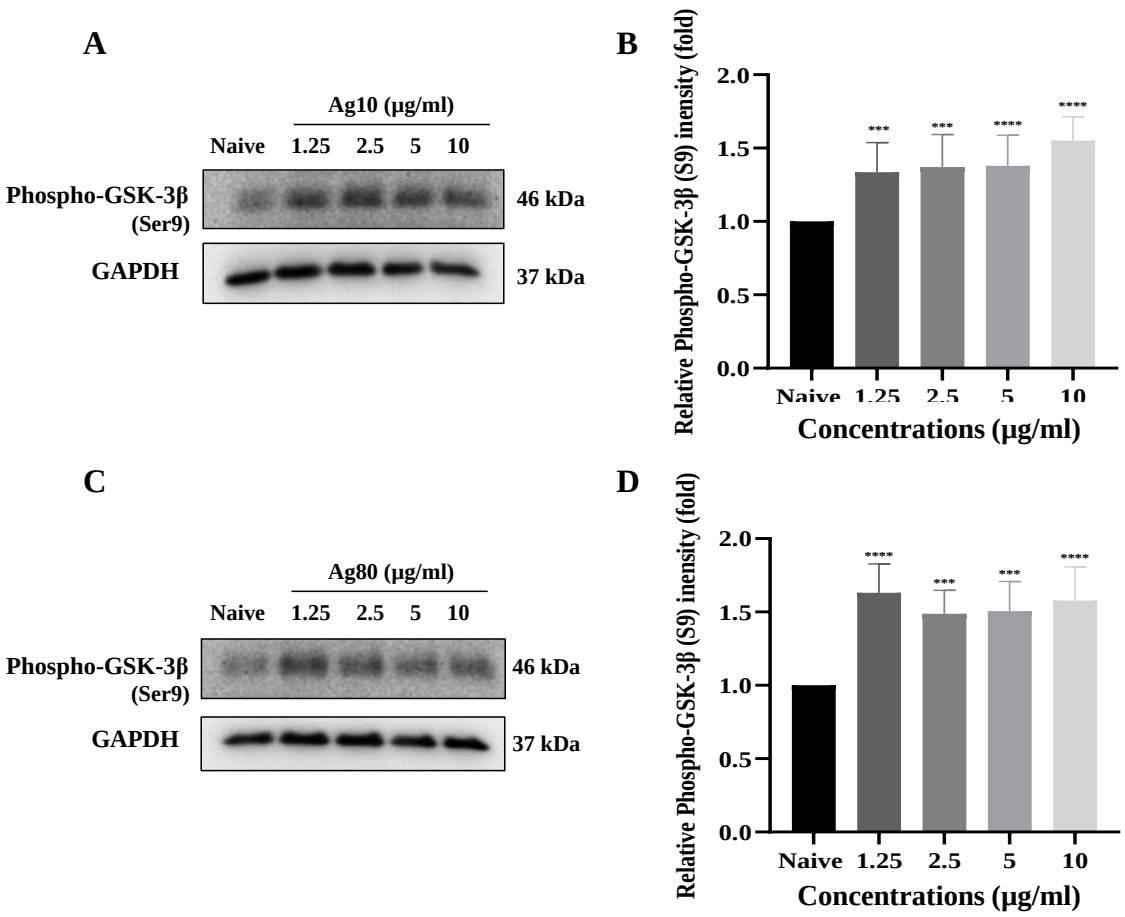


Figure 5.38. The protein expression analysis of phospho-GSK-3β (Ser9) following A549 cells exposure to Ag10 and Ag80 of different concentrations for 24 hours. The representative western blot showing the levels of phospho-GSK-3β (Ser9) protein expression in A549 cells treated with (**A**) Ag10 and (**C**) Ag80 at concentrations of 1.25, 2.5, 5 and 10 µg/ml for 24 hours. Naive represents the protein expression of untreated cells. Bar graphs represent the protein quantification of A549 cells treated with (**B**) Ag10 and (**D**) Ag80. The protein expression was normalised to corresponding GAPDH (loading control). The protein level presented as a protein intensity ratio relative to naive (untreated group). The data expressed with fold unit, bars represent the mean ± SD (n=4). (***) $p < 0.0002$ and (****) $p < 0.0001$ versus untreated group by ANOVA test.

5.3.1.2.2 The effects of AgNPs on the membrane proteins expression of Wnt/β-catenin signalling pathway

It was of interest to further study the impact of AgNPs on Wnt/β-catenin signalling by studying the upstream cascade. Several membrane proteins involved in Wnt/β-catenin signalling were assessed. Subsequent Wnt ligands binding to frizzled membrane receptors lead to bind to LRP5/6 co-receptors, forming an active complex that activates the downstream signalling transduction (Pai et al., 2017). Herein, the LRP6 protein level was analysed. MRC-5 cells demonstrated a concentration-dependent downregulation of LRP6 protein level in cells treated with Ag10 and Ag80. However, substantial suppression in LRP6 was observed at high concentrations (5 and 10 µg/ml) of Ag10 with 0.6- and 0.4-fold, reduction in the relative intensity ratio, respectively and at concentration of 10 µg/ml in Ag80 (0.6-fold) (**Figure 5.39**). The same disruption in LRP6 was reported in A549 cells, in which the smaller size Ag10 decreased the protein level at concentrations of 5 and 10 µg/ml ($p < 0.0001$) and in Ag80 at a concentration of 10 µg/ml ($p < 0.0002$) (**Figure 5.40**). Ag10 revealed more potent effect in attenuating LRP6 activity than Ag80 in both cell lines.

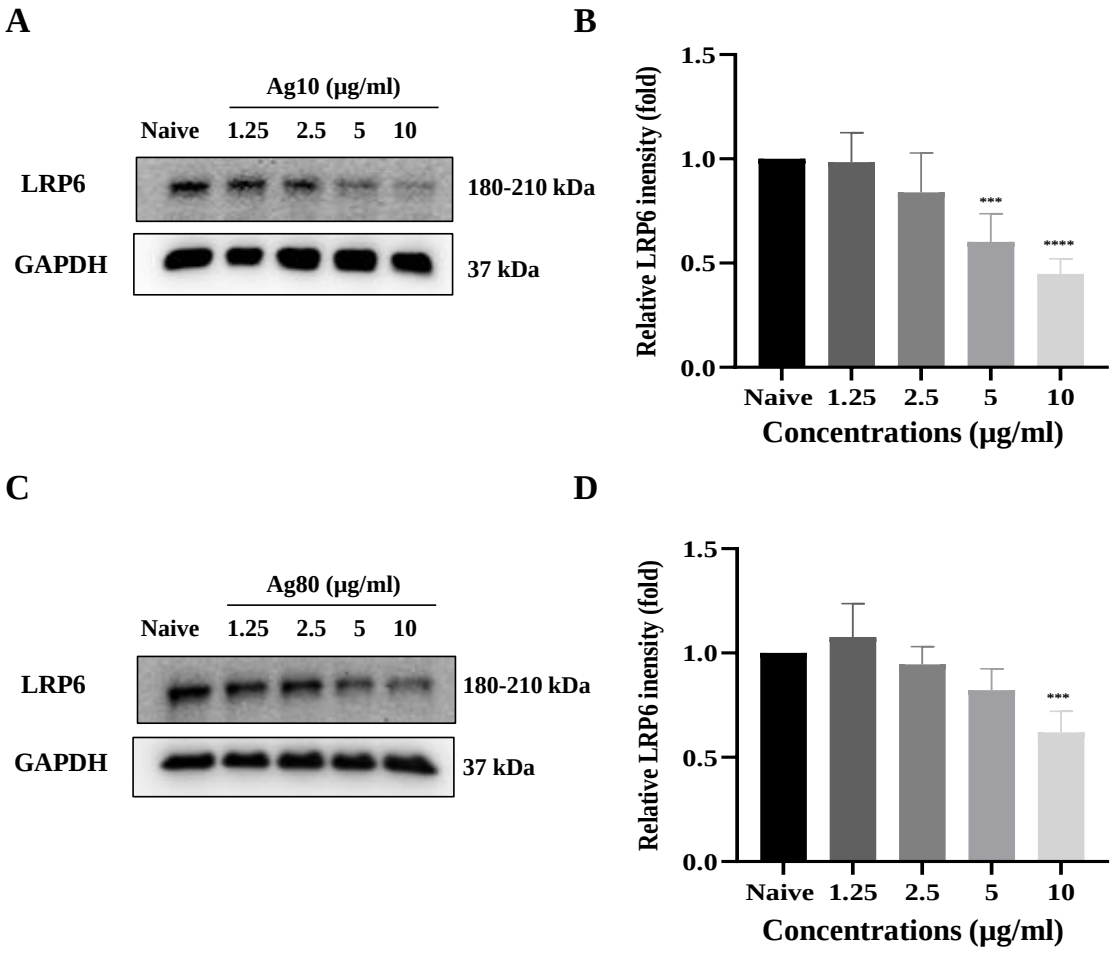


Figure 5.39. The protein expression analysis of LRP6 following MRC-5 cells exposure to Ag10 and Ag80 of different concentrations for 24 hours. The representative western blot showing the levels of LRP6 protein expression in MRC-5 cells treated with (**A**) Ag10 and (**C**) Ag80 at concentrations of 1.25, 2.5, 5 and 10 µg/ml for 24 hours. Naive represents the protein expression of untreated cells. Bar graphs represent the protein quantification of MRC-5 cells treated with (**B**) Ag10 and (**D**) Ag80. The protein expression was normalised to corresponding GAPDH (loading control). The protein level presented as a protein intensity ratio relative to naive (untreated group). The data expressed with fold unit, bars represent the mean ± SD (n=4). (***) $p < 0.0002$ and (****) $p < 0.0001$ versus untreated group by ANOVA test.

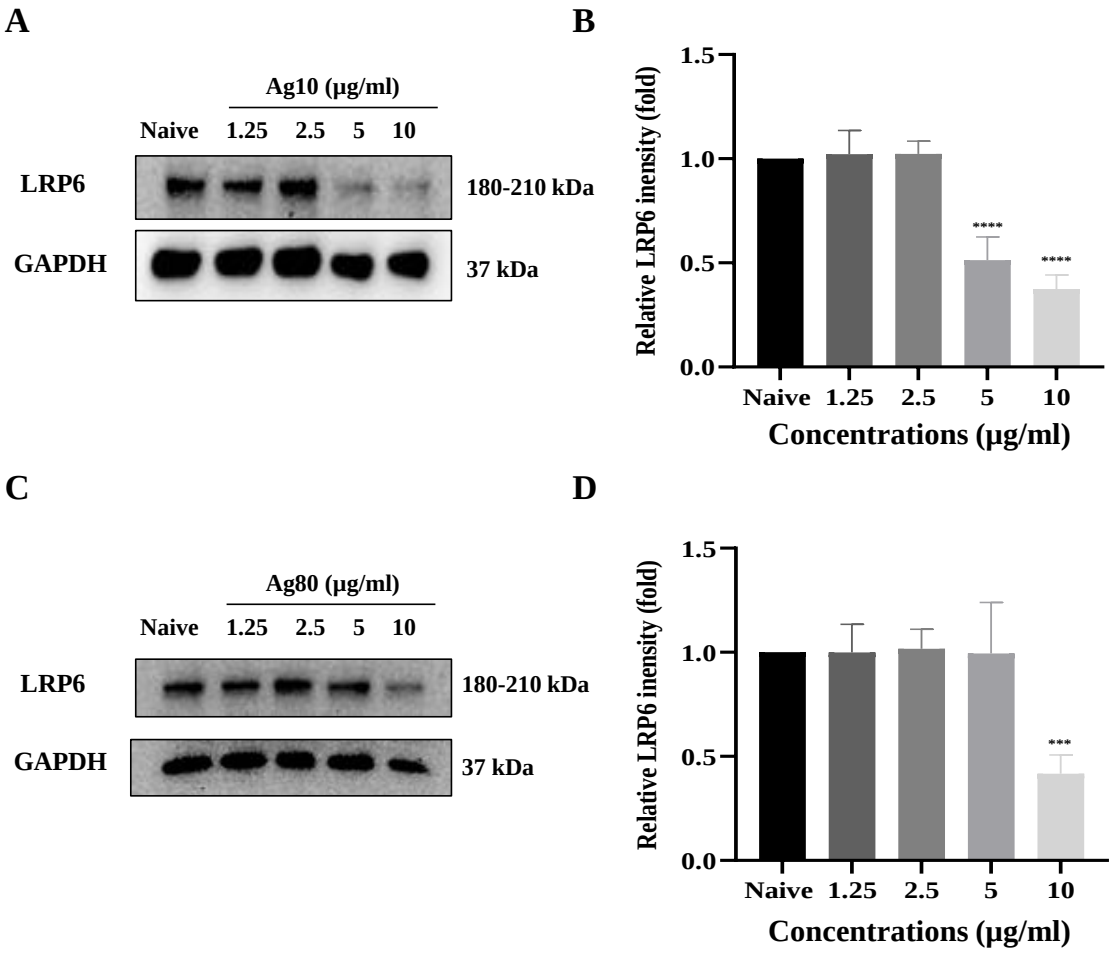


Figure 5.40. The protein expression analysis of LRP6 following A549 cells exposure to Ag10 and Ag80 of different concentrations for 24 hours. The representative western blot showing the levels of LRP6 protein expression in A549 cells treated with (**A**) Ag10 and (**C**) Ag80 at concentrations of 1.25, 2.5, 5 and 10 µg/ml for 24 hours. Naive represents the protein expression of untreated cells. Bar graphs represent the protein quantification of A549 cells treated with (**B**) Ag10 and (**D**) Ag80. The protein expression was normalised to corresponding GAPDH (loading control). The protein level presented as a protein intensity ratio relative to naive (untreated group). The data expressed with fold unit, bars represent the mean ± SD (n=4). (***) $p < 0.0002$ and (****) $p < 0.0001$ versus untreated group by ANOVA test.

Following that, the level of Dvl protein was investigated. The role of Dvl is to transduce the signal to downstream components when the Dvl is activated by binding to the frizzled/LRP5/6 complex in active Wnt signalling (Macdonald et al., 2009). A concentration-dependent reduction was observed in the level of Dvl in MRC-5 cells treated with Ag10 and Ag80. A significant suppression was reported in Ag10 at concentrations of 5 and 10 µg/ml and in Ag80 at a concentration of 10 µg/ml (**Figure 5.41**). Similarly, A549 cells demonstrated a substantial

decrease in Dvl intensity at high concentrations of Ag10 and Ag80 (5 and 10 µg/ml) (**Figure 5.42**). The current findings indicated that AgNPs suppressed the Dvl2 activity which is the positive regulators in Wnt/ β-catenin signalling pathway.

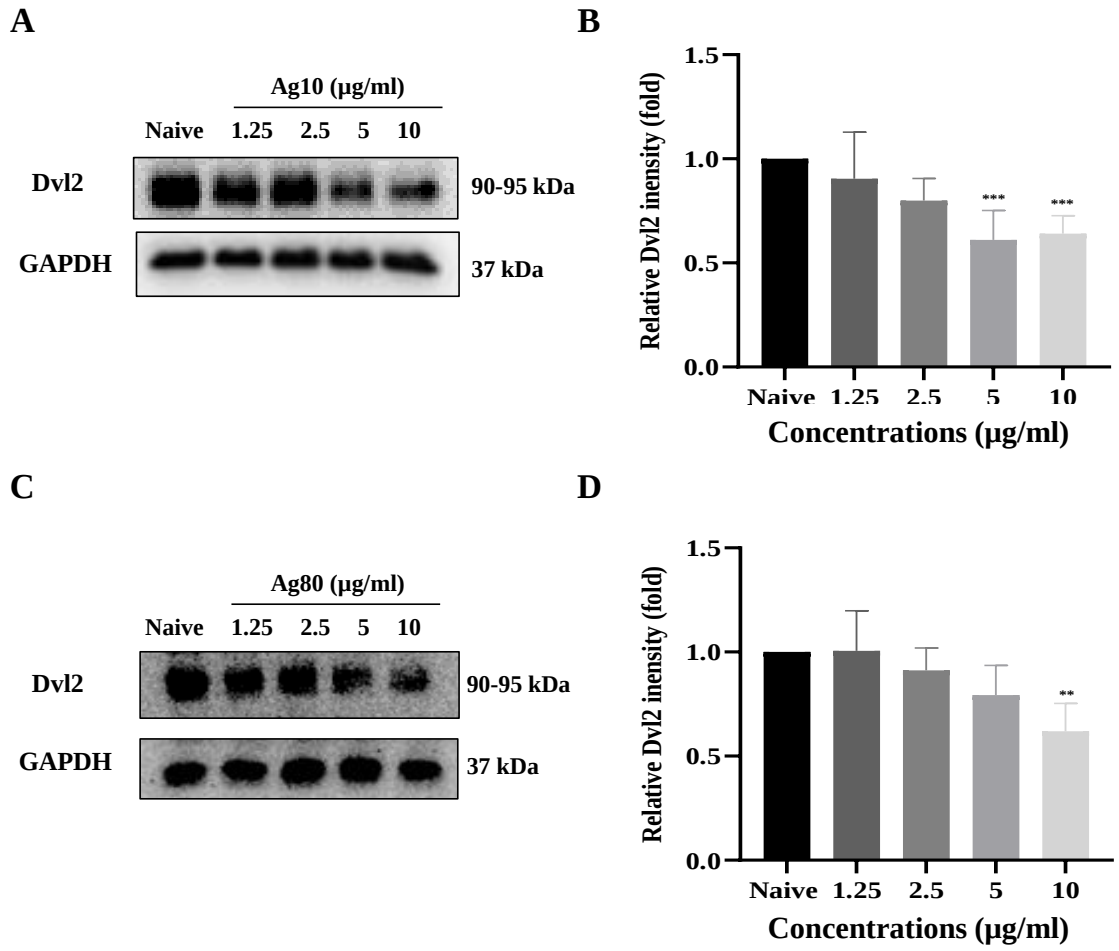


Figure 5.41. The protein expression analysis of Dvl2 following MRC-5 cells exposure to Ag10 and Ag80 of different concentrations for 24 hours. The representative western blot showing the levels of Dvl2 protein expression in MRC-5 cells treated with (**A**) Ag10 and (**C**) Ag80 at concentrations of 1.25, 2.5, 5 and 10 µg/ml for 24 hours. Naive represents the protein expression of untreated cells. Bar graphs represent the protein quantification of MRC-5 cells treated with (**B**) Ag10 and (**D**) Ag80. The protein expression was normalised to corresponding GAPDH (loading control). The protein level presented as a protein intensity ratio relative to naive (untreated group). The data expressed with fold unit, bars represent the mean ± SD (n=4). (**) $p < 0.002$ and (***) $p < 0.0002$ versus untreated group by ANOVA test.

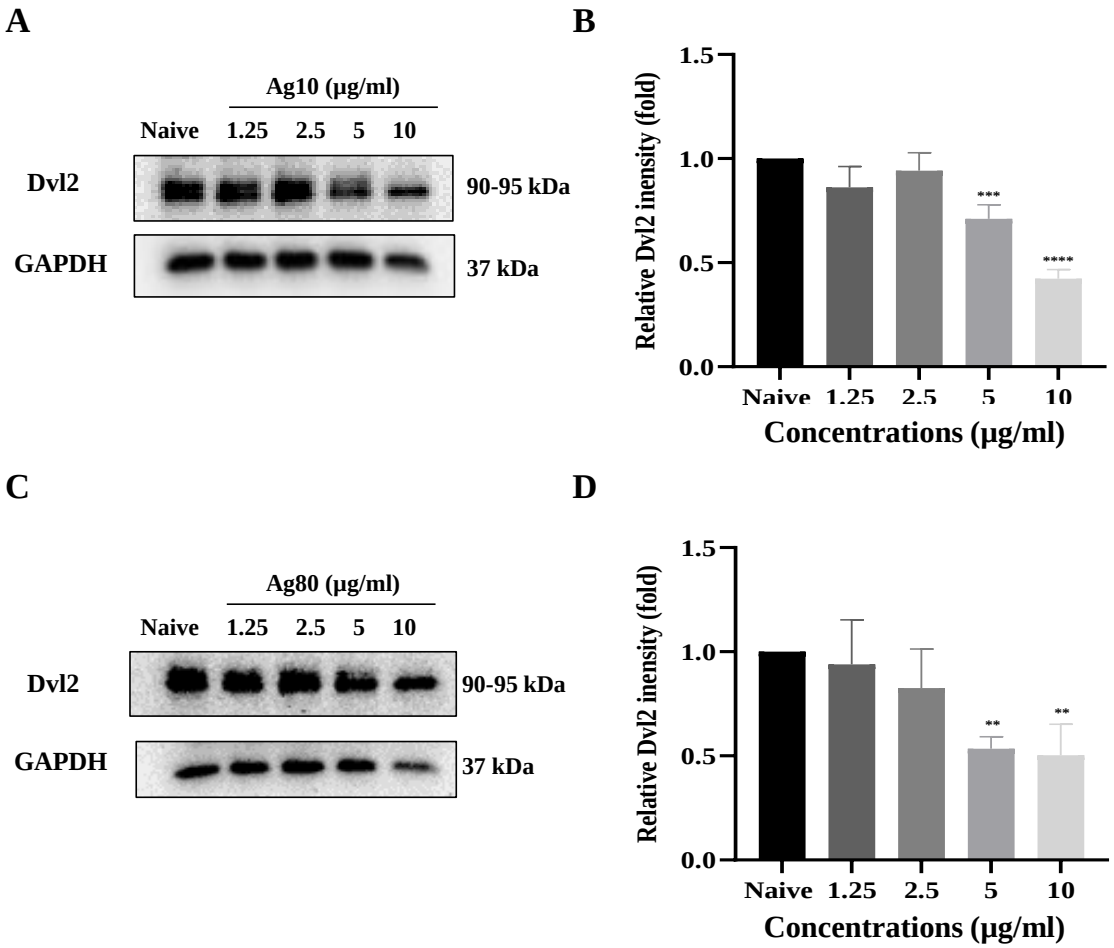


Figure 5.42. The protein expression analysis of Dvl2 following A549 cells exposure to Ag10 and Ag80 of different concentrations for 24 hours. The representative western blot showing the levels of Dvl2 protein expression in A549 cells treated with (**A**) Ag10 and (**C**) Ag80 at concentrations of 1.25, 2.5, 5 and 10 µg/ml for 24 hours. Naive represents the protein expression of untreated cells. Bar graphs represent the protein quantification of A549 cells treated with (**B**) Ag10 and (**D**) Ag80. The protein expression was normalised to corresponding GAPDH (loading control). The protein level presented as a protein intensity ratio relative to naive (untreated group). The data expressed with fold unit, bars represent the mean ± SD (n=4). (**) $p < 0.002$; (***) $p < 0.0002$ and (****) $p < 0.0001$ versus untreated group by ANOVA test.

Another critical component in Wnt/ β-catenin pathway is N-Cadherin. N-Cadherin inactivates Wnt signalling by sequestering β-catenin into cell membrane and subsequently reducing β-catenin in the cytoplasm (Marie and Haÿ, 2013). The activity of N-Cadherin was assessed in this work. The expression of N-Cadherin showed no noticeable changes compared to the untreated group in both MRC-5 and A549 cells exposed to Ag10 and Ag80 (**Figure 5.43 and Figure 5.44**).

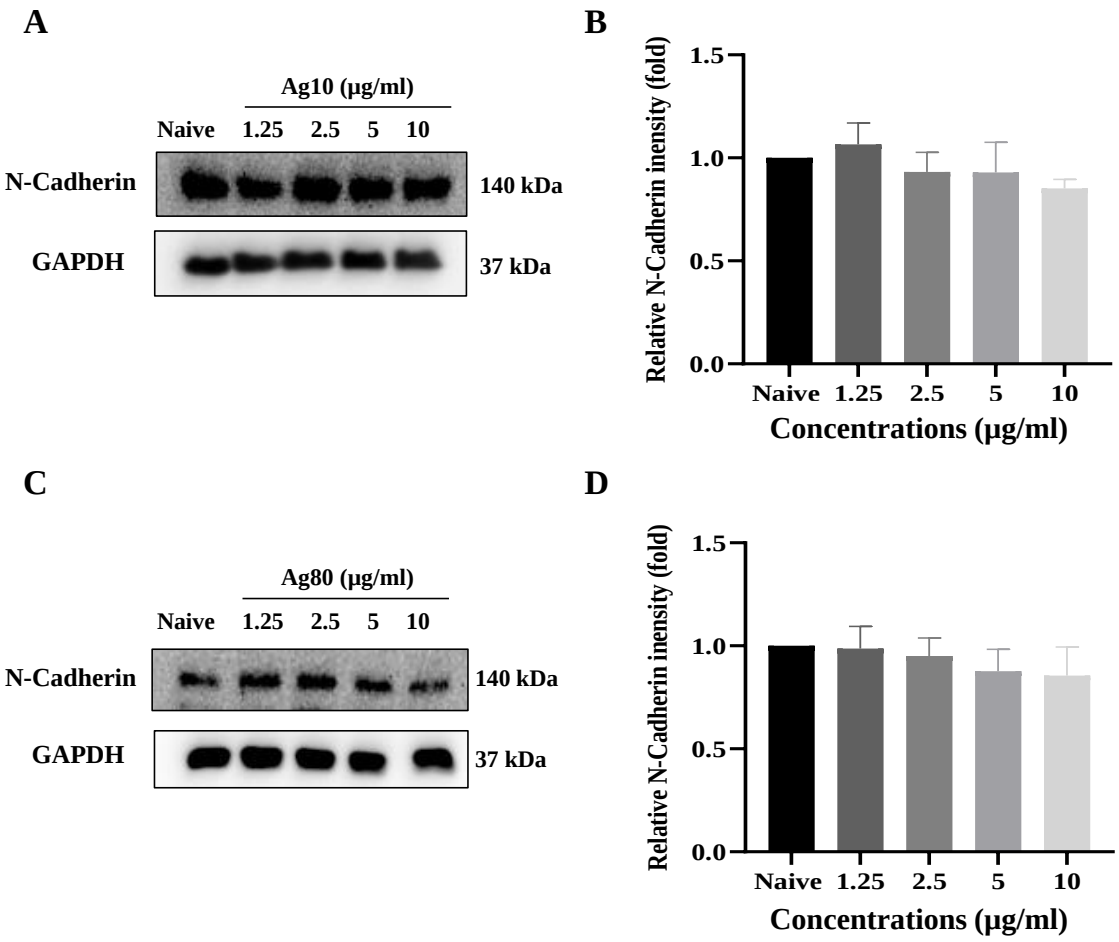


Figure 5.43. The protein expression analysis of N-Cadherin following MRC-5 cells exposure to Ag10 and Ag80 of different concentrations for 24 hours. The representative western blot showing the levels of N-Cadherin protein expression in MRC-5 cells treated with (**A**) Ag10 and (**C**) Ag80 at concentrations of 1.25, 2.5, 5 and 10 µg/ml for 24 hours. Naive represents the protein expression of untreated cells. Bar graphs represent the protein quantification of MRC-5 cells treated with (**B**) Ag10 and (**D**) Ag80. The protein expression was normalised to corresponding GAPDH (loading control). The protein level presented as a protein intensity ratio relative to naive (untreated group). The data expressed with fold unit, bars represent the mean ± SD (n=4).

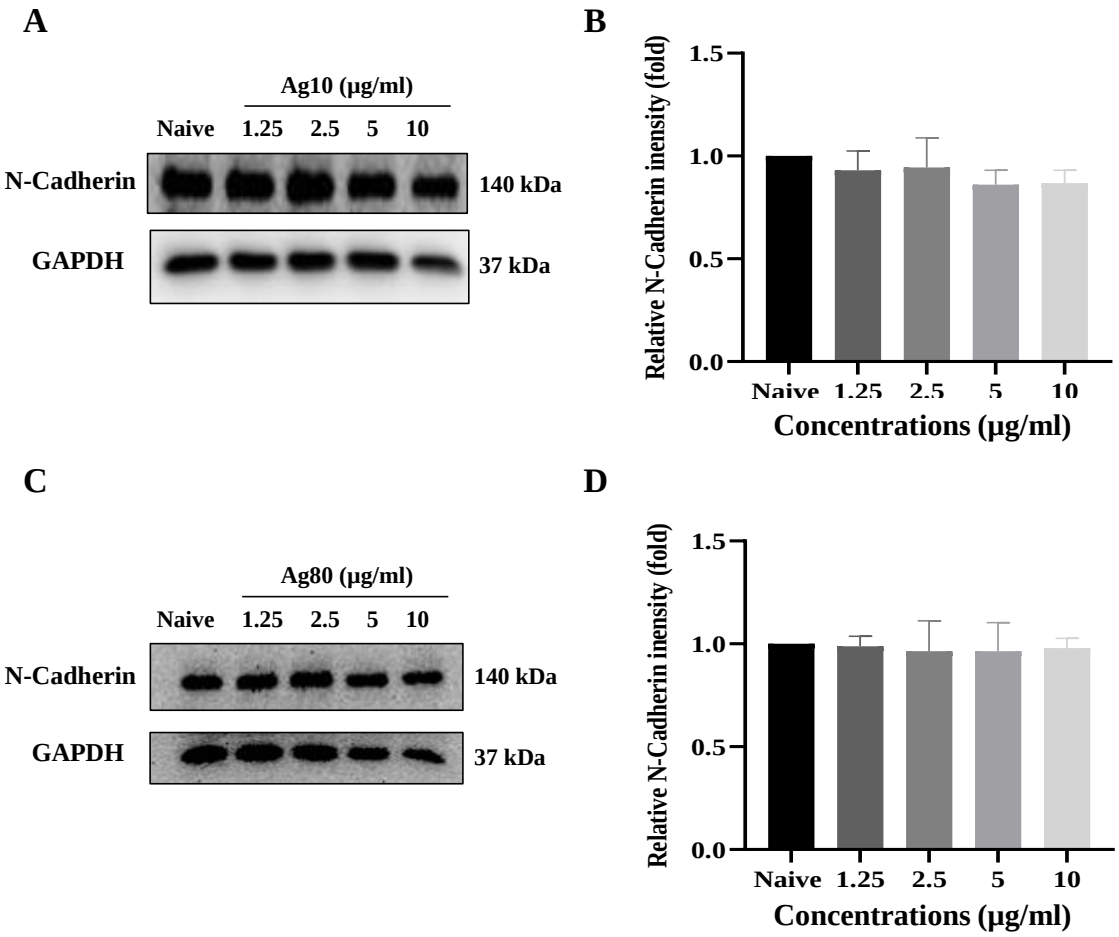


Figure 5.44. The protein expression analysis of N-Cadherin following A549 cells exposure to Ag10 and Ag80 of different concentrations for 24 hours. The representative western blot showing the levels of N-Cadherin protein expression in A549 cells treated with (**A**) Ag10 and (**C**) Ag80 at concentrations of 1.25, 2.5, 5 and 10 µg/ml for 24 hours. Naive represents the protein expression of untreated cells. Bar graphs represent the protein quantification of A549 cells treated with (**B**) Ag10 and (**D**) Ag80. The protein expression was normalised to corresponding GAPDH (loading control). The protein level presented as a protein intensity ratio relative to naive (untreated group). The data expressed with fold unit, bars represent the mean ± SD (n=4).

5.3.1.2.3 Cytoplasmic/nuclear localisation of β-catenin

It was clearly observed from previous findings that AgNPs cause significant modulation on the activity of β-catenin. Therefore, the following assessment was the investigation of the downstream cascade of β-catenin translocation from the cytoplasm to the nucleus. MRC-5 cells were exposed to Ag10 (2.5, 5 and 10 µg/ml) for 24 hours, and then the β-catenin level was assessed in both cytoplasmic and nuclear extracts. As shown in the **Figure 5.45**, there was an increase in the cytoplasmic β-catenin expression compared to the untreated group accompanied with a reduction of β-catenin level in the nuclear extract at high concentrations (5 and 10 µg/ml) compared to the control group. This may indicate a suppression of β-catenin translocation to the nucleus by AgNPs. However, the changing in the β-catenin level was not significant in either cytoplasmic or nuclear extracts in comparison to the untreated group. The present findings showed that Ag10 reduced β-catenin level in the nucleus. This could be the result of the suppression of β-catenin phosphorylation at Ser675 and Ser552 residues as previously evidenced (**Figure 5.36**), which hindered the translocation of β-catenin into the nucleus and lead to sequester β-catenin in the cytoplasm.

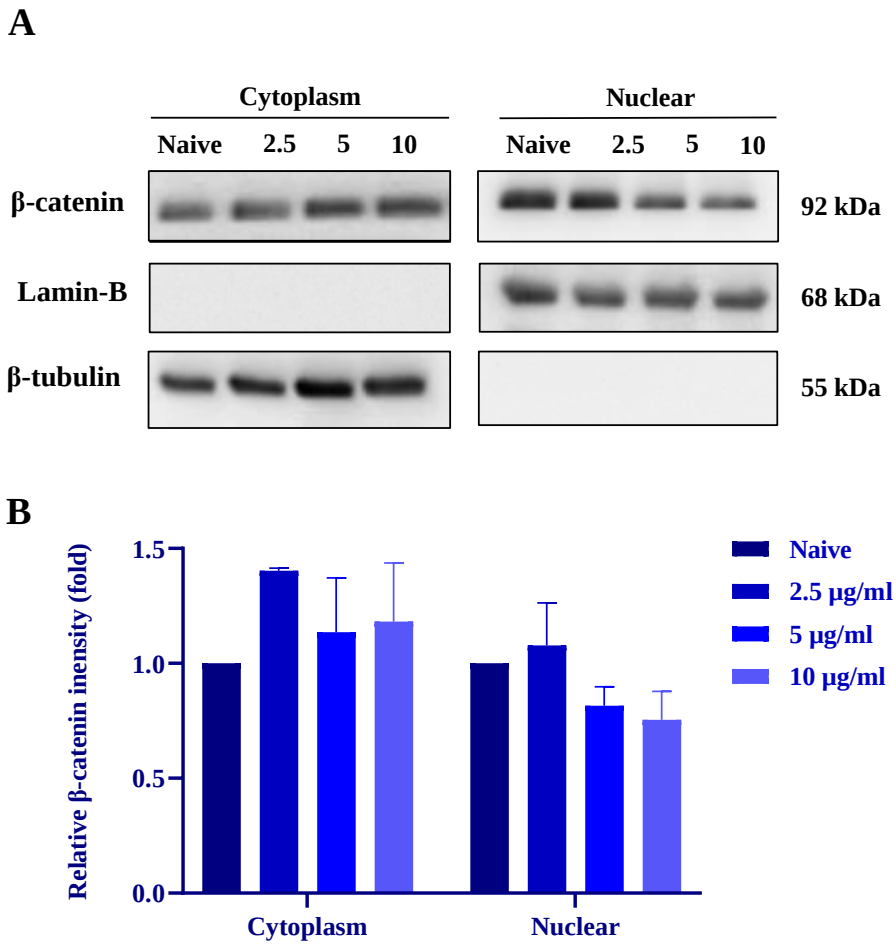


Figure 5.45. The protein expression analysis of β-catenin localisation in the cytoplasm and nucleus following MRC-5 cells exposure to Ag10 of different concentrations for 24 hours. (**A**) The representative western blot showing the levels of β-catenin protein expression in the cytoplasmic and nuclear fractions of MRC-5 cells treated with Ag10 at concentrations of 2.5, 5 and 10 µg/ml for 24 hours. (**B**) Bar graph represents β-catenin protein quantification in both cytoplasm and nuclear fraction. The protein expression was normalised to corresponding Lamin-B and β-tubulin (nuclear and cytoplasmic loading controls, respectively). The protein level presented as a protein intensity ratio relative to naive (untreated group). The data expressed with fold unit, bars represent the mean ± SD (n=3).

To further confirm the β-catenin localisation and translocation form the cytoplasm to the nucleus, the β-catenin was labelled with immunofluorescent staining, and the images were captured using confocal microscopy. As demonstrated in **Figure 5.46**, there was a concentration-dependent reduction in β-catenin intensity compared to the control group. However, it was difficult to justify the β-catenin localisation due to the reduction in the number of viable cells that occurred with increasing the concentration of A10.

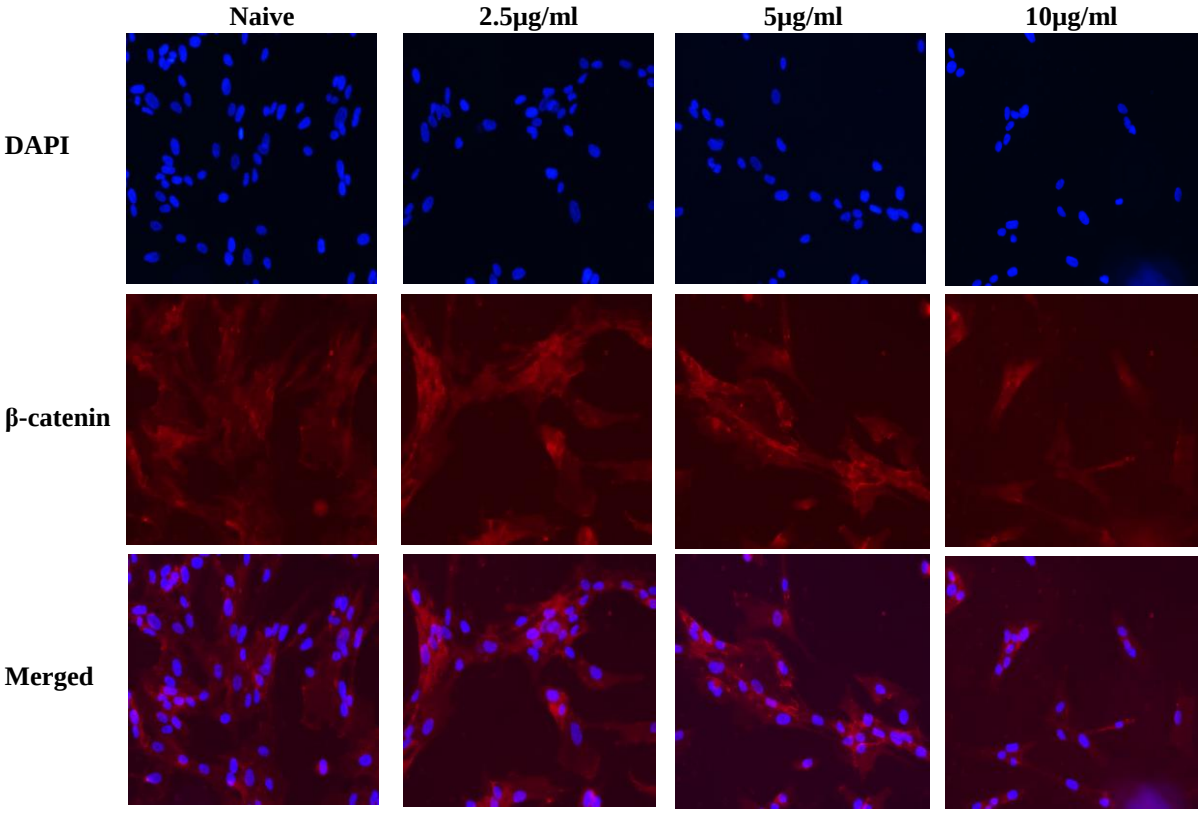


Figure 5.46. Microscopic images of β-catenin localisation following MRC-5 cells exposure to Ag10 of different concentrations for 24 hours. Immunofluorescence staining of MRC-5 cells treated with Ag10 for 24 hours at concentrations of (2.5, 5 and 10 µg/ml). β-catenin-Alexa 549 intensity (red) and DAPI staining stained the nucleus (blue).

5.3.1.2.4 Wnt/β-catenin signalling pathway activation by Wnt activators

In order to further clarify the AgNPs impact on Wnt/β-catenin signalling pathway, a Wnt activator was used prior cells exposure to AgNPs to identify the role of AgNPs in influencing the β-catenin and GSK-3β expressions. Lithium chloride (LiCl) is a Wnt/β-catenin pathway agonist acts by inhibiting GSK-3β activity (Xia et al., 2017a). MRC-5 cells were pre-activated by LiCl then treated with Ag10 of different concentrations (5, 10 and 12.5 µg/ml) for 24 hours.

As illustrated in **Figure 5.47 A and B**, there was an increase in the β-catenin level in cells treated with LiCl alone for 24 hours. There was a concentration-dependent reduction of β-catenin in cells treated with Ag10 alone. It was also observed that cellular incubation with LiCl for 12 hours followed by treating the cells with Ag10 resulted in a reduction of β-catenin expression in a concentration-dependent manner. A significant decrease of GSK-3β following cellular treatment with LiCl then Ag10 of varying concentrations was found compared to untreated group and cells treated with LiCl for 12 hours and then incubated with fresh media for 24 hours (**Figure 5.47 C and D**).

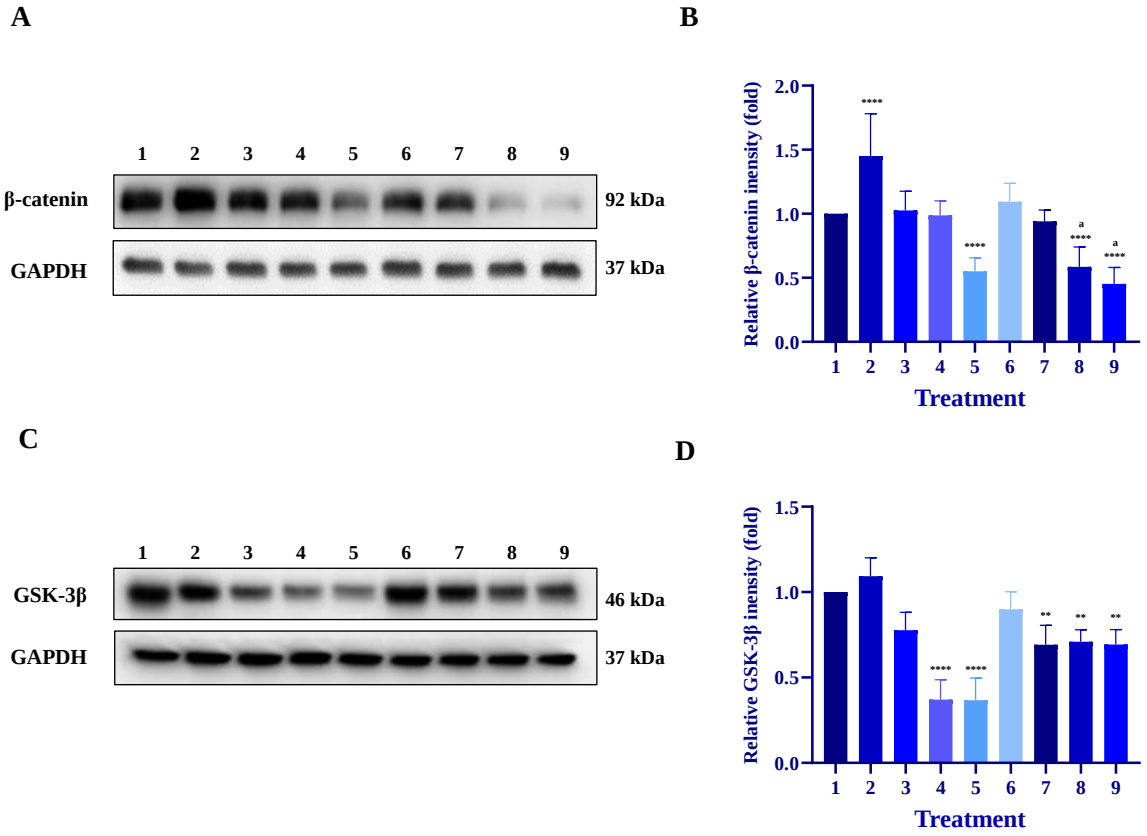


Figure 5.47. The protein expression analysis of β-catenin and GSK-3β following MRC-5 cells exposure to LiCl and Ag10. The representative western blot showing the levels of (**A**) β-catenin and (**C**) GSK-3β protein expressions in MRC-5 cells treated with: Lane (1) untreated; (2) LiCl (20 mM- 24 hours); (3) Ag10 (5 µg/ml- 24 hours); (4) Ag10 (10 µg/ml- 24 hours); (5) Ag10 (12.5 µg/ml- 24 hours); (6) LiCl (20 mM-12 hours) then incubated with fresh media -24 hours; (7) LiCl (20 mM-12 hours) then treated with Ag10 (5 µg/ml- 24 hours); (8) LiCl (20 mM-12 hours) then treated with Ag10 (10 µg/ml- 24 hours) and (9) LiCl (20 mM-12 hours) then treated with Ag10 (12.5 µg/ml- 24 hours). The bar graphs represent the protein quantification of **(B)** β-catenin and **(D)** GSK-3β proteins. The protein expression was normalised to corresponding GAPDH (loading control). The protein level presented as a protein intensity ratio relative to naive (untreated group). The data expressed with fold unit, bars represent the mean ± SD (n=4). (**) $p < 0.002$ and (****) $p < 0.0001$ versus untreated group by ANOVA test. a = $p < 0.05$ versus cells incubated with LiCl (20 mM-12 hours) then incubated with fresh media -24 hours by ANOVA test.

Wnt agonist I is the second Wnt activator was used in this study. Wnt agonist I promotes β-catenin accumulation in the nucleus without suppression of GSK-3β (Liu et al., 2005). MRC-5 cells were pre-activated with Wnt agonist I then exposed to Ag10 for 24 hours. There was a considerable reduction of β-catenin expression in cells treated with Wnt agonist I (25 µM) for 12 hours then exposed to Ag10 for 24 hours compared to the β-catenin level of cells treated with the same concentration of Wnt agonist I alone (**Figure 5.48 A and B**). The level of GSK-3β was also decreased in cells treated with Wnt agonist I (10 and 25 µM) for 12 hours then exposed to Ag10 for 24 hours compared to the level of GSK-3β in cells treated with the same concentration of Wnt agonist I alone (**Figure 5.48 A and C**).

From the current findings of assessing the effect of AgNPs on Wnt/ β-catenin pathway following cellular exposure to both Wnt activators (LiCl and Wnt agonist I), it postulated that AgNPs may directly interact with β-catenin and GSK-3β proteins leading to dysregulation of Wnt/ β-catenin pathway.

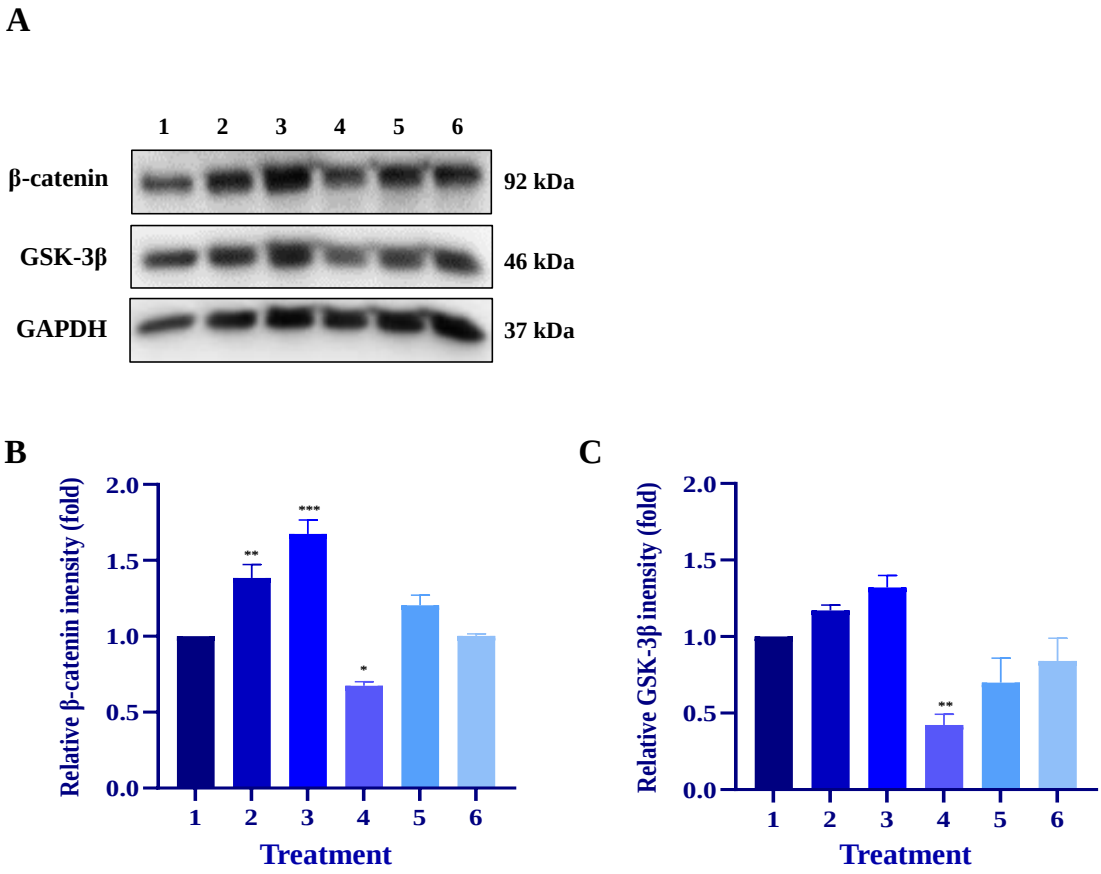


Figure 5.48. The protein expression analysis of β-catenin and GSK-3β following MRC-5 cells exposure to Ag10 and Wnt agonist I. (**A**) The representative western blot showing the levels of β-catenin and GSK-3β protein expressions in MRC-5 cells treated with: Lane (1) untreated; (2) Wnt agonist I (10 µM-24 hours); (3) Wnt agonist I (25 µM-24 hours); (4) Ag10 (10 µg/ml- 24 hours); (5) Wnt agonist I (10 µM-12 hours) then treated with Ag10 (10 µg/ml- 24 hours) and (6) Wnt agonist I (25 µM-12 hours) then treated with Ag10 (10 µg/ml- 24 hours) . The bar graphs represent the protein quantification of (**B**) β-catenin and (**C**) GSK-3β proteins. The protein expression was normalised to corresponding GAPDH (loading control). The protein level presented as a protein intensity ratio relative to naive (untreated group). The data expressed with fold unit, bars represent the mean ± SD (n=3). (*) $p < 0.05$; (**) $p < 0.002$ and (***) $p < 0.0002$ versus untreated group by ANOVA test.

The result demonstrated that AgNPs mediate dysregulation in the Wnt/β-catenin signalling pathway activity. However, it cannot be clearly determined whether the Wnt/β-catenin pathway was in the on or off state after cellular exposure to AgNPs because AgNPs inhibited the activities of both β-catenin which is the core protein for Wnt pathway activity and GSK-3β which is the negative regulator of Wnt pathway. Moreover, the results showed that AgNPs inhibited β-catenin and GSK-3β on Wnt-preactivated cells using Wnt activators (LiCl and Wnt agonist I). The results have also illustrated a suppression of β-catenin translocation into the nucleus and β-catenin was sequestered in the cytoplasm indicated an inhibition of the pathway machinery.

PI3K/AKT signalling pathway crosstalk with Wnt/β-catenin in which AKT plays an important role in β-catenin activation (Fang et al., 2007). Therefore, the downregulation of AKT activity by AgNPs as reported previously in section (5.2.1.2) could explain the observed suppression of β-catenin level. As consequence of Wnt/β-catenin and PI3K/AKT signalling pathways dysregulations by AgNPs thus may disrupt the cell proliferation, cell cycle progression, cell survival as well as cell adhesion and can be responsible for AgNPs induced toxicity.

GSK-3β is associated with the cascades of several signalling pathways that most commonly implicated in cancer including ERK/MAPK, Wnt/β-catenin, PI3K/AKT and mTOR signalling pathways (Mccubrey et al., 2014). In this work, AgNPs mediated the phosphorylation of GSK-3β lead to its inactivation and this can be correlated with AgNPs induced toxicity. In agreement with the present findings, a study observed that AgNPs mediated neurodegeneration by influencing AKT and GSK-3β protein levels (Repar et al., 2018). The latter study reported induction of apoptosis by the reduction of AKT and GSK-3β activities and triggering the pro-apoptotic factors following human astrocytes exposure to citrate-coated AgNPs sized 20 nm for 72 hours and at a concentration of 5 µg/ml. Therefore, the observed suppression of GSK-

3β by AgNPs in the present study may responsible for mediating apoptosis, however, it was difficult to justify the toxic mechanisms underlying GSK-3β inactivation by AgNPs, thus the impact of AgNPs on these pathways should be further investigated.

Collectively, the influence of AuNPs and AgNPs sized 10 and 80 nm on the protein expressions involved in PI3K/AKT and Wnt/β-catenin signalling pathways after 24 hours exposure to MRC-5 and A549 cell lines are summarised in (**Table 5.1 and Table 5.2**). As illustrated in **Table 5.1**, no pattern of AuNPs size-dependent effect on the alteration of the protein expression was observed in both MRC-5 and A549 cells following their exposure to Au10 and Au80. However, only Au10 illustrated to induce significant reduction on phospho-c-Raf and GSK-3β expressions compared to Au80 in MRC-5 cells. A549 cells treated with AuNPs demonstrated significant downregulations of phospho-c-Raf (Ser259) and β-catenin levels compared to MRC-5 cells.

Table 5.1. Summary of AuNPs impacts on the protein expressions involved in PI3K/AKT and Wnt/β-catenin signalling pathways in lung cell lines. The table demonstrates the changes in the protein expressions in both MRC-5 and A549 cells following 24 hours exposure to Au10 and Au80 at high concentration (41 µg/ml). (↓) indicates downregulation of protein expression, (↑) indicates upregulation of protein expression, (↓↓) indicates significant downregulation of protein expression compared to the other size on the same cell line, (↑↑) indicates significant upregulation of protein expression compared to the other size on the same cell line and (-) indicates no change in the protein expression was detected.

Protein	MRC-5		A549	
	Au10	Au80	Au10	Au80
PI3K/AKT signalling pathway				
PDK1	↓	↓	↓	↓
mTOR	-	-	-	-
PTEN	-	-	-	-
AKT	-	-	-	-
Phospho-c-Raf (Ser259)	↓↓	↓	↓	↓
Wnt/β-catenin signalling pathway				
β-catenin	↓	↓	↓	↓
GSK-3β	↓↓	↓	↓	↓
Phospho-GSK-3β (Ser9)	↑	↑	↑	↑↑

In case of AgNPs, no pattern of size-dependent changes in the level of protein expressions involved in PI3K/AKT signalling pathway was noticed in MRC-5 and A549 cells treated with Ag10 and Ag80 (**Table 5.2**). Interestingly, the modulation in Wnt/β-catenin signalling pathway by AgNPs showed a size-dependent alteration in the protein level in both MRC-5 and A549 cells treated with Ag10 and Ag80. The results indicated the significance of AgNPs physicochemical properties which may potentiate distinct alteration in the cell signalling pathways. Also, the results only showed marked reduction in PDK1 and AKT expressions in MRC-5 cell than A549 cells, whereases LRP6 and Dvl proteins were greatly reduced in A549 cells compared to MRC-5 cells.

Moreover, no pronounced cell-type specific effects in the protein expressions changes of both pathways were observed between the healthy and cancerous lung cells exposed to AuNPs and AgNPs. This may raise safety concerns regarding the potential use of AuNPs and AgNPs for cancer treatment. However, the reported dysregulation of PI3K/AKT and Wnt/β-catenin signalling pathways mediated by AuNPs and AgNPs exposure in this study have demonstrated their potential to interfere with the activity of signalling pathways. These findings can still be useful and may open new opportunity for AuNPs and AgNPs to treat several diseases such as diabetes, cardiovascular and Alzheimer's diseases.

Table 5.2. Summary of AgNPs impacts on the protein expressions involved in PI3K/AKT and Wnt/β-catenin signalling pathways in lung cell lines. The table demonstrates the changes in the protein expressions in both MRC-5 and A549 cells following 24 hours exposure to Ag10 and Ag80 at high concentration (10 µg/ml). (↓) indicates downregulation of protein expression, (↑) indicates upregulation of protein expression, (↓↓) indicates significant downregulation of protein expression compared to the other size on the same cell line, (↑↑) indicates significant upregulation of protein expression compared to the other size on the same cell line and (-) indicates no change in the protein expression was detected.

Protein	**MRC-5**		**A549**	
	Ag10	**Ag80**	**Ag10**	**Ag80**
PI3K/AKT signalling pathway				
PDK1	↓	↓	↓	↓
Phospho-PDK1 (Ser241)	↓	↓	↓	↓
mTOR	-	-	-	-
PTEN	-	-	-	-
AKT	↓	↓↓	↓	↓
Phospho-c-Raf (Ser259)	↓	↓	↓	↓
Wnt/β-catenin signalling pathway				
β-catenin	↓↓	↓	↓↓	↓
GSK-3β	↓↓	↓	↓↓	↓
Phospho-GSK-3β (Ser9)	↑	↑	↑	↑
LRP6	↓↓	↓	↓↓	↓
Dvl	↓↓	↓	↓↓	↓
N-Cadherin	-	-	-	-

Taking together, the data have shown that AuNPs and more prominently AgNPs can modulate cell signalling transductions in lung cell lines and thus can be also influenced by the NPs size. As both types of NPs had an influence in PI3K/AKT and Wnt/β-catenin signalling pathways, this offers a promising area for future studies to use NPs as potential therapeutic targets for both cell signalling pathways.

Chapter 6

General discussion and future work

6.1 General discussion

Both AgNPs and AuNPs were extensively reviewed in the first chapter with an emphasis on the NPs physicochemical properties implication in associated toxicity. The collective findings from the literature illustrated some controversy regarding the impact of NPs physicochemical in relation with toxicity (Akter et al., 2018, Yah, 2013). There is still no sufficient information regarding the appropriate NPs characteristics that need to consider for the safe use of NPs with minimal undesirable effects. Therefore, a nanotoxicity investigation of distinct NPs physicochemical properties is necessary to be studied.

The first aim of this research was to study NPs size and composition impact on the NPs toxicity. AgNPs and AuNPs with the three sizes (10, 40 and 80 nm) were used in this work. Both types of NPs with different sizes were characterised and then toxicity assessments were studied in both healthy (MRC-5) and cancerous (A549) lung cells. The second aim was to investigate the impact of AgNPs and AuNPs of different sizes on PI3K/AKT and Wnt/β-catenin signalling pathways, both cell signalling pathways play fundamental roles in the regulation of several cellular physiological functions.

- **Characterisation of AgNPs and AuNPs with different sizes (10, 40 and 80 nm)**

AgNPs and AuNPs of different seizes were initially characterised. The measured average sizes of AgNPs and AuNPs with the three sizes (10, 40 and 80 nm) were successfully correlated to the suppliers nominal sizes measured by TEM. TEM images demonstrated the spherical shape of both AgNPs and AuNPs of the three sizes. Moreover, AgNPs and AuNPs sized 10, 40 and 80 illustrated good monodispersity with appropriate PDI values measured by DLS. Furthermore, the ζ-potential of both types of NPs with different sizes showed good stability with ζ-potential values more negative than -30 mV. Both AgNPs and AuNPs of different sizes

showed changes in their primary sizes as a result of their interaction with serum proteins in cell culture media. The protein adsorption on NPs can lead to a modification in the NPs original sizes (Hansen and Thünemann, 2015). The stability of NPs is highly dependent on the types and concentrations of protein presented in the cell culture media (Izak-Nau et al., 2013).

- **AuNPs show greater biocompatibility than AgNPs in healthy and cancerous lung cell lines; AgNPs mediate size-dependent toxicity**

Toxicity was first studied on the 2D cell culture model of normal (MRC-5) and cancerous (A549) lung cells. Based on the mLDH assay, the measured CC50 values of AgNPs and AuNPs of different sizes showed the biocompatibility of AuNPs compared to AgNPs on both cell lines. In AgNPs, the CC50 values of the three sizes ranged between 6.8 and 26.8 µg/ml after 24 and 48 hours of exposure in both cell lines, whereas the estimated CC50 values were around 28.4-48.5 µg/ml for cells exposed to AuNPs of the three sizes at the same exposure times.

Concentration- and time-dependent toxicity of AgNPs and AuNPs toward their exposure to normal and cancerous lung cells were reported. However, AuNPs elucidated concentration dependency only at high concentrations. As a function of size's impact on toxicity, AgNPs elicited size-dependent toxicity in which Ag10 and Ag40 provoked more toxicity than larger particles (Ag80) in both cell lines. As a function of cell-specific effects, the results illustrated the sensitivity of A549 cells towards their exposure to Ag10 and Ag40 compared to MRC-5 cell lines. On the other hand, MRC-5 cells were more vulnerable to the exposure to Ag80 than A549 cell lines. Similar to the size effect of AgNPs on toxicity, AuNPs exposure to A549 cells demonstrated their high toxicity to smaller sizes of AuNPs compared to larger ones as

followed: 10 > 40 > 80 nm. However, MRC-5 cells showed greater sensitivity to AuNPs of larger sizes 80 and 40 nm.

Previous studies have reported similar identifications of the low or non toxicity of AuNPs in comparison to AgNPs. The safety profile of AuNPs compared to AgNPs was reported with using the same NPs size (20 nm) and coating (peptide-coated) at a concentration range between 10-200 µg/ml and exposed to THP-1-derived human macrophages for 24 and 48 hours (Haase et al., 2011). In another study, AuNPs exhibited the lowest toxicity in comparison to AgNPs of the same size (31 nm) when exposed to the human colorectal adenocarcinoma cells at a concentration range of 2- 10 µg/ml for 24 hours (Schneider et al., 2017). Moreover, the same study elucidated the safety of AuNPs in compared to other metal oxide NPs, such as TiO_2, ZnO and CuO of size ranges 27- 58 nm (Schneider et al., 2017).

As function of size impacts on toxicity, AgNPs sized 4.7 and 47 nm triggered toxicity in a size-dependent pattern when exposed to human pulmonary fibroblast cells for 24 hours at concentration of (1- 25 µg/ml) (Ávalos et al., 2015). On the other hand, the same study found that AuNPs of the three sizes (30, 50 and 90 nm) displayed similar toxicity profile. Another study revealed the size-dependent genotoxicity with citrate-coated AuNPs sized 5 and 50 nm whereas citrate-coated AgNPs induced genotoxicity without obvious size differences response between the two sizes in normal human bronchial epithelial cells (Lebedová et al., 2018). The author demonstrated the high cytotoxicity and genotoxicity of AgNPs of both sizes compared to AuNPs at a concentration range of 1- 50 µg/ml for 24 and 48 hours cells exposure.

The cellular uptake was also investigated in the present study by measuring the shifting of SSC light intensity, which correlated to changes in cell granularity. For AgNPs, Ag80s illustrated the highest scatter of light corresponding to their large size compared to smaller

particles after 24 and 48 hours. On the other hand, time-dependent AuNPs cellular uptake was noticed with both cell lines. MRC-5 cells demonstrated an increase in cell granularity with Au40 and Au80, which can be associated with the detected toxicity. Meanwhile, A549 cells showed the highest cellular uptake of Au10, which is also linked to observed toxicity of smaller size AuNPs. Based on the amount of Ag quantified by ICP-MS, the amounts of internalised Ag detected for Ag10 and Ag80 were higher in A549 than MRC-5 cells, supporting our initial toxicity identification of MRC-5 cells higher resistance to AgNPs than A549 cells. It was suggested that the types of cells illustrate preferential uptake pathways (Albanese and Chan, 2011).

- **Both AgNPs and AuNPs induce mitochondrial-dependent apoptosis and G2/M phase cell cycle arrest; AgNPs but not AuNPs trigger oxidative stress in both lung cells**

The toxicity mechanisms of AgNP and AuNPs sized 10, 40 and 80 nm were studied and the key findings are summarised in **Figure 6.1**. Oxidative stress is suggested to be the major mechanism of NPs associated toxicity (Mortezaee et al., 2019). In the current study, a significant increase in intracellular production of ROS was reported with MRC-5 and A549 cells under the influence of AgNPs of three sizes after 24 hours of incubation. However, no profound ROS generation was noted with AuNPs in either lung cell lines following the same incubation time. Moreover, the AgNPs and AuNPs showed an alteration in the GSH level, which is one of the main defence antioxidants in the cells. AgNPs of different sizes demonstrated a substantial reduction in the GSH/GSSG ratio in size- and concentration-dependent pattern in both cell lines following 24 hours of treatment. On the other side, AuNPs showed a decrease in the GSH/GSSG ratio only at the highest concentration after 24 hours of exposure in both cell lines.

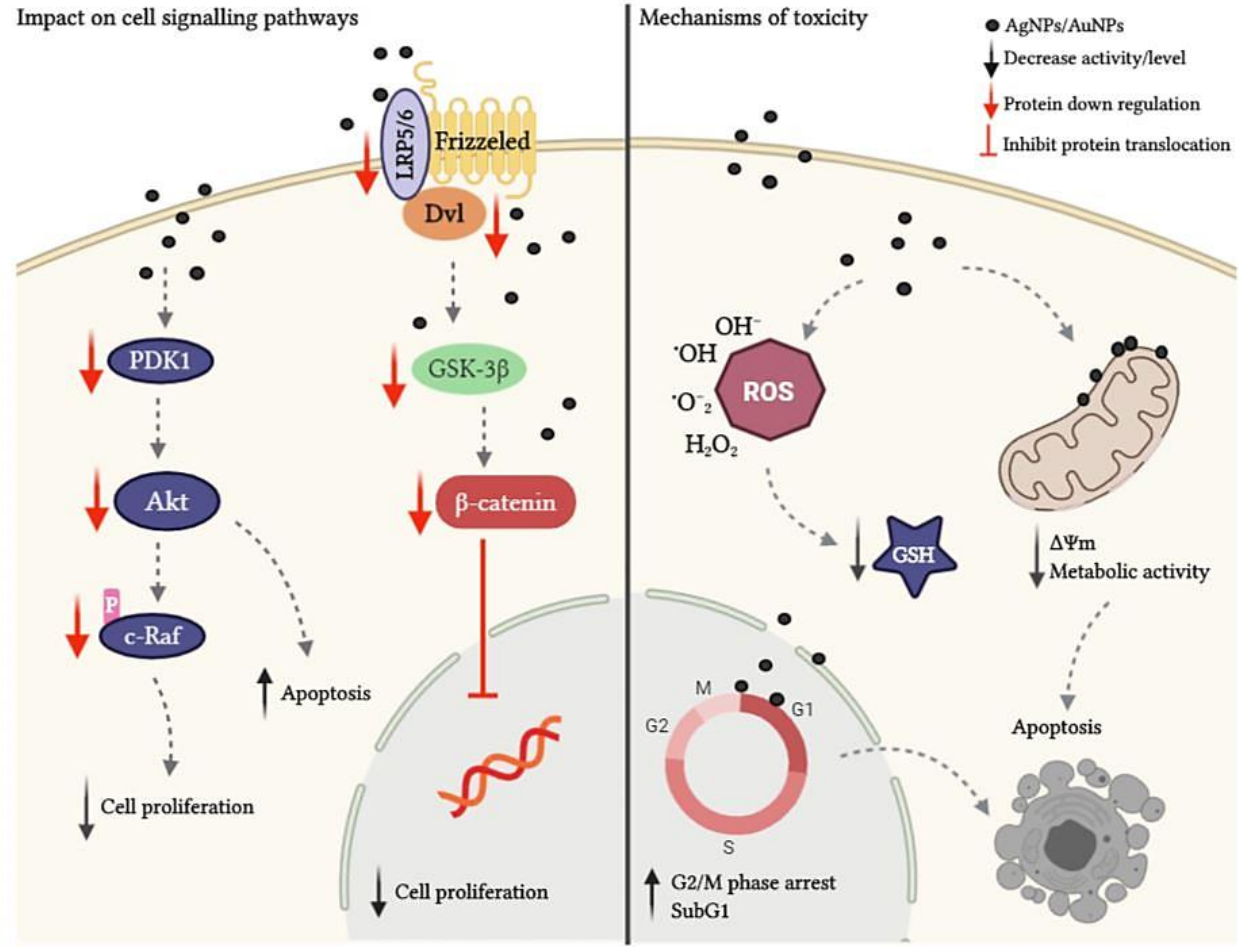


Figure 6.1. Schematic illustration summarised the current study findings of AgNPs and AuNP mechanisms of toxicity and their impacts on cell signalling pathways. The postulated toxicity mechanisms of AgNPs and AuNPs with respect to concentration, size and composition potency differences (right side).The modulation effect of AgNPs and AuNPs on both PI3K/AKT and Wnt/β-catenin signalling pathways (left side). Scheme generated with BioRender.com.

Late apoptosis/necrosis induction was reported following exposure of AgNPs of different sizes to both normal and cancerous lung cells in size-, concentration- and time-dependent patterns. On the other hand, no sign of cell death was detected at 24 hours of MRC-5 cells exposure to the three AuNPs sizes but after 48hours, an increase in the early apoptosis cell death population was reported only at low concentration (26 µg/ml). However, A549 cells exposed to AuNPs of different sizes displayed late apoptosis/necrosis populations that increased

overtime. Schneider et al. (2017) observed high attachment affinity of AgNPs sized 31 nm on the cell surface which caused increase of early and late apoptosis populations in human colorectal adenocarcinoma cells incubated for 24 hours. However, no cell death populations were detected with AuNPs of the same size. Cell apoptosis can be promoted via mitochondrial-dependent pathway. In this work, the mitochondrial membrane potential was affected under the influence of high concentrations of AgNPs and AuNPs of different sizes in both cell lines. Profound loss of mitochondrial membrane potential was detected with Ag10 and Ag40, whereas it was more significant with Au40 and Au80 on MRC-5 and A549 cells.

Both AgNPs and AuNPs showed potential to interfere with the cell cycle progression. It was observed, a potential G2/M phase cell cycle arrest in MRC-5 and A549 cells after 24 hours of incubation to three sizes of AgNPs and more prominently with Ag10. SubG1 phase indicating apoptosis was triggered after 48 hours of AgNPs exposure in MRC-5 and more pronounced effect in A549 cells. In case of AuNPs, G2/M phase cell cycle arrest was reported after 24 hours of exposure in MRC-5 and A549 cells. G2/M phase arrest accompanied with an increase in the accumulated subG1 population were detected after 48 hours of exposure to AuNPs in a concentration-dependent pattern. No size-dependent response in the cell cycle progression was noticed with cell exposed to AuNPs. MRC-5 and A549 cells showed the ability to recover following their 24 hours of exposure to high concentrations of AgNPs of different sizes. Cells treated with Ag10 and Ag40 demonstrated slower recovery rates compared to those treated with the larger size Ag80. Moreover, MRC-5 cells showed more sensitivity towards AgNPs treatment than A549 cells, in which A549 cells rapidly resumed their cell proliferation rate. The same was observed with AuNPs, A549 cells illustrated faster cell proliferation potential following exposure to AuNPs of different sizes in comparison to MRC-5 cells, which

remained affected with their exposure to AuNPs. No size-dependent recovery was observed in cells exposed to AuNPs.

AgNPs and AuNPs showed an influence on the 3D lung multicellular tumour spheroids (A549). A549 spheroids treated with Ag10 and Ag80 showed disruption in the compaction of the spheroids and increases in circumference size at high concentration (12.5 µg/ml) after 24 hours in Ag10 and 48 hours in Ag10 and Ag80. Significant alterations in spheroid integrity were observed with Ag10 more than with Ag80, which supports the size-dependent toxicity observed with the 2D cell culture model. Nevertheless, A549 spheroids revealed no substantial changes of spheroids compaction under the influence of Au10 and Au80, even after a longer time of incubation. Moreover, the cytotoxicity of A549 spheroids treated with AgNPs displayed the presence of dead cells after 48 hours of A549 spheroids incubation with high concentrations of Ag10 and Ag80 and more pronounced dead cells were detected with Ag10. For spheroids treated with Au10 and Au80, only those treated with Au10 demonstrated a slight increase in the dead cell population at 48 hours of exposure to a high concentration. The 3D spheroids cell culture model demonstrated more resistance toward their exposure to AgNPs and AuNPs compared to 2D cell culture model. In agreement to this finding, a study showed the higher toxicity of AgNPs sized 10 nm in 2D monolayer model than 3D spheroids model of primary human hepatocytes (Senyavina et al., 2016). This was explained by the difficult diffusion of AgNPs in the 3D spheroids compared to 2D monolayer which exposed to the same concentration of AgNPs in all the cells.

The toxicity findings were clearly demonstrated that AuNPs is inert and biocompatible than AgNPs. It was noticed that AuNPs required higher concentration and longer incubation time to trigger toxic responses in lung cell lines compared to AgNPs. A previous study suggested that the high toxicity of AgNPs over AuNPs is because AgNPs can more easily oxidise than

AuNPs, which leads to overproduction of ROS and cells undergo extensive oxidative stress (Reidy et al., 2013).

- **AgNPs and AuNPs modulate the activity of the PI3K/AKT pathway in healthy and cancerous lung cell lines**

The PI3K/AKT pathway is widely expressed in many tissues and organs to regulate several physiological functions (Xu et al., 2020a). In the present work, AgNPs and AuNPs sized 10 and 80 nm have demonstrated the potential to interfere with PI3K/AKT cell signalling pathway in MRC-5 and A549 cells. The results evidenced no significant alteration in the PI3K/AKT signalling cascade following exposure to Au10 and Au80 in either cell line. However, at a high concentration (41 µg/ml) of AuNPs of both sizes, a downregulation of PDK1 protein expression was observed, which is responsible for AKT phosphorylation. Therefore, it suggested that AuNPs provoked parietal inactivation of AKT activity and a subsequent reduction in phospho-c-Raf (Ser259) expression.

For cells treated with AgNPs, our finding demonstrated potential alterations of PI3K/AKT signalling transduction following exposure to a high concentration (10 µg/ml) of Ag10 and Ag80 for both cell lines. The implication of AgNPs on PI3K/AKT signalling pathway is suggested to induce cell apoptosis and supress cell proliferation, as illustrated in **Figure 6.1**. Both cell lines showed a reduction in total and phosphorylated forms of PDK1 along with the inhibition of AKT protein expression and subsequent inactivation of the phosphorylated form of c-Raf. The modulation of PI3K/AKT was reported on both cell lines, but it was more profound in the MRC-5 cells. Similar results were observed with Comfort et al. (2011), which investigated the effect of AgNPs and AuNPs sized 10 nm on PI3K/AKT pathway after 24 hours exposure in human epithelial cell line (A431) at a concentration range of 5-25 µg/ml. The study elicited that both NPs inhibited AKT and ERK phosphorylation. However, the

author noticed significant suppression on AKT activity by AuNPs compared to AgNPs. The attenuation effects of AuNPs on AKT and ERK activities were speculated to be the main mechanism of AuNPs in impeding the inflammatory response. Based on the current findings of this study, AgNPs indicated their ability to attenuate PI3K/AKT signalling pathway, with their potential implementation in the development of therapeutic targeting.

- **AgNPs and AuNPs modulate the activity of the Wnt/β-catenin pathway on healthy and cancerous lung cell lines**

The Wnt/β-catenin pathway maintains several biological functions and is found to be incorporated into several pathogeneses, including cancer (Pai et al., 2017). In this study, both AuNPs and AgNPs illustrated to negatively regulate Wnt/β-catenin signalling transduction. AgNPs and AuNPs at high concentrations significantly inhibited β-catenin and GSK-3β activities on both cell lines. The modification was slightly more profound with the smaller size Au10 and Ag10 than larger sizes (Au80 and Ag80). As illustrated in **Figure 6.1**, Ag10 was found to suppress β-catenin expression, which may be due to the effect of Ag10 on AKT downregulation as one of the main regulators for β-catenin phosphorylation. Moreover, Ag10 attenuates β-catenin translocation into the nucleus and thus leads to the sequestration of β-catenin in the cytoplasm. Both Ag10 and Ag80 inactivated the membrane proteins of Wnt/β-catenin pathway including Dvl and LRP6 proteins. The inhibitory effects of Ag10 against Wnt/β-catenin were also confirmed in pre-activated MRC-5 cells with Wnt activators such as LiCl and Wnt agonist I.

Based on our findings, it was difficult to determine whether if the Wnt/β-catenin cell signalling is on the on or off state under the influence of AgNPs and AuNPs. Both NPs inhibited β-catenin and GSK-3β expressions. It suggested that AgNPs and AuNPs may trigger ubiquitin-proteasome degradation pathway resulted in degradation of β-catenin which could explain the

observed reduction of β-catenin level. In case of suppressing the GSK-3β level, AgNPs and AuNPs may directly interact with the protein. Interestingly, the GSK-3β protein consists of phospho-binding pockets, which the NPs may occupies these binding pockets lead to pseudo autoinhibition of GSK-3β protein and upregulation of phospho-GSK-3β expression under the influence of AgNPs and AuNPs as seen previously.

In summary, the findings from the present work demonstrate the good safety profile of AuNPs which can represent a highly attractive non-toxic carrier for drug delivery. Moreover, the results show the cytotoxicity effect of AgNPs which can be used as a promising anticancer agent, however, safety consideration should be carefully addressed toward their exposure to healthy cells. As described earlier, the physicochemical properties of AuNPs and AgNPs can hinder their use for several biomedical applications. As function of NPs size, the 80 nm size of AuNPs and AgNPs exhibit better biocompatibility toward their cellular exposure compared to NPs sized 10 and 40 nm, thereby it is recommended to pay close attention to the NPs size that suitable for use as a safe drug delivery system. Moreover, AuNPs and AgNPs can influence specific cell signalling pathways and this delivers new insight into the possible use of these NPs as a therapeutic target for several diseases.

6.2 Future directions

There are few open questions that still need to be answered with respect to the influence of the composition and size of AgNPs and AuNPs on associated toxicity and NPs impact on cell signalling pathways. Suggestions for further research are described below:

- The main goal of our research was to compare NPs size impact on observed toxicity. The stability of AgNPs and AuNPs were significantly influenced by serum protein in cell culture media. The smaller-size (10 nm) AgNPs and AuNPs were highly prone to form

aggregates. Therefore, it would be useful to further assess NPs interactions with cell culture media components and protein corona formation to understand the consequence of an alteration in the NPs properties. It is desirable to maintain minimal precipitation of NPs in biological media and to consider the possibility of ion release in media as a factor may greatly alter metal NPs behaviour upon their cellular exposure.

- The possibility of metal NPs to dissolve and release metal ions is a critical factor in determining their negative effects. Cellular toxicity of metal NPs is presumed to be dependent on metal ion release. Therefore, it is of interest to investigate whether the observed toxicity of metal NPs is related to the effect of NPs themselves or the presence of released metal ions.

- To build more insight about the safety profile observed with AuNPs compared to AgNPs in lung cell lines, additional work should be carried out, including studying the cellular uptake mechanism of both NPs. Moreover, measuring the toxicity of both NPs at different times of exposure would be helpful to gain more information about NPs detrimental effects on acute and chronic exposure.

- The findings from 3D multicellular lung spheroids model showed lower sensitivity to both AgNPs and AuNPs compared to the 2D monolayer lung model. Therefore, it is recommended to perform further toxicity study on the 3D cell culture modelling as representative model for the *in vitro* study to explore the complex interaction of NPs with cells, which can mimic the *in vivo* models.

- The modulation exerted by AgNPs and AuNPs on PI3K/AKT and Wnt/β-catenin signalling cascades can be further investigated to understand how AgNPs and AuNPs

modify these pathways by assessing the upstream and downstream proteins involved in these signalling pathways.

- Molecular docking can be useful approach to further understand the mechanism behind GSK-3β inhibition by NPs. This technique can predict the NPs interaction with GSK-3β on an atomic level by checking how NPs can fit in the specific binding site of GSK-3β protein.

- The line of investigation of the NPs impact on cell signalling pathways can be extended by using stable isotope labelling by amino acids in cell culture (SILAC)-based proteomics. This approach provides substantial information on a large scale about collections of proteins, including post-translational modification proteins (phosphorylated proteins).

6.3 Conclusion

Our results indicate that the composition of NPs displays an influential impact on toxicity in which AuNPs showed higher biocompatibility compared to AgNPs in MRC-5 and A549 cells. The size of the NPs play important role in toxicity in which smaller sizes (10 and 40 nm) of AgNPs and AuNPs promoted greater toxicity than larger ones (80 nm) in both cells. However, MRC-5 cells were more vulnerable to Au80 and Au40 than Au10. Similar influences were observed in the A549 spheroids, with composition- and size-dependent effects.

AgNPs significantly triggered oxidative stress via overproduction of ROS and glutathione depletion whereas AuNPs promoted oxidative stress only at the highest concentration. Both NPs induce mitochondrial-dysfunction mediated apoptosis. AgNPs and AuNPs suppress the PI3K/AKT pathway which can emphasise apoptosis induction by both NPs in the healthy and cancerous lung cells. Both NPs modulate the Wnt/β-catenin signalling cascade in MRC-5 and A549 cells which assume to interfere with normal cell proliferation and cell cycle progression.

Finally, based on our findings, the potential toxicity of NPs can be dependent on their physicochemical properties. NPs toxicity is controllable and can be manipulated for the safe use of NPs in different biomedical applications.

Chapter 7

References

References

Abdal Dayem, A., Hossain, M. K., Lee, S. B., Kim, K., Saha, S. K., Yang, G.-M., Choi, H. Y. & Cho, S.-G. 2017. The Role of Reactive Oxygen Species (ROS) in the Biological Activities of Metallic Nanoparticles. *International Journal of Molecular Sciences,* 18**,** 120.

Adewale, O. B., Davids, H., Cairncross, L. & Roux, S. 2019. Toxicological Behavior of Gold Nanoparticles on Various Models: Influence of Physicochemical Properties and Other Factors. *International journal of toxicology,* 38**,** 357-384.

Ahmed, S., Ahmad, M., Swami, B. L. & Ikram, S. 2016. A review on plants extract mediated synthesis of silver nanoparticles for antimicrobial applications: A green expertise. *Journal of Advanced Research,* 7**,** 17-28.

Ajdary, M., Moosavi, M. A., Rahmati, M., Falahati, M., Mahboubi, M., Mandegary, A., Jangjoo, S., Mohammadinejad, R. & Varma, R. S. 2018. Health Concerns of Various Nanoparticles: A Review of Their in Vitro and in Vivo Toxicity. *Nanomaterials,* 8**,** 634.

Akter, M., Sikder, M. T., Rahman, M. M., Ullah, A. K. M. A., Hossain, K. F. B., Banik, S., Hosokawa, T., Saito, T. & Kurasaki, M. 2018. A systematic review on silver nanoparticles-induced cytotoxicity: Physicochemical properties and perspectives. *Journal of Advanced Research,* 9**,** 1-16.

Albanese, A. & Chan, W. C. 2011. Effect of gold nanoparticle aggregation on cell uptake and toxicity. *ACS Nano,* 5**,** 5478-5489.

Ali-Boucetta, H., Al-Jamal, K. T., Müller, K. H., Li, S., Porter, A. E., Eddaoudi, A., Prato, M., Bianco, A. & Kostarelos, K. 2011. Cellular Uptake and Cytotoxic Impact of Chemically Functionalized and Polymer-Coated Carbon Nanotubes. *Small,* 7**,** 3230-3238.

Alkawareek, M. Y., Bahlool, A., Abulateefeh, S. R. & Alkilany, A. M. 2019. Synergistic antibacterial activity of silver nanoparticles and hydrogen peroxide. *PloS One,* 14**,** 0220575.

Alkilany, A. M., Nagaria, P. K., Hexel, C. R., Shaw, T. J., Murphy, C. J. & Wyatt, M. D. 2009. Cellular uptake and cytotoxicity of gold nanorods: molecular origin of cytotoxicity and surface effects. *Small,* 5**,** 701-708.

Allouni, Z. E., Cimpan, M. R., Høl, P. J., Skodvin, T. & Gjerdet, N. R. 2009. Agglomeration and sedimentation of TiO2 nanoparticles in cell culture medium. *Colloids and Surfaces B: Biointerfaces,* 68**,** 83-87.

Anedda, A., López-Bernardo, E., Acosta-Iborra, B., Saadeh Suleiman, M., Landázuri, M. O. & Cadenas, S. 2013. The transcription factor Nrf2 promotes survival by enhancing the expression of uncoupling protein 3 under conditions of oxidative stress. *Free Radical Biology and Medicine,* 61**,** 395-407.

Aoki, H., Kang, P. M., Hampe, J., Yoshimura, K., Noma, T., Matsuzaki, M. & Izumo, S. 2002. Direct activation of mitochondrial apoptosis machinery by c-Jun N-terminal kinase in adult cardiac myocytes. *Journal of Biological Chemistry,* 277**,** 10244-10250.

Armstead, A. L. & Li, B. 2016. Nanotoxicity: emerging concerns regarding nanomaterial safety and occupational hard metal (WC-Co) nanoparticle exposure. *International journal of nanomedicine,* 11**,** 6421-6433.

Arvizo, R., Bhattacharya, R. & Mukherjee, P. 2010. Gold nanoparticles: opportunities and challenges in nanomedicine. *Expert opinion on drug delivery,* 7**,** 753-763.

Arvizo, R. R., Bhattacharyya, S., Kudgus, R. A., Giri, K., Bhattacharya, R. & Mukherjee, P. 2012. Intrinsic therapeutic applications of noble metal nanoparticles: past, present and future. *Chemical Society Reviews,* 41**,** 2943-2970.

Asharani, P. V., Hande, M. P. & Valiyaveettil, S. 2009a. Anti-proliferative activity of silver nanoparticles. *BMC Cell Biology,* 10**,** 65.

Asharani, P. V., Low Kah Mun, G., Hande, M. P. & Valiyaveettil, S. 2009b. Cytotoxicity and Genotoxicity of Silver Nanoparticles in Human Cells. *ACS Nano,* 3**,** 279-290.

Aubrey, B. J., Kelly, G. L., Janic, A., Herold, M. J. & Strasser, A. 2018. How does p53 induce apoptosis and how does this relate to p53-mediated tumour suppression? *Cell Death and Differentiation,* 25**,** 104-113.

Aueviriyavit, S., Phummiratch, D. & Maniratanachote, R. 2014. Mechanistic study on the biological effects of silver and gold nanoparticles in Caco-2 cells--induction of the Nrf2/HO-1 pathway by high concentrations of silver nanoparticles. *Toxicology Letters,* 224**,** 73-83.

Avalos, A., Haza, A. I., Mateo, D. & Morales, P. 2014. Cytotoxicity and ROS production of manufactured silver nanoparticles of different sizes in hepatoma and leukemia cells. *Journal of Applied Toxicology,* 34**,** 413-423.

Avalos, A., Haza, A. I., Mateo, D. & Morales, P. 2016. Interactions of manufactured silver nanoparticles of different sizes with normal human dermal fibroblasts. *International Wound Journal,* 13**,** 101-109.

Ávalos, A., Haza, A. I., Mateo, D. & Morales, P. 2015. Effects of silver and gold nanoparticles of different sizes in human pulmonary fibroblasts. *Toxicology mechanisms and methods,* 25**,** 287-295.

Bahadar, H., Maqbool, F., Niaz, K. & Abdollahi, M. 2016. Toxicity of Nanoparticles and an Overview of Current Experimental Models. *Iranian Biomedical Journal,* 20**,** 1-11.

Bai, X., Wang, Y., Song, Z., Feng, Y., Chen, Y., Zhang, D. & Feng, L. 2020. The Basic Properties of Gold Nanoparticles and their Applications in Tumor Diagnosis and Treatment. *International Journal of Molecular Sciences,* 21**,** 2480.

Balfourier, A., Luciani, N., Wang, G., Lelong, G., Ersen, O., Khelfa, A., Alloyeau, D., Gazeau, F. & Carn, F. 2020. Unexpected intracellular biodegradation and recrystallization of gold nanoparticles. *Proceedings of the National Academy of Sciences,* 117**,** 103-113.

Bantz, C., Koshkina, O., Lang, T., Galla, H.-J., Kirkpatrick, C. J., Stauber, R. H. & Maskos, M. 2014. The surface properties of nanoparticles determine the agglomeration state and the size of the particles under physiological conditions. *Beilstein journal of nanotechnology,* 5**,** 1774-1786.

Barathmanikanth, S., Kalishwaralal, K., Sriram, M., Pandian, S. R. K., Youn, H.-S., Eom, S. & Gurunathan, S. 2010. Anti-oxidant effect of gold nanoparticles restrains hyperglycemic conditions in diabetic mice. *Journal of nanobiotechnology,* 8**,** 16-16.

Barbasz, A. & Oćwieja, M. 2016. Gold nanoparticles and ions – friends or foes? As they are seen by human cells U-937 and HL-60. *Journal of Experimental Nanoscience,* 11**,** 564-580.

Barbasz, A., Oćwieja, M. & Roman, M. 2017. Toxicity of silver nanoparticles towards tumoral human cell lines U-937 and HL-60. *Colloids and Surfaces B: Biointerfaces,* 156**,** 397-404.

Barcińska, E., Wierzbicka, J., Zauszkiewicz-Pawlak, A., Jacewicz, D., Dabrowska, A. & Inkielewicz-Stepniak, I. 2018. Role of Oxidative and Nitro-Oxidative Damage in Silver Nanoparticles Cytotoxic Effect against Human Pancreatic Ductal Adenocarcinoma Cells. *Oxidative Medicine and Cellular Longevity,* 2018**,** 8251961.

Bastos, V., Ferreira-De-Oliveira, J. M. P., Carrola, J., Daniel-Da-Silva, A. L., Duarte, I. F., Santos, C. & Oliveira, H. 2017. Coating independent cytotoxicity of citrate- and PEG-coated silver nanoparticles on a human hepatoma cell line. *Journal of Environmental Sciences,* 51**,** 191-201.

Bastos, V., Ferreira De Oliveira, J. M., Brown, D., Jonhston, H., Malheiro, E., Daniel-Da-Silva, A. L., Duarte, I. F., Santos, C. & Oliveira, H. 2016. The influence of Citrate or PEG coating on silver nanoparticle toxicity to a human keratinocyte cell line. *Toxicology Letters,* 249**,** 29-41.

Basu, S., Harfouche, R., Soni, S., Chimote, G., Mashelkar, R. A. & Sengupta, S. 2009. Nanoparticle-mediated targeting of MAPK signaling predisposes tumor to chemotherapy. *Proceedings of the National Academy of Sciences,* 106**,** 7957.

Beer, C., Foldbjerg, R., Hayashi, Y., Sutherland, D. S. & Autrup, H. 2012. Toxicity of silver nanoparticles - nanoparticle or silver ion? *Toxicology Letters,* 208**,** 286-292.

Bhamidipati, M. & Fabris, L. 2017. Multiparametric Assessment of Gold Nanoparticle Cytotoxicity in Cancerous and Healthy Cells: The Role of Size, Shape, and Surface Chemistry. *Bioconjugate Chemistry,* 28**,** 449-460.

Bin-Jumah, M. N., Al-Abdan, M., Al-Basher, G. & Alarifi, S. 2020. Molecular Mechanism of Cytotoxicity, Genotoxicity, and Anticancer Potential of Green Gold Nanoparticles on Human Liver Normal and Cancerous Cells. *Dose-response,* 18**,** 1559325820912154.

Böhmert, L., Niemann, B., Thünemann, A. F. & Lampen, A. 2012. Cytotoxicity of peptide-coated silver nanoparticles on the human intestinal cell line Caco-2. *Archives of Toxicology,* 86**,** 1107-1115.

Boyles, M. S., Kristl, T., Andosch, A., Zimmermann, M., Tran, N., Casals, E., Himly, M., Puntes, V., Huber, C. G., Lütz-Meindl, U. & Duschl, A. 2015. Chitosan functionalisation of gold nanoparticles encourages particle uptake and induces cytotoxicity and pro-inflammatory conditions in phagocytic cells, as well as enhancing particle interactions with serum components. *Journal of Nanobiotechnology,* 13**,** 84.

Boyoglu, C., He, Q., Willing, G., Boyoglu-Barnum, S., Dennis, V. A., Pillai, S. & Singh, S. R. 2013. Microscopic Studies of Various Sizes of Gold Nanoparticles and Their Cellular Localizations. *ISRN Nanotechnology,* 2013**,** 123838.

Brand, M. D., Orr, A. L., Perevoshchikova, I. V. & Quinlan, C. L. 2013. The role of mitochondrial function and cellular bioenergetics in ageing and disease. *The British journal of dermatology,* 169 Suppl 2**,** 1-8.

Breslin, S. & O'driscoll, L. 2013. Three-dimensional cell culture: the missing link in drug discovery. *Drug Discovery Today,* 18**,** 240-9.

Brown, S. D., Nativo, P., Smith, J.-A., Stirling, D., Edwards, P. R., Venugopal, B., Flint, D. J., Plumb, J. A., Graham, D. & Wheate, N. J. 2010. Gold Nanoparticles for the Improved Anticancer Drug Delivery of the Active Component of Oxaliplatin. *Journal of the American Chemical Society,* 132**,** 4678-4684.

Bulte, J. W. & Kraitchman, D. L. 2004. Iron oxide MR contrast agents for molecular and cellular imaging. *NMR in Biomedicine,* 17**,** 484-499.

Burgering, B. M. & Coffer, P. J. 1995. Protein kinase B (c-Akt) in phosphatidylinositol-3-OH kinase signal transduction. *Nature,* 376**,** 599-602.

Cameron, S. J., Hosseinian, F. & Willmore, W. G. 2018. A Current Overview of the Biological and Cellular Effects of Nanosilver. *International Journal of Molecular Sciences,* 19**,** 2030.

Cantley, L. C. & Neel, B. G. 1999. New insights into tumor suppression: PTEN suppresses tumor formation by restraining the phosphoinositide 3-kinase/AKT pathway. *Proceedings of the National Academy of Sciences,* 96**,** 4240.

Cardone, M. H., Roy, N., Stennicke, H. R., Salvesen, G. S., Franke, T. F., Stanbridge, E., Frisch, S. & Reed, J. C. 1998. Regulation of cell death protease caspase-9 by phosphorylation. *Science,* 282**,** 1318-1321.

Carlson, C., Hussain, S. M., Schrand, A. M., Braydich-Stolle, L. K., Hess, K. L., Jones, R. L. & Schlager, J. J. 2008. Unique cellular interaction of silver nanoparticles: size-dependent generation of reactive oxygen species. *The Journal of Physical Chemistry B,* 112**,** 13608-13619.

Carrola, J., Bastos, V., Jarak, I., Oliveira-Silva, R., Malheiro, E., Daniel-Da-Silva, A. L., Oliveira, H., Santos, C., Gil, A. M. & Duarte, I. F. 2016. Metabolomics of silver nanoparticles toxicity in HaCaT cells: structure–activity relationships and role of ionic silver and oxidative stress. *Nanotoxicology,* 10**,** 1105-1117.

Casals, E., Pfaller, T., Duschl, A., Oostingh, G. J. & Puntes, V. 2010. Time Evolution of the Nanoparticle Protein Corona. *ACS Nano,* 4**,** 3623-3632.

Chairuangkitti, P., Lawanprasert, S., Roytrakul, S., Aueviriyavit, S., Phummiratch, D., Kulthong, K., Chanvorachote, P. & Maniratanachote, R. 2013. Silver nanoparticles induce toxicity in A549 cells via ROS-dependent and ROS-independent pathways. *Toxicology in Vitro,* 27**,** 330-338.

Chan, C.-M., Hsiao, C.-Y., Li, H.-J., Fang, J.-Y., Chang, D.-C. & Hung, C.-F. 2019. The Inhibitory Effects of Gold Nanoparticles on VEGF-A-Induced Cell Migration in Choroid-Retina Endothelial Cells. *International Journal of Molecular Sciences,* 21**,** 109.

Chawla, J., Singh, D., Sundaram, B. & Kumar, A. 2018. Identifying Challenges in Assessing Risks of Exposures of Silver Nanoparticles. *Exposure and Health,* 10**,** 61-75.

Chen, X. & Schluesener, H. J. 2008. Nanosilver: A nanoproduct in medical application. *Toxicology Letters,* 176**,** 1-12.

Cheng, X., Tian, X., Wu, A., Li, J., Tian, J., Chong, Y., Chai, Z., Zhao, Y., Chen, C. & Ge, C. 2015. Protein Corona Influences Cellular Uptake of Gold Nanoparticles by Phagocytic and Nonphagocytic Cells in a Size-Dependent Manner. *ACS Applied Materials & Interfaces,* 7**,** 20568-20575.

Chernousova, S. & Epple, M. 2013. Silver as antibacterial agent: ion, nanoparticle, and metal. *Angewandte Chemie International Edition,* 52**,** 1636-1653.

Chithrani, B. D. & Chan, W. C. W. 2007. Elucidating the Mechanism of Cellular Uptake and Removal of Protein-Coated Gold Nanoparticles of Different Sizes and Shapes. *Nano Letters,* 7**,** 1542-1550.

Chithrani, B. D., Ghazani, A. A. & Chan, W. C. W. 2006. Determining the Size and Shape Dependence of Gold Nanoparticle Uptake into Mammalian Cells. *Nano Letters,* 6**,** 662-668.

Cho, E. C., Xie, J., Wurm, P. A. & Xia, Y. 2009. Understanding the role of surface charges in cellular adsorption versus internalization by selectively removing gold nanoparticles on the cell surface with a I2/KI etchant. *Nano Letters,* 9**,** 1080-1084.

Choudhury, D., Xavier, P. L., Chaudhari, K., John, R., Dasgupta, A. K., Pradeep, T. & Chakrabarti, G. 2013. Unprecedented inhibition of tubulin polymerization directed by gold nanoparticles inducing cell cycle arrest and apoptosis. *Nanoscale,* 5**,** 4476-4489.

Chugh, H., Sood, D., Chandra, I., Tomar, V., Dhawan, G. & Chandra, R. 2018. Role of gold and silver nanoparticles in cancer nano-medicine. *Artificial Cells, Nanomedicine and Biotechnology,* 46**,** 1210-1220.

Clevers, H. & Nusse, R. 2012. Wnt/β-catenin signaling and disease. *Cell,* 149**,** 1192-1205.

Cohen, J. M., Teeguarden, J. G. & Demokritou, P. 2014. An integrated approach for the in vitro dosimetry of engineered nanomaterials. *Particle and Fibre Toxicology,* 11**,** 20.

Comfort, K. K., Maurer, E. I., Braydich-Stolle, L. K. & Hussain, S. M. 2011. Interference of silver, gold, and iron oxide nanoparticles on epidermal growth factor signal transduction in epithelial cells. *ACS Nano,* 5**,** 10000-10008.

Condorelli, G., Drusco, A., Stassi, G., Bellacosa, A., Roncarati, R., Iaccarino, G., Russo, M. A., Gu, Y., Dalton, N., Chung, C., Latronico, M. V. G., Napoli, C., Sadoshima, J., Croce, C. M. & Ross, J. 2002. Akt induces enhanced myocardial contractility and cell size in vivo in transgenic mice. *Proceedings of the National Academy of Sciences,* 99**,** 12333.

Connor, E. E., Mwamuka, J., Gole, A., Murphy, C. J. & Wyatt, M. D. 2005. Gold nanoparticles are taken up by human cells but do not cause acute cytotoxicity. *Small,* 1**,** 325-327.

Costa, E. C., De Melo-Diogo, D., Moreira, A. F., Carvalho, M. P. & Correia, I. J. 2018. Spheroids Formation on Non-Adhesive Surfaces by Liquid Overlay Technique: Considerations and Practical Approaches. *Biotechnology Journal,* 13.

Costa, E. C., Moreira, A. F., De Melo-Diogo, D., Gaspar, V. M., Carvalho, M. P. & Correia, I. J. 2016. 3D tumor spheroids: an overview on the tools and techniques used for their analysis. *Biotechnology Advances,* 34**,** 1427-1441.

Coulter, J. A., Jain, S., Butterworth, K. T., Taggart, L. E., Dickson, G. R., Mcmahon, S. J., Hyland, W. B., Muir, M. F., Trainor, C., Hounsell, A. R., O'sullivan, J. M., Schettino, G., Currell, F. J., Hirst, D. G. & Prise, K. M. 2012. Cell type-dependent uptake, localization, and cytotoxicity of 1.9 nm gold nanoparticles. *International journal of nanomedicine,* 7**,** 2673-2685.

Crabb, S. J., Birtle, A. J., Martin, K., Downs, N., Ratcliffe, I., Maishman, T., Ellis, M., Griffiths, G., Thompson, S., Ksiazek, L., Khoo, V. & Jones, R. J. 2017. ProCAID: a phase I clinical trial to combine the AKT inhibitor AZD5363 with docetaxel and prednisolone chemotherapy for metastatic castration resistant prostate cancer. *Investigational New Drugs,* 35**,** 599-607.

Crisponi, G., Nurchi, V. M., Lachowicz, J. I., Peana, M., Medici, S. & Zoroddu, M. A. 2017. Chapter 18 - Toxicity of Nanoparticles: Etiology and Mechanisms. *In:* GRUMEZESCU, A. M. (ed.) *Antimicrobial Nanoarchitectonics.* Elsevier.

Cristiano, B. E., Chan, J. C., Hannan, K. M., Lundie, N. A., Marmy-Conus, N. J., Campbell, I. G., Phillips, W. A., Robbie, M., Hannan, R. D. & Pearson, R. B. 2006. A specific role for AKT3 in the genesis of ovarian cancer through modulation of G(2)-M phase transition. *Cancer Research,* 66**,** 11718-11725.

Cummings, B. S. & Schnellmann, R. G. 2004. Measurement of cell death in mammalian cells. *Current Protocols in Pharmacology,* Chapter 12**,** 1208.

Dadosh, T. 2009. Synthesis of uniform silver nanoparticles with a controllable size. *Materials Letters,* 63**,** 2236-2238.

Dalzon, B., Torres, A., Diemer, H., Ravanel, S., Collin-Faure, V., Pernet-Gallay, K., Jouneau, P.-H., Bourguignon, J., Cianférani, S., Carrière, M., Aude-Garcia, C. & Rabilloud, T. 2019. How reversible are the effects of silver nanoparticles on macrophages? A proteomic-instructed view. *Environmental Science: Nano,* 6**,** 3133-3157.

Danaei, M., Dehghankhold, M., Ataei, S., Hasanzadeh Davarani, F., Javanmard, R., Dokhani, A., Khorasani, S. & Mozafari, M. R. 2018. Impact of Particle Size and Polydispersity Index on the Clinical Applications of Lipidic Nanocarrier Systems. *Pharmaceutics,* 10**,** 57.

Daraee, H., Eatemadi, A., Abbasi, E., Fekri Aval, S., Kouhi, M. & Akbarzadeh, A. 2016. Application of gold nanoparticles in biomedical and drug delivery. *Artificial Cells, Nanomedicine and Biotechnology,* 44**,** 410-422.

Dasgupta, N., Ranjan, S., Mishra, D. & Ramalingam, C. 2018. Thermal Co-reduction engineered silver nanoparticles induce oxidative cell damage in human colon cancer cells through inhibition of reduced glutathione and induction of mitochondria-involved apoptosis. *Chemico-Biological Interactions,* 295**,** 109-118.

Daugherty, R. L. & Gottardi, C. J. 2007. Phospho-regulation of Beta-catenin adhesion and signaling functions. *Physiology,* 22**,** 303-309.

De Matteis, V., Malvindi, M. A., Galeone, A., Brunetti, V., De Luca, E., Kote, S., Kshirsagar, P., Sabella, S., Bardi, G. & Pompa, P. P. 2015. Negligible particle-specific toxicity mechanism of silver nanoparticles: the role of Ag+ ion release in the cytosol. *Nanomedicine: Nanotechnology, Biology, and Medicine,* 11**,** 731-739.

Diehl, J. A., Cheng, M., Roussel, M. F. & Sherr, C. J. 1998. Glycogen synthase kinase-3beta regulates cyclin D1 proteolysis and subcellular localization. *Genes & Development,* 12**,** 3499-511.

Dong, L., Deng, J., Sun, Z. M., Pan, A. P., Xiang, X. J., Zhang, L., Yu, F., Chen, J., Sun, Z., Feng, M. & Xiong, J. P. 2015. Interference with the β-catenin gene in gastric cancer induces changes to the miRNA expression profile. *Tumor Biology,* 36**,** 6973-6983.

Duda, P., Akula, S. M., Abrams, S. L., Steelman, L. S., Martelli, A. M., Cocco, L., Ratti, S., Candido, S., Libra, M., Montalto, G., Cervello, M., Gizak, A., Rakus, D. & Mccubrey, J. A. 2020. Targeting GSK3 and Associated Signaling Pathways Involved in Cancer. *Cells,* 9**,** 1110.

Dumble, M., Crouthamel, M. C., Zhang, S. Y., Schaber, M., Levy, D., Robell, K., Liu, Q., Figueroa, D. J., Minthorn, E. A., Seefeld, M. A., Rouse, M. B., Rabindran, S. K., Heerding, D. A. & Kumar, R. 2014. Discovery of novel AKT inhibitors with enhanced anti-tumor effects in combination with the MEK inhibitor. *PloS One,* 9**,** e100880.

Durán, N., Durán, M., De Jesus, M. B., Seabra, A. B., Fávaro, W. J. & Nakazato, G. 2016. Silver nanoparticles: A new view on mechanistic aspects on antimicrobial activity. *Nanomedicine: Nanotechnology, Biology, and Medicine,* 12**,** 789-799.

Dusinska, M., Rundén-Pran, E., Schnekenburger, J. & Kanno, J. 2017. Chapter 3 - Toxicity Tests: In Vitro and In Vivo. *In:* FADEEL, B., PIETROIUSTI, A. & SHVEDOVA, A. A. (eds.) *Adverse Effects of Engineered Nanomaterials (Second Edition).* Academic Press.

El Badawy, A. M., Luxton, T. P., Silva, R. G., Scheckel, K. G., Suidan, M. T. & Tolaymat, T. M. 2010. Impact of environmental conditions (pH, ionic strength, and electrolyte type) on the surface charge and aggregation of silver nanoparticles suspensions. *Environmental Science & Technology,* 44**,** 1260-1266.

Elechiguerra, J. L., Burt, J. L., Morones, J. R., Camacho-Bragado, A., Gao, X., Lara, H. H. & Yacaman, M. J. 2005. Interaction of silver nanoparticles with HIV-1. *Journal of Nanobiotechnology,* 3**,** 6.

Elsabahy, M. & Wooley, K. L. 2013. Cytokines as biomarkers of nanoparticle immunotoxicity. *Chemical Society Reviews,* 42**,** 5552-5576.

Elsaesser, A. & Howard, C. V. 2012. Toxicology of nanoparticles. *Advanced Drug Delivery Reviews,* 64**,** 129-137.

England, C. G., Gobin, A. M. & Frieboes, H. B. 2015. Evaluation of uptake and distribution of gold nanoparticles in solid tumors. *The European Physical Journal Plus,* 130**,** 231.

Eom, H.-J. & Choi, J. 2010. p38 MAPK Activation, DNA Damage, Cell Cycle Arrest and Apoptosis As Mechanisms of Toxicity of Silver Nanoparticles in Jurkat T Cells. *Environmental Science & Technology,* 44**,** 8337-8342.

Fabrega, J., Luoma, S. N., Tyler, C. R., Galloway, T. S. & Lead, J. R. 2011. Silver nanoparticles: Behaviour and effects in the aquatic environment. *Environment International,* 37**,** 517-531.

Fadeel, B. 2019. The Right Stuff: On the Future of Nanotoxicology. *Frontiers in Toxicology,* 1**,** 1.

Fahrenholtz, C. D., Swanner, J., Ramirez-Perez, M. & Singh, R. N. 2017. Heterogeneous Responses of Ovarian Cancer Cells to Silver Nanoparticles as a Single Agent and in Combination with Cisplatin. *Journal of Nanomaterials,* 2017**,** 5107485.

Falagan-Lotsch, P., Grzincic, E. M. & Murphy, C. J. 2016. One low-dose exposure of gold nanoparticles induces long-term changes in human cells. *Proceedings of the National Academy of Sciences,* 113**,** 13318.

Fang, D., Hawke, D., Zheng, Y., Xia, Y., Meisenhelder, J., Nika, H., Mills, G. B., Kobayashi, R., Hunter, T. & Lu, Z. 2007. Phosphorylation of β-Catenin by AKT Promotes β-Catenin Transcriptional Activity*. *Journal of Biological Chemistry,* 282**,** 11221-11229.

Favi, P. M., Gao, M., Johana Sepúlveda Arango, L., Ospina, S. P., Morales, M., Pavon, J. J. & Webster, T. J. 2015. Shape and surface effects on the cytotoxicity of nanoparticles: Gold nanospheres versus gold nanostars. *Journal of Biomedical Materials Research,* 103**,** 3449-3462.

Fehaid, A. & Taniguchi, A. 2018. Silver nanoparticles reduce the apoptosis induced by tumor necrosis factor-α. *Science and technology of advanced materials,* 19**,** 526-534.

Flores-López, L. Z., Espinoza-Gómez, H. & Somanathan, R. 2019. Silver nanoparticles: Electron transfer, reactive oxygen species, oxidative stress, beneficial and toxicological effects. Mini review. *Journal of Applied Toxicology,* 39**,** 16-26.

Foldbjerg, R., Dang, D. A. & Autrup, H. 2011. Cytotoxicity and genotoxicity of silver nanoparticles in the human lung cancer cell line, A549. *Archives of Toxicology,* 85**,** 743-750.

Foldbjerg, R., Irving, E. S., Hayashi, Y., Sutherland, D. S., Thorsen, K., Autrup, H. & Beer, C. 2012. Global gene expression profiling of human lung epithelial cells after exposure to nanosilver. *Toxicological Sciences,* 130**,** 145-157.

Foldbjerg, R., Olesen, P., Hougaard, M., Dang, D. A., Hoffmann, H. J. & Autrup, H. 2009. PVP-coated silver nanoparticles and silver ions induce reactive oxygen species, apoptosis and necrosis in THP-1 monocytes. *Toxicology Letters,* 190**,** 156-162.

Forkink, M., Smeitink, J. a. M., Brock, R., Willems, P. H. G. M. & Koopman, W. J. H. 2010. Detection and manipulation of mitochondrial reactive oxygen species in mammalian cells. *Biochimica et Biophysica Acta (BBA) - Bioenergetics,* 1797**,** 1034-1044.

Foss Hansen, S., Heggelund, L. R., Revilla Besora, P., Mackevica, A., Boldrin, A. & Baun, A. 2016. Nanoproducts – what is actually available to European consumers? *Environmental Science: Nano,* 3**,** 169-180.

Fraga, S., Faria, H., Soares, M. E., Duarte, J. A., Soares, L., Pereira, E., Costa-Pereira, C., Teixeira, J. P., De Lourdes Bastos, M. & Carmo, H. 2013. Influence of the surface coating on the cytotoxicity, genotoxicity and uptake of gold nanoparticles in human HepG2 cells. *Journal of Applied Toxicology,* 33**,** 1111-1119.

Franco, R., Panayiotidis, M. I. & Cidlowski, J. A. 2007. Glutathione Depletion Is Necessary for Apoptosis in Lymphoid Cells Independent of Reactive Oxygen Species Formation*. *Journal of Biological Chemistry,* 282**,** 30452-30465.

Franke, T. F., Kaplan, D. R. & Cantley, L. C. 1997. PI3K: downstream AKTion blocks apoptosis. *Cell,* 88**,** 435-437.

Fratoddi, I., Venditti, I., Cametti, C. & Russo, M. V. 2015a. How toxic are gold nanoparticles? The state-of-the-art. *Nano Research,* 8**,** 1771-1799.

Fratoddi, I., Venditti, I., Cametti, C. & Russo, M. V. 2015b. The puzzle of toxicity of gold nanoparticles. The case-study of HeLa cells. *Toxicology Research,* 4**,** 796-800.

Freese, C., Uboldi, C., Gibson, M. I., Unger, R. E., Weksler, B. B., Romero, I. A., Couraud, P. O. & Kirkpatrick, C. J. 2012. Uptake and cytotoxicity of citrate-coated gold nanospheres: Comparative studies on human endothelial and epithelial cells. *Particle and Fibre Toxicology,* 9**,** 23.

Fu, P. P., Xia, Q., Hwang, H.-M., Ray, P. C. & Yu, H. 2014. Mechanisms of nanotoxicity: Generation of reactive oxygen species. *Journal of Food and Drug Analysis,* 22**,** 64-75.

García Calavia, P., Bruce, G., Pérez-García, L. & Russell, D. A. 2018. Photosensitiser-gold nanoparticle conjugates for photodynamic therapy of cancer. *Photochemical and Photobiological Sciences,* 17**,** 1534-1552.

Garcia, E. B., Alms, C., Hinman, A. W., Kelly, C., Smith, A., Vance, M., Loncarek, J., Marr, L. C. & Cimini, D. 2019. Single-Cell Analysis Reveals that Chronic Silver Nanoparticle Exposure Induces Cell Division Defects in Human Epithelial Cells. *International Journal of Environmental Research and Public Health,* 16**,** 2061.

Gliga, A. R., Skoglund, S., Wallinder, I. O., Fadeel, B. & Karlsson, H. L. 2014. Size-dependent cytotoxicity of silver nanoparticles in human lung cells: the role of cellular uptake, agglomeration and Ag release. *Particle and Fibre Toxicology,* 11**,** 11.

Gomathi, A. C., Xavier Rajarathinam, S. R., Mohammed Sadiq, A. & Rajeshkumar, S. 2020. Anticancer activity of silver nanoparticles synthesized using aqueous fruit shell extract of Tamarindus indica on MCF-7 human breast cancer cell line. *Journal of Drug Delivery Science and Technology,* 55**,** 101376.

Gopisetty, M. K., Kovács, D., Igaz, N., Rónavári, A., Bélteky, P., Rázga, Z., Venglovecz, V., Csoboz, B., Boros, I. M., Kónya, Z. & Kiricsi, M. 2019. Endoplasmic reticulum stress: major player in size-dependent inhibition of P-glycoprotein by silver nanoparticles in multidrug-resistant breast cancer cells. *Journal of Nanobiotechnology,* 17**,** 9.

Green, A. E. & Rose, P. G. 2006. Pegylated liposomal doxorubicin in ovarian cancer. *International journal of nanomedicine,* 1**,** 229-239.

Greulich, C., Braun, D., Peetsch, A., Diendorf, J., Siebers, B., Epple, M. & Köller, M. 2012. The toxic effect of silver ions and silver nanoparticles towards bacteria and human cells occurs in the same concentration range. *RSC Advances,* 2**,** 6981-6987.

Guadagnini, R., Halamoda Kenzaoui, B., Walker, L., Pojana, G., Magdolenova, Z., Bilanicova, D., Saunders, M., Juillerat-Jeanneret, L., Marcomini, A., Huk, A., Dusinska, M., Fjellsbø, L. M., Marano, F. & Boland, S. 2015. Toxicity screenings of nanomaterials: challenges due to interference with assay processes and components of classic in vitro tests. *Nanotoxicology,* 9 Suppl 1**,** 13-24.

Guo, H., German, P., Bai, S., Barnes, S., Guo, W., Qi, X., Lou, H., Liang, J., Jonasch, E., Mills, G. B. & Ding, Z. 2015. The PI3K/AKT Pathway and Renal Cell Carcinoma. *The Journal of Genetics and Genomics,* 42**,** 343-353.

Gupta, R. & Xie, H. 2018. Nanoparticles in Daily Life: Applications, Toxicity and Regulations. *Journal of environmental pathology, toxicology and oncology,* 37**,** 209-230.

Gurunathan, S., Kang, M.-H. & Kim, J.-H. 2018. Combination Effect of Silver Nanoparticles and Histone Deacetylases Inhibitor in Human Alveolar Basal Epithelial Cells. *Molecules,* 23**,** 2046.

Gustafson, H. H., Holt-Casper, D., Grainger, D. W. & Ghandehari, H. 2015. Nanoparticle uptake: The phagocyte problem. *Nano Today,* 10**,** 487-510.

Haase, A., Tentschert, J., Jungnickel, H., Graf, P., Mantion, A., Draude, F., Plendl, J., Goetz, M. E., Galla, S., Mašić, A., Thuenemann, A. F., Taubert, A., Arlinghaus, H. F. & Luch, A. 2011. Toxicity of silver nanoparticles in human macrophages: uptake, intracellular distribution and cellular responses. *Journal of Physics: Conference Series,* 304**,** 012030.

Hadrup, N., Sharma, A. K., Loeschner, K. & Jacobsen, N. R. 2020. Pulmonary toxicity of silver vapours, nanoparticles and fine dusts: A review. *Regulatory Toxicology and Pharmacology,* 115**,** 104690.

Haider, A. & Kang, I.-K. 2015. Preparation of Silver Nanoparticles and Their Industrial and Biomedical Applications: A Comprehensive Review. *Advances in Materials Science and Engineering,* 2015**,** 165257.

Hameed, A., Fatima, S., Rahman, F. U., Yoon, T.-H., Azam, A., Khan, S., Khan, A. & Islam, N. U. 2014. Synergistic enzyme inhibition effect of cefuroxime by conjugation with gold and silver. *New Journal of Chemistry,* 38**,** 1641-1646.

Hansen, U. & Thünemann, A. F. 2015. Characterization of Silver Nanoparticles in Cell Culture Medium Containing Fetal Bovine Serum. *Langmuir,* 31**,** 6842-6852.

Harhaji, L., Isakovic, A., Raicevic, N., Markovic, Z., Todorovic-Markovic, B., Nikolic, N., Vranjes-Djuric, S., Markovic, I. & Trajkovic, V. 2007. Multiple mechanisms underlying the anticancer action of nanocrystalline fullerene. *European Journal of Pharmacology,* 568**,** 89-98.

He, L., He, T., Farrar, S., Ji, L., Liu, T. & Ma, X. 2017. Antioxidants Maintain Cellular Redox Homeostasis by Elimination of Reactive Oxygen Species. *Cellular Physiology and Biochemistry,* 44**,** 532-553.

Hemmings, B. A. & Restuccia, D. F. 2012. PI3K-PKB/Akt pathway. *Cold Spring Harbor Perspectives in Biology,* 4**,** 011189.

Hillegass, J. M., Shukla, A., Lathrop, S. A., Macpherson, M. B., Fukagawa, N. K. & Mossman, B. T. 2010. Assessing nanotoxicity in cells in vitro. *Wiley interdisciplinary reviews. Nanomedicine and nanobiotechnology,* 2**,** 219-231.

Hsiao, I. L., Hsieh, Y.-K., Wang, C.-F., Chen, I. C. & Huang, Y.-J. 2015. Trojan-Horse Mechanism in the Cellular Uptake of Silver Nanoparticles Verified by Direct Intra- and Extracellular Silver Speciation Analysis. *Environmental Science & Technology,* 49**,** 3813-3821.

Huang, K., Boerhan, R., Liu, C. & Jiang, G. 2017a. Nanoparticles Penetrate into the Multicellular Spheroid-on-Chip: Effect of Surface Charge, Protein Corona, and Exterior Flow. *Molecular Pharmaceutics,* 14**,** 4618-4627.

Huang, K., Ma, H., Liu, J., Huo, S., Kumar, A., Wei, T., Zhang, X., Jin, S., Gan, Y., Wang, P. C., He, S., Zhang, X. & Liang, X. J. 2012. Size-dependent localization and penetration of ultrasmall gold nanoparticles in cancer cells, multicellular spheroids, and tumors in vivo. *ACS Nano,* 6**,** 4483-4493.

Huang, Y.-C., Yang, Y.-C., Yang, K.-C., Shieh, H.-R., Wang, T.-Y., Hwu, Y. & Chen, Y.-J. 2014. Pegylated gold nanoparticles induce apoptosis in human chronic myeloid leukemia cells. *BioMed research international,* 2014**,** 182353.

Huang, Y.-W., Cambre, M. & Lee, H.-J. 2017b. The Toxicity of Nanoparticles Depends on Multiple Molecular and Physicochemical Mechanisms. *International Journal of Molecular Sciences,* 18**,** 2702.

Hughes, J. M., Budd, P. M., Grieve, A., Dutta, P., Tiede, K. & Lewis, J. 2015. Highly monodisperse, lanthanide-containing polystyrene nanoparticles as potential standard reference materials for environmental "nano" fate analysis. *Journal of Applied Polymer Science,* 132**,** 42061.

Huo, Q., Litherland, S. A., Sullivan, S., Hallquist, H., Decker, D. A. & Rivera-Ramirez, I. 2012. Developing a nanoparticle test for prostate cancer scoring. *Journal of Translational Medicine,* 10**,** 44.

Hussain, S., Thomassen, L. C., Ferecatu, I., Borot, M. C., Andreau, K., Martens, J. A., Fleury, J., Baeza-Squiban, A., Marano, F. & Boland, S. 2010. Carbon black and titanium dioxide nanoparticles elicit distinct apoptotic pathways in bronchial epithelial cells. *Particle and Fibre Toxicology,* 7**,** 10.

Ibuki, Y. & Toyooka, T. 2012. Nanoparticle uptake measured by flow cytometry. *Methods in Molecular Biology,* 926**,** 157-166.

Iodice, C., Cervadoro, A., Palange, A., Key, J., Aryal, S., Ramirez, M. R., Mattu, C., Ciardelli, G., O'neill, B. E. & Decuzzi, P. 2016. Enhancing photothermal cancer therapy by clustering gold nanoparticles into spherical polymeric nanoconstructs. *Optics and Lasers in Engineering,* 76**,** 74-81.

Iravani, S., Korbekandi, H., Mirmohammadi, S. V. & Zolfaghari, B. 2014. Synthesis of silver nanoparticles: chemical, physical and biological methods. *Research in Pharmaceutical Sciences,* 9**,** 385-406.

Izak-Nau, E., Voetz, M., Eiden, S., Duschl, A. & Puntes, V. F. 2013. Altered characteristics of silica nanoparticles in bovine and human serum: the importance of nanomaterial characterization prior to its toxicological evaluation. *Particle and Fibre Toxicology,* 10**,** 56.

Jawaid, P., Rehman, M. U., Zhao, Q.-L., Misawa, M., Ishikawa, K., Hori, M., Shimizu, T., Saitoh, J.-I., Noguchi, K. & Kondo, T. 2020. Small size gold nanoparticles enhance apoptosis-induced by cold atmospheric plasma via depletion of intracellular GSH and modification of oxidative stress. *Cell Death Discovery,* 6**,** 83.

Jeevanandam, J., Barhoum, A., Chan, Y. S., Dufresne, A. & Danquah, M. K. 2018. Review on nanoparticles and nanostructured materials: history, sources, toxicity and regulations. *Beilstein journal of nanotechnology,* 9**,** 1050-1074.

Jeyaraj, M., Renganathan, A., Sathishkumar, G., Ganapathi, A. & Premkumar, K. 2015. Biogenic metal nanoformulations induce Bax/Bcl2 and caspase mediated mitochondrial dysfunction in human breast cancer cells (MCF 7). *RSC Advances,* 5**,** 2159-2166.

Jochums, A., Friehs, E., Sambale, F., Lavrentieva, A., Bahnemann, D. & Scheper, T. 2017. Revelation of Different Nanoparticle-Uptake Behavior in Two Standard Cell Lines NIH/3T3 and A549 by Flow Cytometry and Time-Lapse Imaging. *Toxics,* 5**,** 15.

Jog, N. R. & Caricchio, R. 2014. The role of necrotic cell death in the pathogenesis of immune mediated nephropathies. *Clinical Immunology,* 153**,** 243-253.

Johnston, H. J., Hutchison, G., Christensen, F. M., Peters, S., Hankin, S. & Stone, V. 2010. A review of the in vivo and in vitro toxicity of silver and gold particulates: particle attributes and biological mechanisms responsible for the observed toxicity. *Critical Reviews in Toxicology,* 40**,** 328-346.

Kahru, A. & Ivask, A. 2013. Mapping the Dawn of Nanoecotoxicological Research. *Accounts of Chemical Research,* 46**,** 823-833.

Kaiser, J.-P., Roesslein, M., Diener, L., Wichser, A., Nowack, B. & Wick, P. 2017. Cytotoxic effects of nanosilver are highly dependent on the chloride concentration and the presence of organic compounds in the cell culture media. *Journal of Nanobiotechnology,* 15**,** 5.

Kakakhel, M. A., Wu, F., Sajjad, W., Zhang, Q., Khan, I., Ullah, K. & Wang, W. 2021. Long-term exposure to high-concentration silver nanoparticles induced toxicity, fatality, bioaccumulation, and histological alteration in fish (Cyprinus carpio). *Environmental Sciences Europe,* 33**,** 14.

Kanipandian, N., Li, D. & Kannan, S. 2019. Induction of intrinsic apoptotic signaling pathway in A549 lung cancer cells using silver nanoparticles from Gossypium hirsutum and evaluation of in vivo toxicity. *Biotechnology Reports,* 23**,** e00339.

Karakoçak, B. B., Raliya, R., Davis, J. T., Chavalmane, S., Wang, W. N., Ravi, N. & Biswas, P. 2016. Biocompatibility of gold nanoparticles in retinal pigment epithelial cell line. *Toxicology in Vitro,* 37**,** 61-69.

Karthik, C. S., Manukumar, H. M., Ananda, A. P., Nagashree, S., Rakesh, K. P., Mallesha, L., Qin, H. L., Umesha, S., Mallu, P. & Krishnamurthy, N. B. 2018. Synthesis of novel benzodioxane midst piperazine moiety decorated chitosan silver nanoparticle against biohazard pathogens and as potential anti-inflammatory candidate: A molecular docking studies. *International Journal of Biological Macromolecules,* 108**,** 489-502.

Katas, H., Moden, N. Z., Lim, C. S., Celesistinus, T., Chan, J. Y., Ganasan, P. & Suleman Ismail Abdalla, S. 2018. Biosynthesis and Potential Applications of Silver and Gold Nanoparticles and Their Chitosan-Based Nanocomposites in Nanomedicine. *Journal of Nanotechnology,* 2018**,** 4290705.

Kaur, J. & Tikoo, K. 2013. Evaluating cell specific cytotoxicity of differentially charged silver nanoparticles. *Food and Chemical Toxicology,* 51**,** 1-14.

Kennedy, S. G., Kandel, E. S., Cross, T. K. & Hay, N. 1999. Akt/Protein kinase B inhibits cell death by preventing the release of cytochrome c from mitochondria. *Molecular and cellular biology,* 19**,** 5800-5810.

Khan, I., Saeed, K. & Khan, I. 2019. Nanoparticles: Properties, applications and toxicities. *Arabian Journal of Chemistry,* 12**,** 908-931.

Khan, S. A. 2020. Chapter 1 - Metal nanoparticles toxicity: role of physicochemical aspects. *In:* SHAH, M. R., IMRAN, M. & ULLAH, S. (eds.) *Metal Nanoparticles for Drug Delivery and Diagnostic Applications.* Elsevier.

Khanna, P., Ong, C., Bay, B. H. & Baeg, G. H. 2015. Nanotoxicity: An Interplay of Oxidative Stress, Inflammation and Cell Death. *Nanomaterials,* 5**,** 1163-1180.

Khramtsov, A. I., Khramtsova, G. F., Tretiakova, M., Huo, D., Olopade, O. I. & Goss, K. H. 2010. Wnt/β-Catenin Pathway Activation Is Enriched in Basal-Like Breast Cancers and Predicts Poor Outcome. *The American Journal of Pathology,* 176**,** 2911-2920.

Kim, H. R., Kim, M. J., Lee, S. Y., Oh, S. M. & Chung, K. H. 2011. Genotoxic effects of silver nanoparticles stimulated by oxidative stress in human normal bronchial epithelial (BEAS-2B) cells. *Mutation Research,* 726**,** 129-35.

Kim, H. S. & Lee, D. Y. 2018. Near-Infrared-Responsive Cancer Photothermal and Photodynamic Therapy Using Gold Nanoparticles. *Polymers,* 10**,** 961.

Kim, S., Choi, J. E., Choi, J., Chung, K.-H., Park, K., Yi, J. & Ryu, D.-Y. 2009. Oxidative stress-dependent toxicity of silver nanoparticles in human hepatoma cells. *Toxicology in Vitro,* 23**,** 1076-1084.

Kittler, S., Greulich, C., Diendorf, J., Köller, M. & Epple, M. 2010. Toxicity of Silver Nanoparticles Increases during Storage Because of Slow Dissolution under Release of Silver Ions. *Chemistry of Materials,* 22**,** 4548-4554.

Klębowski, B., Depciuch, J., Parlińska-Wojtan, M. & Baran, J. 2018. Applications of Noble Metal-Based Nanoparticles in Medicine. *International Journal of Molecular Sciences,* 19**,** 4031.

Kobayashi, M., Honma, T., Matsuda, Y., Suzuki, Y., Narisawa, R., Ajioka, Y. & Asakura, H. 2000. Nuclear translocation of beta-catenin in colorectal cancer. *British Journal of Cancer,* 82**,** 1689-1693.

Koduru, J. R., Kailasa, S. K., Bhamore, J. R., Kim, K. H., Dutta, T. & Vellingiri, K. 2018. Phytochemical-assisted synthetic approaches for silver nanoparticles antimicrobial applications: A review. *Advances in Colloid and Interface Science,* 256**,** 326-339.

Kovács, D., Igaz, N., Keskeny, C., Bélteky, P., Tóth, T., Gáspár, R., Madarász, D., Rázga, Z., Kónya, Z., Boros, I. M. & Kiricsi, M. 2016. Silver nanoparticles defeat p53-positive and p53-negative osteosarcoma cells by triggering mitochondrial stress and apoptosis. *Scientific Reports,* 6**,** 27902.

Krishnamurthy, N. & Kurzrock, R. 2018. Targeting the Wnt/beta-catenin pathway in cancer: Update on effectors and inhibitors. *Cancer Treatment Reviews,* 62**,** 50-60.

Krug, H. F. 2014. Nanosafety Research—Are We on the Right Track? *Angewandte Chemie International Edition,* 53**,** 12304-12319.

Ksiezak-Reding, H., Pyo, H. K., Feinstein, B. & Pasinetti, G. M. 2003. Akt/PKB kinase phosphorylates separately Thr212 and Ser214 of tau protein in vitro. *Biochimica et Biophysica Acta,* 1639**,** 159-168.

Kumar, A. & Dhawan, A. 2013. Genotoxic and carcinogenic potential of engineered nanoparticles: an update. *Archives of Toxicology,* 87**,** 1883-1900.

Kumar, D., Mutreja, I., Chitcholtan, K. & Sykes, P. 2017a. Cytotoxicity and cellular uptake of different sized gold nanoparticles in ovarian cancer cells. *Nanotechnology,* 28**,** 475101.

Kumar, G., Degheidy, H., Casey, B. J. & Goering, P. L. 2015. Flow cytometry evaluation of in vitro cellular necrosis and apoptosis induced by silver nanoparticles. *Food and Chemical Toxicology,* 85**,** 45-51.

Kumar, V. & Ganesan, S. 2013. Size-dependent in vitro cytotoxicity assay of gold nanoparticles. *Toxicological and Environmental Chemistry,* 95**,** 277-287.

Kumar, V., Sharma, N. & Maitra, S. S. 2017b. In vitro and in vivo toxicity assessment of nanoparticles. *International Nano Letters,* 7**,** 243-256.

Kyriakis, J. M. & Avruch, J. 2001. Mammalian mitogen-activated protein kinase signal transduction pathways activated by stress and inflammation. *Physiological Reviews,* 81**,** 807-869.

Lai, T.-H., Shieh, J.-M., Tsou, C.-J. & Wu, W.-B. 2015. Gold nanoparticles induce heme oxygenase-1 expression through Nrf2 activation and Bach1 export in human vascular endothelial cells. *International journal of nanomedicine,* 10**,** 5925-5939.

Lan, W. C., Lan, W. H., Chan, C. P., Hsieh, C. C., Chang, M. C. & Jeng, J. H. 1999. The effects of extracellular citric acid acidosis on the viability, cellular adhesion capacity and protein synthesis of cultured human gingival fibroblasts. *Australian Dental Journal,* 44**,** 123-130.

Lebedová, J., Hedberg, Y. S., Odnevall Wallinder, I. & Karlsson, H. L. 2018. Size-dependent genotoxicity of silver, gold and platinum nanoparticles studied using the mini-gel comet assay and micronucleus scoring with flow cytometry. *Mutagenesis,* 33**,** 77-85.

Lee, S. H. & Jun, B.-H. 2019. Silver Nanoparticles: Synthesis and Application for Nanomedicine. *International Journal of Molecular Sciences,* 20**,** 865.

Lee, Y. S., Kim, D. W., Lee, Y. H., Oh, J. H., Yoon, S., Choi, M. S., Lee, S. K., Kim, J. W., Lee, K. & Song, C. W. 2011. Silver nanoparticles induce apoptosis and G2/M arrest via PKCζ-dependent signaling in A549 lung cells. *Archives of Toxicology,* 85**,** 1529-1540.

Leicht, D. T., Balan, V., Kaplun, A., Singh-Gupta, V., Kaplun, L., Dobson, M. & Tzivion, G. 2007. Raf kinases: function, regulation and role in human cancer. *Biochimica et Biophysica Acta,* 1773**,** 1196-1212.

Li, J. J., Hartono, D., Ong, C.-N., Bay, B.-H. & Yung, L.-Y. L. 2010. Autophagy and oxidative stress associated with gold nanoparticles. *Biomaterials,* 31**,** 5996-6003.

Li, L., Li, L., Zhou, X., Yu, Y., Li, Z., Zuo, D. & Wu, Y. 2019. Silver nanoparticles induce protective autophagy via Ca2+/CaMKKβ/AMPK/mTOR pathway in SH-SY5Y cells and rat brains. *Nanotoxicology,* 13**,** 369-391.

Li, X., Hu, Z., Ma, J., Wang, X., Zhang, Y., Wang, W. & Yuan, Z. 2018. The systematic evaluation of size-dependent toxicity and multi-time biodistribution of gold nanoparticles. *Colloids and Surfaces B: Biointerfaces,* 167**,** 260-266.

Li, Y., Kröger, M. & Liu, W. K. 2015. Shape effect in cellular uptake of PEGylated nanoparticles: comparison between sphere, rod, cube and disk. *Nanoscale,* 7**,** 16631-16646.

Li, Y., Yue, T., Yang, K. & Zhang, X. 2012. Molecular modeling of the relationship between nanoparticle shape anisotropy and endocytosis kinetics. *Biomaterials,* 33**,** 4965-4973.

Lim, D. H., Jang, J., Kim, S., Kang, T., Lee, K. & Choi, I. H. 2012a. The effects of sub-lethal concentrations of silver nanoparticles on inflammatory and stress genes in human macrophages using cDNA microarray analysis. *Biomaterials,* 33**,** 4690-4699.

Lim, H. K., Asharani, P. V. & Hande, M. P. 2012b. Enhanced genotoxicity of silver nanoparticles in DNA repair deficient Mammalian cells. *Frontiers in genetics,* 3**,** 104-104.

Lin, J., Huang, Z., Wu, H., Zhou, W., Jin, P., Wei, P., Zhang, Y., Zheng, F., Zhang, J., Xu, J., Hu, Y., Wang, Y., Li, Y., Gu, N. & Wen, L. 2014. Inhibition of autophagy enhances the anticancer activity of silver nanoparticles. *Autophagy,* 10**,** 2006-2020.

Lin, Y., Lu, F., Tu, Y. & Ren, Z. 2004. Glucose Biosensors Based on Carbon Nanotube Nanoelectrode Ensembles. *Nano Letters,* 4**,** 191-195.

Liu, J., Wu, X., Mitchell, B., Kintner, C., Ding, S. & Schultz, P. G. 2005. A Small-Molecule Agonist of the Wnt Signaling Pathway. *Angewandte Chemie International Edition,* 44**,** 1987-1990.

Liu, R., Chen, Y., Liu, G., Li, C., Song, Y., Cao, Z., Li, W., Hu, J., Lu, C. & Liu, Y. 2020. PI3K/AKT pathway as a key link modulates the multidrug resistance of cancers. *Cell Death & Disease,* 11**,** 797.

Liu, W., Wu, Y., Wang, C., Li, H. C., Wang, T., Liao, C. Y., Cui, L., Zhou, Q. F., Yan, B. & Jiang, G. B. 2010. Impact of silver nanoparticles on human cells: Effect of particle size. *Nanotoxicology,* 4**,** 319-330.

Liu, Z., Wu, Y., Guo, Z., Liu, Y., Shen, Y., Zhou, P. & Lu, X. 2014. Effects of internalized gold nanoparticles with respect to cytotoxicity and invasion activity in lung cancer cells. *PloS One,* 9**,** 99175.

Logan, C. Y. & Nusse, R. 2004. THE WNT SIGNALING PATHWAY IN DEVELOPMENT AND DISEASE. *Annual Review of Cell and Developmental Biology,* 20**,** 781-810.

Lopez-Chaves, C., Soto-Alvaredo, J., Montes-Bayon, M., Bettmer, J., Llopis, J. & Sanchez-Gonzalez, C. 2018. Gold nanoparticles: Distribution, bioaccumulation and toxicity. In vitro and in vivo studies. *Nanomedicine: Nanotechnology, Biology, and Medicine,* 14**,** 1-12.

López-Muñoz, G. A., Pescador-Rojas, J. A., Ortega-Lopez, J., Salazar, J. S. & Balderas-López, J. A. 2012. Thermal diffusivity measurement of spherical gold nanofluids of different sizes/concentrations. *Nanoscale Research Letters,* 7**,** 423.

Lowry, G. V., Hill, R. J., Harper, S., Rawle, A. F., Hendren, C. O., Klaessig, F., Nobbmann, U., Sayre, P. & Rumble, J. 2016. Guidance to improve the scientific value of zeta-potential measurements in nanoEHS. *Environmental Science: Nano,* 3**,** 953-965.

Lu, P.-J., Huang, S.-C., Chen, Y.-P., Chiueh, L.-C. & Shih, D. Y.-C. 2015. Analysis of titanium dioxide and zinc oxide nanoparticles in cosmetics. *Journal of Food and Drug Analysis,* 23**,** 587-594.

Lushchak, V. I. 2012. Glutathione homeostasis and functions: potential targets for medical interventions. *Journal of Amino Acids,* 2012**,** 736837-736837.

Luyts, K., Napierska, D., Nemery, B. & Hoet, P. H. M. 2013. How physico-chemical characteristics of nanoparticles cause their toxicity: complex and unresolved interrelations. *Environmental Science: Processes & Impacts,* 15**,** 23-38.

Macdonald, B. T., Tamai, K. & He, X. 2009. Wnt/beta-catenin signaling: components, mechanisms, and diseases. *Developmental Cell,* 17**,** 9-26.

Makama, S., Kloet, S. K., Piella, J., Van Den Berg, H., De Ruijter, N. C. A., Puntes, V. F., Rietjens, I. & Van Den Brink, N. W. 2018. Effects of Systematic Variation in Size and Surface Coating of Silver Nanoparticles on Their In Vitro Toxicity to Macrophage RAW 264.7 Cells. *Toxicological Sciences,* 162**,** 79-88.

Malugin, A. & Ghandehari, H. 2010. Cellular uptake and toxicity of gold nanoparticles in prostate cancer cells: a comparative study of rods and spheres. *Journal of Applied Toxicology,* 30**,** 212-217.

Manke, A., Wang, L. & Rojanasakul, Y. 2013. Mechanisms of nanoparticle-induced oxidative stress and toxicity. *BioMed research international,* 2013**,** 942916.

Manning, B. D. & Toker, A. 2017. AKT/PKB Signaling: Navigating the Network. *Cell,* 169**,** 381-405.

Manson, J., Kumar, D., Meenan, B. J. & Dixon, D. 2011. Polyethylene glycol functionalized gold nanoparticles: the influence of capping density on stability in various media. *Gold Bulletin,* 44**,** 99-105.

Marano, F., Hussain, S., Rodrigues-Lima, F., Baeza-Squiban, A. & Boland, S. 2011. Nanoparticles: molecular targets and cell signalling. *Archives of Toxicology,* 85**,** 733-741.

Marassi, V., Di Cristo, L., Smith, S. G. J., Ortelli, S., Blosi, M., Costa, A. L., Reschiglian, P., Volkov, Y. & Prina-Mello, A. 2018. Silver nanoparticles as a medical device in healthcare settings: a five-step approach for candidate screening of coating agents. *Royal Society open science,* 5**,** 171113.

Marie, P. J. & Haÿ, E. 2013. Cadherins and Wnt signalling: a functional link controlling bone formation. *BoneKEy reports,* 2**,** 330-330.

Martínez-Torres, A. C., Zarate-Triviño, D. G., Lorenzo-Anota, H. Y., Ávila-Ávila, A., Rodríguez-Abrego, C. & Rodríguez-Padilla, C. 2018. Chitosan gold nanoparticles induce cell death in HeLa and MCF-7 cells through reactive oxygen species production. *International journal of nanomedicine,* 13**,** 3235-3250.

Mateo, D., Morales, P., Ávalos, A. & Haza, A. I. 2014. Oxidative stress contributes to gold nanoparticle-induced cytotoxicity in human tumor cells. *Toxicology Mechanisms and Methods,* 24**,** 161-172.

Maurer, L. L. & Meyer, J. N. 2016. A systematic review of evidence for silver nanoparticle-induced mitochondrial toxicity. *Environmental Science: Nano,* 3**,** 311-322.

Mazieres, J., He, B., You, L., Xu, Z. & Jablons, D. M. 2005. Wnt signaling in lung cancer. *Cancer Letters,* 222**,** 1-10.

Mccubrey, J. A., Steelman, L. S., Bertrand, F. E., Davis, N. M., Sokolosky, M., Abrams, S. L., Montalto, G., D'assoro, A. B., Libra, M., Nicoletti, F., Maestro, R., Basecke, J., Rakus, D., Gizak, A., Demidenko, Z. N., Cocco, L., Martelli, A. M. & Cervello, M. 2014. GSK-3 as potential target for therapeutic intervention in cancer. *Oncotarget,* 5**,** 2881-2911.

Mcshan, D., Ray, P. C. & Yu, H. 2014. Molecular toxicity mechanism of nanosilver. *Journal of Food and Drug Analysis,* 22**,** 116-127.

Menshykau, D. 2017. Emerging technologies for prediction of drug candidate efficacy in the preclinical pipeline. *Drug Discovery Today,* 22**,** 1598-1603.

Metzger, W., Sossong, D., Bächle, A., Pütz, N., Wennemuth, G., Pohlemann, T. & Oberringer, M. 2011. The liquid overlay technique is the key to formation of co-culture spheroids consisting of primary osteoblasts, fibroblasts and endothelial cells. *Cytotherapy,* 13**,** 1000-1012.

Miethling-Graff, R., Rumpker, R., Richter, M., Verano-Braga, T., Kjeldsen, F., Brewer, J., Hoyland, J., Rubahn, H. G. & Erdmann, H. 2014. Exposure to silver nanoparticles induces size- and dose-dependent oxidative stress and cytotoxicity in human colon carcinoma cells. *Toxicology in Vitro,* 28**,** 1280-1289.

Mihaylova, M. M. & Shaw, R. J. 2011. The AMPK signalling pathway coordinates cell growth, autophagy and metabolism. *Nature Cell Biology,* 13**,** 1016-1023.

Milić, M., Leitinger, G., Pavičić, I., Zebić Avdičević, M., Dobrović, S., Goessler, W. & Vinković Vrček, I. 2015. Cellular uptake and toxicity effects of silver nanoparticles in mammalian kidney cells. *Journal of Applied Toxicology,* 35**,** 581-592.

Mironava, T., Hadjiargyrou, M., Simon, M., Jurukovski, V. & Rafailovich, M. H. 2010. Gold nanoparticles cellular toxicity and recovery: effect of size, concentration and exposure time. *Nanotoxicology,* 4**,** 120-137.

Mohamed, N. 2020. Synthesis of Hybrid Chitosan Silver Nanoparticles Loaded with Doxorubicin with Promising Anti-cancer Activity. *BioNanoScience,* 10**,** 758-765.

Monteiro, D. R., Silva, S., Negri, M., Gorup, L. F., De Camargo, E. R., Oliveira, R., Barbosa, D. B. & Henriques, M. 2013. Silver colloidal nanoparticles: effect on matrix composition and structure of Candida albicans and Candida glabrata biofilms. *Journal of Applied Microbiology,* 114**,** 1175-1183.

Morais, T., Soares, M. E., Duarte, J. A., Soares, L., Maia, S., Gomes, P., Pereira, E., Fraga, S., Carmo, H. & Bastos Mde, L. 2012. Effect of surface coating on the biodistribution profile of gold nanoparticles in the rat. *European Journal of Pharmaceutics and Biopharmaceutics,* 80**,** 185-193.

Mortezaee, K., Najafi, M., Samadian, H., Barabadi, H., Azarnezhad, A. & Ahmadi, A. 2019. Redox interactions and genotoxicity of metal-based nanoparticles: A comprehensive review. *Chemico-Biological Interactions,* 312**,** 108814.

Muhammad, Z., Raza, A., Ghafoor, S., Naeem, A., Naz, S. S., Riaz, S., Ahmed, W. & Rana, N. F. 2016. PEG capped methotrexate silver nanoparticles for efficient anticancer activity and biocompatibility. *European Journal of Pharmaceutical Sciences,* 91**,** 251-255.

Nandhakumar, S., Dhanaraju, M. D., Sundar, V. D. & Heera, B. 2017. Influence of surface charge on the in vitro protein adsorption and cell cytotoxicity of paclitaxel loaded poly(ε-caprolactone) nanoparticles. *Bulletin of Faculty of Pharmacy, Cairo University,* 55**,** 249-258.

Napi, M. L. M., Sultan, S. M., Ismail, R., How, K. W. & Ahmad, M. K. 2019. Electrochemical-Based Biosensors on Different Zinc Oxide Nanostructures: A Review. *Materials,* 12**,** 2985.

Navé, B. T., Ouwens, M., Withers, D. J., Alessi, D. R. & Shepherd, P. R. 1999. Mammalian target of rapamycin is a direct target for protein kinase B: identification of a convergence point for opposing effects of insulin and amino-acid deficiency on protein translation. *The Biochemical journal,* 344**,** 427-431.

Ng, C. T., Tang, F. M., Li, J. J., Ong, C., Yung, L. L. & Bay, B. H. 2015. Clathrin-mediated endocytosis of gold nanoparticles in vitro. *Anat Rec (Hoboken),* 298**,** 418-27.

Nguyen, K. C., Seligy, V. L., Massarsky, A., Moon, T. W., Rippstein, P., Tan, J. & Tayabali, A. F. 2013. Comparison of toxicity of uncoated and coated silver nanoparticles. *Journal of Physics: Conference Series,* 429**,** 012025.

Nguyen, S., Minh Do, N., Truong, K. & Pham, P. 2020. Sodium citrate inhibits proliferation and induces apoptosis of hepatocellular carcinoma cells. *Biomedical Research and Therapy,* 7**,** 3659-3666.

Nitulescu, G. M., Van De Venter, M., Nitulescu, G., Ungurianu, A., Juzenas, P., Peng, Q., Olaru, O. T., Grădinaru, D., Tsatsakis, A., Tsoukalas, D., Spandidos, D. A. & Margina, D. 2018. The Akt pathway in oncology therapy and beyond (Review). *International Journal of Oncology,* 53**,** 2319-2331.

Noël, C., Simard, J. C. & Girard, D. 2016. Gold nanoparticles induce apoptosis, endoplasmic reticulum stress events and cleavage of cytoskeletal proteins in human neutrophils. *Toxicology in Vitro,* 31**,** 12-22.

Nowrouzi, A., Meghrazi, K., Golmohammadi, T., Golestani, A., Ahmadian, S., Shafiezadeh, M., Shajary, Z., Khaghani, S. & Amiri, A. N. 2010. Cytotoxicity of subtoxic AgNP in human hepatoma cell line (HepG2) after long-term exposure. *Iranian Biomedical Journal,* 14**,** 23-32.

Nunes, A. S., Barros, A. S., Costa, E. C., Moreira, A. F. & Correia, I. J. 2019. 3D tumor spheroids as in vitro models to mimic in vivo human solid tumors resistance to therapeutic drugs. *Biotechnology and Bioengineering,* 116**,** 206-226.

Oberdörster, G., Maynard, A., Donaldson, K., Castranova, V., Fitzpatrick, J., Ausman, K., Carter, J., Karn, B., Kreyling, W., Lai, D., Olin, S., Monteiro-Riviere, N., Warheit, D., Yang, H. & Group, A. R. F. T. I. R. F. R. S. I. N. T. S. W. 2005. Principles for characterizing the potential human health effects from exposure to nanomaterials: elements of a screening strategy. *Particle and Fibre Toxicology,* 2**,** 8.

Ortenzio, J., Degn, L., Goldstein-Plesser, A., Mcgee, J. K., Navratilova, J., Rogers, K., Zucker, R. M. & Boyes, W. K. 2019. Determination of silver nanoparticle dose in vitro. *NanoImpact,* 14**,** 100156.

P. J, S., Mukherjee, A. & Chandrasekaran, N. 2016. DNA damage and mitochondria-mediated apoptosis of A549 lung carcinoma cells induced by biosynthesised silver and platinum nanoparticles. *RSC Advances,* 6**,** 27775-27787.

Pai, S. G., Carneiro, B. A., Mota, J. M., Costa, R., Leite, C. A., Barroso-Sousa, R., Kaplan, J. B., Chae, Y. K. & Giles, F. J. 2017. Wnt/beta-catenin pathway: modulating anticancer immune response. *Journal of Hematology & Oncology,* 10**,** 101.

Pan, Y., Leifert, A., Ruau, D., Neuss, S., Bornemann, J., Schmid, G., Brandau, W., Simon, U. & Jahnen-Dechent, W. 2009. Gold nanoparticles of diameter 1.4 nm trigger necrosis by oxidative stress and mitochondrial damage. *Small,* 5**,** 2067-2076.

Pan, Y., Wu, Q., Qin, L., Cai, J. & Du, B. 2014. Gold nanoparticles inhibit VEGF165-induced migration and tube formation of endothelial cells via the Akt pathway. *BioMed research international,* 2014**,** 418624.

Panzarini, E., Mariano, S., Carata, E., Mura, F., Rossi, M. & Dini, L. 2018. Intracellular Transport of Silver and Gold Nanoparticles and Biological Responses: An Update. *International Journal of Molecular Sciences,* 19**,** 1305.

Park, E.-J., Yi, J., Kim, Y., Choi, K. & Park, K. 2010. Silver nanoparticles induce cytotoxicity by a Trojan-horse type mechanism. *Toxicology in Vitro,* 24**,** 872-878.

Park, J., Ha, M. K., Yang, N. & Yoon, T. H. 2017. Flow Cytometry-Based Quantification of Cellular Au Nanoparticles. *Analytical Chemistry,* 89**,** 2449-2456.

Park, J., Lim, D. H., Lim, H. J., Kwon, T., Choi, J. S., Jeong, S., Choi, I. H. & Cheon, J. 2011. Size dependent macrophage responses and toxicological effects of Ag nanoparticles. *Chemical Communications,* 47**,** 4382-4384.

Parnsamut, C. & Brimson, S. 2015. Effects of silver nanoparticles and gold nanoparticles on IL-2, IL-6, and TNF-α production via MAPK pathway in leukemic cell lines. *Genetics and Molecular Research,* 14**,** 3650-3668.

Peng, H. I. & Miller, B. L. 2011. Recent advancements in optical DNA biosensors: exploiting the plasmonic effects of metal nanoparticles. *Analyst,* 136**,** 436-47.

Perde-Schrepler, M., Florea, A., Brie, I., Virag, P., Fischer-Fodor, E., Vâlcan, A., Gurzău, E., Lisencu, C. & Maniu, A. 2019. Size-Dependent Cytotoxicity and Genotoxicity of Silver Nanoparticles in Cochlear Cells In Vitro. *Journal of Nanomaterials,* 2019**,** 6090259.

Pfeffer, C. M. & Singh, A. T. K. 2018. Apoptosis: A Target for Anticancer Therapy. *International Journal of Molecular Sciences,* 19**,** 448.

Piao, M. J., Kang, K. A., Lee, I. K., Kim, H. S., Kim, S., Choi, J. Y., Choi, J. & Hyun, J. W. 2011. Silver nanoparticles induce oxidative cell damage in human liver cells through inhibition of reduced glutathione and induction of mitochondria-involved apoptosis. *Toxicology Letters,* 201**,** 92-100.

Porta, C., Paglino, C. & Mosca, A. 2014. Targeting PI3K/Akt/mTOR Signaling in Cancer. *Frontiers in Oncology,* 4**,** 64.

Prabhu, S. & Poulose, E. K. 2012. Silver nanoparticles: mechanism of antimicrobial action, synthesis, medical applications, and toxicity effects. *International Nano Letters,* 2**,** 32.

Prasad, A., Pospíšil, P. & Tada, M. 2019. Editorial: Reactive Oxygen Species (ROS) Detection Methods in Biological System. *Frontiers in Physiology,* 10**,** 1316-1316.

Pu, P., Zhang, Z., Kang, C., Jiang, R., Jia, Z., Wang, G. & Jiang, H. 2009. Downregulation of Wnt2 and β-catenin by siRNA suppresses malignant glioma cell growth. *Cancer Gene Therapy,* 16**,** 351-361.

Qian, X., Peng, X.-H., Ansari, D. O., Yin-Goen, Q., Chen, G. Z., Shin, D. M., Yang, L., Young, A. N., Wang, M. D. & Nie, S. 2008. In vivo tumor targeting and spectroscopic detection with surface-enhanced Raman nanoparticle tags. *Nature Biotechnology,* 26**,** 83-90.

Qu, Y. & Lü, X. 2009. Aqueous synthesis of gold nanoparticles and their cytotoxicity in human dermal fibroblasts-fetal. *Journal of Biomedical Materials Research,* 4**,** 025007.

Quintero-Quiroz, C., Acevedo, N., Zapata-Giraldo, J., Botero, L. E., Quintero, J., Zárate-Triviño, D., Saldarriaga, J. & Pérez, V. Z. 2019. Optimization of silver nanoparticle synthesis by chemical reduction and evaluation of its antimicrobial and toxic activity. *Biomaterials Research,* 23**,** 27.

Rajeshkumar, S. 2016. Anticancer activity of eco-friendly gold nanoparticles against lung and liver cancer cells. *Journal of Genetic Engineering and Biotechnology,* 14**,** 195-202.

Ramalingam, V., Revathidevi, S., Shanmuganayagam, T., Muthulakshmi, L. & Rajaram, R. 2016. Biogenic gold nanoparticles induce cell cycle arrest through oxidative stress and sensitize mitochondrial membranes in A549 lung cancer cells. *RSC Advances,* 6**,** 20598-20608.

Ramalingam, V., Revathidevi, S., Shanmuganayagam, T. S., Muthulakshmi, L. & Rajaram, R. 2017. Gold nanoparticle induces mitochondria-mediated apoptosis and cell cycle arrest in nonsmall cell lung cancer cells. *Gold Bulletin,* 50**,** 177-189.

Rastogi, A., Zivcak, M., Sytar, O., Kalaji, H. M., He, X., Mbarki, S. & Brestic, M. 2017. Impact of Metal and Metal Oxide Nanoparticles on Plant: A Critical Review. *Frontiers in Chemistry,* 5.

Rauch, J., Kolch, W., Laurent, S. & Mahmoudi, M. 2013. Big Signals from Small Particles: Regulation of Cell Signaling Pathways by Nanoparticles. *Chemical Reviews,* 113**,** 3391-3406.

Reidy, B., Haase, A., Luch, A., Dawson, K. A. & Lynch, I. 2013. Mechanisms of Silver Nanoparticle Release, Transformation and Toxicity: A Critical Review of Current Knowledge and Recommendations for Future Studies and Applications. *Materials (Basel, Switzerland),* 6**,** 2295-2350.

Repar, N., Li, H., Aguilar, J. S., Li, Q. Q., Drobne, D. & Hong, Y. 2018. Silver nanoparticles induce neurotoxicity in a human embryonic stem cell-derived neuron and astrocyte network. *Nanotoxicology,* 12**,** 104-116.

Riaz Ahmed, K. B., Nagy, A. M., Brown, R. P., Zhang, Q., Malghan, S. G. & Goering, P. L. 2017. Silver nanoparticles: Significance of physicochemical properties and assay interference on the interpretation of in vitro cytotoxicity studies. *Toxicology in Vitro,* 38**,** 179-192.

Rinna, A., Magdolenova, Z., Hudecova, A., Kruszewski, M., Refsnes, M. & Dusinska, M. 2014. Effect of silver nanoparticles on mitogen-activated protein kinases activation: role of reactive oxygen species and implication in DNA damage. *Mutagenesis,* 30**,** 59-66.

Rizwan, H., Mohanta, J., Si, S. & Pal, A. 2017. Gold nanoparticles reduce high glucose-induced oxidative-nitrosative stress regulated inflammation and apoptosis via tuberin-mTOR/NF-κB pathways in macrophages. *International journal of nanomedicine,* 12**,** 5841-5862.

Roberts, P. J. & Der, C. J. 2007. Targeting the Raf-MEK-ERK mitogen-activated protein kinase cascade for the treatment of cancer. *Oncogene,* 26**,** 3291-3310.

Roesslein, M., Hirsch, C., Kaiser, J.-P., Krug, H. F. & Wick, P. 2013. Comparability of in vitro tests for bioactive nanoparticles: a common assay to detect reactive oxygen species as an example. *International Journal of Molecular Sciences,* 14**,** 24320-24337.

Rosário, F., Hoet, P., Nogueira, A. J. A., Santos, C. & Oliveira, H. 2018. Differential pulmonary in vitro toxicity of two small-sized polyvinylpyrrolidone-coated silver nanoparticles. *Journal of Toxicology and Environmental Health, Part A,* 81**,** 675-690.

Rosário, F., Hoet, P., Santos, C. & Oliveira, H. 2016. Death and cell cycle progression are differently conditioned by the AgNP size in osteoblast-like cells. *Toxicology,* 368-369**,** 103-115.

Rose, J., Auffan, M., Proux, O., Niviere, V. & Bottero, J.-Y. 2012. Physicochemical Properties of Nanoparticles in Relation with Toxicity. *In:* BHUSHAN, B. (ed.) *Encyclopedia of Nanotechnology.* Dordrecht: Springer Netherlands.

Sambale, F., Wagner, S., Stahl, F., Khaydarov, R. R., Scheper, T. & Bahnemann, D. 2015. Investigations of the toxic effect of silver nanoparticles on mammalian cell lines. *Journal of Nanomaterials,* 16**,** 136765.

Satapathy, S. R., Mohapatra, P., Preet, R., Das, D., Sarkar, B., Choudhuri, T., Wyatt, M. D. & Kundu, C. N. 2013. Silver-based nanoparticles induce apoptosis in human colon cancer cells mediated through p53. *Nanomedicine: Nanotechnology, Biology, and Medicine,* 8**,** 1307-1322.

Savage, D. T., Hilt, J. Z. & Dziubla, T. D. 2019. In Vitro Methods for Assessing Nanoparticle Toxicity. *Methods in Molecular Biology,* 1894**,** 1-29.

Schaeublin, N. M., Braydich-Stolle, L. K., Schrand, A. M., Miller, J. M., Hutchison, J., Schlager, J. J. & Hussain, S. M. 2011. Surface charge of gold nanoparticles mediates mechanism of toxicity. *Nanoscale,* 3**,** 410-420.

Schneider, T., Westermann, M. & Glei, M. 2017. In vitro uptake and toxicity studies of metal nanoparticles and metal oxide nanoparticles in human HT29 cells. *Archives of Toxicology,* 91**,** 3517-3527.

Schwartz, J. A., Price, R. E., Gill-Sharp, K. L., Sang, K. L., Khorchani, J., Goodwin, B. S. & Payne, J. D. 2011. Selective nanoparticle-directed ablation of the canine prostate. *Lasers in Surgery and Medicine,* 43**,** 213-220.

Sengul, A. B. & Asmatulu, E. 2020. Toxicity of metal and metal oxide nanoparticles: a review. *Environmental Chemistry Letters,* 18**,** 1659-1683.

Senyavina, N. V., Gerasimenko, T. N., Pulkova, N. V. & Maltseva, D. V. 2016. Transport and Toxicity of Silver Nanoparticles in HepaRG Cell Spheroids. *Bulletin of Experimental Biology and Medicine,* 160**,** 831-834.

Shao, Y., Wu, C., Wu, T., Yuan, C., Chen, S., Ding, T., Ye, X. & Hu, Y. 2018. Green synthesis of sodium alginate-silver nanoparticles and their antibacterial activity. *International Journal of Biological Macromolecules,* 111**,** 1281-1292.

Sharma, A., Gorey, B. & Casey, A. 2019. In vitro comparative cytotoxicity study of aminated polystyrene, zinc oxide and silver nanoparticles on a cervical cancer cell line. *Drug and chemical toxicology,* 42**,** 9-23.

Shi, X., Wang, J., Lei, Y., Cong, C., Tan, D. & Zhou, X. 2019. Research progress on the PI3K/AKT signaling pathway in gynecological cancer (Review). *Molecular Medicine Reports,* 19**,** 4529-4535.

Shin, S. W., Song, I. H. & Um, S. H. 2015. Role of Physicochemical Properties in Nanoparticle Toxicity. *Nanomaterials,* 5**,** 1351-1365.

Sikora, A., Bartczak, D., Geißler, D., Kestens, V., Roebben, G., Ramaye, Y., Varga, Z., Palmai, M., Shard, A. G., Goenaga-Infante, H. & Minelli, C. 2015. A systematic comparison of different techniques to determine the zeta potential of silica nanoparticles in biological medium. *Analytical Methods,* 7**,** 9835-9843.

Simard, J. C., Durocher, I. & Girard, D. 2016. Silver nanoparticles induce irremediable endoplasmic reticulum stress leading to unfolded protein response dependent apoptosis in breast cancer cells. *Apoptosis,* 21**,** 1279-1290.

Singh, R. P. & Ramarao, P. 2012. Cellular uptake, intracellular trafficking and cytotoxicity of silver nanoparticles. *Toxicology Letters,* 213**,** 249-59.

Singh, S. P., Rahman, M. F., Murty, U. S. N., Mahboob, M. & Grover, P. 2013. Comparative study of genotoxicity and tissue distribution of nano and micron sized iron oxide in rats after acute oral treatment. *Toxicology and Applied Pharmacology,* 266**,** 56-66.

Slavin, Y. N., Asnis, J., Häfeli, U. O. & Bach, H. 2017. Metal nanoparticles: understanding the mechanisms behind antibacterial activity. *Journal of Nanobiotechnology,* 15**,** 65.

Smijs, T. G. & Pavel, S. 2011. Titanium dioxide and zinc oxide nanoparticles in sunscreens: focus on their safety and effectiveness. *Nanotechnology, science and applications,* 4**,** 95-112.

Smith, J. N., Thomas, D. G., Jolley, H., Kodali, V. K., Littke, M. H., Munusamy, P., Baer, D. R., Gaffrey, M. J., Thrall, B. D. & Teeguarden, J. G. 2018. All that is silver is not toxic: silver ion and particle kinetics reveals the role of silver ion aging and dosimetry on the toxicity of silver nanoparticles. *Particle and Fibre Toxicology,* 15**,** 47.

Soenen, S. J., Parak, W. J., Rejman, J. & Manshian, B. 2015. (Intra)Cellular Stability of Inorganic Nanoparticles: Effects on Cytotoxicity, Particle Functionality, and Biomedical Applications. *Chemical Reviews,* 115**,** 2109-2135.

Sokolosky, M., Chappell, W. H., Stadelman, K., Abrams, S. L., Davis, N. M., Steelman, L. S. & Mccubrey, J. A. 2014. Inhibition of GSK-3β activity can result in drug and hormonal resistance and alter sensitivity to targeted therapy in MCF-7 breast cancer cells. *Cell cycle (Georgetown, Tex.),* 13**,** 820-833.

Souza, W., Piperni, S. G., Laviola, P., Rossi, A. L., Rossi, M. I. D., Archanjo, B. S., Leite, P. E., Fernandes, M. H., Rocha, L. A., Granjeiro, J. M. & Ribeiro, A. R. 2019. The two faces of titanium dioxide nanoparticles bio-camouflage in 3D bone spheroids. *Scientific Reports,* 9**,** 9309.

Stern, J. M., Kibanov Solomonov, V. V., Sazykina, E., Schwartz, J. A., Gad, S. C. & Goodrich, G. P. 2016. Initial Evaluation of the Safety of Nanoshell-Directed Photothermal Therapy in the Treatment of Prostate Disease. *International journal of toxicology,* 35**,** 38-46.

Stoehr, L. C., Gonzalez, E., Stampfl, A., Casals, E., Duschl, A., Puntes, V. & Oostingh, G. J. 2011. Shape matters: effects of silver nanospheres and wires on human alveolar epithelial cells. *Particle and Fibre Toxicology,* 8**,** 36.

Strojan, K., Leonardi, A., Bregar, V. B., Križaj, I., Svete, J. & Pavlin, M. 2017. Dispersion of Nanoparticles in Different Media Importantly Determines the Composition of Their Protein Corona. *PloS One,* 12**,** 0169552.

Subramanian, K. & Ponnuchamy, K. 2018. Gold nanoparticles tethered cinnamic acid: preparation, characterization, and cytotoxic effects on MCF-7 breast cancer cell lines. *Applied Nanoscience,* 8**,** 1133-1138.

Sukhanova, A., Bozrova, S., Sokolov, P., Berestovoy, M., Karaulov, A. & Nabiev, I. 2018. Dependence of Nanoparticle Toxicity on Their Physical and Chemical Properties. *Nanoscale Research letters,* 13**,** 44.

Sun, H., Jia, J., Jiang, C. & Zhai, S. 2018. Gold Nanoparticle-Induced Cell Death and Potential Applications in Nanomedicine. *International Journal of Molecular Sciences,* 19**,** 754.

Sun, M., Liu, F., Zhu, Y., Wang, W., Hu, J., Liu, J., Dai, Z., Wang, K., Wei, Y., Bai, J. & Gao, W. 2016. Salt-induced aggregation of gold nanoparticles for photoacoustic imaging and photothermal therapy of cancer. *Nanoscale,* 8**,** 4452-4457.

Sur, I., Cam, D., Kahraman, M., Baysal, A. & Culha, M. 2010. Interaction of multi-functional silver nanoparticles with living cells. *Nanotechnology,* 21**,** 175104.

Surapaneni, S. K., Bashir, S. & Tikoo, K. 2018. Gold nanoparticles-induced cytotoxicity in triple negative breast cancer involves different epigenetic alterations depending upon the surface charge. *Scientific Reports,* 8**,** 12295.

Suresh, A. K., Pelletier, D. A., Wang, W., Morrell-Falvey, J. L., Gu, B. & Doktycz, M. J. 2012. Cytotoxicity induced by engineered silver nanocrystallites is dependent on surface coatings and cell types. *Langmuir,* 28**,** 2727-2735.

Suryawanshi, A., Tadagavadi, R. K., Swafford, D. & Manicassamy, S. 2016. Modulation of Inflammatory Responses by Wnt/β-Catenin Signaling in Dendritic Cells: A Novel Immunotherapy Target for Autoimmunity and Cancer. *Frontiers in Immunology,* 7**,** 460.

Tam, L., Phan, V., Lan, H., Thuy, N., Hien, T., Huy, T., Quy, N., Chinh, H., Tung, L., Tuan, P., Lam, V. & Le, A.-T. 2013. Characterization and antimicrobial activity of silver nanoparticles prepared by a thermal decomposition technique. *Applied Physics A,* 113**,** 613–621.

Teles, M., Reyes-López, F. E., Balasch, J. C., Tvarijonaviciute, A., Guimarães, L., Oliveira, M. & Tort, L. 2019. Toxicogenomics of Gold Nanoparticles in a Marine Fish: Linkage to Classical Biomarkers. *Frontiers in Marine Science,* 6.

Tellez-Gabriel, M., Cochonneau, D., Cadé, M., Jubellin, C., Heymann, M. F. & Heymann, D. 2018. Circulating Tumor Cell-Derived Pre-Clinical Models for Personalized Medicine. *Cancers,* 11.

Teodoro, J. S., Simões, A. M., Duarte, F. V., Rolo, A. P., Murdoch, R. C., Hussain, S. M. & Palmeira, C. M. 2011. Assessment of the toxicity of silver nanoparticles in vitro: a mitochondrial perspective. *Toxicology in Vitro,* 25**,** 664-670.

Terry L. Riss & Moravec, R. A. 2004. Use of Multiple Assay Endpoints to Investigate the Effects of Incubation Time, Dose of Toxin, and Plating Density in Cell-Based Cytotoxicity Assays. *Assay and Drug Development Technologies,* 2**,** 51-62.

Thannickal, V. J. & Fanburg, B. L. 2000. Reactive oxygen species in cell signaling. *American Journal of Physiology-Lung Cellular and Molecular Physiology,* 279**,** 1005-1028.

Theodorou, I. G., Ryan, M. P., Tetley, T. D. & Porter, A. E. 2014. Inhalation of silver nanomaterials--seeing the risks. *International Journal of Molecular Sciences,* 15**,** 23936-74.

Toduka, Y., Toyooka, T. & Ibuki, Y. 2012. Flow cytometric evaluation of nanoparticles using side-scattered light and reactive oxygen species-mediated fluorescence-correlation with genotoxicity. *Environmental Science & Technology,* 46**,** 7629-7636.

Toulany, M., Maier, J., Iida, M., Rebholz, S., Holler, M., Grottke, A., Jüker, M., Wheeler, D. L., Rothbauer, U. & Rodemann, H. P. 2017. Akt1 and Akt3 but not Akt2 through interaction with DNA-PKcs stimulate proliferation and post-irradiation cell survival of K-RAS-mutated cancer cells. *Cell Death Discovery,* 3**,** 17072.

Valenta, T., Hausmann, G. & Basler, K. 2012. The many faces and functions of β-catenin. *EMBO Journal,* 31**,** 2714-2736.

Vales, G., Suhonen, S., Siivola, K. M., Savolainen, K. M., Catalán, J. & Norppa, H. 2020. Size, Surface Functionalization, and Genotoxicity of Gold Nanoparticles In Vitro. *Nanomaterials,* 10**,** 271.

Van Der Zande, M., Undas, A. K., Kramer, E., Monopoli, M. P., Peters, R. J., Garry, D., Antunes Fernandes, E. C., Hendriksen, P. J., Marvin, H. J., Peijnenburg, A. A. & Bouwmeester, H. 2016. Different responses of Caco-2 and MCF-7 cells to silver nanoparticles are based on highly similar mechanisms of action. *Nanotoxicology,* 10**,** 1431-1441.

Vance, M. E., Kuiken, T., Vejerano, E. P., Mcginnis, S. P., Hochella, M. F., Jr., Rejeski, D. & Hull, M. S. 2015. Nanotechnology in the real world: Redeveloping the nanomaterial consumer products inventory. *Beilstein journal of nanotechnology,* 6**,** 1769-1780.

Vanden Berghe, T., Grootjans, S., Goossens, V., Dondelinger, Y., Krysko, D. V., Takahashi, N. & Vandenabeele, P. 2013. Determination of apoptotic and necrotic cell death in vitro and in vivo. *Methods,* 61**,** 117-129.

Varela, J. A., Bexiga, M. G., Åberg, C., Simpson, J. C. & Dawson, K. A. 2012. Quantifying size-dependent interactions between fluorescently labeled polystyrene nanoparticles and mammalian cells. *Journal of Nanobiotechnology,* 10**,** 39.

Venugopal, K., Rather, H. A., Rajagopal, K., Shanthi, M. P., Sheriff, K., Illiyas, M., Rather, R. A., Manikandan, E., Uvarajan, S., Bhaskar, M. & Maaza, M. 2017. Synthesis of silver nanoparticles (Ag NPs) for anticancer activities (MCF 7 breast and A549 lung cell lines) of the crude extract of Syzygium aromaticum. *Journal of Photochemistry and Photobiology B: Biology,* 167**,** 282-289.

Verheyen, E. M. & Gottardi, C. J. 2010. Regulation of Wnt/beta-catenin signaling by protein kinases. *Developmental Dynamics,* 239**,** 34-44.

Verma, A., Uzun, O., Hu, Y., Hu, Y., Han, H. S., Watson, N., Chen, S., Irvine, D. J. & Stellacci, F. 2008. Surface-structure-regulated cell-membrane penetration by monolayer-protected nanoparticles. *Nature Materials,* 7**,** 588-595.

Vermes, I., Haanen, C. & Reutelingsperger, C. 2000. Flow cytometry of apoptotic cell death. *Journal of Immunological Methods,* 243**,** 167-190.

Vijayakumar, S. & Ganesan, S. 2012. Cytotoxicity Assay on Gold Nanoparticles with Different Stabilizing Agents. *Journal of Nanomaterials,* 2012**,** 734398.

Völker, C., Oetken, M. & Oehlmann, J. 2013. The Biological Effects and Possible Modes of Action of Nanosilver. *In:* WHITACRE, D. M. (ed.) *Reviews of Environmental Contamination and Toxicology Volume 223.* New York, NY: Springer New York.

Vrček, I. V., Žuntar, I., Petlevski, R., Pavičić, I., Dutour Sikirić, M., Ćurlin, M. & Goessler, W. 2016. Comparison of in vitro toxicity of silver ions and silver nanoparticles on human hepatoma cells. *Environmental Toxicology,* 31**,** 679-692.

Vyas, S. P. & Goswami, R. 2019. Size-dependent cellular uptake and TLR4 attenuation by gold nanoparticles in lung adenocarcinoma cells. *Nanomedicine: Nanotechnology, Biology, and Medicine,* 14**,** 229-229–253.

Wada, T. & Penninger, J. M. 2004. Mitogen-activated protein kinases in apoptosis regulation. *Oncogene,* 23**,** 2838-2849.

Wang, J., Li, J., Guo, G., Wang, Q., Tang, J., Zhao, Y., Qin, H., Wahafu, T., Shen, H., Liu, X. & Zhang, X. 2016. Silver-nanoparticles-modified biomaterial surface resistant to staphylococcus: new insight into the antimicrobial action of silver. *Scientific Reports,* 6**,** 32699.

Wang, L., Jiang, X., Ji, Y., Bai, R., Zhao, Y., Wu, X. & Chen, C. 2013. Surface chemistry of gold nanorods: origin of cell membrane damage and cytotoxicity. *Nanoscale,* 5**,** 8384-8391.

Wang, S.-H., Lee, C.-W., Chiou, A. & Wei, P.-K. 2010. Size-dependent endocytosis of gold nanoparticles studied by three-dimensional mapping of plasmonic scattering images. *Journal of Nanobiotechnology,* 8**,** 33.

Wang, X., Ji, Z., Chang, C. H., Zhang, H., Wang, M., Liao, Y.-P., Lin, S., Meng, H., Li, R., Sun, B., Winkle, L. V., Pinkerton, K. E., Zink, J. I., Xia, T. & Nel, A. E. 2014. Use of Coated Silver Nanoparticles to Understand the Relationship of Particle Dissolution and Bioavailability to Cell and Lung Toxicological Potential. *Small,* 10**,** 385-398.

Wang, Z., Xia, T. & Liu, S. 2015. Mechanisms of nanosilver-induced toxicological effects: more attention should be paid to its sublethal effects. *Nanoscale,* 7**,** 7470-7481.

Wei, L., Lu, J., Xu, H., Patel, A., Chen, Z.-S. & Chen, G. 2015. Silver nanoparticles: synthesis, properties, and therapeutic applications. *Drug Discovery Today,* 20**,** 595-601.

Williams, K. M., Gokulan, K., Cerniglia, C. E. & Khare, S. 2016. Size and dose dependent effects of silver nanoparticle exposure on intestinal permeability in an in vitro model of the human gut epithelium. *Journal of Nanobiotechnology,* 14**,** 62.

Wu, D., Ma, Y., Cao, Y. & Zhang, T. 2020. Mitochondrial toxicity of nanomaterials. *Science of the Total Environment,* 702**,** 134994.

Wu, K., Yang, Y., Zhang, Y., Deng, J. & Lin, C. 2015. Antimicrobial activity and cytocompatibility of silver nanoparticles coated catheters via a biomimetic surface functionalization strategy. *International journal of nanomedicine,* 10**,** 7241-7252.

Wu, Z., Guan, R., Tao, M., Lyu, F., Cao, G., Liu, M. & Gao, J. 2017. Assessment of the toxicity and inflammatory effects of different-sized zinc oxide nanoparticles in 2D and 3D cell cultures. *RSC Advances,* 7**,** 12437-12445.

Xia, M.-Y., Zhao, X.-Y., Huang, Q.-L., Sun, H.-Y., Sun, C., Yuan, J., He, C., Sun, Y., Huang, X., Kong, W. & Kong, W.-J. 2017a. Activation of Wnt/β-catenin signaling by lithium chloride attenuates d-galactose-induced neurodegeneration in the auditory cortex of a rat model of aging. *FEBS open bio,* 7**,** 759-776.

Xia, Q., Li, H., Liu, Y., Zhang, S., Feng, Q. & Xiao, K. 2017b. The effect of particle size on the genotoxicity of gold nanoparticles. *Journal of Biomedical Materials Research,* 105**,** 710-719.

Xia, Y., Zhang, X., Bo, A., Sun, J. & Li, M. 2018. Sodium citrate inhibits the proliferation of human gastric adenocarcinoma epithelia cells. *Oncology Letters,* 15**,** 6622-6628.

Xin, L., Wang, J., Fan, G., Che, B., Cheng, K. & Dong, G. 2016. Comparative oxidative stress elicited by nanosilver in stable HSPA1A promoter-driven luciferase reporter HepG2 and A549 cells. *Toxicology Research,* 5**,** 1298-1305.

Xu, F., Na, L., Li, Y. & Chen, L. 2020a. Roles of the PI3K/AKT/mTOR signalling pathways in neurodegenerative diseases and tumours. *Cell & Bioscience,* 10**,** 54.

Xu, L., Wang, Y.-Y., Huang, J., Chen, C.-Y., Wang, Z.-X. & Xie, H. 2020b. Silver nanoparticles: Synthesis, medical applications and biosafety. *Theranostics,* 10**,** 8996-9031.

Xue, Y., Zhang, T., Zhang, B., Gong, F., Huang, Y. & Tang, M. 2016. Cytotoxicity and apoptosis induced by silver nanoparticles in human liver HepG2 cells in different dispersion media. *Journal of Applied Toxicology,* 36**,** 352-360.

Yah, C. S. 2013. The toxicity of Gold Nanoparticles in relation to their physiochemical properties. *Biomedical Research,* 24**,** 400-413.

Yang, D. & Wong, W. P. 2016. Small but Mighty: Nanoparticles Probe Cellular Signaling Pathways. *Developmental Cell,* 37**,** 397-398.

Yao, C., Zhang, L., Wang, J., He, Y., Xin, J., Wang, S., Xu, H. & Zhang, Z. 2016. Gold Nanoparticle Mediated Phototherapy for Cancer. *Journal of Nanomaterials,* 2016**,** 5497136.

Yaqoob, S. B., Adnan, R., Rameez Khan, R. M. & Rashid, M. 2020. Gold, Silver, and Palladium Nanoparticles: A Chemical Tool for Biomedical Applications. *Frontiers in Chemistry,* 8.

Yi, C., Liu, D., Fong, C. C., Zhang, J. & Yang, M. 2010. Gold nanoparticles promote osteogenic differentiation of mesenchymal stem cells through p38 MAPK pathway. *ACS Nano,* 4**,** 6439-6448.

Yuan, Y. G., Peng, Q. L. & Gurunathan, S. 2017. Effects of Silver Nanoparticles on Multiple Drug-Resistant Strains of Staphylococcus aureus and Pseudomonas aeruginosa from Mastitis-Infected Goats: An Alternative Approach for Antimicrobial Therapy. *International Journal of Molecular Sciences,* 18**,** 569.

Yuan, Y. G., Zhang, S., Hwang, J. Y. & Kong, I. K. 2018. Silver Nanoparticles Potentiates Cytotoxicity and Apoptotic Potential of Camptothecin in Human Cervical Cancer Cells. *Oxidative Medicine and Cellular Longevity,* 2018**,** 6121328.

Yurdasiper, A., Arıcı, M. & Ozyazici, M. 2018. Chapter 7 - Nanopharmaceuticals: Application in inhaler systems. *In:* SHEGOKAR, R. & SOUTO, E. B. (eds.) *Emerging Nanotechnologies in Immunology.* Boston: Elsevier.

Zaman, S., Wang, R. & Gandhi, V. 2014. Targeting the apoptosis pathway in hematologic malignancies. *Leukemia & Lymphoma,* 55**,** 1980-1992.

Zamora-Justo, J. A., Abrica-González, P., Vázquez-Martínez, G. R., Muñoz-Diosdado, A., Balderas-López, J. A. & Ibáñez-Hernández, M. 2019. Polyethylene Glycol-Coated Gold Nanoparticles as DNA and Atorvastatin Delivery Systems and Cytotoxicity Evaluation. *Journal of Nanomaterials,* 2019**,** 5982047.

Zhang, H. & Zhang, C. 2014. Transport of silver nanoparticles capped with different stabilizers in water saturated porous media. *Journal of Materials and Environmental Science,* 5**,** 231-236.

Zhang, X.-F. & Gurunathan, S. 2016. Combination of salinomycin and silver nanoparticles enhances apoptosis and autophagy in human ovarian cancer cells: an effective anticancer therapy. *International journal of nanomedicine,* 11**,** 3655-3675.

Zhang, Z., Singh, R. & Aschner, M. 2016. Methods for the Detection of Autophagy in Mammalian Cells. *Current Protocols in Toxicology,* 69**,** 1-26.

Zhao, P., Li, N. & Astruc, D. 2013. State of the art in gold nanoparticle synthesis. Coord Chem Rev 257(3-4):638-665. *Coordination Chemistry Reviews,* 257**,** 638–665.

Zhou, G., Liu, N., Wang, Z., Shi, T., Gan, J., Wang, Z. & Zhang, J. 2017. Quantitative analysis of gold and carbon nanoparticles in mammalian cells by flow cytometry light scattering. *Journal of Nanoparticle Research,* 19**,** 78.

Zhu, B., Li, Y., Lin, Z., Zhao, M., Xu, T., Wang, C. & Deng, N. 2016. Silver Nanoparticles Induce HePG-2 Cells Apoptosis Through ROS-Mediated Signaling Pathways. *Nanoscale Research Letters,* 11**,** 198.

Zhu, G.-X., Gao, D., Shao, Z.-Z., Chen, L., Ding, W.-J. & Yu, Q.-F. 2021. Wnt/β-catenin signaling: Causes and treatment targets of drug resistance in colorectal cancer (Review). *Mol Med Rep,* 23**,** 105.

Zielinska, E., Zauszkiewicz-Pawlak, A., Wojcik, M. & Inkielewicz-Stepniak, I. 2017. Silver nanoparticles of different sizes induce a mixed type of programmed cell death in human pancreatic ductal adenocarcinoma. *Oncotarget,* 9**,** 4675-4697.

Zimmermann, S. & Moelling, K. 1999. Phosphorylation and regulation of Raf by Akt (protein kinase B). *Science,* 286**,** 1741-1744.

Zorova, L. D., Popkov, V. A., Plotnikov, E. Y., Silachev, D. N., Pevzner, I. B., Jankauskas, S. S., Babenko, V. A., Zorov, S. D., Balakireva, A. V., Juhaszova, M., Sollott, S. J. & Zorov, D. B. 2018. Mitochondrial membrane potential. *Analytical Biochemistry,* 552**,** 50-59.

Zucker, R. M., Daniel, K. M., Massaro, E. J., Karafas, S. J., Degn, L. L. & Boyes, W. K. 2013. Detection of silver nanoparticles in cells by flow cytometry using light scatter and far-red fluorescence. *Cytometry A,* 83**,** 962-972.

Zucker, R. M., Ortenzio, J., Degn, L. L., Lerner, J. M. & Boyes, W. K. 2019. Biophysical comparison of four silver nanoparticles coatings using microscopy, hyperspectral imaging and flow cytometry. *PloS One,* 14**,** 0219078.

Chapter 8

Appendix

Appendix

Table A1. Stability measurement of AgNPs in Ham's F-12 Nutrient Mixture. AgNPs of different sizes (10-80nm) and at a concentration of 10 µg/ml were incubated in Ham's F-12 Nutrient Mixture with serum (10% FBS) at 37°C for 30 mins, 24 hrs and 48 hrs. The changes in AgNPs sizes were measured using DLS.

AgNPs	30 mins		24 hrs		48 hrs	
	Size	**PDI**	**Size**	**PDI**	**Size**	**PDI**
Ag10	60 ±7	0.1 ±0	27 ±3	0.4 ±0	17 ±1	0.6 ±0
Ag40	62 ±1	0.2 ±0	97 ±2	0.4 ±0	40 ±1	0.3 ±0
Ag80	118 ±2	0.1 ±0	133 ±1	0.1 ±0	67 ±1	0.1 ±0

Table A2. Stability measurement of AuNPs in Ham's F-12 Nutrient Mixture. AuNPs of different sizes (10-80nm) and at a concentration of 26 µg/ml were incubated in Ham's F-12 Nutrient Mixture with serum (10% FBS) at 37°C for 30 mins, 24 hrs and 48 hrs. The changes in AuNPs sizes were measured using DLS.

AuNPs	30 mins		24 hrs		48 hrs	
	Size	**PDI**	**Size**	**PDI**	**Size**	**PDI**
Au10	24 ±1	0.4 ±0	24 ±1	0.4 ±0	12 ±0	0.4 ±0
Au40	58 ±2	0.2 ±0	61 ±2	0.2 ±0	41 ±1	0.2 ±0
Au80	109 ±1	0.1 ±0	109 ±1	0.1 ±0	110 ±1	0.1 ±0

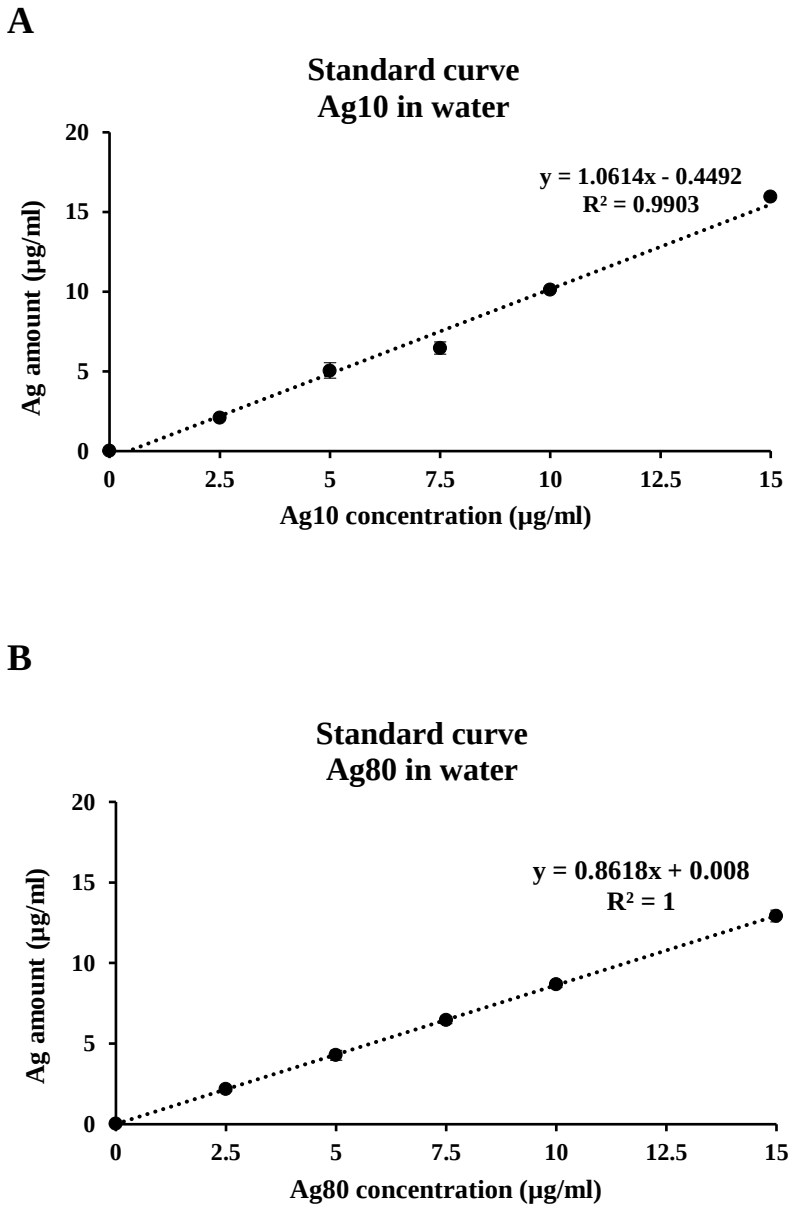


Figure A1. Standard curves of Ag10 and Ag80 in water using ICP-MS. The amount of Ag measured by ICP-MS based on different concentrations (2.5- 15 µg/ml) of Ag10 (**A**) and Ag80 (**B**) in water.

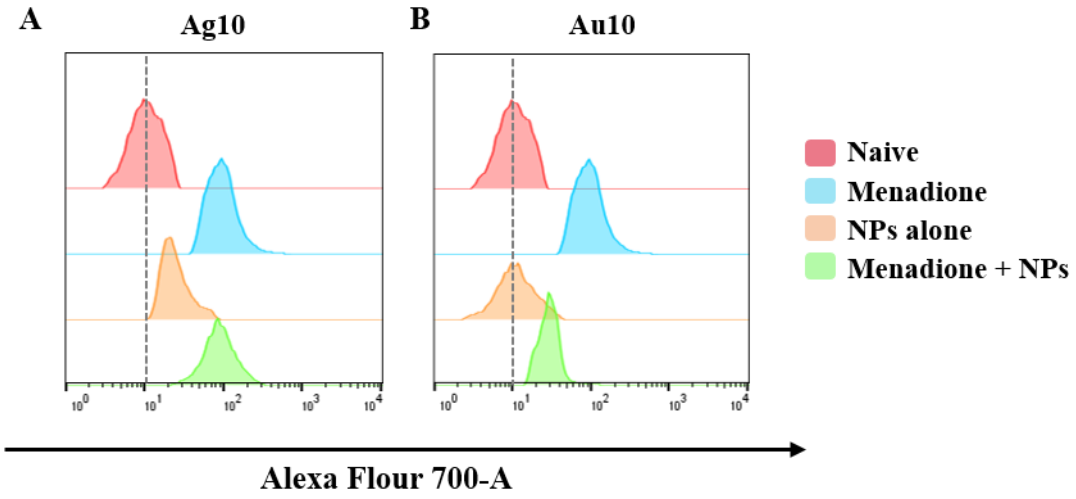


Figure A2. Analysis of AgNPs and AuNPs interference with CellRox™ deep red assay. A549 cells treated with Ag10 at 10 µg/ml (**A**), Au10 at 36 µg/ml (**B**), Menadione at 50 µM (positive control) and a combination of Ag10 or Au10 with Menadione for 24 hrs. No changes in the intensity produced from cells treated with Menadione alone and Menadione with NPs indicating no interference with the assay.

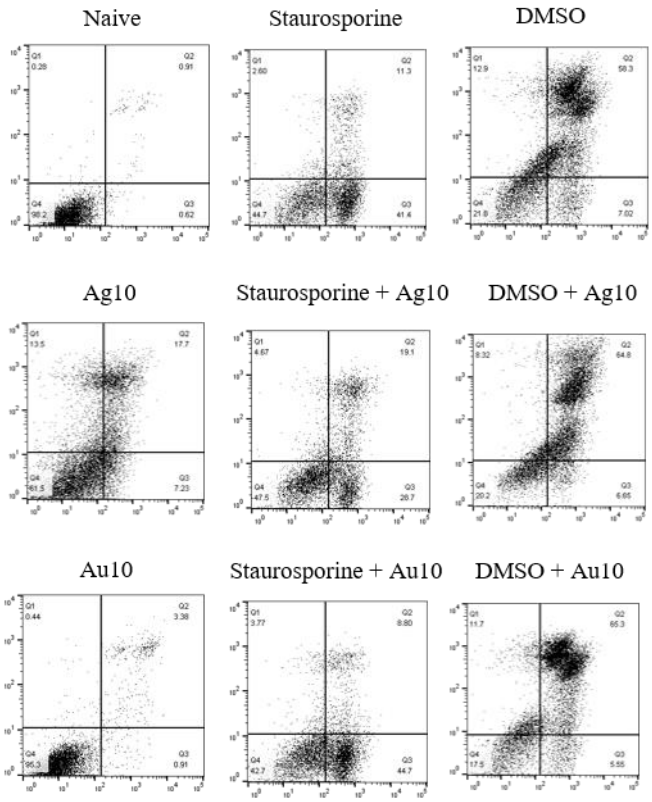


Figure A3. Analysis of AgNPs and AuNPs interference with Alexa Fluor® 488 Annexin V/Dead cell apoptosis assay. A549 cells treated with Ag10 at 10 µg/ml, Au10 at 36 µg/ml, Staurosporine at 1 µM (apoptosis inducer), DMSO at 10% (necrosis inducer), and a combination of Ag10 or Au10 with apoptosis or necrosis inducers for 24 hrs. No profound changes in the intensity produced from cells treated with apoptosis or necrosis inducers alone and apoptosis and necrosis inducers with NPs indicating no interference with the assay.

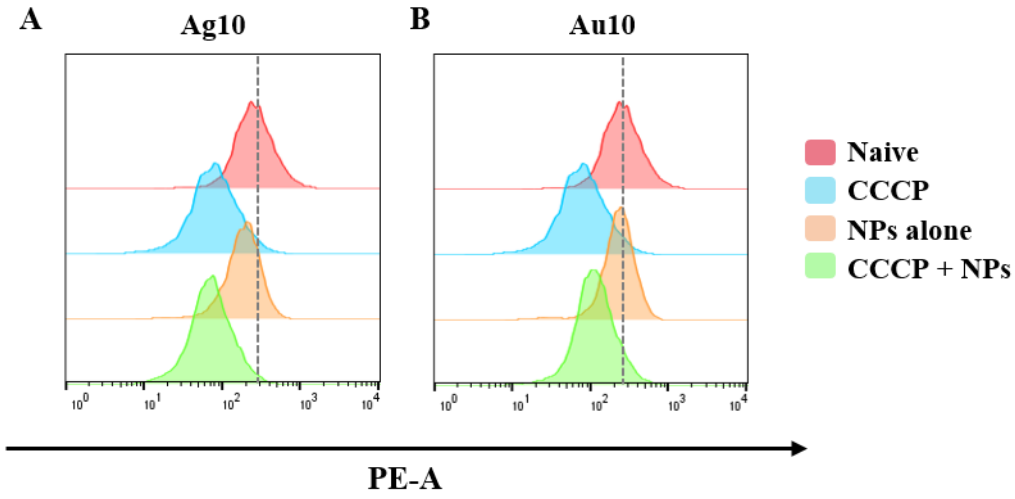


Figure A4. Analysis of AgNPs and AuNPs interference with MitoProbe™,TMRM assay. A549 cells treated with Ag10 at 10 µg/ml (**A**), Au10 at 36 µg/ml (**B**), CCCP at 50 mM (positive control) and a combination of Ag10 or Au10 with CCCP for 24 hrs. No changes in the intensity produced from cells treated with CCCP alone and CCCP with NPs indicating no interference with the assay.

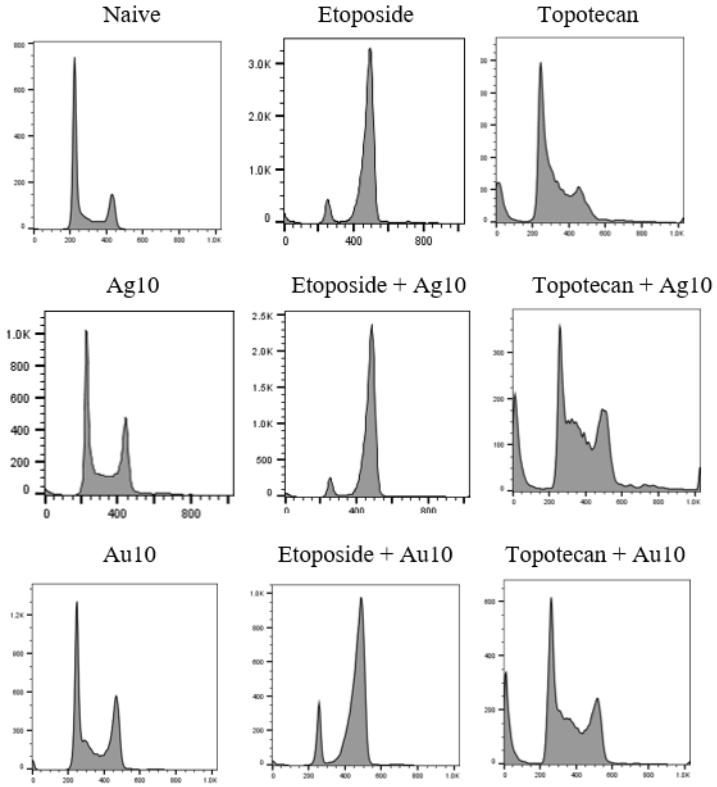


Figure A5. Analysis of AgNPs and AuNPs interference with FxCycle™ PI/RNase Staining. A549 cells treated with Ag10 at 10 µg/ml, Au10 at 36 µg/ml, Etoposide at 10 µM (G2/M phase inducer), Topotecan at 1 µM (G1/S phase inducer), and a combination of Ag10 or Au10 with G1/S or G2/M phase inducers for 24 hrs. No profound changes in the intensity produced from cells treated with G1/S or G2/M phase inducers alone and G1/S and G2/M phase inducers with NPs indicating no interference with the assay.

Conference oral presentation:

Hanouf Bafhaid, Zubair Ahmed, Youcef Mehellou, Hanene Ali-Boucetta. "A Nanotoxicology Investigation: Exploring the size effects of silver and gold nanoparticles on lung cells". International Conference On Nanomedicine And Nanobiotechnology 2019, Munich, Germany (October, 2019).

Abstract:

Unfortunately, nanotoxicology literature does not present a homogenous finding in regards to the cytotoxicity of nanoparticles and discrepancies are still present between the different conclusions. While the biological responses and cellular-uptake of nanoparticles are predominately influenced by their different physiochemical properties, a systematic nanotoxicology framework is still lacking.

This study aims to systematically compare the impact of different composition and different sizes (10, 40 and 80nm) of spherical silver (AgNP) and gold (AuNP) nanoparticles on cellular toxicity and assess the changes mediated by these nanoparticles following their exposure to human adenocarcinoma alveolar basal epithelial cells (A549) and normal lung fibroblasts (MRC-5). The size and charge of the nanoparticles were characterised using dynamic light scattering and transmission electron microscopy. Their cytotoxicity effects were then studied using MTT, mLDH assays and the mechanism(s) of cell death investigated using Annexin-V/PI, reactive oxygen species (ROS) and glutathione depletion. On A549 cells, we found that CC50 (50% cytotoxic concentration) of Ag10 and Au10 after 24hrs are 11.7 and 42.2µg/ml respectively which suggests that AuNP are safer than AgNP. It was interesting to see that the smaller sizes (10,40nm) of AgNP and AuNP demonstrate more cytotoxicity in comparison to their bigger counterparts (80nm). This could be due to their enhanced cellular uptake due to their small size, as we found the amount of silver -taken-up by A549 cells after 24hrs exposure to Ag10 and Ag80 measured by ICP-MS are 4 and 3µg/ml, respectively. Necrotic cell death was observed in a size, concentration and time dependent manner following exposure to AgNP for 24 and 48hrs (more than 15% Annexin (+)/PI (+)) in both cell lines. Induction of oxidative stress was also found after 24hrs post- exposure to all sizes of AgNP on both cell lines, while AuNP showed an increase in ROS generation only at the highest concentration (40µg/ml). After 24hrs exposure to AgNP, the amount of reduced glutathione was significantly depleted in a size and dose-dependent manner with up to 80% decrease in reducing glutathione levels after A594 exposure to Ag10. AuNP illustrated a reduction effect on reduced glutathione in

A549 and MRC-5 cells at the highest concentration which correlates with the detected ROS levels.

In summary, our findings highlight that the size of nanoparticles can influence their interaction with cells. AgNP of smaller sizes (10 and 40nm) showed detrimental effects on lung cells after 24 and 48hrs of exposure. AuNP demonstrated a good safety profile comparing to AgNP of the same size, emphasising that nanoparticle composition has also an impact on their cellular toxicity. However, MRC-5 and A549 cells display similar trend of toxicity toward AgNP, which is associated with the release of silver ions.

While size and chemical composition were the key determinant factors in defining the toxicity of our silver & gold nanoparticles, the ultimate goal of this work is to create a systematic nanotoxicology framework in order to validate current literature and to pave the development nanoparticles for biomedical applications.